Ewelina Kalwarczyk

Nanoparticles in complex fluids

Advisor: Prof. ICHF dr hab. Marcin Fiałkowski

The presented dissertation was prepared within
the International Ph.D. in Chemistry Studies at the
Institute of Physical Chemistry of the Polish Academy of Sciences
Department of Soft Condensed Matter and Fluids
Kasprzaka 44/52, 01-224 Warsaw, Poland.

Warsaw, August 2012

Acknowledgements

I would like to thank my advisor, Professor Marcin Fiałkowski, for creating an outstanding scientific community, his support and many priceless advices on my research.

Thanks to Professor Robert Hołyst, the Director of the Institute of Physical Chemistry PAS and a head of Department of Soft Condensed Matter and Fluids, for creating the opportunity to study in his department and for many fruitful discussions.

Thanks to all employees of the Department of Soft Condensed Matter IPC PAS for creating a wonderful and inspiring scientific atmosphere. In particular, I thank Dr. Maciej Paszewski for introducing me to the mysteries of the synthesis of nanoparticles. I thank Dr. Stefan A. Wieczorek and Msc. Natalia Ziębacz for their help in conducting and analyzing the results of dynamic light scattering measurements. I would like to thank Msc. Karolina Urbaniak, Msc. Monika Pyzalska, MSc. Monika Gołoś and Ms Joanna Kęska for their contribution to the results of my research.

I would like to acknowledge Professor Ewa Górecka and Dr Damian Pociecha, from Structural Research Laboratory of Department of Chemistry University of Warsaw, for invaluable assistance in carrying out measurements using X-ray scattering.

The work was supported by the project operated within the Foundation for Polish Science Team Programme co-financed by the EU "European Regional Development Fund" TEAM/2010-6/4.

List of papers

(1) Kalwarczyk, E., Golos M., Holyst R., Fialkowski M., Polymer-induced ordering and phase separation in ionic surfactants, *J. Colloid Int. Sci.*, **342**, 93 (2010) (**IF=3.066**)

(2) Kalwarczyk, E., Paszewski M., Xin X., Gorecka E., Pociecha D., Holyst R., Fialkowski M. New one-pot technique to introduce charged nanoparticles into a lyotropic liquid crystal matrix, *Langmuir*, **27**, 3937 (2011) (**IF=4.268**)

(3) Holyst R., Bielejewska A., Szymanski J., Wilk A., Patkowski A., Gapinski J., Zywocinski A., Kalwarczyk T., Kalwarczyk, E., Tabaka M., Ziebacz N., Wieczorek S.A., Scaling form of viscosity at all length-scales in poly(ethylene glycol) solutions studied by fluorescence correlation spectroscopy and capillary electrophoresis, *Phys. Chem. Chem. Phys.*, **11**, 9025 (2009) (**IF=3.453**)

(4) Xin X., Li H., Wieczorek S.A., Szymborski T., Kalwarczyk, E., Ziebacz N., Gorecka E., Pociecha D., Holyst R., Incorporation of carbon nanotubes into a lyotropic liquid crystal by chase separation in the presence of a hydrophilic polymer , *Langmuir*, **26**, 3562 (2010) (**IF=4.268**)

(5) Xin X., Li H., Kalwarczyk, E., Kelm A., Fialkowski M., Gorecka E., Pociecha D., Holyst R., Single-Walled Carbon Nanotube/Lyotropic Liquid Crystal Hybrid Materials Fabricated by a Phase Separation Method in the Presence of Polyelectrolyte, *Langmuir*, **26**, 8821 (2010) (**IF=4.268**)

(6) Li H., Xin X., Kalwarczyk T., Kalwarczyk, E., Niton P., Holyst R., Hao JC., Reverse Vesicles from a Salt-Free Catanionic Surfactant System: A Confocal Fluorescence Microscopy Study, *Langmuir*, **26**, 15210 (2010) (**IF=4.268**)

(7) Hou, S., Ziębacz, N., Wieczorek, S. A., Kalwarczyk, E., Sashuk, V., Kalwarczyk, T., Kamiński, T.S., Hołyst, R. Formation and Structure of PEI/DNA Complexes: Quantitative Analysis *Soft Matter* **7**, 6967 (2011) (**IF=4.457**)

(8) Winkler, K., Paszewski, M., Kalwarczyk, T., Kalwarczyk, E., Gorecka, E., Pociecha, D., Wojciechowski, T., Holyst, R., Fialkowski, M., Ionic Strength-Contolled Deposition of Charged Nanoparticles on Solid Substrate *J. Phys Chem. C* **115**, 19096 (2011) (**IF=4.520**)

List of patent applications

(1) Robert Hołyst, Marcin Fiałkowski, Ewelina Kalwarczyk, Monika Pyzalska, Joanna Kęska, Monika Gołoś, Karolina Urbaniak; **P-387151** "Sposób strącania i porządkowania roztworów jonowych środków powierzchniowo czynnych w mieszaninach wody i rozpuszczalników polarnych"

(2) Robert Hołyst, Marcin Fiałkowski, Ewelina Kalwarczyk, Monika Pyzalska, Joanna Kęska, Monika Gołoś, Karolina Urbaniak; **P-387292** "Sposób strącania i porządkowania roztworów kationowych środków powierzchniowo czynnych w rozpuszczalnikach polarnych, zwłaszcza w wodzie"

(3) Ewelina Kalwarczyk, Marcin Fiałkowski, Robert Hołyst, Maciej Paszewski, Xia Xin; **P-389326** "Sposób wprowadzania hydrofilowych, naładowanych nanocząstek do uporządkowanych faz surfaktantów"

(4) Maciej Paszewski, Marcin Fiałkowski, Ewelina Kalwarczyk, Tomasz Kalwarczyk, Katarzyna Winkler, Robert Hołyst; **P-391217** "Metoda pokrywania powierzchni nanocząstkami"

(5) Maciej Paszewski, Marcin Fiałkowski, Ewelina Kalwarczyk, Tomasz Kalwarczyk, Katarzyna Winkler, Robert Hołyst; **EN.700114.GB** "Method of coating material surfaces with nanoparticles"

Koncepcja rozprawy doktorskiej

Nanotechnologia jest prężnie rozwijającą się dziedziną nauki zapoczątkowaną w latach 50 XX wieku przez Richarda P. Feynmana wykładem „There's Plenty of Room at the Bottom". Wykorzystuje ona obiekty o różnej strukturze przestrzennej oraz różnym składzie, jednakże mające jedną podstawową cechę wspólną – rozmiar mniejszy niż 100 nanometrów. Metody otrzymywania oraz charakteryzacja nanoobiektów o ściśle określonej geometrii i rozmiarze są przedmiotem badań w ośrodkach naukowych na całym świecie. Współcześnie obserwujemy bardzo intensywny transfer nanotechnologii z laboratoriów do codziennego życia. Nanocząstki coraz częściej można znaleźć jako składniki leków, kosmetyków, farb, opon samochodowych, opakowań produktów spożywczych a nawet tekstyliów. Często są one składnikami płynów złożonych takich jak roztwory micelarne, roztwory polimerów czy uporządkowane fazy ciekłych kryształów. Poznanie właściwości takich układów jest interesujące ze względów poznawczych, umożliwiłoby także projektowanie materiałów o ściśle zadanej strukturze i właściwościach. Z tego powodu celowym wydaje się zbadanie układów składający się z nanocząstek oraz płynów złożonych o określonej strukturze takich jak roztwory micelarne oraz uporządkowane fazy liotropowych ciekłych kryształów.

W swojej pracy doktorskiej zbadam układy składające się z hydrofilowych, naładowanych nanocząstek metali szlachetnych (Au oraz Ag) oraz półprzewodnikowych typu „core/shell" – „jądro/otoczka" (CdSe/ZnS) wprowadzonych do płynów o różnym stopniu złożoności. W przypadku układów o bardzo złożonej strukturze wewnętrznej – liotropowych ciekłych kryształów – zbadana zostanie możliwość wbudowywania nanocząstek do uporządkowanych faz, a następnie możliwość tworzenia z nich stałych, porowatych struktur zawierających wbudowane nanocząstki. Dla płynów o niższym stopniu złożoności (roztwory micelarne) zbadane zostanie oddziaływanie pomiędzy micelami a nanocząstkami w zależności od stężenia oraz wielkości części hydrofilowej surfaktantu.

The concept of dissertation

Nanotechnology is a rapidly developing field of science started in the 50 century by Richard P. Feynman's lecture, "There's Plenty of Room at the Bottom". It uses objects with different spatial structure and a different composition, but with one major thing in common - a size smaller than 100 nanometers. Methods of obtaining and characterization of nano-objects with well-defined geometry and size are the subject of research in scientific institutions around the world. Today we observe a very intense transfer of nanotechnology from laboratories to everyday life. Nanoparticles are increasingly found as components of drugs, cosmetics, paints, tires, food packaging and even fabrics. Often, they are components of complex fluids such as micellar solutions, polymer solutions or ordered phases of liquid crystals. Understanding the properties of such systems is interesting for cognitive reasons, it would also enable the design of materials with well-defined structure and properties. For this reason it is advisable to investigate systems consisting of nanoparticles and complex fluids such as micellar solutions and lyotropic ordered phases of liquid crystals.

In my dissertation, I examine the systems consisting of hydrophilic charged noble metal (Au and Ag) and semiconductor core/shell (CdSe/ZnS) nanoparticles immersed in liquids of varying complexity. In the case of systems with very complex internal structure - lyotropic liquid crystals - I examine the incorporation of nanoparticles into ordered phases, and then the possibility to create solid, porous structures containing embedded nanoparticles. In the case of fluids of lower complexity (micellar solutions) I examine the interaction between micelles and nanoparticles depending on the concentration and size of the hydrophilic part of surfactant.

Theses

1) Phase separation and ordering in the ionic surfactant-based systems can be obtained via polymer-induced phase separation.

2) The polymer induced phase separation in systems consisting of surfactant and nanoparticles can be used as a method for direct incorporation of nanoparticles into various ordered phases of surfactants.

3) Fluorescence quenching of negatively charged semiconductor quantum dots in the presence of nonionic surfactant is a result of formation of surfactant coating at the surface of the quantum dots. The coating consists of two layers of surfactant molecules and and is formed in adsorption process following the first-order kinetics.

Table of contents

Abbreviations and symbols

$f(\kappa r)$ – Henry function

χ – molar fraction of negatively charged nanoparticles in the system

χ^* – titration point

χ_{Ag} – molar fraction of Ag-nanoparticles

ϵ – constant of the dimension of J/mol

η – viscosity of a fluid

Γ – parameter in DLS, inverse of inflection point of autocorrelation function

$\gamma^{poly}_{\mathrm{H_2O}}$ – the activity coefficients of water in the polymer-rich phase

$\gamma^{surf}_{\mathrm{H_2O}}$ – the activity coefficients of water in the surfactant-rich phase

κ^{-1} – Debye length

λ – wavelength

λ_{em} – emission (fluorescence) wavelength

$\mu^0_{\mathrm{H_2O}}$ – the chemical potential of water in the standard state

$\mu^{poly}_{\mathrm{H_2O}}$ – the chemical potential of water in the polymer-rich phase

$\mu^{surf}_{\mathrm{H_2O}}$ – the chemical potential of water in the surfactant-rich phase

ν – the mass fraction of the polar solvent

ϕ_{salt} – the molar fraction of a salt

$\phi^{\star}_{\mathrm{salt}}$ – the threshold molar fraction of salt

ψ – the fraction of the diffuse ions

p – percentage concentration of the polymer solution expressed in the form of a common fraction

N – number of atoms in nanoparticle

$\mathrm{N_s}$ – number of atoms at the surface of nanoparticle

$\mathrm{N_{agg}}$ – aggregation number

$\mathrm{P_s}$ – percentage of surface atoms with respect to total number of atoms

τ – delay time

τ_{q} – time of quenching of quantum dots

θ – angle between incident ray and scattered plane

ε – dielectric constant of medium

$\varepsilon_{\mathrm{abs}}$ – molar absorption coefficient (attenuation coefficient)

ζ-potential – zeta-potential

A – absorbance

a – lattice constant for hexagonal phase

$a_{\mathrm{H_2O}}^{poly}$ – activity of water in the polymer-rich phase

$a_{\mathrm{H_2O}}^{surf}$ – activity of water in the surfactant-rich phase

B – fitting parameter in power-law equation

c – molar concentration of a sample

C_{NP}^{0} – initial concentration of nanoparticles

c_{Ag}^{0}, c_{Au}^{0} – initial molar concentration of Ag- and Au-nanoparticles solution respectively

$C_{\mathrm{NP}}^{\mathrm{pol}}$ – concentration of the nanoparticles remaining in polymer-rich phase after the phase separation

$C_{\mathrm{PEG}}^{\mathrm{low}}$ – the lower threshold mass fraction of PEG

$C_{\mathrm{PEG}}^{\mathrm{up}}$ – the upper threshold mass fraction of PEG

C_{p} – the mass fraction of polymer in the sample

$C_{\mathrm{p}}^{\star}$ – threshold mass fractions of the polymer

C_{s} – the mass fraction of surfactant in the sample

$C_{\mathrm{s}}^{\mathrm{m}}$ – the minimal mass fraction of the surfactant in the surfactant-rich phase needed to get an ordered (hexagonal) phase

c_{Ag}, c_{Au} – temporary molar concentration of Ag- and Au-nanoparticles respectively

c_{surf} – molar concentration of surfactant

D – translational diffusion coefficient

d – interplanar spacing, also - the distance between layers in lamellar phase

$G(\tau)$ – intensity-intensity autocorrelation function

h – the Planck's constant

I – intensity of transmitted light

$I(t)$ – intensity of scattering signal at time t, in DLS

I_0 – intensity of incident light

I_{b}, I_{s} – intensity of DLS signal comming from big and small particles respectively

k_{B} – Boltzmann's constant

l – absorption path length

$m_{\mathrm{H_2O}}$ – the mass of water

$m_{\mathrm{H_2O}}^{poly}$ – the mass of water in the polymer-rich phase

$m_{\mathrm{H_2O}}^{surf}$ – the mass of water in the surfactant-rich phase

M_{poly} – the molar mass of the polyelectrolyte

m_{pol} – the mass of polar solvent

m_{p} – the mass of polymer

m_{solv} – the mass of solvent

M_{surf} – the molar mass of the surfactant

m_{s} – the mass of surfactant

M_{w} – molecular weight

M_{n} – number-averaged molecular weight

M_{w} – weight-averaged molecular weight

n – the average number of counterions released from the dissociation of the polyelectrolyte molecule

$N_{\mathrm{NP}}^{\mathrm{LLC}}$ – number of nanoparticles transferred into the LLC phase

N_{-}, N_{+} – number of moles of the negatively and positively charged nanoparticles respectively

N_{b}, N_{s} – number of big and small particles respectively

N_{salt} – the number of moles of the salt

N_{s} – the number of moles of the surfactant

N_{Ag}, N_{Au} – number of Ag- and Au-nanoparticles in solution

$N_{\mathrm{surf/QD}}$ – number of surfactant molecules attributable to one quantum dot

p – momentum of the particle

q – scattering vector

Q_{-}, Q_{+} – total net charge over the negatively and positively charged nanoparticles, respectively

$Q_{\mathrm{QD}(-)}, Q_{\mathrm{Ag}(-)}, Q_{\mathrm{Au}(-)}, Q_{\mathrm{Ag}(+)}, Q_{\mathrm{Au}(+)}$, – net charge of nanoparticles mentioned in subscript

R – the gas constant

r – radius of an object, for example nanocrystal

r_a – atomic radius

$r_{\mathrm{Ag}(+)}, r_{\mathrm{QD}(-)}$ – radius of Ag(+) and QD(-) nanoparticles, respectively

$R_{\mathrm{h,mic}}$ – hydrodynamic radii of micelles

$R_{\mathrm{h,QD}}$ – hydrodynamic radii of quantum dot

R_{g} – radius of gyration

$R_{\mathrm{h,b}}$, $R_{\mathrm{h,s}}$ – hydrodynamic radius of big and small particles respectively

R_{h} – hydrodynamic radius

r_{mic} – radius of the micelle

T – temperature

t – time

U_{E} – electrophoretic mobility

V^0 – initial volume of nanoparticles solution

V^{pol} – volume of the polymer-rich phase

V_{Ag}, V_{Au} – volume of Ag- and Au-nanoparticles solution respectively

$x^{poly}_{\mathrm{H_2O}}$ – molar fraction of water in the polymer-rich phase

$x^{surf}_{\mathrm{H_2O}}$ – molar fraction of water in the surfactant-rich phase

x_{poly} – the molar fraction of the polyelectrolyte molecules in the polymer-rich phase

x_{surf} – the molar fraction of the surfactant

Z – number of oxygen atoms one PEG molecule

m – number of carbon atoms in the alkyl chain of C_mE_n

n – number of oxyethylene units in the polar head of C_mE_n

C_mE_n – polyoxyethylene glycol monoalkylether

NMe_4OH – tetramethylammonium hydroxide

A – baseline of correlation function

Ag(+), Au(+) – silver and gold nanoparticles coated with positively charged ligand - TMA

Ag(-), Au(-) – silver and gold nanoparticles coated with negatively charged ligand - MUA

AgDA – silver nanoparticles coated with decanoic acid

AgMUA – silver nanoparticles coated with MUA

AgTMA – silver nanoparticles coated with TMA

AR – aspect ratio (i. e. length / width)

AuDDA – gold nanoparticles coated with dodecylamine

AuMUA – gold nanoparticles coated with MUA

AuTMA – gold nanoparticles coated with TMA

B – intercept of correlation function

CMC – critical micelle concentration

CPB – hexadecylpyridinium bromide

CTAB – cetyltrimethylammonium bromide

DA – decanoic acid

DDA – dodecylamine

DDAB – didodecyldimethylammonium bromide

DLS – dynamic light scattering

DSS – dodecanesulfonic acid, sodium salt

DTAC – dodecyltrimethylammonium chloride

F(q) – form factor

FWHM – full width of half maximum

I (q) – total scattering intensity in SAXS

L – number of shells in nanoparticle

LLC – lyotropic liquid crystal

MUA – 11-mercaptoundecanoic acid

NPs – nanoparticles

PAAS – poly(acrylic acid, sodium salt)

PDDAC – poly(diallyldimethylammonium chloride)

PDI – polydispersity index

PEG – polyethylene glycol

PEI – polyethylenimine

PIPS – polymer-induced phase separation

PSS – poly(sodium 4-styrenesulfonate)

PVA – polyvinyl alcohol

QD – quantum dot

QD(-) – CdSe/ZnS core/shell quantum dots coated with negatively charged ligand

QY – quantum yield

S(q) – structure factor

SAM – self-assembled monolayer

SAXS – small angle X-ray scattering

SDS – sodium dodecyl sulfate

SEM – scanning electron microscopy

SERS – surface-enhanced Raman scattering

SPR – surface plasmon resonance

TBAB – tetrabutyl ammonium borohydride

TEM – transmission electron microscopy

TEOS – tetraethyl orthosilicate

TMA – N,N,N-trimethyl(11-mercaptoundecyl) ammonium chloride

TMOS – tetramethyl orthosilicate

TTAB – tetradecyltrimethylammonium bromide

WAXS – wide angle X-ray scattering

1 Introduction

A modern, twenty-first-century chemistry, not only continues the research conducted in previous centuries, but also brings together various branches of science and technology. The overall objective of this action is usually the desire to create entirely new materials characterized by an interesting combination of physicochemical properties. During the study described in this dissertation I followed this trend, and connected selected issues of nanotechnology and soft matter. In particular I combined nanoparticles (NPs), i.e. particles whose size is one billionth of a meter, with liquids having complex internal structure. An example of this type of liquids, called complex fluids, are solutions of surfactants and of polymers. One of the key achievements of the research presented is the development of the method which allows the formation of new "nanostructured" materials consisting of NPs enclosed in a soft or solid template of a prescribed internal structure.

The dissertation is organized into four Chapters (Introduction, Experimental part, Results, and Summary), each of which is further divided into Sections. Because this dissertation covers selected issues of nanotechnology and of soft matter, the Introduction is divided into two sections. Section 1.1 contains the basics of nanotechnology, with particular emphasis on spherical NPs, their properties, synthesis and self-organization. Section 1.2 introduces the main issues in the field of soft matter, especially the behavior of surfactants and polymers in aqueous solutions.

The Experimental part, sums up the information related to experimental side of my research. Section 2.1 includes basics of experimental techniques used in my studies. Section 2.2 describes procedures for the synthesis and functionalization of NPs. Section 2.3 contains specification of the chemicals used in experiments.

The essential part of this dissertation (Results) is divided into three sections. In Section 3.1 I described the phenomenon observed in solutions consisting of ionic surfactant, ionic or nonionic polymer and water. I found, that the addition of a proper polymer induces the phase separation process. Additionally, it may lead to ordering of molecules inside the surfactant-rich phase. I named the observed phenomenon: the polymer-induced phase separation (PIPS). In the case of ionic surfactants, PIPS is preferably caused by the addition of polyelectrolyte with the same charge as that of surfactant. In Section 3.2 I demonstrated that polymer-induced phase separation, described in Section 3.1, is a great tool to fabricate novel “nanostructured”

materials. In particular, I showed that PIPS may be used to incorporate charged NPs into ordered phases of ionic or nonionic surfactants. Additionally, I succeed to convert this kind of soft nanocomposite into solid form. In Section 3.3, I contained the results of studies on the dispersion of NPs in fluids with a low degree of complexity, that is, in micellar solutions of surfactants. I demonstrated that non-ionic surfactants adsorb at the surface of NPs functionalized with carboxylic acid groups. In the case of semiconductor quantum dots (QDs) functionalized with COOH groups, the adsorption of surfactant leads to the quenching of fluorescence. Each section of the Results is completed with separate section, which contains conclusions of the results. The key findings of the dissertation are overviewed in Summary.

1.1 Nanomaterials - properties, methods of synthesis, self-assembly, and applications

Nanotechnology is a young and rapidly expanding field of modern science. In general, it deals with creating, processing and use of materials whose size is of the order of one billionth of a meter. Although the minimization in science is the observed trend for a long time, it is difficult to define the start of nanotechnology. Many people link it with the lecture "There is plenty of room at the bottom" by Richard Feynman. This lecture took place on December 26, 1956 at the annual meeting of the American Physical Society at the California Institute of Technology. During his lecture, Feynman did not use the term "nano" because it did not exist at that time. However, he put on issues and ideas that are currently addressed by nanotechnology and its tools[1]. This makes this American physicist, and Nobel prize laureate, a father of nanotechnology. The prefix "nano" came to the metric system in 1960, indicating a factor of 10^{-9}. Nano, from the Greek $\nu\alpha\nu o\varsigma$, means a dwarf that is something very, very tiny. The definition of nanotechnology, however, appeared more than ten years later, in 1974, at the International Conference on Precision Engineering. At this conference Noiro Taniguchi from Tokyo University of Science, postulated that "Nano-technology mainly consists of the processing of, separation, consolidation, and deformation of materials by one atom or by one molecule"[2].

As its building blocks nanotechnology uses nanomaterials. Although the International Union of Pure and Applied Chemistry (IUPAC) does not specify a definition of nanomaterial, it is commonly accepted that nanomaterials are objects that have at least one dimension in the range of 1 and 100 nanometers. Nanoobjects are a kind of bridge between the world of atoms/molecules and the world of complex microscopic structures formed by human or by nature. The comparison of nanomaterials with objects of different sizes (from meters to tenths of a nanometer - angstroms) is presented in Figure 1.

This Section focuses on nanomaterials and it is organised as follows: Section 1.1.1 discusses the main properties of nanomaterials resulting from their size. Section 1.1.2 focuses on the basic methods of preparation of nanomaterials. Section 1.1.3 discusses methods of organizing nanomaterials in complex, hierarchical structure. Last Section (1.1.4) is devoted to selected applications of nanomaterials in various branches of science and technology.

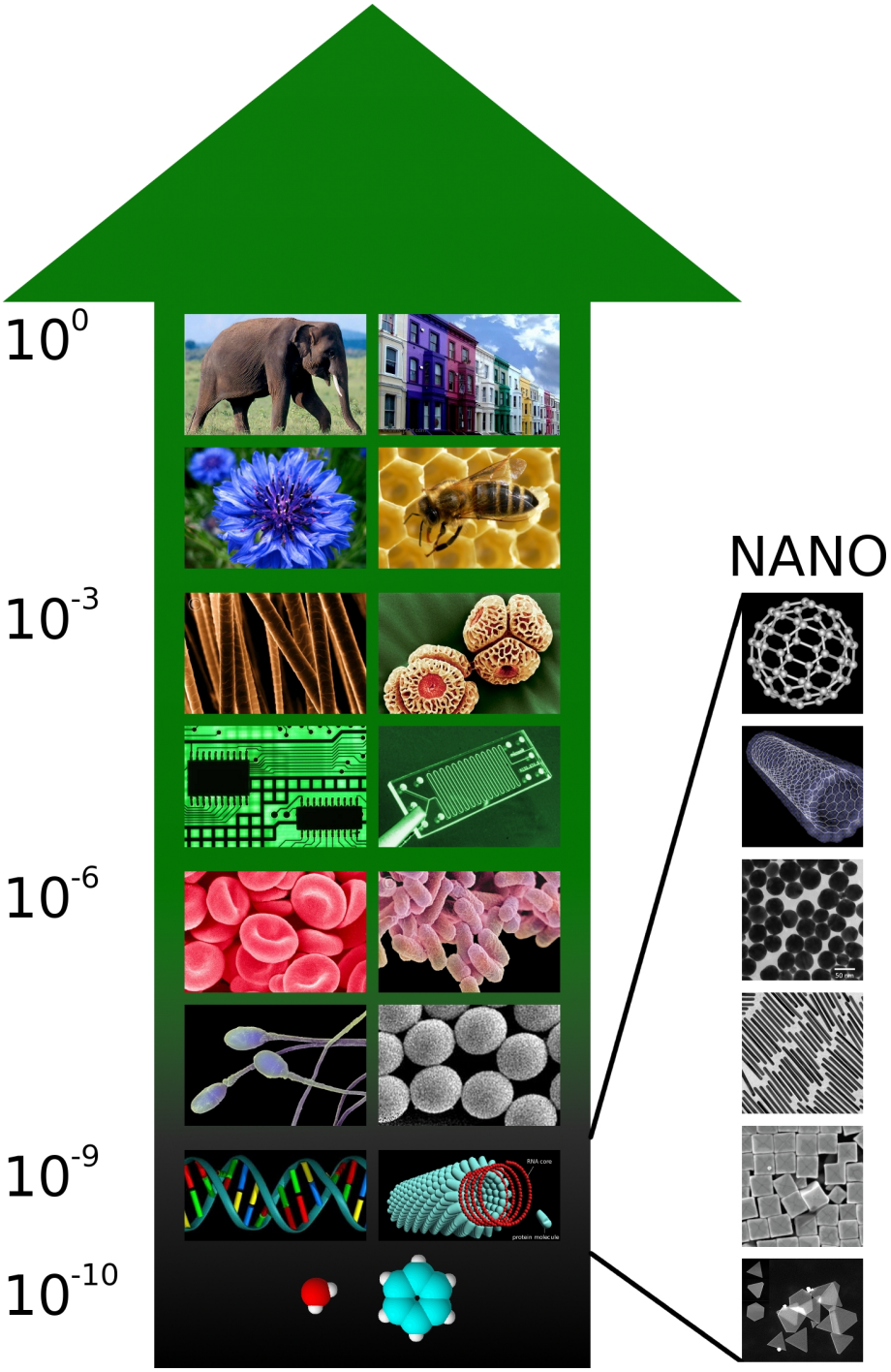

Figure 1: Different size scales - a comparison of nanomaterials with different objects of a size from meters to angstoms, formed by human or by nature. Meter-size is represented by animals, buildings, plants and insects. Milimeter-size is depicted by the size of hair, pollens, microchips and microfluidic systems. Micrometer-size objects are particularized by cells, bacteria, sperm and polymer microspheres. Nanometer-size objects are represented by DNA as well as TMV virus and angstrom-sized objects - by simple molecules like water or benzene. The examples of synthetic nanomaterials are fullerenes, carbon nanotubes, metal NPs, nanorods, nanocubes and nanoplates. Sources of images contained in this figure are collected on page 170.

1.1.1 Selected properties at the nanoscale

As shown in Figure 1, the sizes of nano-materials are intermediate between the typical size of atoms (simple molecules) and size of microscopic objects. This fact accounts for unique properties of nanomaterials, which are presented in this Section.

I. Size and the number of atoms

What does the nano-size mean in practice? In the case of NP that has nano-size in all of its dimensions, nanometer size means that the particle consists of a few to several thousands of atoms. For example, the atomic radius of gold is 0.135 nm[3]. This means that ten gold atoms arranged in a row give the total length of 2.7 nm. NPs are usually represented as spheres, but in reality, they can be well described by polyhedrons. The smallest ideal NPs, called clusters, consist of a strictly limited number of atoms arranged in shells. These defined number of atoms are called magic numbers. The relationship between the number of shells (L) and the number of atoms (N) in NP is described by the Equation (1)[4]. Geometric solution of the Equation (1) with indicated number of atoms and number of shells is shown in Figure 2.

$$N = \frac{10L^3 + 15L^2 + 11L + 3}{3} \tag{1}$$

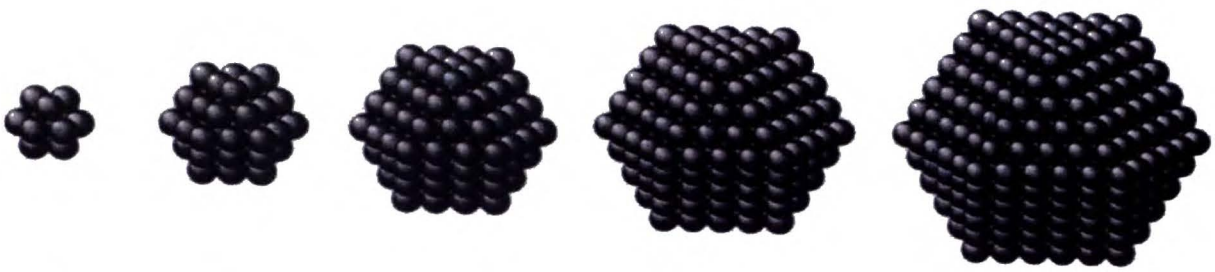

Figure 2: Metal nanocrystals in closed-shell configuration with magic number of atoms.[5]

Perfect clusters exist not only in theory but are also isolated and characterized in practice[6–9]. Synthesis of such small structures with ideal geometry often requires a very sophisticated methods or experimental conditions. The geometry of typical NPs sometimes deviates from ideality, but it does not affect the size-dependent properties of these particles.

Clearly visible thing that makes nanomaterials differ from their bulk counterparts is the number of atoms on the surface with respect to volume. Surface atoms are different from those in the volume, even if we consider the same material. The reason for this difference is the number of neighboring atoms, the so-called coordination number. The number of neighboring atoms translates directly into surface energy of the atom, which in turn affects its reactivity. Atoms with higher coordination numbers have lower surface energy and are, therefore, less reactive. Inner atoms are surrounded on all sides by other atoms, which causes that they are stabilized by their presence. Atoms on the surface, and, especially, at the edges or corners are surrounded by smaller numbers of atoms, are less stabilized, and as a result have greater surface energy.[10] Graphical illustration of the differences in coordination number on the example of small crystal with simple cubic lattice is shown in Figure 3.

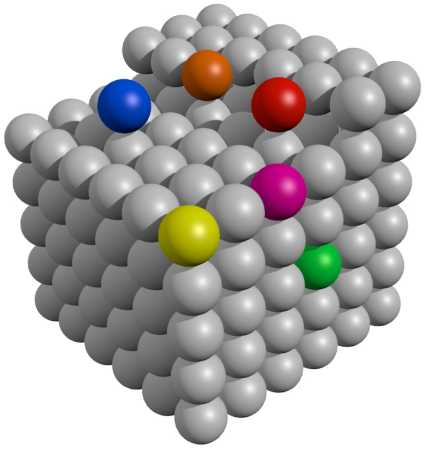

Figure 3: Schematic representation of different coordination numbers for small crystal with simple cubic unit. The numbers of neighbours are: 6 (not indicated) for bulk atom, 5 (green) for surface atom, 4 (violet) for edge atom, 3 (yellow) for corner atom and (orange) kink atom, 2 (red) for atom adsorbed on a step, and 1 (blue) for atom adsorbed on the surface.

In the case of a cubic crystal, each internal atom is surrounded by six other atoms. It has the largest number of neighbors, which makes it the best-stabilized (it has the lowest surface energy). An atom that is located on the crystal surface (green) has slightly smaller number of neighbors (slightly higher energy). Edge (violet), corner (yellow) or kink (orange) atoms have even higher energies by the fact that they are less stabilized. Atom that is adsorbed on the surface (blue) has only one neighbor atom and as a result it is the less stable (has the highest energy). Such adsorbed atoms are the most reactive in the whole crystal. Lower stabilisation and higher energy is the reason for some specific properties of surface atoms like lower melting

temperature or greater reactivity (including catalytic activity). The number of surface atoms in respect to all atoms in the object is commonly described by the surface-to-volume ratio[10].

Let's consider spherical crystal of radius, r, consisting of N atoms with atomic radius r_a. In this case, the total number of atoms

$$\mathrm{N} = \frac{\frac{4}{3}\pi r^3}{\frac{4}{3}\pi r_a^3} = \left(\frac{r}{r_a}\right)^3 \tag{2}$$

and the number of atoms on the surface of the crystal, $\mathrm{N_s}$ is equal to

$$\mathrm{N_s} = \frac{4\pi r^2}{4\pi r_a^2} = 4\left(\frac{r}{r_a}\right)^2 \tag{3}$$

Taking Equations (2) and (3) together, the percentage, $\mathrm{P_s}$, of atoms on the surface with respect to total number of atoms,

$$\mathrm{P_s} = \frac{\mathrm{N_s}}{\mathrm{N}} \times 100\% = \frac{4\left(\frac{\mathrm{r}}{\mathrm{r_a}}\right)^2}{\left(\frac{\mathrm{r}}{\mathrm{r_a}}\right)^3} \times 100\% = 4\left(\frac{\mathrm{r}}{\mathrm{r_a}}\right)^{-1} \times 100\% \tag{4}$$

which finally gives:

$$\mathrm{P_s} = 4\mathrm{N}^{-\frac{1}{3}} \times 100\% \tag{5}$$

The geometrical interpretation of Equation (5) is shown in Figure 4.

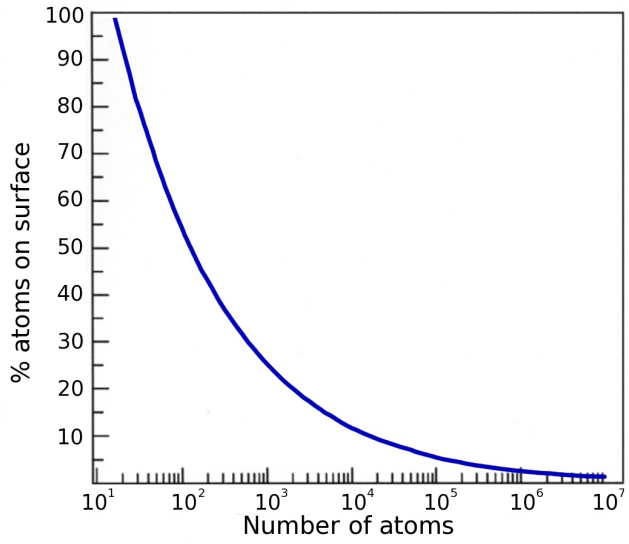

Figure 4: Evolution of the fraction of the surface atoms as a function of total number of atoms in the particle.[4] The calculation is based on Equation (5).

According to Equation (5), the percentage of surface atoms is proportional to the cube root of the total number of atoms in crystal. This means that for very small particles (consisting of several atoms) exactly or nearly 100% of the atoms is located on the surface. As the number of atoms in the cluster increases, the fraction of surface atoms decreases. When the number of atoms is in the order of 10^7, the fraction of atoms on the surface is lower than 1%. In practice, 10^7 of atoms correspond to a crystal size of 150 nm.[4]

As already mentioned, the surface atoms are more reactive than those in bulk. This fact is widely used in catalysis[11,12], in which the developed surface area is highly desirable. Nanomaterials fulfill this condition, therefore they are used as catalysts for various reactions. The application of nanomaterials in catalysis is discussed in Section 1.1.4.

II. Shapes and composition of the nanocrystals

Nanomaterials are limited by size, but are not limited in shape. The most common nanomaterials are spherical NPs. However, these are not the only possible and the observed shapes of nano-objects. Among non-spherical NPs, one can find: nanorods, nanowires, nanoplates, nanocubes, nanotetrapods, and others. TEM images of nanomaterials with different shapes are presented in Figure 5.

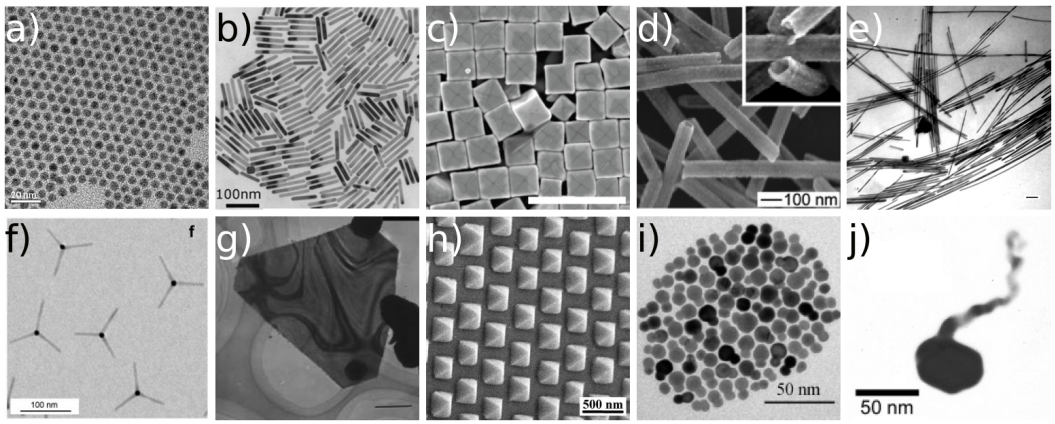

Figure 5: Selected nanomaterials with different shapes: (a) Au NPs[13], (b) Au nanorods[14], (c) Au nanocubes[15], (d) Pd/Ag nanotubes[16], (e) Ag nanowires[17], (f) CdSe/CdS nanotetrapods[18], (g) Au triangular nanoplate[19], (h) nanopyramids[20], (i) $CoPt_3$/Au nanodumbells[21] and (j) Au nanotadpole[22]

Nanomaterials can be made of different starting materials. The most popular are nanoobjects composed of one type of material - for example, metal NPs (Au, Ag, Pt, Fe, Co, Cd). Some nanomaterials are composed of more than one type of atoms, for example, semiconductor CdSe NPs or magnetic Fe_2O_3 NPs. In the case of nanomaterials composed of more than one type of atom, there are two basic ways of arrangement of atoms within the material. In the first, the atoms are uniformly distributed inside the material (like zinc and oxygen atoms in ZnO NP). In the second, the atoms of different elements are found only in strictly defined areas of the material (e.g. gold and silver atoms in Au (core)/Ag (shell) NP). In the case of core/shell NPs atoms of one type are located within the inner sphere (core) while others form the outer layer (shell) of the particle. In this dissertation, I deal with spherical metal NPs (gold and silver) and spherical semiconductor core/shell NPs (CdSe/ZnS).

III. Optical properties of nanomaterials

Due to the basics of quantum mechanics, every particle is associated with its own matter wave. The wavelength of this matter wave, λ, known as de Broglie wavelength, is described by the Equation (6) in which h is the Planck's constant and p is the momentum of the particle.

$$\lambda = \frac{h}{p} \tag{6}$$

When the size of the object is within the nanoscale, the de Broglie wavelength is comparable to its size. In such a case, the properties of the object begin to be dominated by the rules of quantum mechanics. This is what makes the properties of nano-objects intermediate between the properties of individual atoms and of bulk materials[23]. To illustrate the existence of intermediate properties of nanomaterials, let us consider the evolution of the density of electronic states with increasing size of the object. Each electron in an atom is ascribed to its own atomic orbital of a discrete energy level. When we combine atoms to form a molecule, atomic orbitals are mixed and form molecular orbitals. Those orbitals have also discrete energy levels. In bulk materials consisting of huge number of atoms and as a result huge number of electrons, the electronic structure is completely different. In this case the electrons are described as a superposition of plane waves that are extended through the whole material. The resulting electronic structure of a bulk material does not exhibit discrete energy levels but broad energy bands.

The electronic structure of a nanomaterials is intermediate between that of atoms or molecules

and that of bulk solid. As in case of atoms and molecules the energy levels of nanocrystal are discrete. There are, however, some differences. The density of energy levels is much larger and the spacing between them is much smaller than in case of atoms or molecules. On the other hand, the electronic structure of nanomaterials is similar to that observed for bulk materials. Energy levels of nano-materials are also grouped into bands separated by energy gap. The difference is that the spacing between energy levels in the bands are much larger than in bulk materials. In nanomaterials, band structure is discrete rather than continuous[23]. As the size of the nanoobject increases, the spaces between the energy levels decrease. For this reason even small changes in the size result in significant changes of the electronic structure.

The electronic structure of nanomaterials and its changes with size gives rise to the size-dependent absorption and fluorescence of **semiconductor quantum dots**[24]. As shown in the Figure 6, maxima of absorption and fluorescence spectra of semiconductor QDs are moving towards longer wavelengths while increasing the size of the nanocrystals. This phenomenon is extremely sensitive to changes in particle size. As shown in the Figure 6, the resize of the

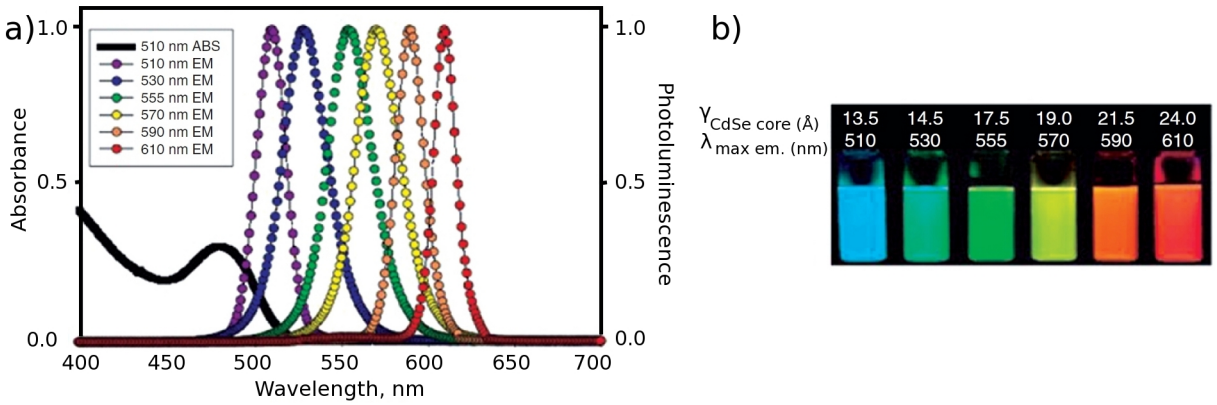

Figure 6: (a) Absorption and emission spectra of six different CdSe/ZnS core/shell QD dispersion and (b) photograph demonstrating the size-dependent fluorescence of QD dispersions.[24] As the size of the CsSe core increases from 1.35 nm to 2.4 nm, the color of emitted light changes from blue to red.

core of 1.05 nm, result in 100 nm change in emission wavelength. The overall fluorescence of quantum dots is a result of two types of processes, that is, intrinsic states emission and surface states emission. Surface states are energy levels localized in the surface region of material[25]. The proportion between intrinsic and surface states emission depends on the composition of QD. It was recently shown[26] that the contribution of surface states emission is nearly 70% in case of CdSe core QDs. It was also shown that the pasivating of CdSe core with ZnS shell

results in drop of this contribution to about 30%.

Size-dependent changes in optical properties are observed not only in the case of semiconductor QDs, but also in metal nanocrystals. Colloidal solutions of metal NPs also exhibit strong absorption of visible light (see Figure 7) . Location of maximum of absorption also changes (shift toward longer wavelengths) with increasing size of the NPs. This shift, however, is much smaller than in the case of semiconductor NPs. As shown in Figure 7, sizing NPs from 30 to 100 nm (i.e. 70 nm) changes the position of absorption maximum of about 50 nm.

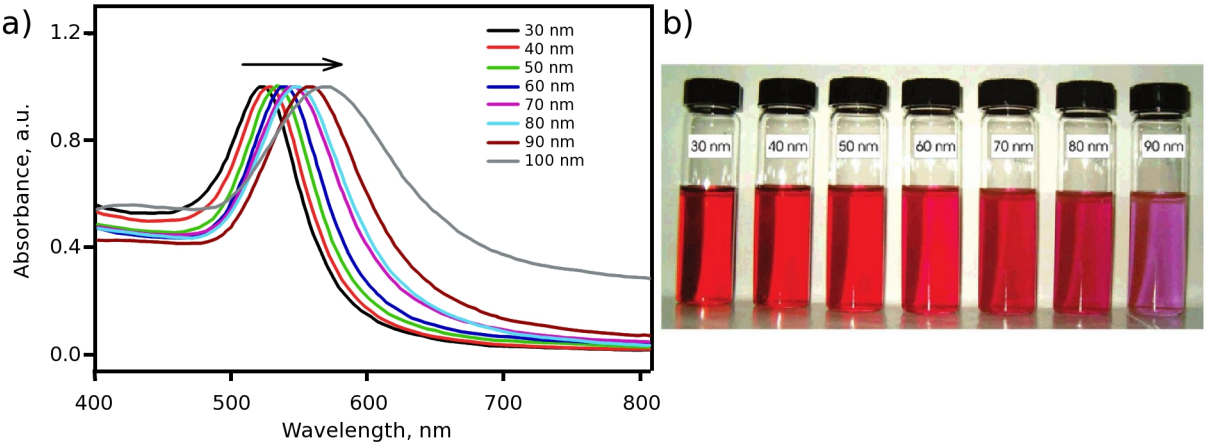

Figure 7: (a) The absorption spectra of Au NPs of a different size. The arrow indicates the direction of shifting the position of the absorption maximum with increasing size of the NPs. (b) The pictures of corresponding NPs solutions[27].

Although the change in optical properties is evident both in the case of semiconductor and metal NPs, the origin of this phenomenon in both cases is different. As it was discussed, the absorption and the emission spectra of semiconductor nanocrystals are a consequence of transitions between quantized energy states. However, the shape of the absorption spectra of metallic NPs (and other metal nanostructures of a dimension smaller than the wavelength of an exciting light) result from collective oscillation of electron density at the surface. This phenomenon is known as **surface plasmon resonance, SPR**[28,29] and it is shown schematically in Figure 8.

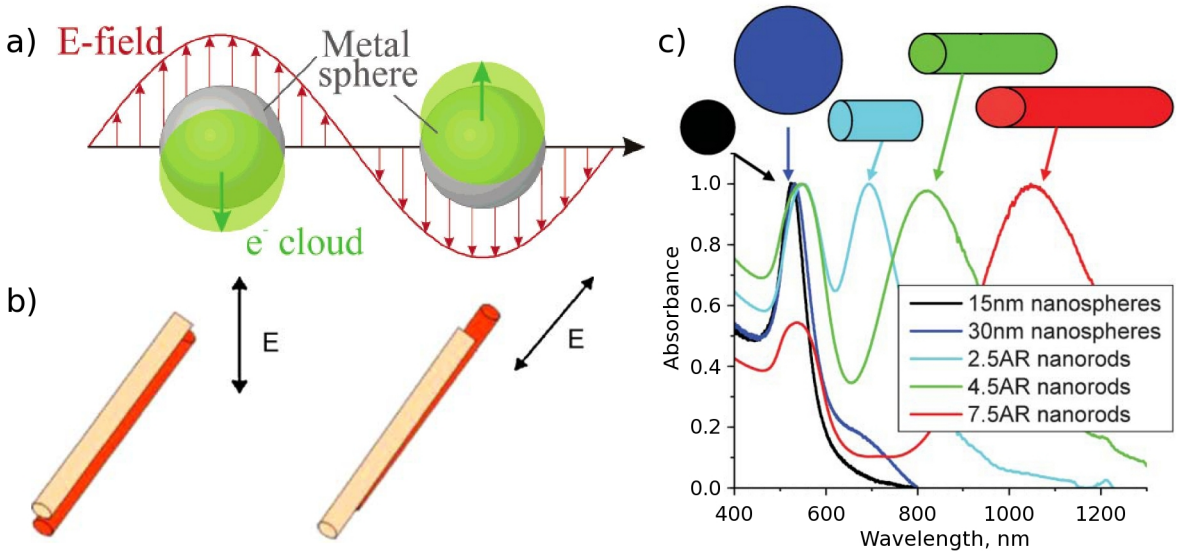

Figure 8: The scheme of surface plasmon resonance - collective oscillations of electron density at the surface of small metal particles: (a) spherical particle[30], (b) rod-like particle[31]. (c) Surface plasmon absorption of gold nanocrystals differing in shape and size (AR refers to aspect ratio, that is the proportion between length and width of nanorod) .[29]

The position of the maxima of absorption (and observed color of the sample) reflects the frequency of electron oscillations. It depends on the type of metal (usually gold, silver or platinum), size, size distribution and on the surrounding medium[30]. Surface plasmon absorption is also very sensitive to the shape of the nanostructure, for example: spherical particles have one absorption band whereas nanorods have two bans corresponding to the electron oscillations perpendicular and along the major axis of the nanorod (transverse and longitudinal band respectively).[32] As it was mentioned, in the case of spherical NPs, the maximum of absorption shifts towards longer wavelengths as the size of particles increases. Similarly, in the case of nanorods, the maxima of absorption corresponding to transverse and longitudinal modes shift toward longer wavelengths as the nanorod increases in its size and length, respectively. The first (and still current) explanation of the optical properties of colloidal solutions of gold, and other solutions containing spherical NPs of metal, was proposed by the German physicist Gustav Mie in 1908. In his work[33,34], he explained the shift of the absorption maximum with increasing size of NPs by solving Maxwell's equations. He stated that, in general, the absorption of spherical gold solutions is a result two properties of the metallic gold: the absorptivity and the reflectivity. The color of the colloidal gold solution is a result of balance between these two properties.

1.1.2 Nanoparticle synthesis and modification of their surface

As illustrated schematically in Figure 9, there are, in general, two types of approaches to the synthesis of nanomaterials: *top-down* and *bottom-up*. The *top-down* approach refers to the physical techniques and procedures in which nanomaterials are formed from bigger, bulk structures by the reduction of their size. The examples are grinding[35], etching[36] or litography[37]. The *bottom-up* strategy relates to the methods in which nanomaterials are produced directly from atoms or molecules. The most common example is the wet chemical synthesis of nanocrystals[38–42], that is the synthesis of nanomaterials from simple organic/inorganic compounds in liquid medium. Selected examples of chemical synthesis of nanomaterials are discussed further. In this dissertation NPs were prepared using bottom-up approach, as is is described in details in Section 2.2.1.

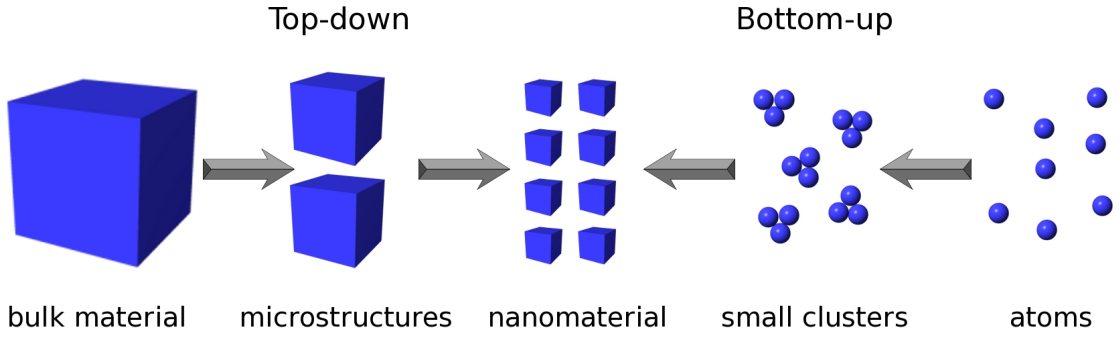

Figure 9: Two approaches to the synthesis of nanomaterials: from left – top-down approach, from right – bottom-up approach.

Although the bottom-up approach is nothing new in chemistry (colloidal chemistry has been practiced for centuries), the interest in this method of preparation of nanomaterials is still large. This interest is reflected by the number of publications and books on this subject. In particular, according to "Web of Knowledge" database the number of publications on nano synthesis exceeds 9 000 results. Among those publications one can easily found the description of chemical synthesis of nanomaterials of different shapes (e.g. spherical NPs[40,43], nanorods[14,31]), composition (e.g. Au[13,39,40,42], Ag[13,40,44], Pt[40,45,46], Co[47]), size[48,49], and size distribution[40,49].

Even for spherical gold NPs there are many possible synthetic routes[43,50,51]. There are also several ways of classification of these methods. One of them is the distinction between single-phase and biphase methods. In the case of the single-phase methods, all chemical reactions leading to the formation of NPs take place in one and the same phase. This phase can be

aqueous (like in case of so called "citrate reduction" introduced by Turkevich[38]) or organic (like in the method described by Jana and Peng[40] – the one used in this dissertation). In the biphase method, the synthesis of NPs is carried out in two-phase system (consisting of polar and nonpolar phase). In this case some processes occur in polar phase (e. g. dissolution of the metallic precursor) and the rest (e. g. reduction of the precursor and stabilization of NPs) in the nonpolar phase. Biphase methods require the use of phase-transfer reagent, which enables the transfer of appropriate reagents through the phase boundary. An example of biphase method is the Brust-Shriffin method[39]. The desired size of NP is obtained either in one[39,41] or in two-step[40,42,49] (so called "seeded-growth") procedure, the last of which was used in this dissertation. One can also find more sophisticated methods of Au NPs synthesis conducted in surfactant matrices[52–56] (micelles or ordered phase), microemulsions[57] and the methods involving physical processes like thermolysis[58] or laser ablation[59].

A common feature of wet chemical synthesis of metal NPs is the reduction of precursor metal compound to the form of atoms and subsequent self-assembly of those metal atoms to the form of smaller or bigger clusters. Typical precursors in the synthesis of gold NPs are $AuCl_3$[40], $HAuCl_4$[38,39,60,61] and $AuCl(PPh_3)$[13]. The most popular reducing compounds used in the synthesis of gold NPs include $NaBH_4$[39,61], hydrazine[40], tetrabuthylammonium borohydride[40], tetraoctylammonium bromide[39] and acetic acid[61]. In the case of two-step reactions (like the one used in this dissertation), two different reducing agents are used. The first reducer (stronger one, for example tetrabutyl ammonium borohydride) is used to reduce the precursor to the form of small NPs called "seeds". Second reducing agent (weaker one, e.g. hydrazine) is used to induce growth of small NPs into bigger once. The activity of the reducing agent used in growth step is typically too weak to reduce metal ions without presence of nucleation centers (seeds)[49]. The use of two reducing agents of different reducing activity allows for synthesis of large NPs with low size distribution[49].

Due to the very high surface energy, nanomaterials are metastable state of matter, and they tend to aggregate without appropriate protection. To ensure the stability of NPs and protect them against the aggregation, the synthesis is typically conducted in the presence of compounds that form protecting shell. The type of capping substance depend on the material of nanocrystal and its further application. In case of gold colloids the most popular coating ligands are sulfur-containing organic compounds like thiols[39] or disulfides[62]. This is due to the

high affinity of sulfur to gold. Other types of ligands used to protect NPs against aggregation include amines[40] and phosphines[63]. Absorbed ligands form a monolayer at the surface of nanocrystal. The molecules in this layer are ordered which causes that they are often called self-assembled monolayers (SAMs). Nanocrystals stabilized with coating layer are commonly known as monolayer protected clusters. The scheme of self-assembled monolayer formed by thiols on a gold surface together with the anatomy and characteristics of the layer is shown in Figure 10b.

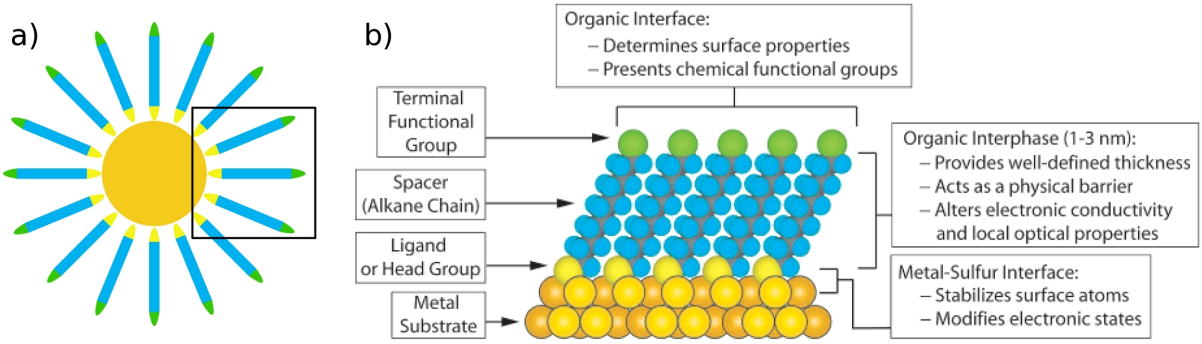

Figure 10: (a) Scheme of a NP coated with protecting layer of thiols. (b) Scheme of ideal self-assembled monolayer (SAM) of alkanethiolates supported on a structure of gold NPs.[64]

As it was mentioned, the primary role of capping agents is to ensure the stability of nanocrystals. It is however not the only one. The second one is to provide desired properties like hydrophilicity, hydrophobicity, the presence of defined charge or biocompatibility. This cause that the chemistry of coating ligands is very rich and sophisticated. There are three approaches to introduce desired functional group on the NP, as it is shown schematically in Figure 11. The first one is the synthesis of NPs in the presence of proper stabilizing ligand[39] (Figure 11a). The second one involves the synthesis of NPs coated with intermediate ligand and then modify the ligand during subsequent reactions[65,66] (Figure 11b). The third approach is to synthesize NPs with stabilizing ligand of a one type and than replace it with another one during, so called, ligand exchange reaction[40,67] (Figure 11c). The original ligand may be replaced completely or partly. This depends on many factors including the affinity of ligands head group to the NP surface, chain length of ligands and their steric bulkiness[65,66,68] . In particular, in case of gold NPs, amines are replaced totally by thiols due to higher affinity of sulfur to gold[69].

In this dissertation, as a final product, I used thiol-coated metal NPs. The desired coverage was obtained using the ligand exchange approach, (cf. Figure 11c) using amines as intermediate stabilizing ligands. The exact procedures of NP synthesis and their surface modification employed are described in Section 2.2.1.

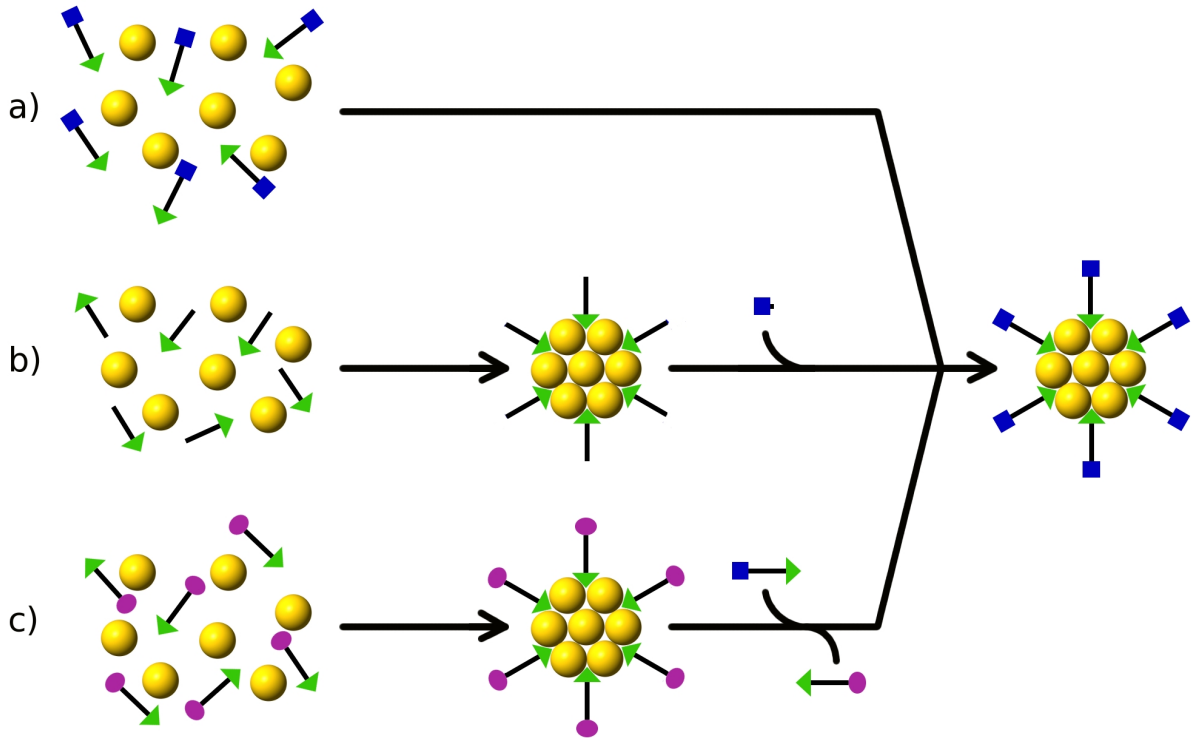

Figure 11: Three ways to achieve proper coverage of the NP: (a) direct synthesis using the appropriate ligand, (b) modification of the ligands on the NP surface and (c) ligand exchange reaction.

1.1.3 Self-assembly of nanomaterials

One of the main tasks of nanotechnology is the use of nano-objects to create more complex structures. Apart from special cases such as the movement of atoms with scanning tunneling microscope[70], it is extremely difficult to manipulate individual atoms or nanoobjects, so that they form a specific pattern or structure. The easiest way to attain this objective is to involve the forces of nature (laws of chemistry and physics) to do the job. This approach, often referred to as the self-assembly, is used both for creating nanoobjects of a certain size and shape (as outlined in the previous Section) and to create higher hierarchical structures using nano-objects as building blocks. Self-assembly is also the method used in this dissertation to synthesize NPs (compare Section 2.2), and to fabricate "nanostructured" materials (see Sections 3.2 and 3.3). Some examples of self-assembled nanomaterials are shown in Figure 12.

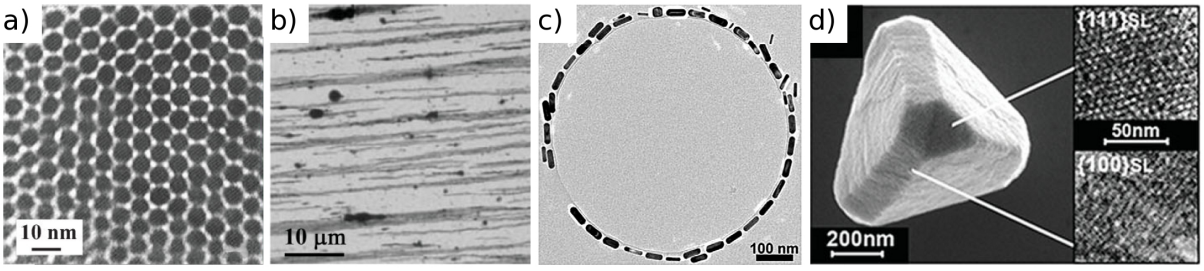

Figure 12: The examples of nanomaterials assemblies: a) Ag NPs assembled into two-dimensional hexagonal close packed structure[71], b) magnetic γ-Fe_2O_3 NPs assembled into nanowires upon magnetic field[72], c) gold nanorods assembled into ring (end-to-end fashion) during solvent (CH_2Cl_2) evaporation[73], d) oppositely charged NPs assembled into diamond-like (ZnS) crystals with truncated tetrahedron morphologies[67].

Self-assembly is defined as “autonomous organization of components into patterns or structures without human intervention”[74,75]. It can be driven either by direct intermolecular interactions (hydrogen bonds, hydrophobic interactions, van der Waals interaction, electrostatic interaction or molecular recognition reactions), by using external fields/forces[76] (magnetic, electric or flow field) or templates. In the last case, the term template refers to any surface-modified object containing active sites suitable for selective NP deposition[77]. The examples of commonly used templates are surfactants and polymers[78].

Self-assembly is commonly divided into dynamic and static[74]. The distinction between these two types is associated with energy dissipation. In the case of *dynamic self-assembly*,

the interaction responsible for the creation of structures or patterns appear only if the system dissipates energy[74,79]. The structure formed via this type of self-assembly evolves depending on the amount of energy supplied to- and dispersed from the system[79]. Most examples of dynamic self-assembly can be derived from nature, e.g. bacterial colony growth, mitosis in eukaryotic cells, reaction-diffusion waves in Belousov-Zabotynski reaction or Rayleigh-Bénard convection cells. Given the fact that nature is a source of inspiration for nanotechnology, the interest in dynamic self-assembly is growing, although it is a challenge for researchers. There are several works devoted to the foundations of a dynamic self-assembly[79] however, in general, the process is poorly understood.

As the design and control over dynamic self-assembled structures is a difficult task, most of research is focused on the second type of self-assembly, that is, on *static self-assembly*. In this case, the system is in global or local equilibrium and it does not dissipate energy. The structure formed via this type of self-assembly is fixed which means that once it is formed it does not change under the influence of external conditions.[79] For this reason, most examples of static self-assembly structures include crystals (atomic, ionic or molecular). Another example are complex structures formed by thermo- or lyotropic liquid crystals (which are discussed in Section 1.2.3), block copolymer assemblies or molecular sieves. Static self-assembly is also represented by self-assembled monolayers and various equilibrium structures composed of nanomaterials.

In this dissertation, I used the static self-assembly in several variants. Firstly, to create NPs and coat them with protecting, self-assembled monolayers (see Section 2.2). Secondly, to obtain various ordered structures of surfactants (see Section 3.1). Finally, to form diverse soft and solid nanocomposites (see Section 3.2).

1.1.4 Applications of nanoparticles

Despite the fact that nanotechnology is a relatively young field of science, nanomaterials are already used in many branches of both the science and technology. Furthermore, new, promising applications of nanomaterials still come to light. To narrow the considerations of this Section, I selected only some of the most important applications of nanomaterials, with special emphasis on the use of spherical NPs.

I. Catalysis.

One of the basic application of nanomaterials, especially metal NPs , relates to catalysis[11,12]. Despite the fact that some metals, like gold, do not exhibit catalytic activity in bulk, they are good catalysts when their size is reduced to the nanoscale. This results from the increase of the percentage of surface atoms, discussed in Section 1.1.1. The examples of chemical reactions that are catalysed by gold NPs include: CO[80,81] and CH_3OH[82] oxidation, O_2 reduction[83,84] and hydrogenation of unsaturated compounds[85]. Limiting factor of the catalytic activity is the development of the surface. For this reason, to get the best performance of the NP-containing catalyst, NPs must be well-separated. This goal is achieved by the use of specific supports on which NPs are deposited. The examples of such supports are oxides (Co_3O_4, Fe_2O_3, TiO_2)[86] and mesoporous silica[87]. Catalysts containing NPs are prepared in various ways including precipitation of NP on the substrate, chemical vapor deposition[88], pulsed laser deposition[89] or direct growth of nanostructures in/on the support[90].

II. Biology and medicine.

Another area of application of nanomaterials refers to biology and medicine[91–95]. This follows from two simple facts. First, the size of the NPs is smaller than the size of the cells. In fact, NPs are comparable (in the terms of size) with cell components. Second, NPs can be easily functionalized with biomolecules such as proteins or DNA. This causes that nanomaterials can be easily introduced to various locations within the cell. NPs can be used for example: as drug-delivery agents[96], in the phototermal therapy of cancer[97] or to detect specific nucleotides[98]. Recently, the group of Opałło shown that film electrodes prepared by layer-by-layer assembly of oppositely charged NPs (gold/carbon[99], carbon/carbon[100], silicate/carbon[101]) can be used for selective detection of biologically important molecules, such dopamine[101]. Semiconductor

NPs are often used as fluorescent markers to visualize specific areas within the cell.[24,91,102,103] In this field, semiconductor NPs have many advantages compared to existing, traditional markers.[104] First of all, they have greater photostability what causes that observed samples do not fade under the influence of long continuous illumination. Additionally, multicolor images can be obtained simpler – by a single wavelength excitation of cells tagged with NPs of different size.

III. Optical applications

Wide branch of NPs applications is related to their optical properties, discussed in Section 1.1.1. Optical application of NPs are different in case of metal and semiconductor NPs. In case of metal NPs, the applications relates mainly to surface plasmon absorption. An example is optical detection of various molecules based on the changes of absorption spectra of NPs in solution[105,106]. Another example of optical application of metal NPs are surface-enhanced Raman scattering (SERS) substrates[107] that can be used to detect molecules adsorbed on the surface. Metal NPs are also proposed to be useful as components of nonlinear optical devices[108]. In the case of semiconductor nanocrystals, the optical applications are based on specific electronic structure. A lot of works relate to the use of QDs in electroluminescent devices such as light emitting diodes[109–111], solar cells[112–116] or lasers[117].

IV. Other applications

In addition to catalytic, bio-inspired and optical applications, nanomaterials find their place in various fields of science and technology. First of all they are used as doping materials to improve the mechanical properties of materials[118]. Nanomaterials are used as components of textiles, for example in water-[119] and oil-resistant[120] clothes or in antibacterial fabrics[121]. They are also used as components of cosmetics, in particular ZnO and TiO particles are used to provide UV protection.

At present, it seems that the future of NPs lies in the field of smart materials that are capable to self-organize or take specific functions in response to external conditions. Such materials should lead to the development of a new generation of electronic devices, especially computers.

1.2 Complex fluids

In the previous Section (1.1) I discussed various aspects of nanomaterials and reviewed the use of NPs in selected branches of science and technology. Note that in practical applications, NPs are mainly used as modifiers (for example as cosmetic ingredients or as the catalytic centers in the catalysts). In such cases, they are not alone but in company of other materials. In particular, NPs occur together with complex fluids, which are the subject of discussion in this Section.

The notion of a complex fluid can be explained by reference to a simple fluid. Simple fluids are those that do not posses any internal structure. They are homogeneous at the molecular level. Examples are pure solvents or typical solutions (what we intuitively understand under the concept of solution). Complex fluids are those that have internal structure and are heterogeneous at the molecular level. Examples include micellar solutions of surfactants and solutions of polymers (polymer networks). Quite often, the structure of complex fluids is periodic. This periodicity occurs, for example, in ordered phases of surfactants and of liquid crystals. Selected examples of complex fluids are schematically shown in Figure 13.

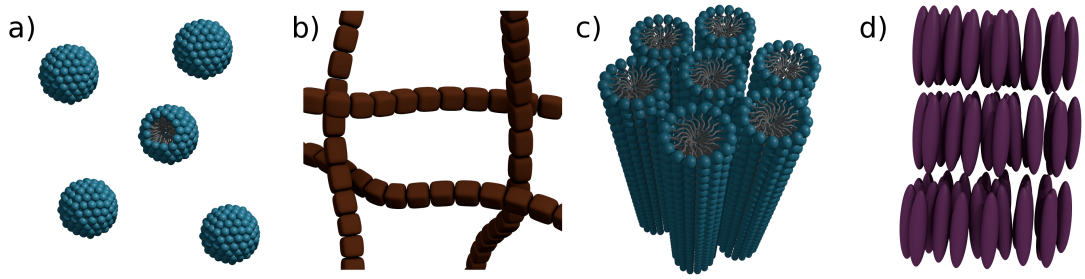

Figure 13: Schematic representation of selected examples of complex fluids: (a) micellar solution of surfactant, (b) a polymer network, (c) the hexagonal phase of surfactant, (d) smectic-A phase formed by rod-like liquid crystal.

This Section provides the description of the main properties of surfactants and polymers - complex fluids used in this dissertation. Section 1.2.1 defines the concept of surfactant and presents the main division of these substances. Sections 1.2.2 and 1.2.3 describe phase behavior of surfactants: gathering at interfaces, micellization and formation of ordered phases. Sections 1.2.4 and 1.2.5 discuss basic concepts of polymers and polyelectrolytes. Section 1.2.6 deals with a variety of interactions between surfactants and polymers. The last Section (1.2.7) reviews the use of surfactants to create mesoporous silica.

1.2.1 Surfactants

The term surfactant stands for *surface active agent*. It describes substances that act on the surface and decrease surface tension or interface tension (by adsorbing at air/liquid or liquid/liquid interface)[25]. Surfactants are the specific group of organic compounds that are **amphiphilic**. It means that every surfactant consist of two basic parts: one that is soluble in a given fluid (lyophilic) and the second that is insoluble in this fluid (lyophobic). When water is used as solvent, then we say about hydrophilic and hydrophobic part, respectively. Schematic representation of surfactant molecule is shown in Figure 14.

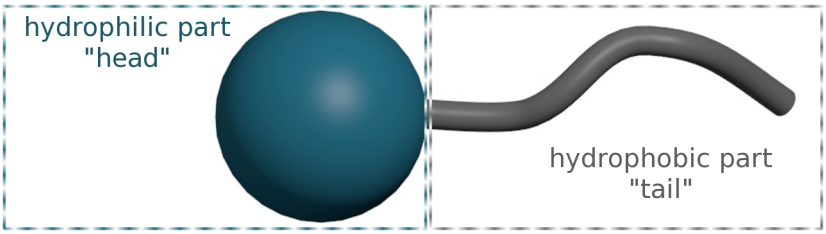

Figure 14: Schematic representation of surfactant molecule. Hydrophilic unit (head) is shown in blue and hydrophobic unit (tail) is shown in grey.

Typical amphiphile molecule consists of one hydrophilic ("head") and one hydrophobic ("tail") part. The polar part of the surfactant can be ionic (like sulfate) or nonionic group (like polyoxyethylene chain), and the character of this unit determines most of the properties of the amphiphile. Hydrophobic unit is usually linear or branched hydrocarbon chain of a length 8 – 18 carbon atoms[122]. As it was mentioned, typically, one hydrophilic head is connected to one hydrophobic tail. There are, however, some exceptions such as molecules containing more hydrophobic units. There is also a specific group - gemini surfactants - that consist of two identical, twin, molecules whose hydrophilic units are connected with few carbon atoms spacer[122].

I. Classification of surfactants

The nature of the hydrophilic part is diverse and therefore it is used as the main criteria of surfactants' classification. In general, we can distinguish three main groups of surfactants: ionic (anionic, cationic), nonionic and zwitterionic. Classification of surfactants with respect to the nature of the hydrophilic group is shown in Figure 15. Individual groups of surfactants are discussed below.

The ionic class of surfactants is the largest one. It divides into anionic and cationic subclass with respect to the charge of the polar group. In **anionic surfactants**, the hydrophilic unit is negatively charged. It can be realized by few types of groups, from which the most common are: carboxylate, sulfate, sulfonate and phosphate. The counterions used are typically sodium, potassium, ammonium, calcium, magnesium and various protonated alkyl amines. Anionics are the most popular of all types of surfactants (especially in the detergents formulation) what is caused by the simplicity and low cost of their manufacture. The most common example of anionic surfactant is sodium dodecyl sulfate, SDS, consisting of negatively charged sulfate group attached to 12-carbon linear alkyl chain. SDS is a component of a wide range of industrial products such as engine degreasers, floor cleaners and car wash soaps. It is also used in cosmetics like toothpastes, shampoos, shower-gels and shaving foams[122,123].

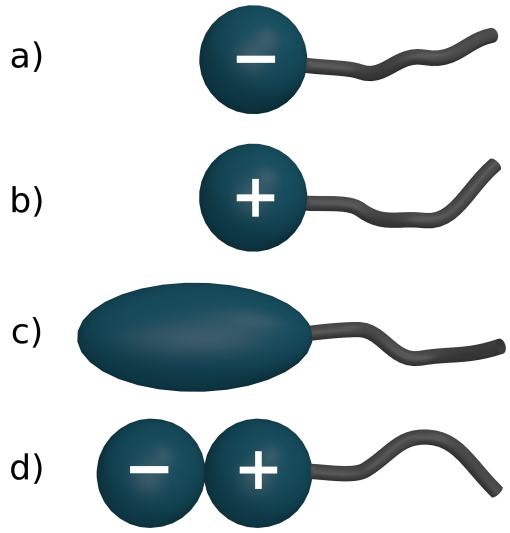

Figure 15: Classification of the surfactants due to the charge of the polar head. Ionic surfactants may have either negative charge - anionic (a) or positive charge - cationic (b). Nonionic surfactants (c) do not have any charge, and zwitterionic have two subunits with both negative and positive charge.

In the case of **cationic surfactants**, the polar group carries the positive charge. It is mainly realized by introducing of nitrogen atom in the form of amine or quaternary ammonium salt. Due to the positive charge, cationics adsorb strongly on negatively charged surfaces like metals, minerals, plastics or fibers. Therefore, most of their applications (anti-corrosion agents, dispersants, antistatic agents, fabric softeners, hair conditioners) are related to their adsorption properties[122,124]. The example of the cationic surfactant is cetyltrimethylammonium bromide,

CTAB, in which the positive charge comes from ammonium group and the hydrophobic tail is a 16-carbon linear alkyl chain. CTAB and other cationic surfactants are widely used as stabilizers in synthesis of gold nanomaterials of a different shapes including spheres[40] and rods[17,125].

In **nonionic surfactants**, the polar group is usually polyether chain and rarely polyhydroxyl chain. Because of the polymeric character, the size of the hydrophilic unit may be varied nearly at will. In practice, it rarely consists of more than 10 subunits. The particularly important group of nonionic surfactants are the fatty alcohol ethoxylates (also known as polyoxyethylene glycol monoalkylethers). They are abbreviated to C_mE_n where m denotes the number of carbon atoms in the alkyl chain and n is the number of oxyethylene units in the polar head. C_mE_n surfactants are used in liquid and powder detergents as well as in various industrial applications[122,126].

In **zwitterionic surfactants** the polar group contain two charged subunits with opposite charge. The positively charged group is almost always ammonium group. The negatively charged group may vary, however the carboxylate is the most common. Zwitterionic surfactants are sometimes called amphoteric, however this two terms are not equal. Amphoteric surfactants also contain two subunits, however neither cationic nor anionic site is permanently charged. The net charge of the substance varies with pH. When the pH changes from low to high the net charge of amfoteric surfactant changes from cationic, through zwitterionic to anionic. As a result amfoteric surfactant has stable zwitterionic form only in a certain pH range[122,124].

In this dissertation I used selected ionic surfactants, both anionic and cationic, as well as $C_{12}E_n$ nonionic surfactants. All surfactants used are specified in Section 2.3.

1.2.2 The main properties of surfactants - gathering at interfaces and micellisation

The size and nature of both hydrophilic and hydrophobic part influences to some extent the properties of the surfactant. One of them is a tendency to gather at the interface. In case of air/water interface, surfactant molecules arrange themselves in such a way that hydrophilic parts stay in water whereas hydrophobic parts stay in the air to minimize their contact with water. Similarly, in case of oil/water interface hydrophilic heads stay in water phase while hydrophobic tails are directed into the oil phase, as it is shown in Figure 16a.

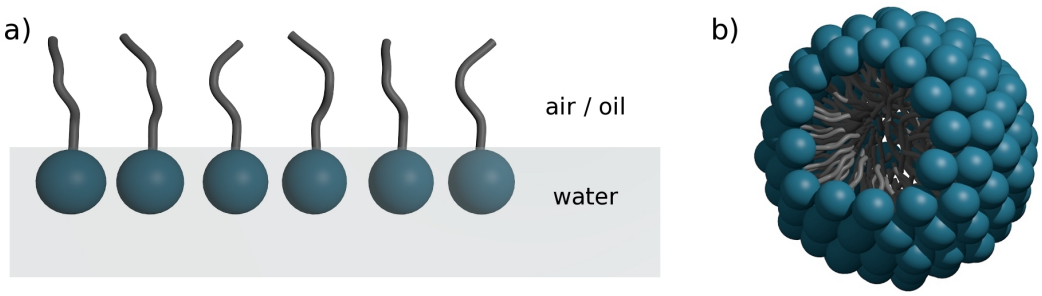

Figure 16: Schematic representation of (a) surfactant molecules at the air/water (or oil/water) interface (b) normal, spherical micelle.

In solution, surfactant molecules present another interesting property - self-assembling into bigger aggregates called micelles[127]. The core of the normal micelle is hydrophobic and it is composed of hydrophobic hydrocarbon chains. The surface of normal micelle is hydrophilic and it consists of polar units of surfactants. The shape of the micelle may be spherical or extended (ellipsoidal or rod-like) and it depends on the geometrical proportion between "head" and "tail" subunit[127,128]. For some surfactants, the shape of the micelle can vary with the concentration of surfactant in the solution. Schematic representation of a normal, spherical micelle is shown in Figure 16b.

Surfactants form micelles above certain concentration called *critical micelle concentration*, CMC. CMC is defined phenomenologically (for given temperature) as a point in which the number of surfactants's molecules associated into micelle increases sharply. Below CMC, the surfactant molecules are freely dispersed in the solution and the quality of such dispersion is defined by the solubility of the compound. Above CMC, micelles coexist with free unassociated molecules, called unimers. CMC depends strongly on the surfactant structure and other parameters like temperature, presence of salt or cosolutes[127,129]. The number of molecules that form the micelle may vary because of the fact that the micelles are in equilibrium with unimers.

The average number of surfactant molecules that form micelle is referred to as the *aggregation number*, N_{agg} [127,128].

1.2.3 Ordered phases formed by surfactants

As it was discussed in the previous Section (1.2.2), above CMC surfactant molecules bring together to form micelles. Usually, they are initially spherical and gradually elongate to the rod-like form. Further increase of surfactant concentration, leads to the arrangement of surfactant molecules into geometrically more complex structures, called phases. The arrangement of surfactant molecules (or group of its molecules) in such phases is very similar to the arrangement of molecules within phases formed by normal (thermotropic) liquid crystals. Thus the surfactants are often referred to as *lyotropic liquid crystals*, LLC. The prefix "lyo-" indicates that ordered phases are formed under the influence of solvent and as a result the type of the ordered phase is determined mostly by amphiphile concentration. This distinguishes surfactants from typical (thermotropic) liquid crystals, that is rod-like or disk-like molecules, for which the type of ordering is governed mainly by temperature [130–132]. The most common LLC phases are: hexagonal, lamellar, cubic and their corresponding reversed phases [133,134]. Schematic representation of these phases is shown in Figure 17a, b, c.

Hexagonal phase is formed by infinitely long (at least in theory) cylindrical micelles arranged in hexagonal array. The interior of those micelles is formed by hydrocarbon chains, whereas the exterior is formed by polar head groups. The schematic representation of hexagonal phase is shown in Figure 17a. *Lamellar phase* (see Figure 17b) have a sandwich-like structure. It consists of parallel bilayers of surfactant separated with the layers of water. Each bilayer is a plane-like structure consisting of surfactant molecules arranged into tail-to-tail fashion and as a result - shielded by the polar groups from the contact with water. *Cubic phase* is the most complicated structure formed by surfactants. This is bicontinuous phase consisting of two independent, non-crossing water and surfactant channels. The surfactant sublattice is sometimes referred as branched micelle. The cross section of such structure is similar to that observed for elongated micelle: hydrophobic core surrounded by hydrophilic corona. Unlike the others, cubic phase one may exist in several different types designated as Ia3d, Pn3m, Im3m. The common feature of all cubic phases is the bicontinuous nature. Schematic representation of cubic phase is shown in Figure 17c. *Reversed phases* are the last group of LLC

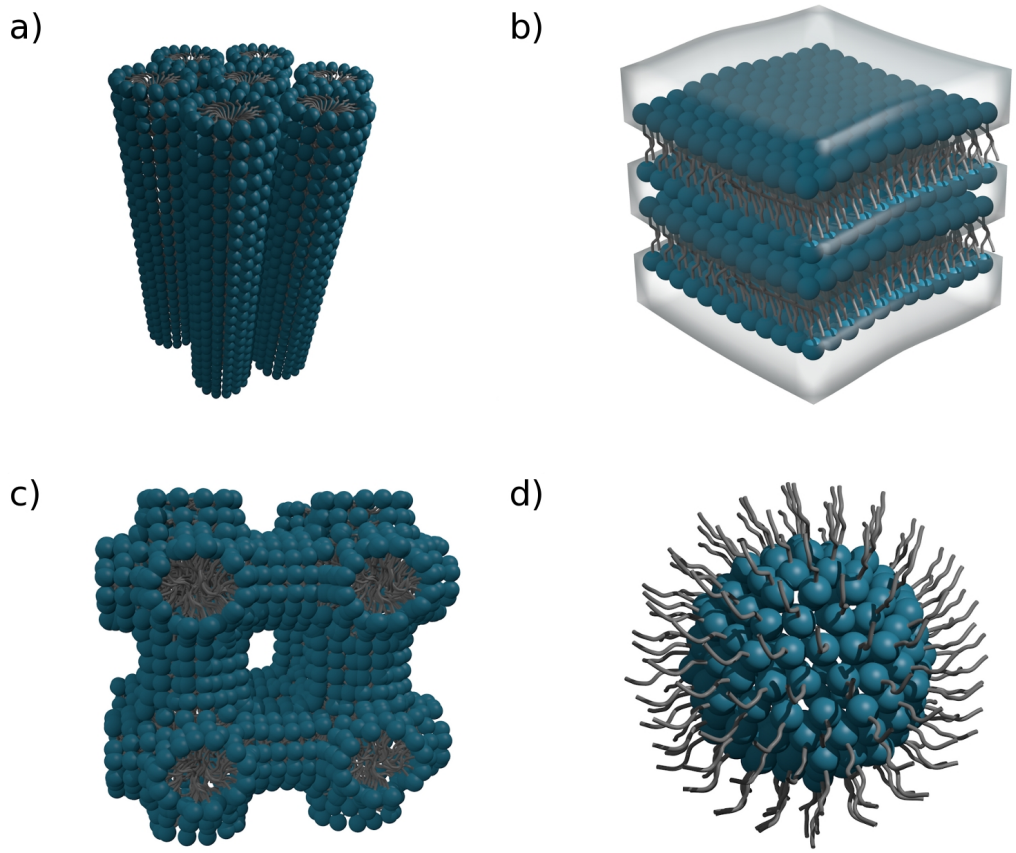

Figure 17: Types of ordered phases observed in surfactant/water systems: a) hexagonal, b) lamellar, c) cubic phase, d) reversed micelle.

phases. The difference between normal and reversed phase is in the way of arranging the surfactant molecules into subunits. In normal phases the interior is hydrophobic and the exterior is hydrophilic whereas in reversed (micellar, hexagonal, cubic) phases the core is formed by hydrophilic head-groups and the corona is formed by hydrophobic hydrocarbon chains. The example of the reverse phase - reversed micelle is shown schematically in Figure 17d. All the complicated self-assembled structures of surfactants are made up of smaller subunits, such as micelles (spherical or elongated) and bilayers. This makes, that the phases differ in the degree of continuity. Hexagonal phase is continuous in one dimension, lamellar is continuous in two dimensions and cubic phases have a three-dimensional continuity[133,135]. This also causes that with increasing concentration of surfactant in surfactant/water binary mixture (thus increasing complexity of their internal structure), the viscosity of such mixture increases significantly.

According to the definition of LLC, the occurrence of various phases is determined by the composition, that is the ratio between surfactant and solvent in a binary mixture. For practical reasons, the existence of ordered phases of surfactants is presented graphically on the temperature vs composition graph. This type of graphs are called phase diagrams. The typical sequence of the occurrence of individual phases in surfactant/water binary mixture, with increasing the concentration of surfactant, is as follows. Firstly, below CMC, the solution contains free, unasociated surfactant molecules. Then, above CMC, miceles start to form. After that, there are successively: hexagonal, cubic and lamellar phases. Finally, one or more reversed phases and solid surfactant. Topology of the phase diagram of surfactant is schematically shown in Figure 18.

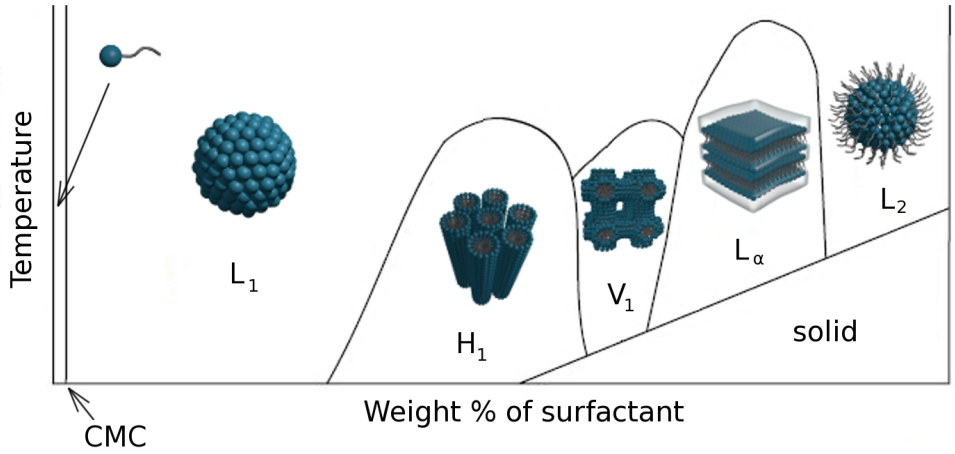

Figure 18: Typical topology of the phase diagram for surfactant/water binary mixture.[129] The graphical panels on the diagram represents (from left to right): the solution of free surfactant molecules, micellar (L_1), hexagonal (H_1), cubic (V_1), lamellar (L_α) and reversed micellar (L_2) phase respectively.

It should be noted that each surfactant has its own unique phase diagram. Even small modification of the structure, such as the type of counterion in ionic surfactant or the number of oxyethylene units in polar group of nonionic surfactants C_mE_n, may change the phase diagram significantly. It is also worth to notice the fundamental differences between the phase diagrams of ionic and nonionic surfactants. In the case of ionic surfactants, phase behavior is determined almost exclusively by the composition of a binary (surfactant/water) mixture and the temperature has a negligible effect. The sequence of occurrence of ordered phases is generally consistent with that shown in Figure 18, that is after the micellar solution there are successively hexagonal, cubic, lamellar, reversed phases and solid surfactant. In the case of nonionic surfactants, particularly surfactants with oligo (ethylene oxide) chain as the polar group, the

temperature significantly affect the phase behavior of binary mixture. At relatively low temperatures, the sequence of phases LLC is the same as for ionic surfactants and consistent with the presented in Figure 18. An important difference occurs during increase the temperature of binary mixture of a fixed composition. In particular, heating of the micellar solution (with fixed composition) usually leads to turbidity of the solution. This turbidity is caused by the spontaneous division of of the solution into two phases differing in the concentration of surfactant. Further increasing the temperature of the mixture leads to a sequence of new phases such as sponge phase or reversed micellar phase. This behavior of non-ionic surfactants is caused by the decrease in hydrophilicity of the oxyethylene groups with increasing temperature and as a result, weakening their interaction with water molecules[136]. Examples of phase diagrams of surfactants used in this dissertation are given in Section 2.3 (Figure 35).

1.2.4 Polymers and polyelectrolytes

Polymers are the macromolecules consisting of small repeatable units – monomers – conected with each other in a repeatable manner[137]. The polymer may consist of one or more types of monomers. In the latter case we speak of the copolymer.

The number of monomers connected with each other in a polymer chain is known as a degree of polymerization and it is one of the physical quantities that characterize every polymer. This parameter is often used to distinguish polymers from oligomers, that is a macromolecules composed of a few monomers. The exact value of the degree of polymerization that distinguishes oligomers from polymers is still the mater of debate and it is between 10 and 100. The main difference between the polymers and oligomers is, that in the case of polymer – adding or subtracting a single monomer does not change the physicochemical properties of substance. In the case of oligomers, however, a slight change of chain length causes a significant change in physicochemical properties[138].

Polymers are also characterized by mass. One can distinguish two types of masses for polymers: weight-averaged molecular weight (M_{w}) and number-averaged molecular weight (M_{n}). The ratio of this two masses, namely $M_{\mathrm{w}}/M_{\mathrm{n}}$ is known as polydispersity index (PDI). The polymer whose macroscopic sample consists of polymers having the same degree of polymerization is called monodisperse. Truly monodisperse polymers are that made by nature, for example proteins. Synthetic polymers are usually polydisperse - they have broad distribution of degrees

of polymerisation. The narrowness of the degree of polymerisation may be obtain during post-synthetic procedures including separation of the polymers due to their masses with the use of ultracentrifuge. This procedure may lead to obtain samples of moderate monodispersity. It is generally accepted that polymer sample is considered as monodisperse when its PDI is lower than 1.1.[139]

Because of the huge diversity of the available monomers, there is no one exact way of polymer classification.[139] The first and probably the most natural division of polymers is into biological (such as DNA, proteins and polysaccharides) and non-biological ones.

Non-biological polymers are categorized due to the polarity of monomers into:

- non-polar (e.g. polystyrene)
- polar, but water-insoluble (e.g. poly(methyl methacrylate))
- water soluble (e.g. polyethylene glycol)
- ionizable polymers, or polyelectrolytes (e.g. poly(styrenesulfonate))

Polymers are also classified according to their structure (see Figure 19) into:

- linear - monomers are connected one after another
- branched - some monomers form side chains in the main chain
- cross-linked - few simple polymer chains are connected with each other, forming a network

Polymers containing ionizable groups in the monomers are called **polyelectrolytes**. In aqueous solutions, polyelectrolytes are dissociated what makes that the polymer chain is charged. Polyelectrolytes (like simple electrolytes) are divided into strong and weak depending on their dissociation ability. Strong polyelectrolytes are charged regardless of pH. In case of weak polyelectrolytes the degree of dissociation, and thus the charge of the polymer, depends strictly on pH. Namely, they are charged when pH > pKa.

Similarly to ionic surfactants, polyelectrolytes are grouped with respect to the sign of the carried charge into:

- anionic - negatively charged (e.g. poly(styrenesulfonate))
- cationic - positively charged (e.g. polyethyleneimine)
- zwitterionic or amfoteric - containing charged monomers of a different sign

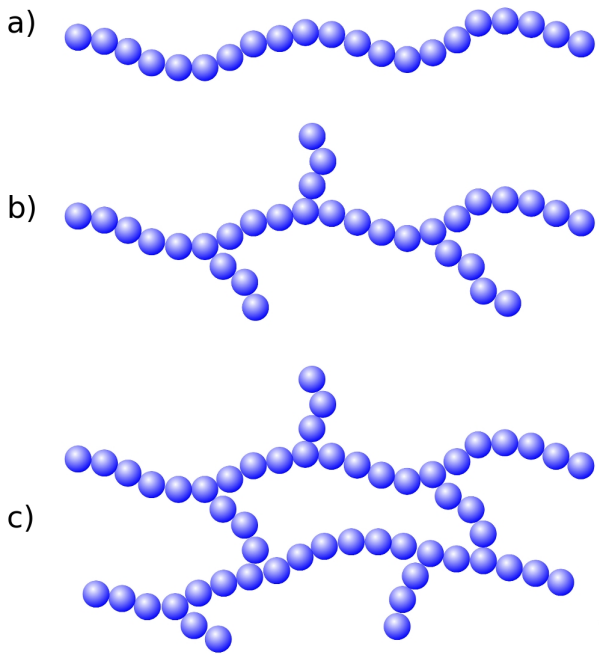

Figure 19: Classification of polymers according to their structure: a) linear, b) branched, c) cross-linked.

In this dissertation I used only simple, synthetic linear polymers (both ionic and nonionic). Specification and structures of used polymers are given in Chapter 2.3.

1.2.5 Polymers in solution

When polymer is dissolved in solution, it may interact with solvent molecules. This interaction as well as the interaction between monomers influences the conformation of the macromolecule. Most of the polymers in solution form random coils, what means that monomers are oriented randomly in space although they are connected with adjoining units. Random coil is not a specified shape but a statistical distribution of all the shapes present in the population of the macromolecules[140]. This type of conformation is preferred when there are no specific interaction between monomers. However when interactions occur other conformation are preferred. To illustrate the difference between the structure of polymers with and without specific interaction one may compare the structure of nonionic polymers and polyelectrolytes in aqueous solution. In case of nonionic polymers, there are no specific interactions between monomers so the polymer adopt a random coil conformation. In case of polyelctrolytes, there is a strong repulsion between monomers, what result in elongation of polymer chain up to rod-like conformation. The repulsion between monomers can be reduced by the addition of salt. This

screening effect of salt result in the change of polyelectrolyte conformation from elongated to coiled. Another fine example of the influence of specific interaction between monomers on the polymer conformation is the double helix of the DNA. DNA is biological polymer in which nucleotides are the repeatable units. Structure of the DNA – double helix – is a result of specific interactions – hydrogen bonds between base pairs.

Polymer chain in solution is typically characterized by its radius of gyration. Radius of gyration, R_g, is defined as the average distance from the center of the gravity of polymer chain to its periphery. It may be described as an averages radius of all polymer conformation measured from its center of gravity. When we compare R_g values of nonionic polymer (coiled) and polyelectrolyte (elongated) of the same chain length, it occurs that R_g is bigger for charged polymer. Schematic representation of the difference in R_g for coiled and elongated polymers is schematically shown in Figure 20.

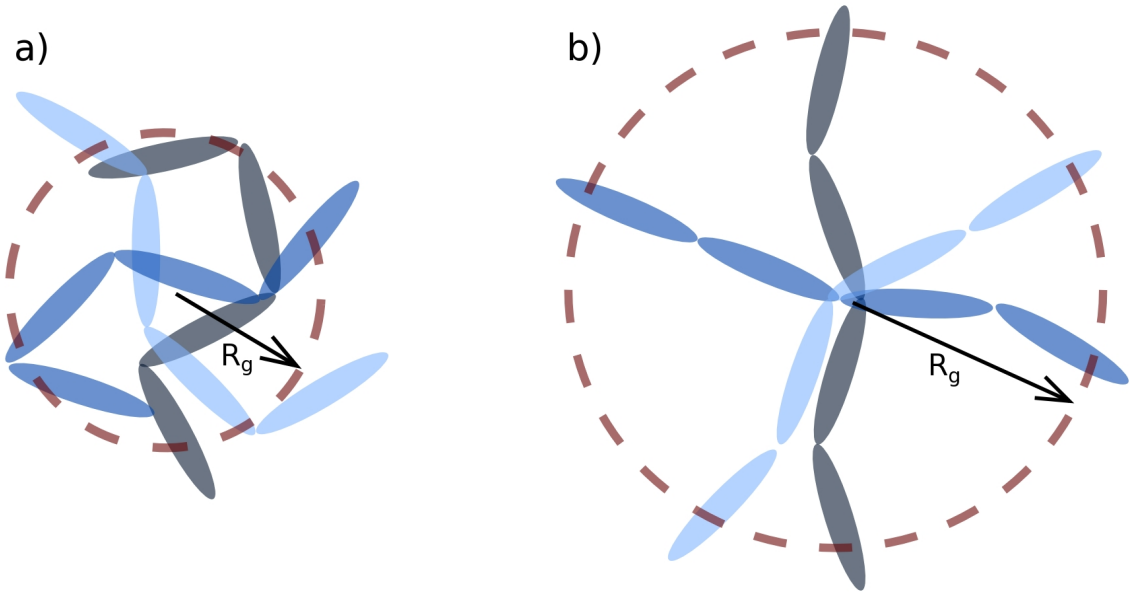

Figure 20: Schematic representation of radius of gyration of nonionic (a) and ionic (b) polymer consisting of same number of monomers.

1.2.6 Interaction of surfactants with polymers: association and phase separation

Solutions containing both surfactants and polymers are very important from application point of view. This cause the large interest in the interaction between those components and its consequences. The topic was started in 1940s and is still continuing now. Most of the available literature concerns the association that may occur in such systems. Due to the applications (mainly in cosmetics), the most extensively studied system is the mixture of anionic surfactant, sodium dodecyl sulfate, SDS and nonionic polymer, polyethylene glycol, PEG. As it was mentioned in Section 1.2.1, one of the most important property of surfactants is their ability to lower the surface (or interfacial) tension. In aqueous surfactant solution the surface tension decreases as long as the surfactant concentration is lower than the CMC. Above CMC surface tension value is nearly constant and independent on the surfactant concentration.

The situation changes if the solution contain both surfactant and polymer molecules. In such a case, at a concentration known as the critical association concentration, surfactant molecules start to attach to the polymer chain[141] forming a complex. In this complex, surfactant molecules form micelles around the polymer segments. This situation is usually described by a "pearl-necklace model"[142] that is presented graphically in Figure 21[142].

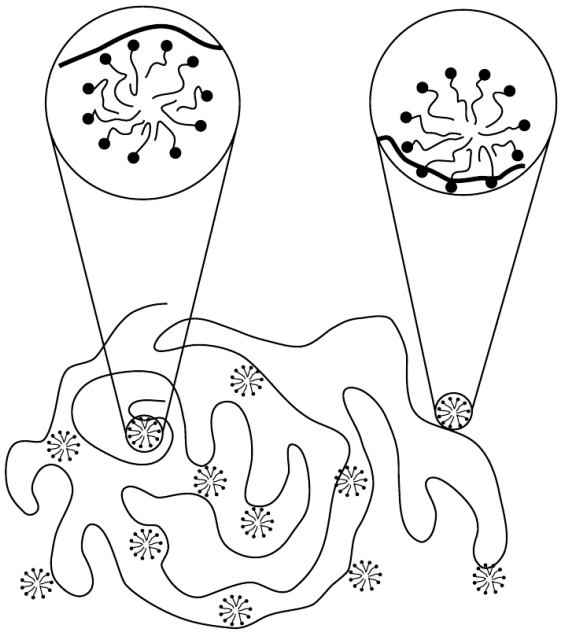

Figure 21: Pearl-necklace model ilustrating the polymer - surfactant complex. From " Surfactants and polymers in aqueous solution"[142] p. 281.

Critical association concentration is typically lower than CMC. The formation of surfactant-polymer complex results in decrease of surface activity of surfactant. The surface tension saturates at certain value and it stays constant as long as surfactant molecules associate to polymer chain. Further addition of surfactant lead to the saturation of the polymer with surfactant, what result in recovery of its surface activity. The association described above is observed in case of nonionic polymers and ionic (especially anionic) surfactants[143].

The association may also occur in the solution of oppositely charged polyelectrolyte and ionic surfactant[143]. It results, however, in phase separation. This follows from the fact that strong attractive interaction between charged groups of opposite sign leads to the formation of two phases. One of those phases is rich in both species (their complex) and the second is rich in counterions, and eventually the excess of one of the species.

Apart from phase separation observed in the solution of ionic surfactants and polyelectrolytes of opposite charge (called associative phase separation), there is a second type of phase separation, known as segregative one. In this case the mixture separates spontaneously into two phases. One of them is enriched in surfactant (typically upper phase) and the second is enriched in polymer (typically the bottom phase). Segregative phase separation may occur in three types of mixtures: (i) nonionic surfactant and nonionic polymer[144–147], (ii) ionic surfactant and ionic polyelectrolyte of opposite charge with high concentration of simple salt[148], (iii) ionic surfactant and ionic polyelectrolyte of the same charge[148].

In the solutions containing nonionic surfactants and nonionic polymers, there are no specific attractive interactions between hydrophilic segments. For this reason, the association is not observed. Instead, the segregative phase separation may occur. The studies on phase behavior of such concentrated mixtures was started in 1990s[144,145] and was also continued recently by the group of Hołyst[146,147].

The explanation of the phase separation in nonionic surfactant/nonionic polymer mixture is given by the analogy to the mixtures of colloids and nonadsorbing polymers in a common good solvent[146,149,150]. In such a mixture, the phase separation is driven by the depletion interaction. Each colloidal particle is surrounded by its depletion zone of a size that is comparable with the radius of gyration of the polymer. The polymer cannot enter this zone because it would cause a great loss of its conformational entropy. If two particles are so close to each other that their depletion zones overlap, the imbalance of the osmotic pressure is created. This im-

balance pushes the particles together and finally results in the phase separation of the mixture into colloid-rich and surfactant-rich phase[151]. Recently, the group of Hołyst expand the topic of phase separation in mixtures of this type asking a question if it is possible to *"design the condition for which the solution of polymers and surfactants exhibits ordering"*. The work[146] contains not only experimental data but also simple theoretical model consistent with experimental results. The model is based on the experimental observation that polymer-rich phase do not contain any micelles what imply that the interface between coexisting phases act as a semipermeable membrane. This membrane is permeable only for water molecule what indicates that the thermodynamic equilibrium in the system is set by the chemical potential of water in two phases[146]. In general, the proposed model may be applied in any surfactant/polymer mixture what makes it very useful in preparation of ordered phases of surfactant of a desired type of ordering.

As it was discussed above, ionic surfactants associate to the polyelectrolyte of opposite charge what typically result in precipitation of the complex. The addition of salt may reduce this effect, by screening the charges, and facilitate the mixing. Further addition of electrolyte may however invert the situation again and lead to the segregative phase separation[148].

Phase separation of a segregative character is also possible in the mixtures of surfactants and polyelectrolytes bearing the same charge, however there is extremely small number of examples of such mixtures in the literature. The one that can be found, is the mixture of anionic surfactant, SDS and anionic polysaccharide, sodium hyaluronate[148]. This mixture separates spontaneously for high surfactant and polyelectrolyte concentration. This behavior is attributed to the substantial entropy loss of the counterions during the phase separation because of the differences in the charge densities[148]. Additionally, the phase separation in mixtures of this type can be additionally facilitated by the addition of salt.

1.2.7 Surfactants as templates

As it was discussed in Section 1.2.3, concentrated surfactant solutions exhibit a variety of ordered phases called lyotropic liquid crystalline phases. Those LLC phases may be used as a templates in formation of other materials with clearly defined internal structure, especially in the formation of nanocomposites. In such cases, surfactant governs the alignment of the obtained material and therefore surfactants are commonly described as structure-directing agents.

As it was mentioned in Section 1.1.2, surfactant solution can be used as reacting medium for NP synthesis and their presence may be crucial for the shape of grown nanostructures[17,40,125]. Ordered phases of various surfactants can be used to create soft nanocomposite materials containing embedded NPs. To create this type of hybrid material, two approaches are used. The first is the direct growth of nanoobjects inside the surfactant phase[52–56]. The second is the simple mixing of NPs with previously prepared LLC phase[152–156]. The latter approach was recently used to fabricate composite materials containing metal,[52,53,152–154] semiconductor,[52,54] and magnetic[155,156] NPs or nanorods[55,56]

Surfactants are also used as templates for porous materials of a well defined internal structure. Solids having pore diameters in the range of 2 - 50 nm are referred to as the mesoporous materials[157]. In nature, mesoporous materials are represented by zeolites. The first reports describing the preparation of this type of materials based on liquid crystal templates comes from 1990s. Prototype materials consisted of silica walls arranged in a hexagonal structure was designated as MCM-41.[158,159] The obtained ordering of the walls depicted the cylindrical hexagonal structure of used surfactant and the pore size was varied by using surfactants of a different chain length[158]. Typical transission electron micrographs of hexagonally ordered silica is shown in Figure 22.

The synthetic procedure of mesoporous materials formation requires the use of inorganic precursor, surfactant and acid or base (to adjust the pH). For mesoporous silica, the most common precursors are organosilicates such as tetramethyl orthosilicate, TMOS, and tetraethyl orthosilicate, TEOS. Typical structure directing agents are cationic surfactants, especially quaternary ammonium salts. The formation of mesoporous structure is based on the hydrolysis of inorganic precursor and its further condensation in the water chnnels of the surfactant template. Crude material is subsequently dried and calcinated in high temperature (about 500 °C) to remove the LLC template and leave pure inorganic walls of a great periodicity. Although the first

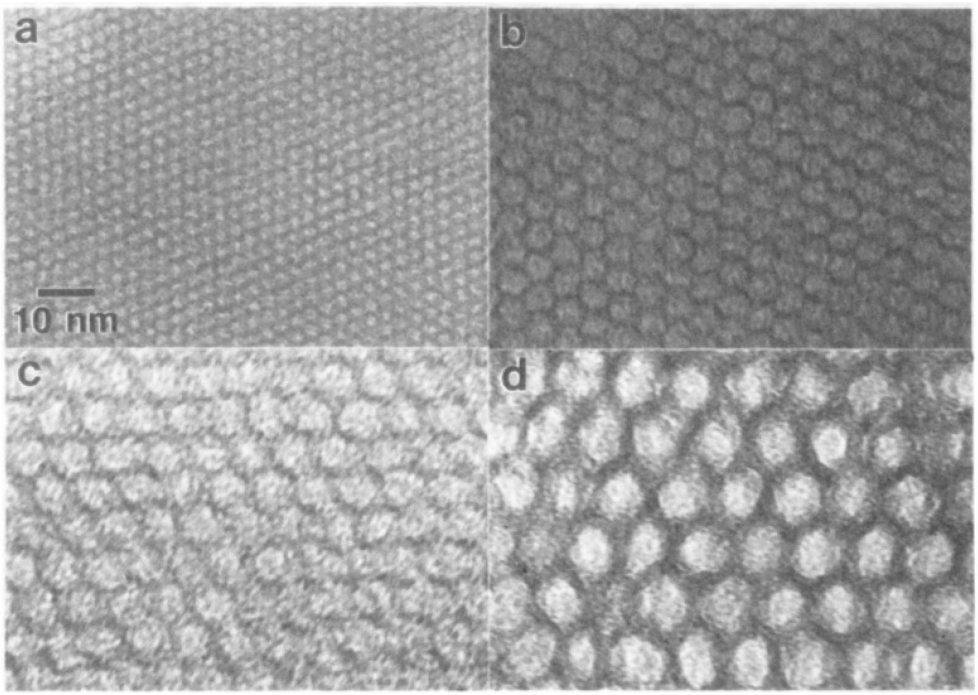

Figure 22: Transmission electron micrographs of hexagonal silica (MCM-41) having different pore sizes: a) 2 nm, b) 4 nm, c) 6.5 nm, d) 10 nm.[158]

works concerns formation of hexagonal silica,[158–160] other types of ordering like cubic[160–162] or lamellar[160–162] may be easily obtained. Furthermore, mesoporous materials includes not only silica, but also metal oxides (e.g. TiO_2, ZrO_2, Al_2O_3, Nb_2O_5, WO_3, HfO_2, SnO_2) and mixed oxides (e.g. $SiTiO_4$, $ZrTiO_4$, Al_2TiO_5, ZrW_2O_8)[163]. Due to the large, tunable pore sizes and expanded surface area mesoporous materials have several potential applications in catalysis[164,165], in separation processes and in host-guest chemistry[166].

2 Experimental part

In this Chapter, I describe the experimental techniques and procedures used in this dissertation. This Chapter is organized as follows. Section 2.1 contains the basics of experimental techniques that were used during my research. Section 2.1.1 describes polarized optical microscopy. Section 2.1.2 refers small and wide angle X-ray scattering. Section 2.1.3 depicts dynamic light scattering. Section 2.1.4 deals with the basics of zeta-potential measurements. Section 2.1.5 recalls the main issues of spectroscopic techniques.

Section 2.2 is dedicated to different experimental procedures. Section 2.2.1 includes the procedures of synthesis and functionalisation of gold and silver NPs. Section 2.2.2 refers the UV-Vis titration of oppositely charged NPs. Section 2.2.3 describes the formation of silica-based mesophase doped with NPs.

Last Section (2.3) contains the characterization of the substances used in my research. It includes the list of substances together with their purities and suppliers. It also contains a list of critical micelle concentration and phase diagrams of surfactants.

2.1 Research techniques used

2.1.1 Polarized optical microscopy

In this dissertation, polarized optical microscope was used to investigate the samples of lyotropic liquid crystals in order to determine the their ordering. The LLC phases were examined in pure form (water solution) or with addition of NPs. The basics of image formation in polarized optical microscope is explained in Figure 23. This type of microscope is equipped with two crossed polarizers placed before and after the sample. First polarizer (before the sample) enables to pass only the light having certain polarization. The second polarizer, called also analyzer, is oriented perpendicularly to the first one. If the are no sample or if the sample is isotropic (does not change the polarization plane), then the second polarizer cuts of every light what result in completely black image. However, if the sample is anisotropic, it reorients the polarization plane of light so that part of light can pass through the second polarizer. In the latter case bright colorful images are formed.

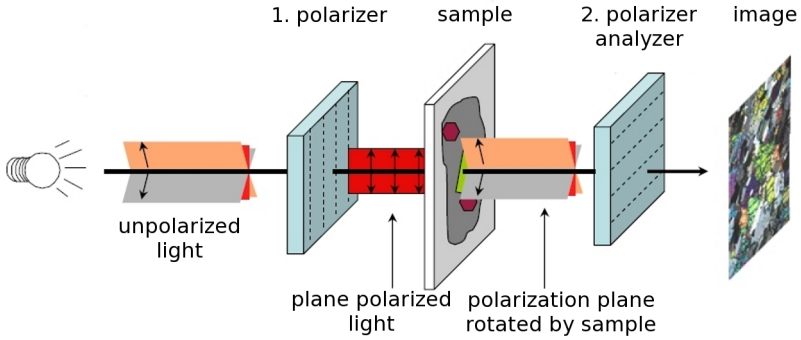

Figure 23: The scheme of the image formation in polarized optical microscope, from Ref. 167.

The example of anisotropic samples that can be visualized by polarized optical microscope are ordered phases of lyotropic liquid crystals (hexagonal or lamellar). Every ordered phase has its own typical features, visible in polarized optical microscopy images. Those images, known as textures, can be used to verify the type of ordering in the samples of lyotropic liquid crystals. The examples of LLC textures are shown in Figures 39 and 51.

The textures were investigated using Nikon Eclipse E400 polarized optical microscope equipped with LINKAM THMS 600 heating/cooling stage controlled by the LinkSys 2.36 software. The images were acquired and processed with the use of the image analyzer software Lucia G. The observations were carried out in the temperature 25 °C. Experiments were con-

ducted in the laboratories of the Institute of Physical Chemistry PAS.

2.1.2 Small and wide angle X-ray scattering

In this dissertation, X-ray scattering analysis were used to characterize short and long-range order within the samples. Both methods are based on the Bragg's law, given by the Equation (7):

$$2dsin(\theta) = n\lambda \Longrightarrow d = \frac{n\lambda}{2sin(\theta)}. \tag{7}$$

In this equation, n is an integer, λ is wavelength of incident wave, θ is the angle between incident ray and scattered plane and d is the interplanar spacing. The Bragg's law, illustrated on Figure 24, defines the θ angles needed for constructive interference of reflected X-rays.

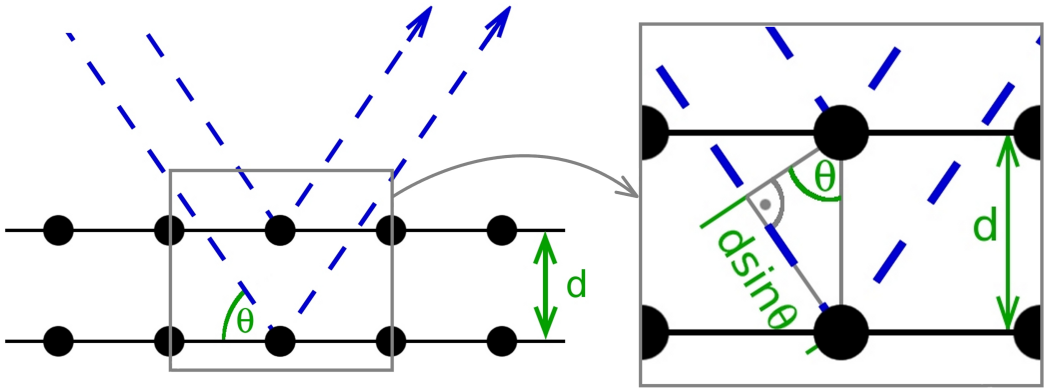

Figure 24: The ilustration of Bragg's law.

Small (SAXS) and wide (WAXS) angle X-ray scattering methods give diffraction patterns of the same type as in powder diffraction methods although they do not require crystallinity of the sample. They allow examination of a completely disordered samples or samples containing only partially ordered domains. As the names imply, small (SAXS) and wide (WAXS) angle X-ray scattering techniques differ in angle at which the scattering pattern is collected. This difference is shown schematically in Figure 25. According to the Bragg's diffraction law (Equation (7)) scattering angles are inversely proportional to the interplanar spacing. It means, that the reflexes from planes separated by few nanometers are observed for low scattering angles (0 – 4°) whereas smaller spacings (sub-nanometer) give constructive interference for wide angles (4 – 170°). Typically, SAXS/WAXS experimental results are plotted on scattered intensity

vs. 2θ or scattered intensity vs. scattering vector, q, plot. The scattering vector is defined as:

$$q = \frac{4\pi sin\theta}{\lambda} \tag{8}$$

and it contains information about the wavelength of X-rays. The use of q instead of 2θ makes it easier to compare experimental data obtained with the use of X-ray sources of different wavelengths.

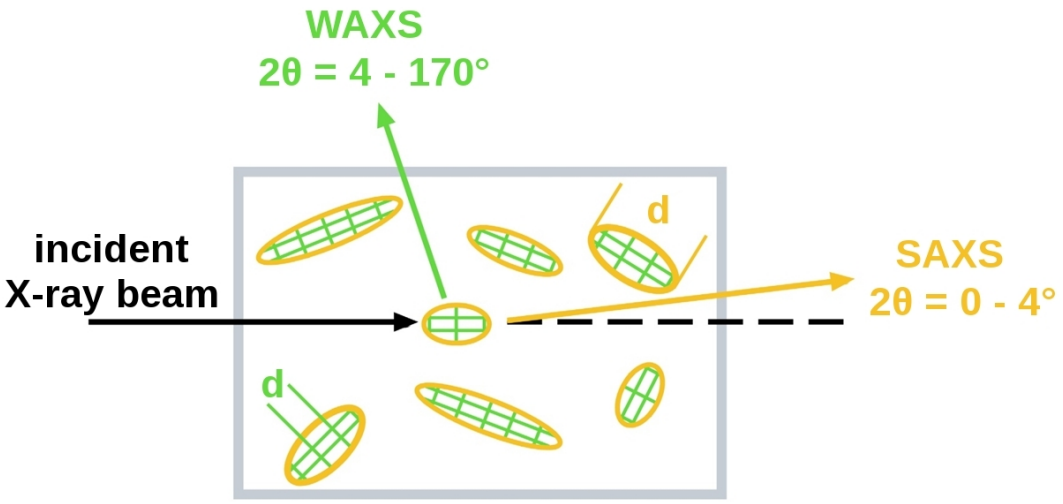

Figure 25: Schematic representation of the main difference between small (SAXS) and wide (WAXS) angle X-ray scattering, i.e. the difference in scattering angle.

I. SAXS determination of size and size distribution of spherical NPs.

SAXS is often used to determine the shape and/or their size and size distribution. This follows from the fact that the total scattering intensity, I (q), consists of two parts:

$$\mathrm{I}(q) = \mathrm{F}(q)\mathrm{S}(q). \tag{9}$$

The first one is the form factor, F(q), and the second is the structure factor, S(q). F(q) carries information on the particle radius of gyration whereas S(q) contains information about the interactions between particles and their mutual arrangement. If we consider a dilute solution of non-interacting, monodisperse particles, then S(q) = 1. Under this conditions, for very low scattering angles:

$$\mathrm{I}(q) \approx \mathrm{I}(0)\exp(-\frac{1}{3}R_g^2q^2) \tag{10}$$

where I(0) is the forward scattering. Equation (10) is typically referred to as a Guinier approximation and is the basis to draw a Guinier (i.e. ln(I(q)) vs. q^2) plot. For ideal monodisperse systems Guinier plot gives a linear function whose slope yields the radius of gyration of particles. Guinier approximation is valid only for very small angles, that is for $q < 1.3/R_g$ [168,169]. If the solution contains particles of same shape but different in size, the appropriate analysis of I(q) yield the size distribution of particles. An example of Guinier plot for Au NPs, synthesized in the Institute of Physical Chemistry, is shown in Figure 26.

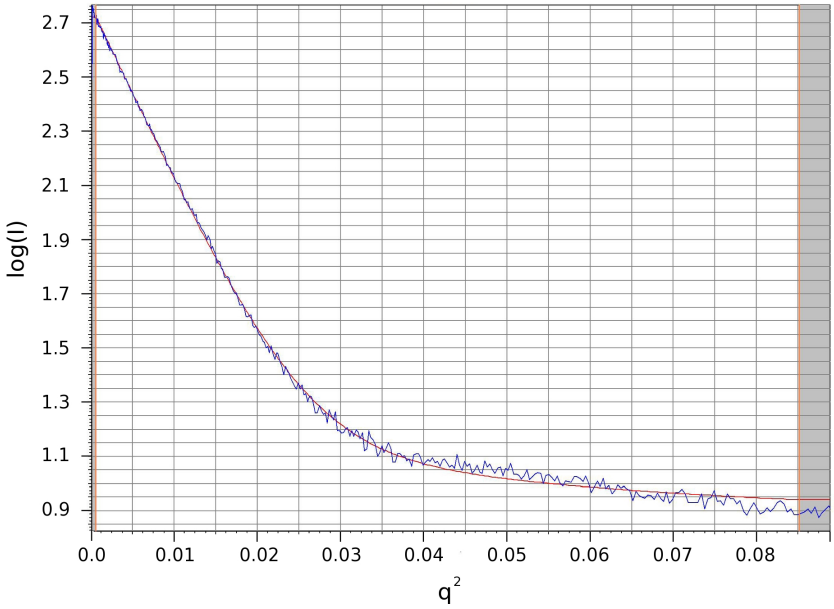

Figure 26: Guinier plot for Au NPs: blue curve – experimental data, red curve – fit to the data. The initial part of the graph can be approximated by a linear function. Radius of gyration of studied NPs is equal to (2.02 $\pm$ 0.48) nm.

II. SAXS characterisation of ordered phases of lyotropic liquid crystals.

Small angle X-ray scattering is also used to determine and characterize the nanometer-scale regularities within samples such as liquid crystalline phases. A set of diffraction fringes is characteristic for each ordered phase. Formation of the diffraction fringes for hexagonal and lamellar phase is shown schematically in Figure 27. For the hexagonal phase one may obtain three diffraction fringes ((010), (110), (020)), whose positions are to each other as $1 : \sqrt{3} : 2$. The characteristic distance for hexagonal phase, a, that is, distance between the centers of cylindrical micelles can be easily determined from the position of the first diffraction fringe, by

applying the Equation (11).

$$a = \frac{2d}{\sqrt{3}} \tag{11}$$

Diffraction pattern for lamellar phase consists of equally spaced fringes. Position of the first band corresponds directly to the distance between the bilayers (d) of the lamellar phase. The following fringes correspond to successive harmonics.

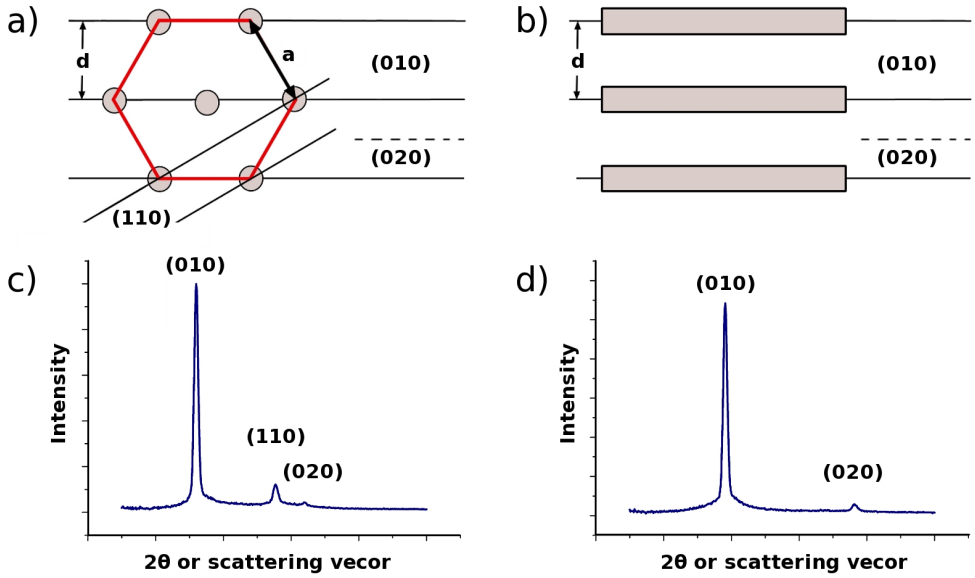

Figure 27: Scheme of diffraction fringes formation for hexagonal (a) and lamellar (b) phases. Circles and rectangles denote the cylindrical micelles of hexagonal phase and bilayers of lamellar phase respectively. Typical SAXS pattern for hexagonal (c) and lamellar (d) phase respectively.

In this dissertation small angle X-ray scattering was used to:

- determine the size/size distribution of spherical gold and silver NPs (cf. Figure 26)
- determine the type of ordered phase of lyotropic liquid crystals (cf. Figure 48) and to characterize their characteristic distances (a and d for hexagonal and lamellar phase respectively).

The small angle X-ray scattering patterns were obtained with the Bruker Nanostar system, the patterns were registered with Vantec 2000 area detector. The CuK (α = 1.54 Å) radiation was used. The samples were prepared in Lindemann capillaries (1.5 mm in diameter). The signal intensities were obtained through integration of the 2D patterns over azimuthal angle. The measurement were carried out in temperature 25 °C.

Wide angle X-ray scattering was used to investigate silicated LLC phases containing NPs and the samples formed after their calcination – mesoporous silica (see Figure 57 and Figure 58). The samples were powdered and analyzed with the Bruker D8 GADDS system (point beam CuKα, Gebel mirror, collimator 0.5 mm). The WAXS patterns were registered with Hi Star area detector. The measurements were performed in temperature 25 °C. Both SAXS and WAXS experiments were conducted in the Structural Research Laboratory of the University of Warsaw.

2.1.3 Dynamic light scattering

Dynamic light scattering, DLS, (also known as photon correlation spectroscopy) is a technique used to determine the size of objects (nano-and microparticles) contained in the solution. This technique is based on several basic assumptions:

1. If the particles are small compared to the wavelength of incident light, then they scatter light in an isotropic way (same in all directions). Light scattered at various particles interferes constructively or destructively depending on the arrangement of the particles, as it is shown in Figure 28.

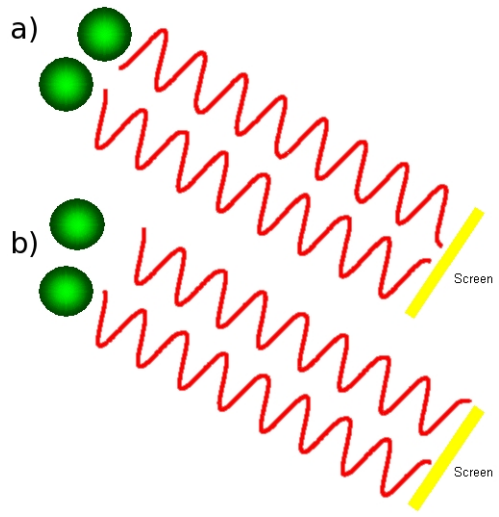

Figure 28: Effect of particle orientation on the result of interference of scattered light: (a) destructive interference, (b) constructive interference.[170]

2. Location of the particles in the solution is not static but is constantly changing due to collisions with solvent molecules (Brownian motion). This leads to continuous changes in the arrangement of molecules and therefore to the fluctuations of the observed scattered light.

Fluctuations in the DLS signal contain information about the dynamic properties of solute molecules, especially about their translational diffusion coefficient.[171] The larger the particles are, the slower the velocity of their Brownian motion. Small particles bombarded by solvent molecules move rapidly and over long distances. Large particles move more slowly and definitely closer. Translational diffusion coefficient (D) of an object with a radius r in a fluid of a viscosity η and temperature T is described by Stokes-Einstein equation:

$$D = \frac{k_{\mathrm{B}}T}{6\pi\eta r}, \tag{12}$$

in which k_{B} is the Boltzmann's constant. The radius r in Equation (12) is known as hydrodynamic radius and it is defined as a radius of a sphere moving with the same diffusion coefficient. Therefore, the resulting value of the hydrodynamic radius is the most accurate for spherical objects.

The original DLS signal is a noise, as it is shown schematically in Figure 29. To extract information from this noise one has to use intensity - intensity autocorrelation function $G(\tau)$ given by Equation (13).

$$G(\tau) =< I(t)I(t+\tau) > \tag{13}$$

In autocorrelation procedure, the intensity of signal obtained for a given time ($I(t)$) is compared with the same signal shifted by a delay time, τ. If the signal does not change then the result of autocorrelation function is equal to unity. However, if the signal at the time $t + \tau$ is entirely different than for t, then the correlation is zero.

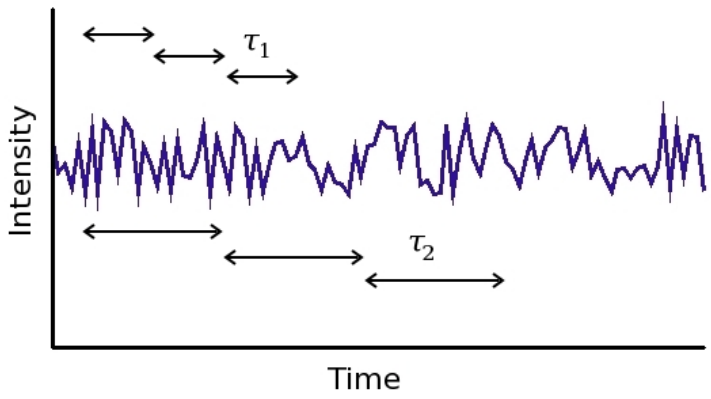

Figure 29: Schematic representation of the original DLS signal (intensity vs. time) and the interpretation of delay time, τ.

DLS signal reflects intensity fluctuations resulting from changes in the mutual position of the objects. In the case of large number of monodisperse particles the correlation is close to unity for very short times, and it decays exponentially in time:

$$G(\tau) = \mathrm{A}(1 + \mathrm{B}\exp(-2\Gamma\tau)). \tag{14}$$

In Equation (14), A is the baseline, B is the intercept of correlation function and

$$\Gamma = Dq^2 \tag{15}$$

contains information about the translational diffusion coefficient. The value of Γ can be read out directly from the chart of the autocorrelation function because it is equal to the inverse of inflection point. Wave vector, q, in Equation (15) is defined as:

$$q = \frac{4\pi n}{\lambda} sin\frac{\theta}{2} \tag{16}$$

where n is a refractive index of the dispersant, λ is the wavelength of the laser and θ is the scattering angle.

If the autocorrelation function has few inflection points (few different values of Γ), it means that the solution contains objects that differ in the value of hydrodynamic radius. The presence of two different objects may not be apparent at first glance. This follows from the fact that according to the Rayleigh approximation, the intensity of scattered light is proportional to the sixth power of particle size[172]. This means that if the solution contains equal number of 5 nm and 50 nm-sized objects, the intensity of scattered light coming from 50 nm-sized particles is 10^6 times greater than the one originating from 5 nm-sized particles.

In this dissertation dynamic light scattering was used to determine hydrodynamic radii of:

- metal and semiconductor NPs (cf. Figure 61)
- surfactant micelles in the solution of a given concentration (cf. Figure 64)
- NPs with adsorbed surfactants (cf. Figure 68)

The details of the DLS experiment were as follows: The measurements were carried out using the Stabilite 2017 Argon ion laser (λ = 514 nm) or He - Ne laser (λ = 633 nm) at various

angles, from 30° to 150°. The Fourier transform of the intensity-intensity correlation function $G(q;t)$ was measured as a function of the scattering wave vector, q, and time, t. All measurements were carried out at 25 °C. DLS experiments were conducted in the laboratories of the Institute of Physical Chemistry PAS.

2.1.4 Zeta-potential measurements

According to IUPAC, electrokinetic potential, ζ, is defined as a potential that drop across the mobile part of the double layer and that is responsible for electrokinetic phenomena[25]. Negative value of ζ means that the potential decreases from the bulk of the liquid phase towards the interface. ζ - potential is a commonly used to characterize colloidal systems, especially their stability in solutions.

To explain the concept of zeta potential more accurately, let us consider a single, negatively charged colloidal particle. The presence of such particles affects the distribution of ions in solution, as it is shown in Figure 30. Directly at the surface of the charged particle, the Stern layer - a layer of firmly adsorbed counterions is created. Beyond, the positive ions are still attracted to the negatively charged colloidal particle, however, they are also repelled by the positive ions from the Stern layer. This leads to the creation of another layer of ions, called the diffusion layer. The concentration of positive ions in the diffusion layer gradually decreases with increasing distance from the surface of the colloid, and finally reaches a value as in the depths of the solution. Stern layer together with the diffusion layer is called the electrical double layer[173,174].

If a charged particle moves (e. g. due to gravity) it moves together with ions from the Stern layer and a portion of ions from the diffusion layer. It is believed that inside the diffusion layer there is a hypothetical limit within which ions with a colloidal particle form a stable entity. If a particle moves, the ions contained within this boundary move together with it. This theoretical limit is called the surface of hydrodynamic shear or slipping plane. The ζ-potential is the potential that exists at slipping plane[175], as it is shown in Figure 30. It should be noted that ζ - potential is not equivalent to the surface potential, nevertheless for many applications it is its fairly good approximation.

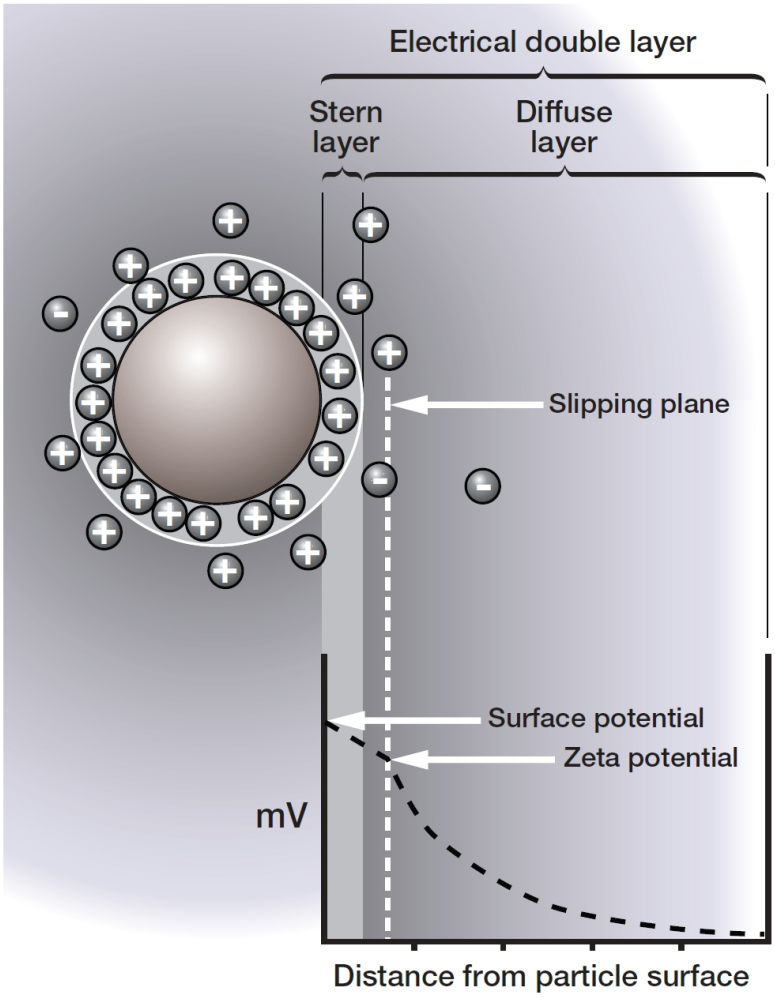

Figure 30: Schematic representation of electrical double layer, slipping plane and ζ - potential for negatively charged particle.[175]

The ζ - potential is measured using the electrophoresis phenomenon that is the movement of charged particles under the influence of an external electric field. The velocity of such particles, known as electrophoretic mobility, U_{E}, depends on the gradient of the electric field, dielectric constant of medium (ε), its viscosity (η), and ζ - potential. The dependence of electrophoretic mobility on these parameters is described by the Henry equation (Equation (17)).

$$U_{\mathrm{E}} = \frac{2\varepsilon\zeta f(\kappa r)}{3\eta} \tag{17}$$

Factor $f(\kappa r)$, known as Henry function, depends on the Debye length, κ^{-1}, and the radius of the particle, r. For the approximation of Henry function two values are used: 1.5 or 1.0.[175] The value of 1.5 (Smoluchowski approximation) is used for aqueous solutions, especially for

solutions that contain particles larger than 0.2 μm dissolved in the electrolyte solution having a concentration greater than 10^{-3} mol/dm^3. The value of 1.0 (Huckel approximation) is used for small particles dissolved in a solution of low dielectric constant, especially for particles dispersed in non-aqueous solutions. In presented experiments I used the Smoluchowski approximation ($f(\kappa r)$ = 1.5).

To determine the ζ - potential from Henry equation, one need to determine electrophoretic mobility. The experiment is conducted in a cell with a capillary at the ends of which there are two electrodes. Under the influence of an applied electric field, ions and particles in the solution migrate toward the electrode of opposite sign. Particle velocity is measured using the Doppler effect, and then expressed in unit field strength as their mobility.

In this dissertation, Zetameter (Zetasizer Nano, Malvern Instruments Ltd.) was used to determine ζ-potential of charged NPs as well as NPs with adsorbed surfactant molecules. The measurements were carried out at 25 °C. ζ-potential measurements were conducted in the laboratories of the Institute of Physical Chemistry PAS.

2.1.5 Spectroscopic techniques

Spectroscopic techniques are commonly used to determine spectral characteristics of studied systems. The ability to absorb or emit photons is closely related to the electronic structure of given molecule. As it was discussed in Section 1.1.1, in case of metal NPs, the absorption of light in UV-Vis range is a result of surface plasmon resonance.

Measurement of absorption spectra is one of the main procedures performed during laboratory tests. During the measurement the sample is illuminated by a light source of defined spectral characteristics. After passing through the sample, the intensity of incident light is weakened. The attenuation of light is the result of two processes, absorption and scattering, the sum of which is called attenuation (formerly - extinction). The intensity of transmitted light (I) depends on the intensity of incident light (I_0), molar concentration of a sample, c, absorption path length, l, and molar absorption coefficient (attenuation coefficient), ε_{abs}. The exact relation is given by Lambert-Beer law, (Equation (18)) which also gives the definition of absorbance (A).

$$A = log_{10}\frac{I_0}{I} = \varepsilon_{\text{abs}} cl \tag{18}$$

The Lambert-Beer law states that the absorbance is a linear function of concentration. It makes that the Equation (18) is useful to determine the concentration of the sample of a known attenuation coefficient. The illustration of Lambert-Beer law is shown in Figure 31. The change of absorbance as a function of wavelength is known as the absorption spectra. In this dissertation

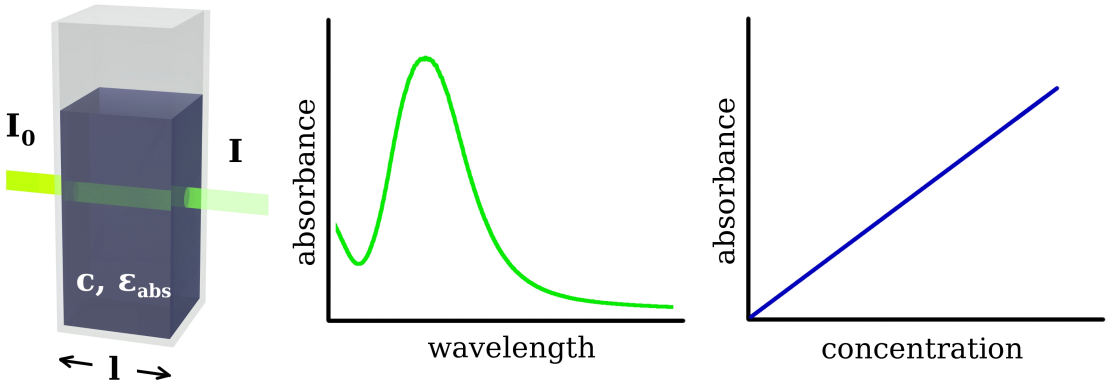

Figure 31: The ilustration of Lambert-Beer law.

spectroscopic techniques were used to:

- collect the absorption spectra of various samples, mainly solutions containing NPs (cf. Figures 46, 47 a, and 45)
- collect the emission (fluorescence) spectra of semiconductor QDs (i.e. Figure 62)

The UV-Vis absorption spectra were recorded on Shimadzu MultiSpec-1501 spectrometer or on Ocean Optics 2000+ spectrophotometer in the spectral range 190 – 800 nm. The samples were measured in a quartz cuvette of 1 mm path length.

The fluorescence spectra were recorded on Ocean-Optics USB 2000+ spectrophotometer in the range 190-1000 nm in quartz micro cuvette (10 mm of path length). The fluorescence was excited using laser diode (λ = 405 nm). The spectra were recorded automatically every 10 seconds. The experiments were performed in Okolab incubator in the temperature 25.0 °C. Experiments were carried out in laboratories of the Institute of Physical Chemistry PAS.

2.2 Experimental procedures

2.2.1 Synthesis and functionalization of nanoparticles

I. Synthesis of gold nanoparticles.

Gold NPs were synthesized according to the known procedure described by Jana and Peng[40]. The original procedure was magnified three times. The described procedure is two-step method, what allows for better control over the size and the dispersity of NPs. In the first step small NPs (seeds) were prepared and in the second step the seeds were grown to bigger NPs. The reduction of gold precursor was done with the use of two different reducing agents, that is tetrabutyl ammonium borohydride (TBAB) and hydrazine. TBAB was used in the first step, whereas hydrazine – in the second step. The synthesis was conducted in the presence of surfactant – didodecyldimethylammonium bromide (DDAB) and coating ligand – dodecylamine (DDA), what result in formation of dodecylamine coated NPs, AuDDA. Alkylamines are not as good capping agents as alkanetiols because of the weaker binding to the gold surfaces. The protecting alkylamine coating can be easily replaced with other type of coating during ligand exchange reaction. As a result, one batch of AuDDA can be used to prepare series of NPs solutions having gold core of a same size but differing in terms of coating. Chemical structures of the main compounds used for synthesis and functionalization of gold NPs are shown in Figure 34.

Preparation of gold seeds

Firstly, about 13 ml of 0.1 M DDAB solution was prepared by dissolving 0.694 g DDAB in 12.975 g of toluene. 29.5 mg of gold precursor, $HAuCl_4$ x 3 H_2O, was dissolved by sonication in 7.5 ml of DDAB solution. Then 270 mg of DDA was added and the mixture was sonicated to dissolve DDA completely. Finally 75 mg of TBAB was dissolved in DDAB solution and then injected to the gold solution during vigorous stirring. The addition of TBAB (reducing agent) to the gold solution result in immediate change of color of the solution from orange to dark brown, what indicates the formation of NPs. After addition of TBAB, the solution was stirred for about 15 minutes and then aged overnight in room temperature.

Seeding growth of gold nanoparticles

Firstly the growing solution of gold precursor was prepared by dissolving, via sonication, 292.5 mg of $HAuCl_4$ x 3 H_2O, 1.5 g of DDAB and 2.775 g of DDA in 75 ml (64.87 g) of toluene. Then, previously prepared seeds solution was added and resulting solution was mixed. Next, the solution of reducing agent (0.2 M hydrazine in DDAB solution) was prepared by dissolving 192 mg of hydrazine in 30 ml of 0.1 M DDAB solution (1.39 g of DDAB in 25.95 g of toluene). As prepared hydrazine solution was added dropwise (for about 10 minutes) during vigorous stirring of the solution. Finally, the solution was mixed for about 15 minutes.

II. Synthesis of silver nanoparticles

Silver NPs, similarly to gold ones, were prepared according to the procedure described by Jana and Peng[40] magnified three times. The synthesis was single-step reaction and used the mixture of hydrazine and tetrabutyl ammonium borohydride (TBAB) as the reducing agent.The synthesis was conducted in the presence of decanoic acid (DA) and dodecylamine (DDA) and resulted in formation of decanoic acid stabilized silver NPs, AgDA. The initial DA coating was further changed into thiols during ligand exchange reaction. Chemical structures of the main compounds used for synthesis and functionalization of silver NPs are shown in Figure 34.

The procedure of AgDA synthesis was as follows. Firstly, the reaction media was prepared by dissolving 516 mg of DA in 30 ml (26 g) of toluene. Next, 516 mg of hydrazine was dissolved by sonication in DA solution. Then the solution of the second reducing agent was prepared by dissolving 2.5 mg of TBAB in 8.67 g of toluene. 0.3 ml of as prepared TBAB solution was added to the reaction solution. Subsequently, the silver precursor was prepared by dissolving 51 mg of silver acetate in 0.6 ml of 1 M DDA solution (prepared by dissolving 0.185 g of DDA in 0.74 g of toluene). Finally, the solution of silver precursor was injected to the reaction solution during vigorous stirring. The color of the mixture changed into deep brown few minutes after addition of silver precursor, what indicated the formation of NPs. The stirring was continued for about 15 minutes to complete the reaction.

III. Functionalization of gold and silver nanoparticles

As prepared gold (AuDDA) and silver (AgDA) NPs were functionalized by ligand exchange reaction that is schematically shown on Figure 32. The procedures of functionalization and puryfication was based on the literature[67].

NPs were coated with ω-functionalized thiols: 11-mercaptoundecanoic acid (MUA) and N,N,N-trimethyl(11-mercaptoundecyl) ammonium chloride (TMA). Both ligands made NPs water soluble. Additionally they fit up NPs with electrostatic charge: negative in case of MUA and positive in case of TMA.

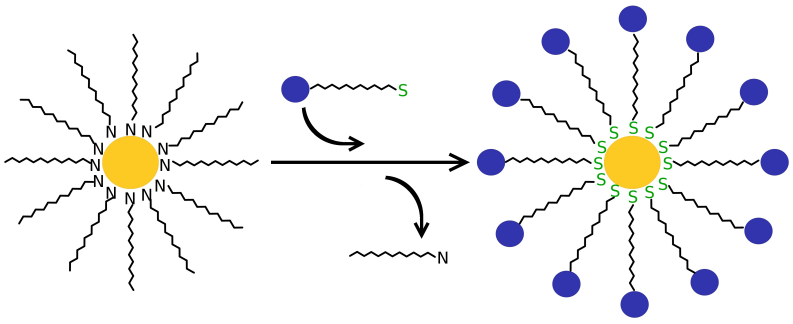

Figure 32: Scheme of the ligand exchange reaction. Yellow and blue circles represent respectively the cores of NPs, and terminal functional groups of ligands.

Preparation of AuMUA

Typically, the solution containing 22 mg of MUA, 4 g of methanol and 5 droplets of tetramethylammonium hydroxide, NMe_4OH, (in the form of 25% solution in methanol) was added to 13 g of crude AuDDA solution. The mixture was allowed to react for at least 1 hour. If the NPs did not precipitate in this time, than about 10 ml of methanol was added to induce precipitation. The precipitate was separated by centrifugation of the sample (3000 - 4000 rpm, 5 - 10 min) and decantation of the supernatant. The precipitate was then washed with ethyl acetate (3 x 15 ml). After each addition of ethyl acetate the sample was centrifuged and the supernatant was decanted. To purify AuMUA the precipitate was dissolved in about 2 ml of deionized water with addition of 3 droplets of NMe_4OH and re-precipitated with 50 ml of acetone. The precipitate was then separated, washed with ethyl acetate (3 x 15 ml) and dried. Finally, dry precipitate was dissolved in 50 g of deionized water with addition of few droplets of NMe_4OH (to adjust the pH to about 11).

Preparation of AuTMA

Analogously to the synthesis of AuMUA, the solution containing 22 mg of TMA and 4 g of methanol was added to 13 g of crude AuDDA solution. The mixture was relaxed for at least an hour. The precipitate was separated (by centrifugation of the sample and decantation of the supernatant) and washed with ethyl acetate (3 x 15 ml). Next, AuTMA was purified by dissolving in 2 ml of methanol and re-precipitating it with about 50 ml of ethyl acetate. The precipitate was again separated, washed with ethyl acetate (3 x 15 ml), dried and finally dissolved in 50 g of deionized water.

Preparation of AgMUA

The solution containing 27 mg of MUA, 1 g of methanol and 4 droplets of NMe_4OH (25% in methanol) was added to 13.4 g of crude AgDA solution. The mixture was relaxed for at least an hour during which the black precipitate appeared. The precipitate was separated (by centrifugation of the sample and decantation of the supernatant) and washed with ethyl acetate (3 x 15 ml). AgMUA was then dissolved in about 1 ml of deionized water with 3 droplets of NMe_4OH and re-precipitated with 50 ml of acetone. The precipitate was again collected, washed with 10 ml of ethyl acetate and dried. AgMUA were finally dissolved in 48.2 g of deionized water with addition of NMe_4OH (to adjust the pH to about 11).

Preparation of AgTMA

The solution of 27 mg of TMA in 1 g of methanol was added to 13.4 g of crude AgDA solution. The mixture was allowed to relax for at least an hour during which precipitation occured. The precipitate was separated (by centrifugation of the sample and decantation of the supernatant) and washed with ethyl acetate (3 x 15 ml). The purification of AgDA was done by dissolving the precipitate in about 2 ml of methanol and re-precipitating it with 40 ml of ethyl acetate. Finally AgTMA were separated, washed with 15 ml of ethyl acetate, dried and dissolved in 48.4 g of water.

2.2.2 UV-Vis titration of oppositely charged nanoparticles

According to the literature, the mixture of oppositely charged NPs is stable as long as the net charge of the NP mixture is different than zero[67]. At this point, called electroneutral point, the precipitation of aggregated NPs occurs. In order to determine the electroneutral point accurately, and define the range of stability of the mixture of oppositely charged NPs, one can perform UV-Vis titration. This result from the fact, that the precipitation of NPs aggregates results in sharp decrease of absorbance of the mixture. UU-Vis titration is based on controlling the changes in absorbance of the mixture caused by successive additions of small portions of NPs of one type.

To explain the procedure for the titration of oppositely charged NPs, let us consider a situation in which the solution of positively charged NPs, AuTMA, is titrated with the solution of negatively charged NPs, AgMUA. Denotr The initial concentrations of the solutions are c^0_{Au} and c^0_{Ag} for AuTMA and AgMUA, respectively. The volumes of AuTMA and AgMUA solutions in the mixture are V_{Au} and V_{Ag}, respectively. At the beginning of the procedure, absorption spectra of both, initial solutions of NPs are collected. After the addition of AgMUA to AuTMA, the mixture is stirred for at least 3 minutes, and then the absorption spectra is collected. The molar fraction of AgMUA NPs, χ_{Ag}, changes during process according to Equation (19) in which N_{Ag} denotes the number of Ag NPs and N_{Au} denotes the number of Au NPs.

$$\chi_{\mathrm{Ag}} = \frac{N_{\mathrm{Ag}}}{N_{\mathrm{Ag}} + N_{\mathrm{Au}}} = \frac{c^0_{\mathrm{Ag}} V_{\mathrm{Ag}}}{c^0_{\mathrm{Ag}} V_{\mathrm{Ag}} + c^0_{\mathrm{Au}} V_{\mathrm{Au}}} \tag{19}$$

Temporary concentrations, c_{Au} and c_{Ag}, of AuTMA and AgMUA NPs in the mixture change according to Equations (20) and (21) respectively.

$$c_{\mathrm{Au}} = \frac{c^0_{\mathrm{Au}}}{1 + \frac{\chi_{\mathrm{Ag}}}{1-\chi_{\mathrm{Ag}}} \cdot \frac{c^0_{\mathrm{Au}}}{c^0_{\mathrm{Ag}}}} \tag{20}$$

$$c_{\mathrm{Ag}} = \frac{c^0_{\mathrm{Au}}}{\frac{1-\chi_{\mathrm{Ag}}}{\chi_{\mathrm{Ag}}} + \frac{c^0_{\mathrm{Au}}}{c^0_{\mathrm{Ag}}}} \tag{21}$$

Application of UV-Vis titration in this dissertation is described in Section 3.2.3.

2.2.3 Fabrication of a Silica-Based Mesophase Doped with Nanoparticles

As it was mentioned in Section 1.2.7, LLC phases can be used to prepare mesoporous materials of a well defined internal structure. To fabricate the silica-based mesophase doped with NPs, I carried out the hydrolysis and condensation of TEOS under basic conditions[162,176]. I used alkaline hydrolysis method because the NPs coated with MUA were stable only in alkaline environment. To obtain the LLC matrix, I induced phase separation in aqueous solution consisting of CTAB (0.20 g), PDDAC (0.63 g) and AuMUA solution (0.63 g). The resulting mass fractions of surfactant and polymer (with respect to water) were 15% and 10% respectively (cf. Equations (22) – (27)). When the phase separation was completed, I removed the polymer-rich phase and characterized surfactant-rich phase using SAXS. The obtained doped LLC phase represented hexagonal ordering with characteristic distance a = 6.25 nm. In order to transform soft LLC phase into silica-based mesophase, I added 0.37 g of TEOS and 0.04 g of NMe_4OH (25 wt. % solution in methanol) to the obtained LLC phase. I mixed the sample for fer minutes and finally I placed in an oven at 100 °C for 20 h in order to complete the condensation process. As prepared silica-based mesophase was characterized using WAXS. The results of this characterization are described in details in Section 3.2.6.

2.3 Characterisation of substances

This Section contains the specification of the substances used in this dissertation. Subtitles below refer to groups of substances used.

Nonionic surfactants

(1) pentaethylene glycol monododecyl ether, ($C_{12}E_5$, Fluka, > 98%)
(2) hexaethylene glycol monododecyl ether, ($C_{12}E_6$, Fluka > 98%)
(3) heptaethylene glycol monododecyl ether, ($C_{12}E_7$, Sigma Aldrich $\geq$98%)
(4) octaethylene glycol monododecyl ether ($C_{12}E_8$, Fluka > 98%)
(5) nonaethylene glycol monododecyl ether ($C_{12}E_9$, Fluka)
(6) decaethylene glycol monododecyl ether ($C_{12}E_{10}$, Sigma Aldrich)
(7) Brij 35 (main component: tricosaethylene glycol dodecyl ether ($C_{12}E_{23}$, Sigma Aldrich).

Cationic surfactants

(1) cetyltrimethylammonium bromide (CTAB, $M_{\mathrm{w}} = 364.46$, Sigma, 99%)
(2) tetradecyltrimethylammonium bromide (TTAB, $M_{\mathrm{w}} = 336,41$, Sigma, 99%)
(3) dodecyltrimethylammonium chloride (DTAC, $M_{\mathrm{w}} = 263,89$, Sigma, 99%)
(4) hexadecylpyridinium bromide (CPB, $M_{\mathrm{w}} = 384,44$, Fluka, 97%)

Anionic surfactants

(1) sodium dodecyl sulfate (SDS, $M_{\mathrm{w}} = 288,38$, Sigma, 98.5%)
(2) dodecanesulfonic acid, sodium salt (DSS, $M_{\mathrm{w}} = 272,38$, Sigma, 99%)

Nonionic polymers

(1) poly(ethylene glycol) (PEG, $M_{\mathrm{w}} \sim$ 20 000, Fluka)
(2) poly(ethylene glycol) (PEG, M_{n} from 570 to 630, Sigma Aldrich)
(3) poly(ethylene glycol) (PEG, M_{w} = 400, Sigma Aldrich)
(4) hexaethylene glycol (PEG, n = 6, Sigma Aldrich, 97%)
(5) tetraethylene glycol (PEG, n = 4, Sigma Aldrich, 99%)
(6) polyvinyl alcohol (PVA, $M_{\mathrm{w}} \sim$ 27 000, Fluka)

Cationic polyelectrolytes

(1) poly(diallyldimethylammonium chloride) (PDDAC, M_w from 100 000 to 200 000, Sigma, 20% aqueous solution)
(2) polyethylenimine (PEI, $M_w \sim 800$, Sigma, 50% aqueous solution)

Anionic polyelectrolytes

(1) poly(sodium 4-styrenesulfonate) (PSS, $M_w \sim 70\,000$, Sigma)
(2) poly(acrylic acid, sodium salt) (PAAS, $M_w \sim 15\,000$, Sigma, 35% aqueous solution)

Inorganic salts

(1) sodium chloride (NaCl, Chempur)
(2) nickel nitrate, hexahydrate ($Ni(NO_3)_2 \cdot 6\,H_2O$, Sigma)
(3) copper sulphate ($CuSO_4$, POCh)
(4) cobalt sulphate, heptahydrate ($CoSO_4 \cdot 7\,H_2O$, POCh)
(5) manganese sulphate, pentahydrate ($MnSO_4 \cdot 5\,H_2O$, Wako Pure Chemicals Industries)
(6) sodium nitrate ($NaNO_3$, Chempur)

Solvents

(1) acetone (99.5%, Chempur)
(2) ethanol (96%, Linegal Chemicals)
(3) methanol (99.8%, POCH Basic)
(4) ethyl acetate (99.8%, POCH Basic)
(5) toluene (99.5%, POCH Basic)

Compounds used for synthesis and functionalization of metal NPs

(1) gold(III) chloride trihydrate ($HAuCl_4$ x 3 H_2O, $\geq$ 99.9%, Sigma Aldrich
(2) silver acetate (CH_3COOAg, 99%, Sigma Aldrich)
(3) didodecyldimethylammonium bromide (DDAB, $\geq$ 98.0%, Fluka)
(4) dodecylamine (DDA, $\geq$ 99.5%, Fluka)
(5) decanoic acid (DA, $\geq$ 98.0%, Sigma)
(6) tetrabutyl ammonium borohydride (TBAB, 98%, Aldrich)
(7) hydrazine (N_2H_4, 98%, Sigma-Aldrich)

(8) tetramethylammoniumhydroxide (NMe_4OH, 25 wt. % solution in methanol, Aldrich)

(9) 11-mercaptoundecanoic acid (MUA, 95%, Sigma Aldrich)

(10) N,N,N-trimethyl(11-mercaptoundecyl) ammonium chloride (TMA, pure, synthesized by M. Paszewski, ICHF PAN)

Formation of mesoporous silica

(1) tetraethyl-orthosilicate (TEOS, $\geq$ 98.0%, Fluka) - silica precursor

Quantum dots

(1) cadmium selenide / zinc sulphide (CdSe/ZnS) core/shell semiconductor nanocrystals coated with octadecylamine and amphiphilic polymer with COO^- surface groups (λ_{em} = 540 nm, quantum yield, QY, > 30%, FWHM = 35 nm, 8μM solution in water, Ocean Nanotech)

(2) cadmium selenide / zinc sulphide (CdSe/ZnS) core/shell semiconductor nanocrystals coated with octadecylamine and amphiphilic polymer with COO^- surface groups (λ_{em} = 620 nm, QY > 50%, FWHM = 25 nm, 8μM solution in water, Ocean Nanotech)

All chemicals were used as delivered. For aqueous solutions, Millipore deionized water (15MΩ cm) was used. Chemical structures of surfactants and polymers are shown in Figure 33. Chemical structures of the main compounds used for synthesis and functionalization of metal NPs are shown in Figure 34. The literature values of the critical micelle concentrations of the surfactants used in experiments are collected in Table 1. Phase diagrams of selected surfactants (both nonionic and ionic) are collected in Figure 35.

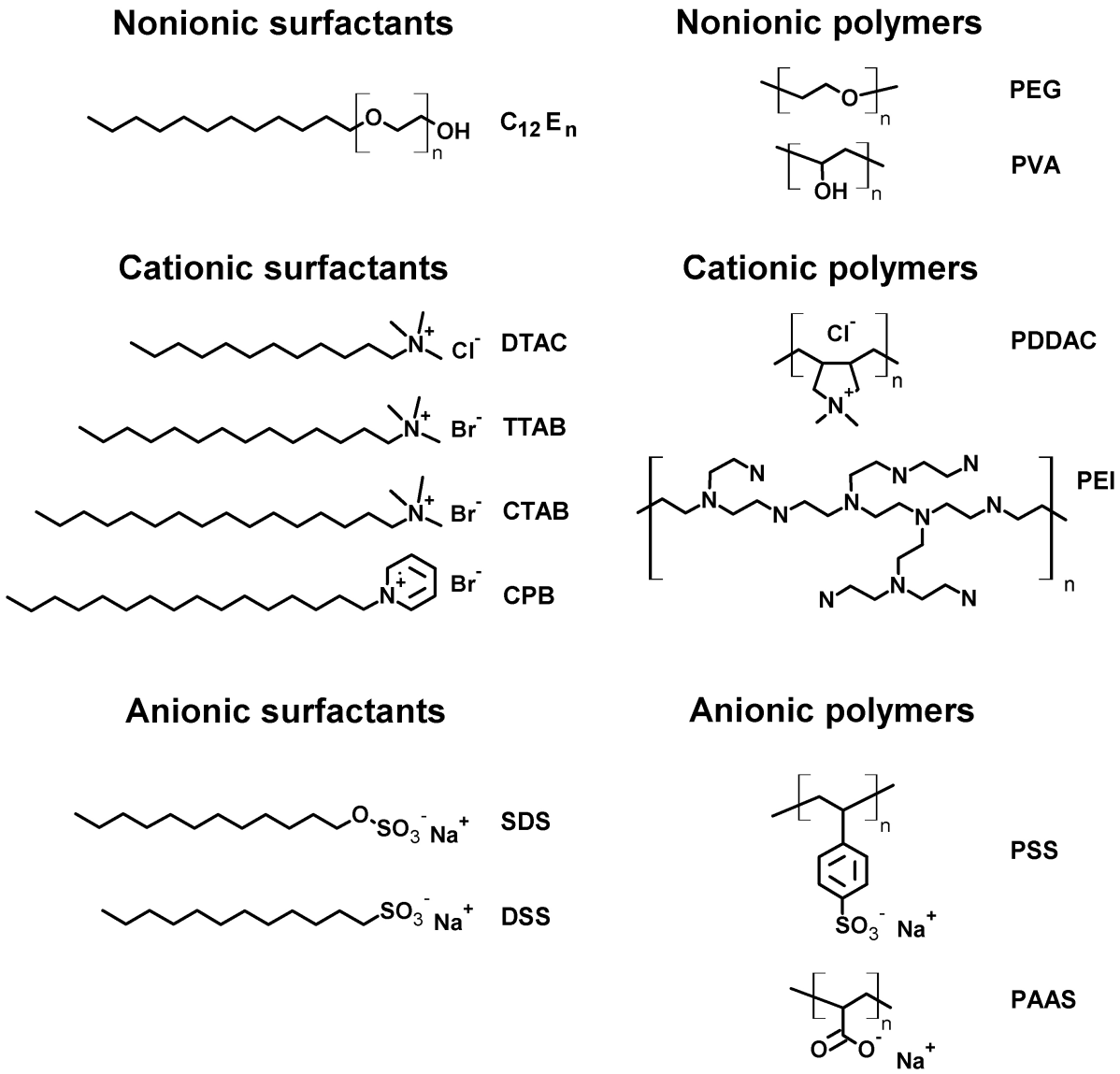

Figure 33: Chemical structures of the surfactants and polymers used in the experiments. Surfactants: oligoethylene glycol monododecyl ethers ($C_{12}E_n$), cetyltrimethylammonium bromide (CTAB), tetradecyltrimethylammonium bromide (TTAB), dodecyltrimethylammonium chloride (DTAC), hexadecylpyridinium bromide (CPB), sodium dodecyl sulfate (SDS), dodecanesulfonic acid, sodium salt (DSS). Polymers: poly(ethylene glycol) (PEG), polyvinyl alcohol (PVA), poly(diallyldimethylammonium chloride) (PDDAC), polyethylenimine (PEI), poly(sodium 4-styrenesulfonate) (PSS), poly(acrylic acid, sodim salt) (PAAS).

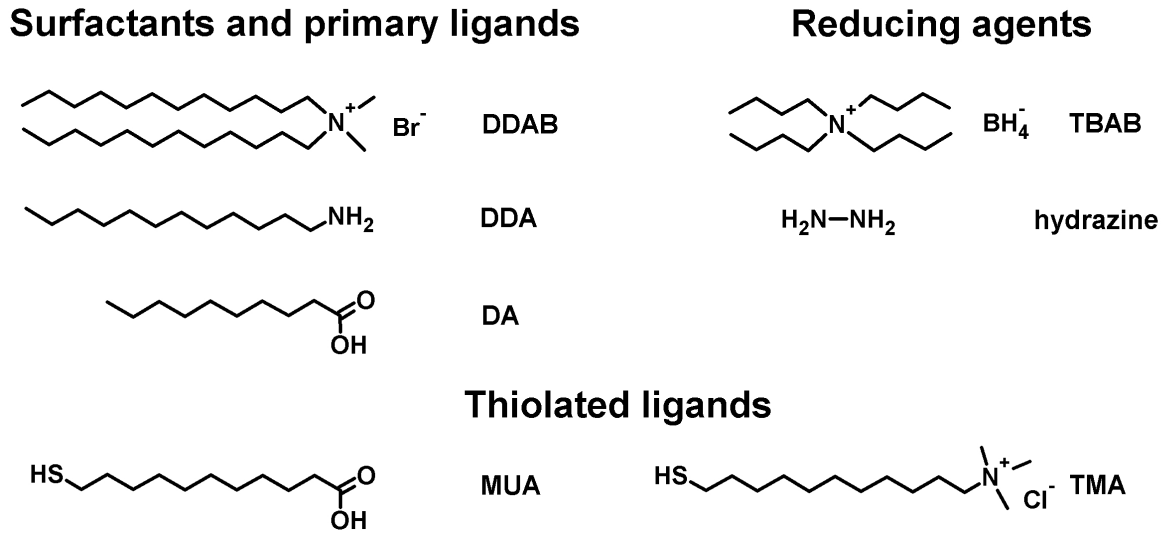

Figure 34: Chemical structures of the main compounds used for synthesis and functionalization of metal NPs. Surfactants and primary ligands: didodecyldimethylammonium bromide (DDAB), dodecylamine (DDA), decanoic acid (DA). Reducing agents: tetrabutyl ammonium borohydride (TBAB), hydrazine. Thiolated ligands: 11-mercaptoundecanoic acid (MUA), N,N,N-trimethyl(11-mercaptoundecyl) ammonium chloride (TMA).

Surfactant	CMC	Reference
$C_{12}E_5$	6.5 $\times 10^{-5}$ M	127
$C_{12}E_6$	6.8 $\times 10^{-5}$ M	127
$C_{12}E_7$	6.9 $\times 10^{-5}$ M	127
$C_{12}E_8$	7.1 $\times 10^{-5}$ M	127
$C_{12}E_9$	1.6 $\times 10^{-4}$ M	177
$C_{12}E_{10}$	8.0 $\times 10^{-5}$ M	178
$C_{12}E_{23}$	3.5 $\times 10^{-5}$ M	179
CTAB	0.9 $\times 10^{-3}$ M	180
TTAB	3.86 $\times 10^{-3}$ M	181
DTAC	21.5 $\times 10^{-3}$ M	182
CPB	0.65 $\times 10^{-3}$ M	183
SDS	8.16 $\times 10^{-3}$ M	184
DSS	8.55 $\times 10^{-3}$ M	185

Table 1: The literature values of CMC of used surfactants.

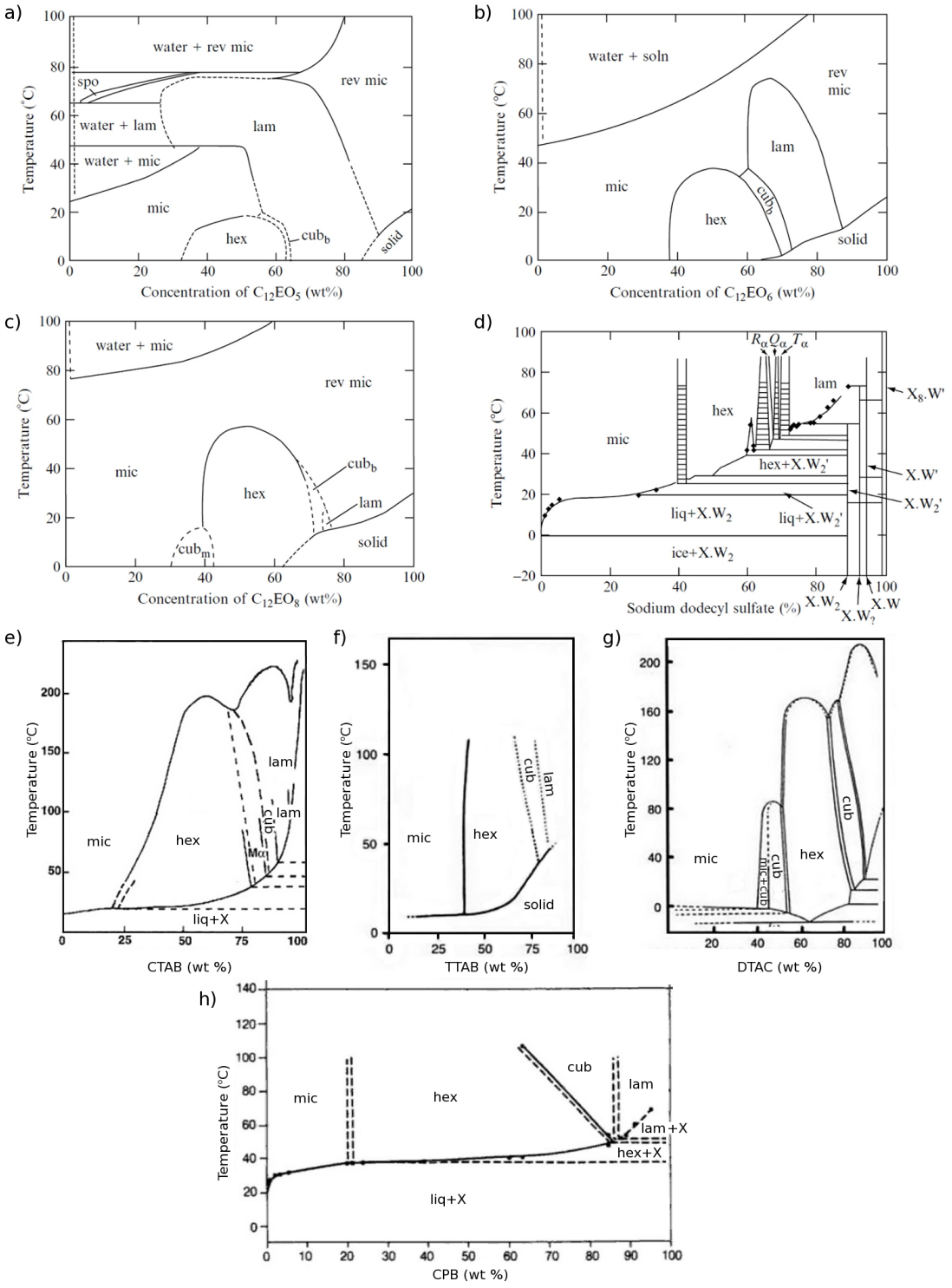

Figure 35: Phase diagrams of selected surfactants used in the research: a) $C_{12}E_5$ [186], b) $C_{12}E_6$ [186], c) $C_{12}E_8$ [186], d) SDS [187], e) CTAB [188], f) TTAB [189], g) DTAC [189], h) CPB [190].

3 Results

This Chapter of the dissertation is divided into three Sections, each of which refers to the following scientific publications: The first Section (3.1) is devoted to the phase separation in systems consisting of ionic surfactants and ionic or nonionic polymers. It is based on the article published in 2010 in Journal of Colloid and Interface Science (Ref. 191).

The second Section (3.2) is devoted to fabrication of soft and solid nanocomposites. It describes the incorporation of hydrophilic NPs (metallic and/or semiconductor) to the ordered phases of lyotropic liquid crystals using polymer-induced phase separation - the method described in Section 3.1. Section 3.2 is based on the research published in 2011 in Langmuir (Ref. 192).

Last Section (3.3) refers to the behavior of NPs in diluted surfactant solutions. In particular, it describes the adsorption of nonionic surfactants the surface of semiconductor QDs. This absorption leads to the quenching of the fluorescence of QDs. Section 3.3 is based on recently obtained results, that are prepared for publication.

3.1 From dilute to condensed systems - polymer induced phase separation for ionic surfactants

3.1.1 Introduction

Solutions of surfactants exhibit a variety of self-assembled structures[193,194]. As it was discussed in Sections 1.2.2 and 1.2.3, they can aggregate to form micelles or vesicles or condense to from ordered structures of complex morphologies. The formation of the ordered structures is based on the phase separation/ordering processes[195–199]. In binary mixtures of surfactant and water the phase transition is caused by the dehydration of the surfactant hydrophilic heads and - at fixed temperature - is controlled by the concentration of the surfactant molecules in the system. The dehydration increases the influence of the van der Waals attraction between the surfactant micelles. In the case of ternary surfactant/polymer/water mixtures the phase separation is driven by different forces. Namely, adding water-soluble polymer to the binary mixture induces attractive interactions between micelles, which is also referred as to the depletion interactions[200]. The depletion interactions are driven by entropy changes. The entropic depletion forces are known to cause phase separation in colloids and emulsions composed of small and large particles[200,201].

In the colloids (or micelles)/polymers mixtures the depletion forces have also geometrical origins and result from changes in the conformational entropy of the polymer chains[149,150,202,203]. Namely, the geometric constrains prevent the center of mass of a polymer molecule from getting closer to the micelle than a certain characteristic distance. This distance is, approximately, a sum of the radius of gyration of a polymer, R_{g}, and the radius of the micelle, r_{mic}. The center of mass of a polymer cannot get closer to the micelle because it would result in a decrease in its conformational entropy. For this reason, when two micelles are separated by a distance smaller than $2(r_{\mathrm{mic}} + R_{\mathrm{g}})$, polymer coils cannot enter between them. As a result, the region between the micelles is depleted with respect to the polymer concentration. The polymers outside the depletion zone between the micelles induce an osmotic pressure causing an effective attraction between the micelles. This osmotic pressure pushes the micelles together and leads to the phase separation into the colloid-rich phase and polymer-rich phase[151].

Walz and Sharma[204] developed a model for calculating the depletion interactions between two charged particles immersed in a solution of like-charged macromolecules. The authors predicted that the electrostatic interactions can increase both the magnitude and range of the depletion forces. The effect of the polyelectrolyte on the stability of solutions of charged particles against aggregation has also been confirmed experimentally[205–207].

As it was mentioned in Section 1.2.6, the phase separation processes induced by the addition of nonionic water-soluble polymers in solutions of nonionic surfactants have recently been investigated[146,147,208]. It has been shown[146] that the addition of poly(ethylene glycol) (PEG) to the aqueous solution of nonionic surfactant $C_{12}E_6$ (n-dodecyl hexaoxyethylene glycol monoether) can result in the separation of the system into the polymer-rich and the surfactant-rich phases. The surfactant-rich phase exhibits hexagonal structure which is composed of cylindrical micelles (channels) packed in a hexagonal array. Also, it has been demonstrated[147] that the hexagonal ordering can be induced provided that (1) the radius of gyration of the polymer added to the system is larger than the size of the water channels in the hexagonal phase, and (2) the polymer reduces the separation temperature to below the temperature of the hexagonal-isotropic phase transition in a binary surfactant-water mixture.

The mixtures of surfactants and polymers have recently been extensively studied[194,209–212] because of their importance to industrial applications[193,209,210]. They play an important role in cosmetics, detergents, pharmaceuticals, pesticides, or enhanced oil recovery. Surfactants, in their ordered phases, can be used as end products themselves or applied as templates[159,213–215] that are further processed to obtain complex micro- or nano-structured materials. For instance, hexagonal phases self-assembled in surfactant mixtures may be filled with metal NPs[152,153].

In this part of the dissertation, I demonstrate for the first time that the electrostatic interactions can enhance the depletion forces in the mixtures of surfactant and polyelectrolyte and lead to the phase separation and further ordering of ionic surfactants. The purpose of this part is to investigate the process of the phase separation in aqueous solutions of ionic surfactants and polyelectrolytes as well as in aqueous solutions of ionic surfactants and nonionic polymers.

Four types of mixtures were studied:

(1) cationic surfactant and cationic polyelectrolyte,
(2) anionic surfactant and anionic polyelectrolyte,
(3) aqueous solutions of cationic surfactant and nonionic polymer,
(4) aqueous solutions of anionic surfactant and nonionic polymer.

In the case of cationic surfactants and nonionic polymers the effect of inorganic salt on the phase separation was also investigated in details. All types of the experiments I performed are schematically represented in Figure 36. As a main result, I show that by adding either the polyelectrolytes or nonionic polymers along with inorganic salts to the surfactant solution one can induce phase separation over a wide range of initial surfactant concentrations. The resulting concentration of surfactant molecules in the surfactant-rich phase is high enough to form ordered structures.

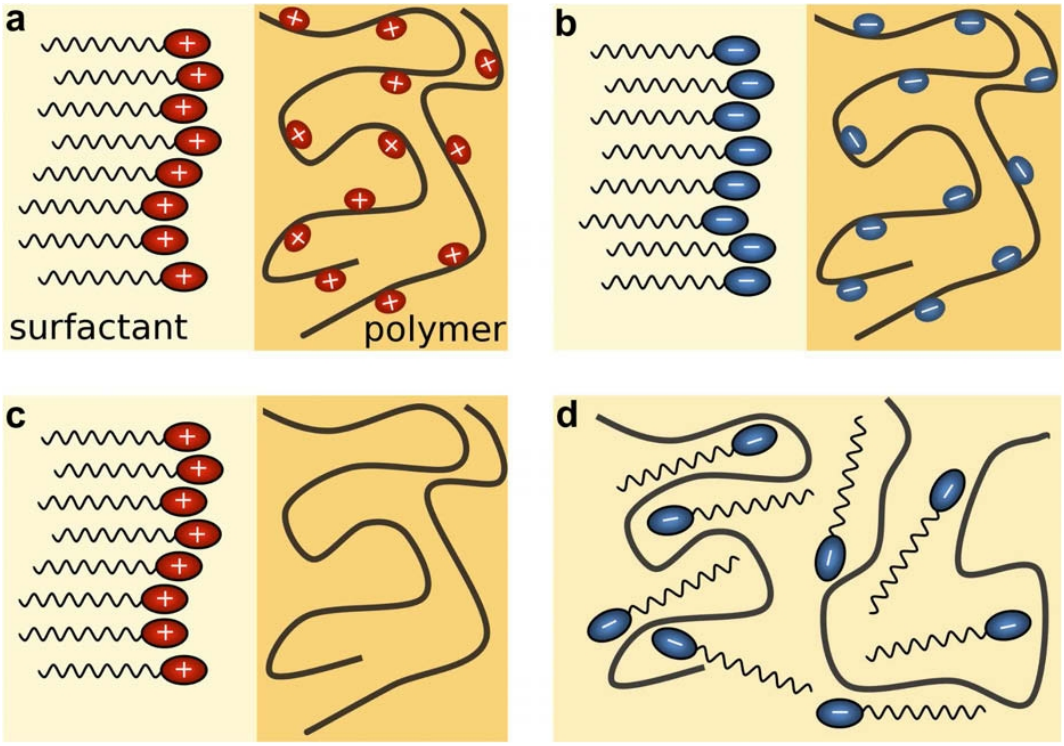

Figure 36: Schematic representation of four types of studied experimental systems: (a) mixture of cationic surfactant and cationic polyelectrolyte, (b) mixture of anionic surfactant and anionic polyelectrolyte, (c) mixture of cationic surfactant and nonionic polymer – either undoped or doped with inorganic salt, and (d) mixture of anionic surfactant and nonionic polymer. For the cases (a) – (c) the phase separation occurs for sufficiently high mass fraction of polyelectrolyte or nonionic polymer and salt. In the case (d) the phase separation was not observed.

3.1.2 Sample preparation

The samples were prepared in ambient conditions at the room temperature (about 25 °C). The solutions were prepared by dissolving surfactants and polyelectrolytes/polymers in a solvent in appropriate weight proportions. As a solvent I applied (i) either pure water or (ii) a mixture of water and one of the two organic polar solvents: acetone or ethanol. To calculate the mass fraction of surfactant, C_{s}, and polymer, C_{p}, in the sample, the following formulas were applied:

$$C_{\mathrm{s}} = \frac{m_{\mathrm{s}}}{m_{\mathrm{s}} + m_{\mathrm{solv}}}, \tag{22}$$

$$C_{\mathrm{p}} = \frac{m_{\mathrm{p}}}{m_{\mathrm{p}} + m_{\mathrm{solv}}}, \tag{23}$$

where m_{s}, m_{p}, m_{solv} are, respectively, the mass of surfactant, polymer, and the solvent. In order to determine the exact mass of polymer and solvent in the sample of a known surfactant and polymer concentration, Equations (22) and (23) needed to be transformed to the following forms.

$$m_{\mathrm{p}} = m_{\mathrm{s}} \frac{C_{\mathrm{p}}(1 - C_{\mathrm{s}})}{C_{\mathrm{s}}(1 - C_{\mathrm{p}})}, \tag{24}$$

$$m_{\mathrm{solv}} = m_{\mathrm{s}} \frac{(1 - C_{\mathrm{s}})}{C_{\mathrm{s}}} \tag{25}$$

$$m_{\mathrm{p}} = \frac{1}{\mathrm{p}} m_{\mathrm{s}} \frac{C_{\mathrm{p}}(1 - C_{\mathrm{s}})}{C_{\mathrm{s}}(1 - C_{\mathrm{p}})}, \tag{26}$$

$$m_{\mathrm{solv}} = m_{\mathrm{s}} \frac{(1 - C_{\mathrm{s}})}{C_{\mathrm{s}}} - (1 - \mathrm{p})\mathrm{m_p}, \tag{27}$$

Equations (24) and (25) were valid in the case of samples, in which the polymer was used in the pure form, whereas Equations (26) and (27) were valid in case where an aqueous polymer solution with a percentage concentration, p. If the solvent was a mixture of water and a polar solvent (acetone or ethanol), the mass of the solvent was calculated as a sum of the mass of water and the mass of the polar solvent, $m_{\mathrm{solv}} = m_{\mathrm{H_2O}} + m_{\mathrm{pol}}$. The amount of the polar solvent, ν, was expressed as the mass fraction,

$$\nu = \frac{m_{\mathrm{pol}}}{m_{\mathrm{sol}}}. \tag{28}$$

In experiments where the system was doped with inorganic salt, the amount of salt was measured relative to the content of the surfactant in the solution, as the molar fraction

$$\phi_{\mathrm{salt}} = \frac{N_{\mathrm{salt}}}{N_{\mathrm{s}}}, \tag{29}$$

where N_{salt} and N_{s} denote, respectively, the number of moles of the salt and the surfactant.

To obtain homogeneous solutions the samples were first heated up to about 60 °C and thoroughly blended using a magnetic stirrer. After that, in order to remove gas bubbles from the bulk of the solution, the samples were ultracentrifuged (using the Hettich Universal 32 centrifuge). Before the examination, the samples were allowed to relax at the room temperature. The mixtures were initially clear (transparent). The process of phase separation was accompanied by the formation of a cloudy phase. The cloudy and the clear phases were separated by a sharp interface and corresponded, respectively, to the surfactant-rich and the polymer-rich phases. If the process of the phase separation took place, the cloudy phase showed up usually 1 or 2 h after the sample preparation. If the sample remained clear for more than 10 h I assumed that the phase separation does not occur. Typically, the volume of the sample was about 10 cm^3.

To determine the threshold concentrations of salt in the experiments with the solutions of CTAB and PEG doped with NaCl, the salt was added successively to the system starting from the molar fraction $\phi_{\mathrm{salt}} = 0$. The amount of salt was increased by either 0.05 or 0.1. Each time after the addition of NaCl the solutions were blended using magnetic stirrer at the room temperature and then relaxed for a couple of hours. A photograph of the sample – a mixture of CTAB (C_{s} = 15%) and PEG (C_{p} = 5%) doped with NaCl ($\phi_{\mathrm{salt}} = 0.6$) – taken before and after the phase separation is shown in Figure 37.

3.1.3 Optical studies

When the separation process took place, the cloudy (surfactant-rich) phase was further investigated with the optical microscopy with the purpose of determining whether it represents an ordered or disordered phase. The samples for the microscope studies were prepared in the following way (cf. Figure 38). First, with the aid of a syringe, a small portion of the cloudy phase was placed between two glass plates of the diameter of about 15 mm. Prior to use, the plates were cleaned in the ultrasound cleaner and washed in acetone and methanol. The dis-

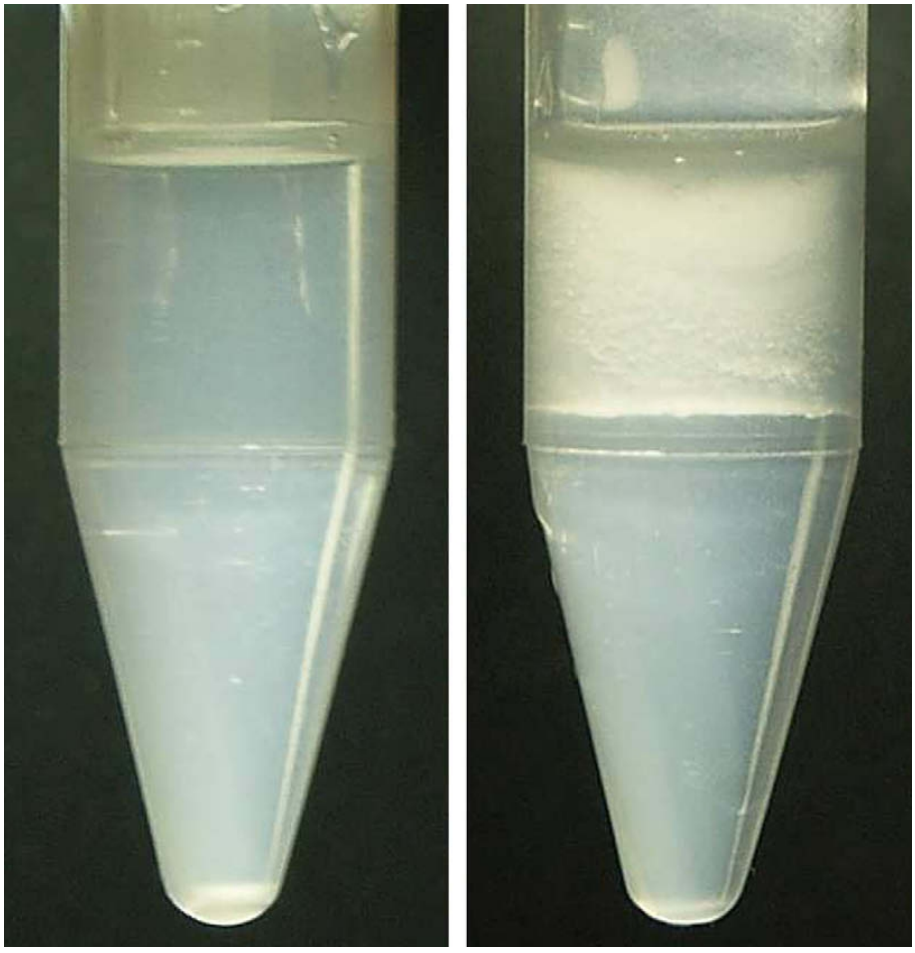

Figure 37: The mixture of CTAB (C_{s} = 15%) and PEG (C_{p} = 5%) doped with NaCl ($\phi_{\mathrm{salt}} = 0.6$) before (left) and after (right) the phase separation process. The cloudy and the clear region in the right picture corresponds to the surfactant-rich and the polymer-rich phase, respectively. The time difference between the pictures is about five hours.

tance between the plates – controlled with the use of aluminum spacers – was 100 μm. Finally, the sample was sealed with the glue "Poxipol" to prevent water from evaporating during the observations. The sample was investigated using optical microscope equipped with crossed polarizers. To determine the type of the ordering, the texture of the sample was compared to the textures of the hexagonal phases formed by aqueous solutions of the surfactant (with known type of ordering, based on the phase diagrams[193,194,216]). An example of the texture of the surfactant-rich phase obtained from the CTAB/PDDAC/water ternary mixture and the texture of the hexagonal phase observed in CTAB/water binary mixture (25 wt.-%) is shown in Figure 39.

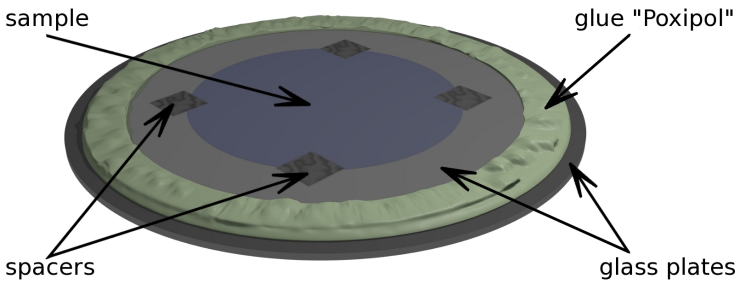

Figure 38: Scheme of sample prepared for polarized optical microscopy studies.

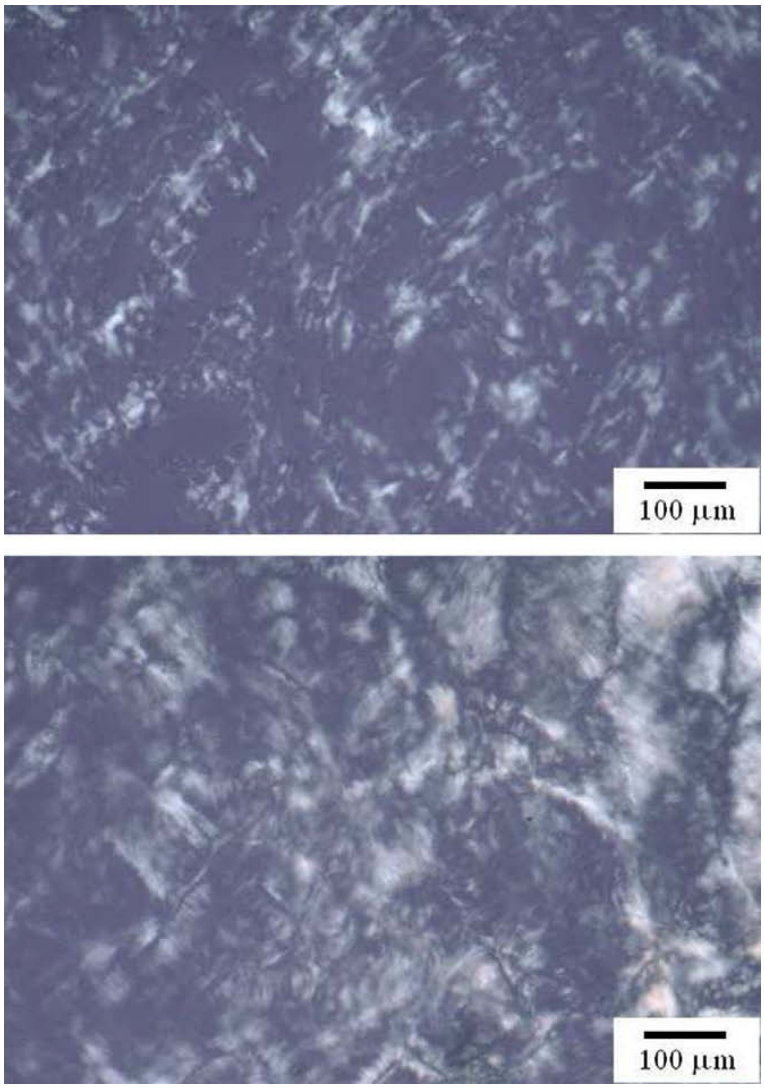

Figure 39: The photograph of the texture of the surfactant-rich phase which emerged in the mixture of CTAB (C_{s} = 5%) and PDDAC (C_{p} = 16%) as a result of the phase separation (top), and (bottom) the texture of the hexagonal phase observed in the aqueous solution of CTAB at the surfactant mass fraction 25 wt. %, at the temperature 25 °C. Pictures obtained from the optical microscopy under crossed polarizers. As seen, the concentration of the surfactant molecules in the surfactant-rich phase is high enough to induce the hexagonal ordering.

3.1.4 Phase separation in mixtures of ionic surfactants and polyelectrolytes

I. Cationic surfactant and cationic polyelectrolyte

To investigate the phase separation in the system composed of cationic surfactant and cationic polyelectrolyte I performed a systematical study of aqueous solutions of CTAB and PDDAC. We employed the CTAB/PDDAC mixtures for the following seven mass fractions of the surfactant: 3%, 5%, 7%, 10%, 12%, 15%, and 20%. For each of the above mass fractions of CTAB, I determined the threshold mass fractions, $C_{\mathrm{p}}^{\star}$, of PDDAC. The threshold mass fraction was estimated in the following way: For the mass fractions of the polyelectrolyte lower than $C_{\mathrm{p}}^{\star}$ the mixture did not separate, for the mass fractions higher than $C_{\mathrm{p}}^{\star}$ it separated into the surfactant-rich and the polyelectrolyte-rich phases. I found that the phase separation can be induced by addition of the polyelectrolyte for a wide range of the surfactant mass fractions. I observed the separation in the systems in which the mass fraction of CTAB was close to that corresponding to the spontaneous ordering of the hexagonal phase in the binary mixture CTAB/water (about 20 wt.%) as well as in the mixtures of low mass fraction of the surfactant. I found that the amount of the polyelectrolyte needed to induce the phase separation process decreased with the mass fraction of the surfactant. In the mixture of high surfactant mass fraction, containing 15% CTAB, the phase separation was induced by a small admixture (of the order of 2.5%) of PDDAC. In the mixture of low surfactant mass fraction ($\sim$ 3%), the phase separation took place when the mass fraction of the polyelectrolyte reached about 18.5%. The dependence of the threshold mass fraction of the polyelectrolyte on the surfactant mass fraction for the CTAB/PDDAC/ water ternary mixture studied is shown in Figure 40.

The analysis of the textures, carried out using the optical microscopy under crossed polarizers, revealed that for all mass fractions of CTAB used, the surfactant-rich phases exhibited the hexagonal order. This result is not surprising in view of the fact that at the temperatures higher than 20 °C the first ordered phase observed in the CTAB/water binary mixture is the hexagonal phase[194], which occurs for the mass fraction of CTAB about 25% (cf. phase diagram of CTAB shown in Figure 35).

Note also that the molar concentration corresponding to the surfactant mass fraction C_{s} = 3%, at which the phase separation was observed in my experiments is, approximately, only 80 times bigger than the critical micelle concentration, $\mathrm{CMC}_{\mathrm{CTAB}}$ = 0.9 mM[180]. Thus, by addition of the polyelectrolyte I can induce the phase separation in a wide range of the surfactant concen-

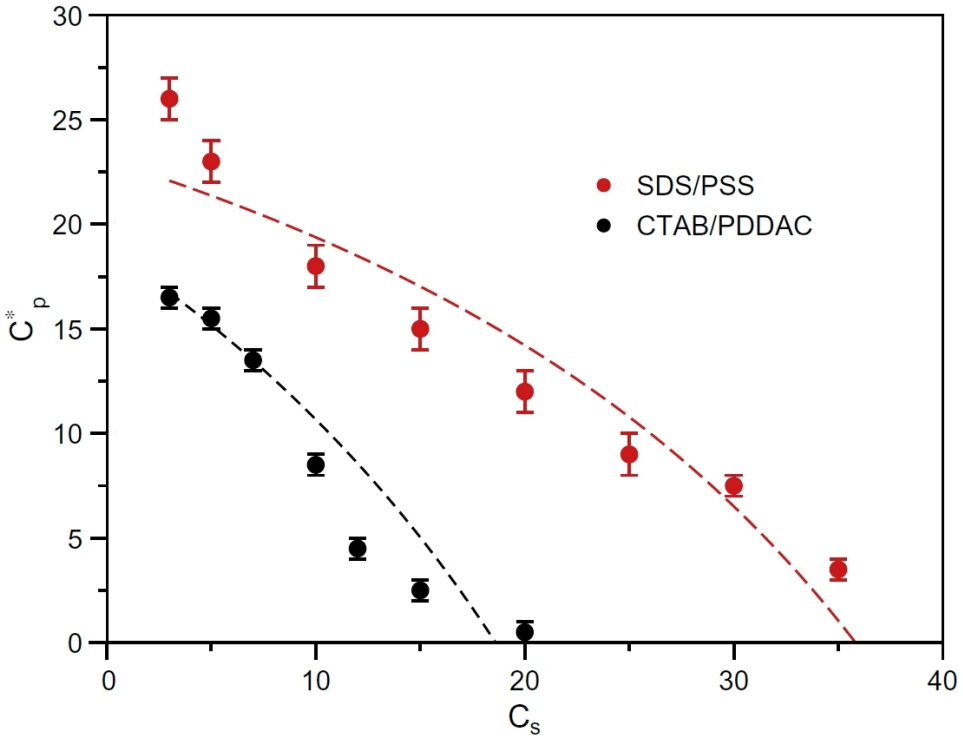

Figure 40: Phase diagram for the aqueous solutions of CTAB/PDDAC (cationic surfactant/cationic polyelectrolyte) and SDS/PSS (anionic surfactant/anionic polyelectrolyte) plotted in the surfactant mass fraction (C_s) – polyelectrolyte mass fraction (C_p) plane. The data points represent the threshold mass fractions, $C_\mathrm{p}^\star$, of the polyelectrolytes needed to induce the phase separation process. The threshold mass fractions were determined for selected mass fractions of the surfactant at the temperature 25 °C. For the mass fractions of the polyelectrolytes higher than $C_\mathrm{p}^\star$ the mixtures separate into the surfactant-rich and the polymer-rich phases. The dashed lines represent least-squares fit of Equation (40) to the experimental data.

trations.

To demonstrate the robustness of the effect studied I also carried out a number of experiments with other cationic surfactants: TTAB, CPB, and CTAB, and two other cationic polyelectrolytes: PDDAC and PEI. As a solvent either water, mixtures of ethanol and water, or mixtures of acetone and water was used. I did not perform detailed studies of the phase diagram for these systems. That is, in contrast to the CTAB/PDDAC/water system, I did not determine the threshold mass fractions of the polyelectrolytes. The aim of the experiments was simply to show that it is possible to find the mass fraction of the polyelectrolyte, C_p, at which the phase separation occurs for given mass fraction of the surfactant, C_s. The results of the experiments are summarized in Table 2. The values of C_p listed in the last column represent the mass fractions of the polyelectrolyte that was sufficient to induce the phase separation.

surfactant	polyelectrolyte	solvent	$C_{\rm s}$ (wt %)	$C_{\rm p}$ (wt %)
TTAB	PDDAC	w	20	20
TTAB	PDDAC	w	30	10
TTAB	PEI	w	30	20
TTAB	PDDAC	w+a (5%)	30	10
CPB	PDDAC	w	15	5
CPB	PDDAC	w+a (5%)	15	10
CTAB	PDDAC	w+a (5%)	10	15
CTAB	PDDAC	w+a (95.5%)	15	15
CTAB	PDDAC	w+e (5%)	15	10

Table 2: Examples of the polymer-induced phase ordering observed in different cationic surfactant/cationic polyelectrolyte systems. The symbols "w", "w+a", and "w+e" refer, respectively, to water, mixture of water and acetone, and mixture of water and ethanol. The numbers in brackets denote the amount of acetone/ethanol, ν, in the solvent mixture (see Equation (28)). The polymer mass fractions, $C_{\rm p}$, are not the threshold mass fractions. The values of the threshold mass fractions have been investigated in detail only for the CTAB/PDDAC/water system. Here I only show that the same effect is observed for other systems.

II. Anionic surfactant and anionic polyelectrolyte

To study the phase separation in the system composed of anionic surfactant and anionic polyelectrolyte I employed aqueous solutions of SDS and PSS. The SDS/PSS/water ternary mixture was investigated for the following nine mass fractions of SDS: 3%, 5%, 10%, 15%, 20%, 25%, 30%, 35%, and 40%. For each of the above mass fractions of the surfactant, we determined the threshold mass fractions of the polyelectrolyte, $C_{\rm p}^{\star}$, above which the phase separation was observed. I found that for all the surfactant mass fractions the phase separation process can be induced by increasing the content of the polyelectrolyte in the mixture. As in the case of the cationic surfactant/cationic polyelectrolyte system discussed previously, I observed that the amount of the polyelectrolyte necessary for the phase separation process to occur decreased with the mass fraction of the surfactant. For example, in the mixture of high SDS content ($C_{\rm s}$ = 35%), the phase separation was induced by a relatively small amount of PSS ($C_{\rm p} \sim 3.5\%$) in the solution. In the mixture of low surfactant mass fraction ($C_{\rm s}$ = 3%), the phase separation occurred for the mass fraction of the polyelectrolyte $C_{\rm p} \sim 26\%$. The dependence of the threshold polyelectrolyte mass fraction on the surfactant mass fraction for the system

studied is presented in Figure 40. Based on the optical microscopy studies of the textures, I found that for all the mass fractions of SDS, the surfactant-rich phases represented the hexagonal ordering. I also noted that the amount of surfactant in the mixture (C_{s} = 3%) at which the phase separation was induced is, approximately, only 13 times bigger than the critical micelle concentration, $\mathrm{CMC_{SDS}}$ = 8.16 mM[184].

I also investigated three other systems: SDS/PAAS/water, DSS/PAAS/water, and a solution of SDS and PSS in the mixture of water and acetone. My goal was to confirm the effect of polyelectrolyte on the phase separation and to demonstrate that it is possible to find the mass fraction of the polyelectrolyte, C_{p}, at which the phase separation takes place for given mass fraction of the surfactant, C_{s}. In contrast to the SDS/PSS/water system, I did not perform detailed studies of the phase diagram and did not determine the threshold mass fractions of the polyelectrolytes. The results of the experiments are summarized in Table 3.

surfactant	polyelectrolyte	solvent	C_{s} (wt %)	C_{p} (wt %)
SDS	PAAS	w	10	20
SDS	PSS	w + a (5%)	15	20
DSS	PAAS	w	10	15

Table 3: Examples of the polymer-induced phase ordering observed in different anionic surfactant/anionic polyelectrolyte systems. The symbols "w", "w+a", stand for water and mixture of water and acetone, respectively. The number in bracket denotes the content, ν, of acetone in the solvent mixture (see Equation (28)). The polymer mass fractions, C_{p}, are not the threshold mass fractions. The values of the threshold concentration have been investigated in detail only for the SDS/PSS/water system. Here I only show that the same effect is observed for other systems.

III. Effect of inorganic salt

To investigate the effect of salt on the phase separation, I conducted series of experiments on both the SDS/PSS/water and CTAB/ PDDAC/water systems employing NaCl as the inorganic salt. The experiments were carried out at the temperature 25 °C. I found that in each system the addition of the salt resulted in lowering of the mass fraction of the polyelectrolyte, $C_{\mathrm{p}}^{\star}$, needed to induce the phase separation. However, for the systems studied, the salt added without the polyelectrolyte did not induce the hexagonal ordering in the surfactant-rich phase. The dependence of $C_{\mathrm{p}}^{\star}$ on the molar fraction of NaCl for the SDS/PSS/water system for the surfactant

mass fraction C_s = 20% is shown in Figure 41. As seen, $C_p^\star$ decreases with the increasing content of the salt added and saturates at about ϕ_{salt} = 1.0. Similar effect was observed for the CTAB/PDDAC/water system. For this system, for the surfactant mass fraction C_s = 10%, I found that the addition of NaCl lowers the threshold mass fraction of the polyelectrolyte from $C_p^\star$ = 9.5% (observed for ϕ_{salt} = 0.0) to $C_p^\star$ = 2.5% for ϕ_{salt} = 1.0.

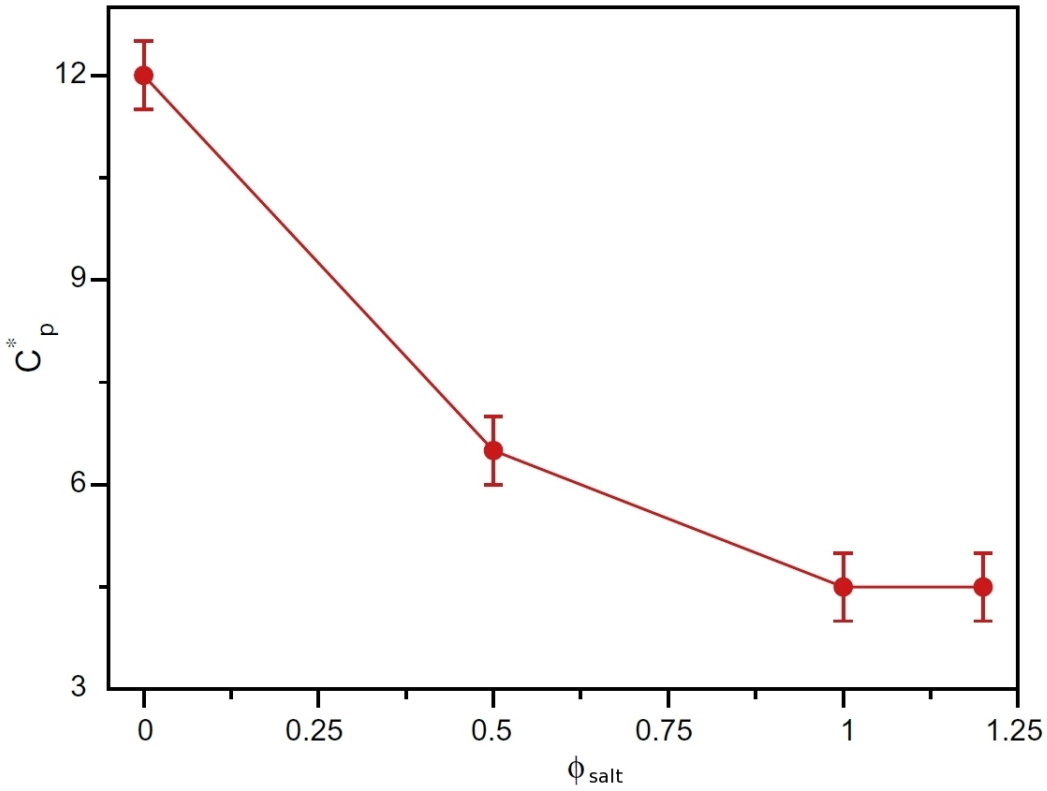

Figure 41: The threshold mass fraction, $C_p^\star$, of the polyelectrolyte (PSS) needed to induce the phase separation/ordering process in the SDS/PSS/water system as a function of the molar fraction, (ϕ_{salt}), of the NaCl added. The mass fraction of the surfactant (SDS) is C_s = 20%, the experiment was conducted at the temperature 25 °C. For the mass fractions of the polyelectrolyte higher than $C_p^\star$ the mixtures separate into the ordered (hexagonal) surfactant-rich and the polymer-rich phases. The solid lines are plotted as guides for the eye.

3.1.5 Phase separation in mixtures of ionic surfactants and nonionic polymers

I. Cationic surfactant and nonionic polymer doped with inorganic salt Aqueous solutions of CTAB and PEG were used to investigate the phase separations in cationic surfactant/nonionic polymer system. I studied three surfactant mass fractions of CTAB: 10%, 15%, and 20%, and the mass fractions of PEG in the range from 1% to 50%. For each the mass fractions I examined the effect of the salt on the phase separation. I found that for each of the mass fractions of CTAB

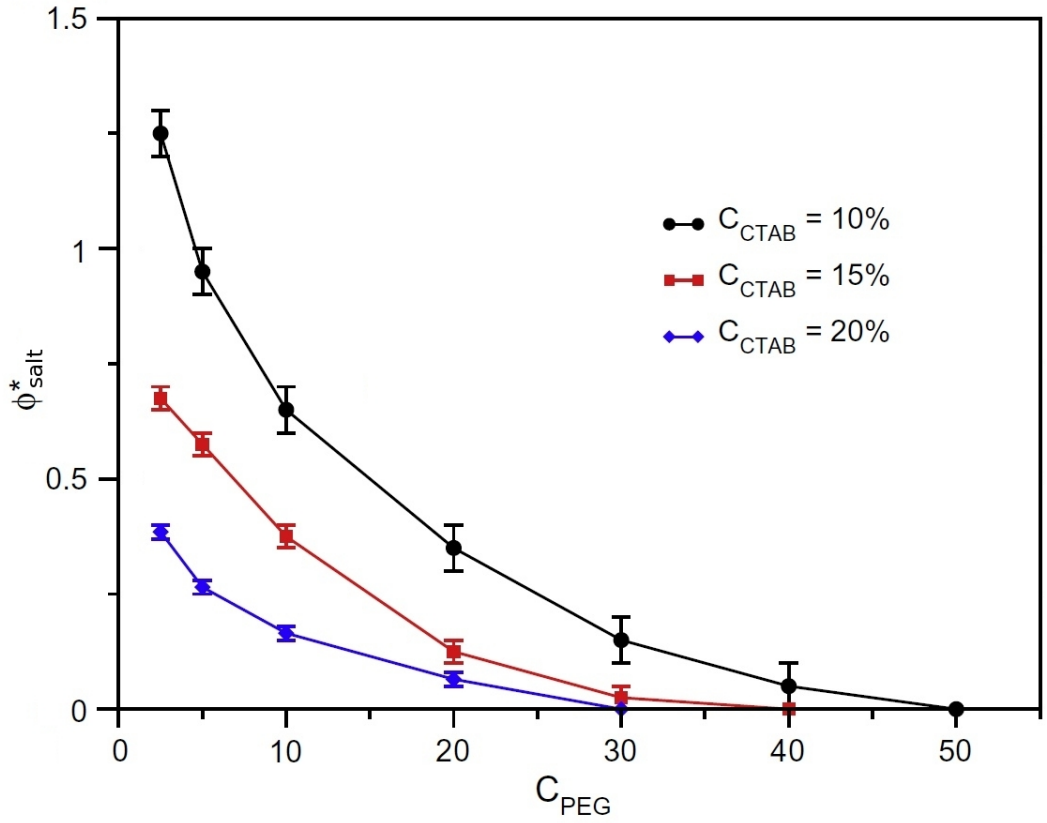

Figure 42: The threshold molar fraction, $\phi^{\star}_{\rm salt}$, of NaCl needed to induce the phase separation in the aqueous solutions of CTAB/PEG/NaCl at the temperature 25 °C, plotted as a function of the mass fraction of PEG for three mass fractions of CTAB: 10, 15, and 15%. The solid lines are drawn as guides for the eye. For the molar fractions of the salt above $\phi^{\star}_{\rm salt}$ the system separates into the surfactant- and the polymer-rich phases.

studied there existed two threshold mass fractions of PEG: (i) the upper threshold mass fraction, $C^{\rm up}_{\rm PEG}$, above which the phase separation takes place without the addition of the salt, and (ii) the lower threshold mass fraction, $C^{\rm low}_{\rm PEG}$, below which the phase separation could not be induced by the addition of the salt. The values of $C^{\rm up}_{\rm PEG}$ decreased with the mass fraction of CTAB. For the mass fractions of CTAB $C_{\rm s}$ = 10%, 15%, and 20%, the upper threshold mass fractions of PEG,

$C^{\rm up}_{\rm PEG}$, were estimated as 50%, 40%, and 30%, respectively. The value of the lower threshold mass fraction was approximately the same for the three mass fractions of CTAB studied. It was estimated as $C^{\rm low}_{\rm PEG} \approx 2\%$.

For each mass fraction of CTAB, for the mass fractions of PEG in the range between $C^{\rm low}_{\rm PEG}$ and $C^{\rm up}_{\rm PEG}$, I determined the threshold molar fraction of NaCl, $\phi^{\star}_{\rm salt}$, representing the minimal amount of the salt needed to induce the phase separation. If the amount of NaCl was lower than $\phi^{\star}_{\rm salt}$ the mixture did not separate; for $\phi_{\rm salt} \geq \phi^{\star}_{\rm salt}$ the mixture separated into the surfactant-rich and the polyelectrolyte-rich phases. The values of $\phi^{\star}_{\rm salt}$ as a function of the mass fraction of PEG are plotted for three mass fractions of CTAB in Figure 42. From the optical microscopy studies of the textures, I found that for all mixtures, the surfactant-rich phase represented the hexagonal ordering. I also confirmed the robustness of the effect of inorganic salt on the phase separation by studying variety of other systems being aqueous solutions of cationic surfactants and nonionic polymers. The aim of my experiments was to find – for a given mass fraction of surfactant and polyelectrolyte – the molar fraction of inorganic salt that was sufficient to induce the phase separation. In contrast to the CTAB/PEG/water system, I did not find the threshold molar fraction of salt needed to induce the phase ordering. Results of the experiments are presented in Table 4. Note that for each mixture listed in Table 4 the phase separation did not take place in the absence of inorganic salt.

II. Anionic surfactant and nonionic polymer

To study the phase separation in the system composed of anionic surfactant and nonionic polymer I used solutions of SDS and PEG. I investigated mixtures of the following percentage compositions of the surfactant and the polymer: (10%, 0.5 – 60%), (20%, 5 – 30%), (30%, 5 – 35%), (35%, 5 – 20%), and (45%, 5 – 30%). The first terms in the brackets refer to the mass fractions of SDS, and the second terms denote the ranges of the mass fractions of PEG employed. In the experiments, the mass fractions of the polymer were sampled with $\Delta C_{\rm p}$ = 5%. Note here that the viscosity of the mixture increases rapidly with the content of PEG. For this reason I did not use samples with the polymer mass fractions higher than about 60%. For any of the mixtures studied the phase separation process did not occur. Also, in order to check possible effect of inorganic salt on the phase separation, for selected mass fractions of SDS, NaCl was added to the mixture. I found that the salt induced the phase separation only for the

surfactant	polymer	salt	C_{s} (wt %)	C_{p} (wt %)	ϕ_{salt}
CTAB	PEG	$Ni(NO_3)_2 \cdot 6\,H_2O$	10	10	0.7
CTAB	PEG	$CuSO_4$	10	10	0.7
CTAB	PEG	$CoSO_4 \cdot 7\,H_2O$	10	10	0.7
CTAB	PEG	$MnSO_4 \cdot 5\,H_2O$	10	10	0.7
CTAB	PEG	$NaNO_3$	10	10	0.7
CTAB	PVA	NaCl	20	30	1.0
TTAB	PEG	NaCl	10	10	1.3
TTAB	PEG	NaCl	15	10	0.6
TTAB	PVA	NaCl	30	3	1.0
CPB	PEG	NaCl	10	10	1.0
CPB	PEG	NaCl	15	10	0.6
CPB	PVA	NaCl	18	3	1.0
CPB	PVA	$CoSO_4 \cdot 7\,H_2O$	18	3	1.0
CPB	PVA	$Ni(NO_3)_2 \cdot 6\,H_2O$	18	3	0.8
DTAC	PEG	NaCl	35	15	1.5

Table 4: Examples of the phase ordering induced in different cationic surfactant/nonionic polymer systems doped with inorganic salt. For each mixture listed, the phase separation did not occur in the absence of the salt. The molar fractions, ϕ, are not the threshold fractions. The values of the threshold molar fractions have been investigated in detail only for the mixture CTAB/PEG/water doped with NaCl. Here I only demonstrate that the same effect is observed for other systems.

highest total mass fractions of PEG and SDS, when the salt was added in a relatively high molar fraction ($\phi_{\mathrm{salt}} = 2.0$).

3.1.6 Discussion

I. Ionic surfactant/polyelectrolyte

The mechanism of the polyelectrolyte-induced phase separation in the ionic surfactant/-polyelectrolyte system can be explained in terms of the chemical potential of water in the surfactant- and polymer-rich phases. It was found in Ref. 146 that the interface between these two coexisting phases acts as a semipermeable membrane[217]. That is, this interface is permeable to water (and small ions) but not to large polyelectrolyte molecules. Therefore, the thermodynamic equilibrium in the system is determined by the equality of the chemical potential of water in the surfactant-rich phase, $\mu^{surf}_{\mathrm{H_2O}}$, and in the polymer-rich phase, $\mu^{poly}_{\mathrm{H_2O}}$,

$$\mu^{surf}_{\mathrm{H_2O}}(x^{surf}_{\mathrm{H_2O}}) \;=\; \mu^{poly}_{\mathrm{H_2O}}(x^{poly}_{\mathrm{H_2O}}), \tag{30}$$

where $x^{surf}_{\mathrm{H_2O}}$ and $x^{poly}_{\mathrm{H_2O}}$ denote, respectively, molar fraction of water in the surfactant- and the polymer-rich phase. The chemical potentials are the following functions of the activities, $a^{surf}_{\mathrm{H_2O}}$ and $a^{poly}_{\mathrm{H_2O}}$, of water in the surfactant-rich and the polymer-rich phase:

$$\mu^{surf}_{\mathrm{H_2O}}(x^{surf}_{\mathrm{H_2O}}) \;=\; \mu^{0}_{\mathrm{H_2O}} + RT\ln a^{surf}_{\mathrm{H_2O}}, \tag{31}$$

$$\mu^{poly}_{\mathrm{H_2O}}(x^{poly}_{\mathrm{H_2O}}) \;=\; \mu^{0}_{\mathrm{H_2O}} + RT\ln a^{poly}_{\mathrm{H_2O}}, \tag{32}$$

where $\mu^{0}_{\mathrm{H_2O}}$ denotes the chemical potential of water in the standard state, T is the temperature, and R is the gas constant. The water activities are linked with the molar fractions by the relations $a^{surf}_{\mathrm{H_2O}} = \gamma^{surf}_{\mathrm{H_2O}} x^{surf}_{\mathrm{H_2O}}$, and $a^{poly}_{\mathrm{H_2O}} = \gamma^{poly}_{\mathrm{H_2O}} x^{poly}_{\mathrm{H_2O}}$, where $\gamma^{surf}_{\mathrm{H_2O}}$ $\gamma^{poly}_{\mathrm{H_2O}}$ denote, respectively, the activity coefficients of water in the surfactant and polymer-rich phase. The molar fractions of water both in the surfactant- and polymer-rich phase are close to unity, and, consequently, $\gamma^{surf}_{\mathrm{H_2O}} \approx \gamma^{poly}_{\mathrm{H_2O}} \approx 1$. Thus, from Equations (30), (31), and (32) one gets

$$\ln x^{surf}_{\mathrm{H_2O}} \;=\; \ln x^{poly}_{\mathrm{H_2O}}, \tag{33}$$

The molar fraction of water in the surfactant-rich phase can be estimated based on the molar fraction, x_{surf} of the surfactant. The space between the charged micelles is filled with water and the counterions released by the surfactant molecules (Na^+ for SDS and Br^- for CTAB). Some

fraction of the counterions are bound to the surface of the micelles and form an immobile layer (referred also to as the Stern layer). The rest of the counterions are weakly associated with the micelles and form a diffuse layer. Only the latter affect the molar fraction of water in the surfactant-rich phase. Denote the fraction of the diffuse ions by ψ ($\psi \leq 1$). Then, $x_{\mathrm{H_2O}}^{surf}$ is given by

$$x_{\mathrm{H_2O}}^{surf} \approx 1 - \psi x_{\mathrm{surf}}. \tag{34}$$

In the polymer-rich phase two types of ions are present: the charged polyelectrolyte molecules and the accompanying counterions (Na^+ for PSS and Cl^- for PDDAC). If I denote the average number of counterions released from the dissociation of the polyelectrolyte molecule as n ($n \gg 1$) the molar fraction of water in the polymer-rich phase is given by

$$x_{\mathrm{H_2O}}^{poly} = 1 - (1+n)x_{\mathrm{poly}} \approx 1 - nx_{\mathrm{poly}}, \tag{35}$$

where x_{poly} is the molar fraction of the polyelectrolyte molecules in the polymer-rich phase. From Equations (33), (34), and (35), one gets the following condition for the quality of the chemical potentials of water in both the phases:

$$\psi x_{\mathrm{surf}} = n x_{\mathrm{poly}}, \tag{36}$$

I note that, in general, the exchange of small ions between the polymer- and surfactant-rich phases can occur. That is, the counterions released from the surfactant molecules can migrate to the polymer-rich phase and these released from the dissociation of the polyelectrolyte molecules migrate to the surfactant-rich phase. However, the number of polyelectrolyte molecules in the polymer-rich phase and the number of surfactant molecules in the surfactant-rich phase remains unchanged. Thus, to maintain the electrical neutrality, the total number of counterions of either type is constant in both the phases. It follows that the molar fractions of the counterions are fixed. Consequently, the condition (36) is valid even if the surfactant and the polyelectrolyte releases different types of counterions, provided they are monovalent.

The relation (36) allows to predict the amount of polyelectrolyte needed to induce the phase separation in the system. Denote by $C_{\mathrm{s}}^{\mathrm{m}}$ the minimal mass fraction of the surfactant in the

surfactant-rich phase needed to get an ordered (hexagonal) phase. If the mixture separates into the polymer- and the surfactant-rich phase, the ordering takes place in the latter phase when the mass fraction, $C_{\rm s}$, of the surfactant in this phase is larger than or equal to $C_{\rm s}^{\rm m}$. In the following, I find the mass of the polyelectrolyte, $m_{\rm p}$, that has to be added to the binary solution of surfactant/water of the mass fraction $C_{\rm s}$ to induce the ordering in the surfactant-rich phase after the phase separation. At equilibrium, water distributes between the two coexisting phases according to Equation (36). The mass of the surfactant, $m_{\rm s}$, that is sufficient to induce the phase ordering corresponds to the mass fraction of the surfactant equal to $C_{\rm s}^{\rm m}$. The mass of water, $m_{\rm H_2O}^{surf}$, in the surfactant-rich phase is then given by

$$m_{\rm H_2O}^{surf} = \frac{1-C_{\rm s}^{\rm m}}{C_{\rm s}^{\rm m}} m_{\rm s}, \tag{37}$$

The total mass, $m_{\rm H_2O}$ of water in the system is

$$m_{\rm H_2O} = \frac{1-C_{\rm s}}{C_{\rm s}} m_{\rm s}. \tag{38}$$

The conservation of the mass of water yields

$$m_{\rm H_2O}^{surf} + m_{\rm H_2O}^{poly} = m_{\rm H_2O}, \tag{39}$$

where $m_{\rm H_2O}^{poly}$ is the mass of water in the polymer-rich phase. Combining Equations (36) – (39) one gets the following relationship between the threshold mass fraction, $C_{\rm p}^{\star}$, of the polyelectrolytes needed to induce the phase separation/ordering process and the surfactant mass fraction, $C_{\rm s}$, in the mixture:

$$\frac{C_{\rm p}^{\star}}{1-C_{\rm p}^{\star}} = K\frac{M_{\rm poly}}{M_{\rm surf}}\left(\frac{C_{\rm s}^{\rm m}}{1-C_{\rm s}^{\rm m}} - \frac{C_{\rm s}}{1-C_{\rm s}}\right), \tag{40}$$

where $K = \psi/n$; $M_{\rm poly}$ and $M_{\rm surf}$ are, respectively, the molar mass of the polyelectrolyte and the surfactant.

I fitted the relation (40) to the experimental data obtained for the SDS/PSS/water and CTAB/-PDDAC/water systems. The quantity K and the value $C_{\rm s}^{\rm m}$ were the fitting parameters. The results of the fitting are shown in Figure (40). As seen, the dependencies obtained based on

Equation (40) agree fairly well with the experimental data. For the SDS/PSS/water mixture I obtained $K_{\rm an}$ = 2.21 10^{-3} and $C_{\rm s}^{\rm m}$ = 35.8% (slightly lower than the value $\sim$ 40% following from the phase diagram of the SDS/water mixture[193]). Assuming a complete dissociation, one PSS molecule releases the number n of counterions equal to the number of the composing monomers. For the average molar mass $M_{\rm PSS}$ = 70,000, one gets$n \approx 340$. This value, combined with the ratio $K_{\rm an}$ obtained, gives reasonable estimate of the fraction of the diffuse ions in the surfactant-rich phase $\psi_{\rm an} = K_{\rm an} n = 0.75$. For the CTAB/PDDAC/water system the fit of Equation (40) yielded $K_{\rm cat}$ = 2.47 10^{-3}, and $C_{\rm s}^{\rm m}$ = 18.6% (close to the value $\sim$ 20% that follows from the phase diagram of the CTAB/water mixture[194]). Large mass polyelectrolytes do not dissociate completely but some part of the counterions remain bounded with polyions[218]. Additionally, PDDAC is known[219] to entrap water molecules. The polymer-fixed water contains the Cl^- anions that do not contribute to the water activity in the polymer-rich phase. Thus, the effective number, $n_{\rm eff}$, of the anions released into the solvent by one PDDAC molecule is lower than the number n of the monomers composing the PDDAC molecule. In the experiments I used PDDAC of the average molar mass $M_{\rm PDDAC}$ = 150,000, corresponding to $n \approx 929$. To estimate $n_{\rm eff}$ I assumed that the fraction of the diffuse anions in the surfactant-rich phase is of the order of unity, $\psi_{\rm cat} \sim 1.0$. From the value $K_{\rm cat}$ obtained I got $n_{\rm eff} = \psi_{\rm cat}/K_{\rm cat} \sim 400$. That is, the PDDAC molecule releases into the solvent roughly a half of all possible counterions.

II. Ionic surfactant/nonionic polymer

In the following, I discuss the phase separation occurring in the mixture of ionic (cationic) surfactant and non-ionic polymer (PEG) without the addition of salt. As in the case of the ionic surfactant/polyelectrolyte system, I consider the chemical equilibrium between water molecules in the surfactant-rich and the polymer-rich phase. The main contribution to the chemical potential of water in the surfactant-rich phase is due to the presence of the ions. It is written as (cf. Equation (31))

$$\mu_{\rm H_2O}^{surf} = \mu_{\rm H_2O}^0 + RT \ln a_{\rm H_2O}^{surf} \approx \mu_{\rm H_2O}^0 - RT\psi x_{\rm surf} \qquad (41)$$

In the PEG-rich phase the main contribution to the chemical potential comes from the interactions of water molecules with oxygen atoms in the polymer chains[146]. If I assume that one PEG molecule consists of Z oxygen atoms ($Z \approx 457$ for PEG 20 000) the chemical potential

of water in the PEG-rich phase can be written as

$$\mu_{\mathrm{H_2O}}^{poly} \approx \mu_{\mathrm{H_2O}}^{0} - RTx_{\mathrm{PEG}} - \epsilon Z x_{\mathrm{PEG}}, \tag{42}$$

where x_{PEG} is molar fraction of the PEG molecules, and ϵ is some constant of the dimension of J/mol. In Equation (42), the product of Z and x_{PEG} approximates the average number of the oxygen atoms per one water molecule in the PEG-rich phase. Equating (41) and (42) I get

$$x_{\mathrm{surf}} \approx \frac{\epsilon}{RT}\frac{Z}{\psi}x_{\mathrm{PEG}} \tag{43}$$

The last term in Equation (42) was neglected since x_{PEG} is negligibly small compared with x_{surf}. Combining Equation (43) with Equations (37) – (39), I obtain the following relation between the mass fraction of PEG, $C_{\mathrm{PEG}}^{\mathrm{up}}$, above which the phase separation occurs without the addition of salt for a given surfactant mass fraction, C_{s}:

$$\frac{C_{\mathrm{PEG}}^{\mathrm{up}}}{1-C_{\mathrm{PEG}}^{\mathrm{up}}} = \frac{RT\psi}{Z\epsilon}\frac{M_{\mathrm{PEG}}}{M_{\mathrm{surf}}}\left(\frac{C_{\mathrm{s}}^{\mathrm{m}}}{1-C_{\mathrm{s}}^{\mathrm{m}}} - \frac{C_{\mathrm{s}}}{1-C_{\mathrm{s}}}\right), \tag{44}$$

where $C_{\mathrm{s}}^{\mathrm{m}}$ is the minimal mass fraction of the surfactant needed to induce the phase ordering in the surfactant/water system. According to Equation (44), $C_{\mathrm{PEG}}^{\mathrm{up}}$ decreases with the increasing C_{s}. This agrees well with the results of the experiments on the CTAB/PEG/water system.

As I found, the nonionic polymer can induce the phase separation and ordering for cationic surfactant (CTAB) only. It is, however, not clear why the phase ordering is not induced in the solution of anionic surfactant (SDS) by the addition of the nonionic polymer (PEG). This fact can be attributed to the presence of the interactions between PEG and the sulfate groups of the SDS molecules[210,212,213,220,221]. As it was mentioned in Section 1.2.6, the SDS molecules bind to the PEG chains to form aggregates. This effect can prevent the micelles from condensing into ordered structures. Further studies are needed to elucidate this phenomenon.

III. The effect of salt

To discuss the effect of salt on the phase separation I invoke the Donnan effect (equilibrium)[222]. The Donnan equilibrium establishes between two ionic solutions that are separated by a semipermeable membrane allowing the passage of selected ions. To illustrate the Donnan effect assume that, initially, one side (I) of the semipermeable membrane contains a solution consisting of permeable cations such as Na^+ with some impermeable large anions, and the other side (II) contains pure solvent. After addition of NaCl (that dissociates into Na^+ and Cl^- ions, which are permeable to the membrane) an equilibrium between ion concentrations on both sides establishes. The resulting concentration of NaCl is higher on the side II of the membrane. This uneven distribution of the salt is due to the presence of the immobile anions on side I that create an electrostatic potential repelling the Cl^- anions. Overall, the salt added tends to equalize the total concentrations of ions on both sides of the membrane and reduces the osmotic pressure.

In the system composed of ionic surfactant and polyelectrolyte or ionic surfactant and nonionic polymer, the phase boundary between the polymer- and the surfactant-rich phase acts as a semipermeable membrane. That is because the interface is permeable for small ions and is impermeable neither for the charged polyelectrolyte molecules, polymer molecules, nor for the charged surfactant micelles. In the ionic surfactant/polyelectrolyte system, due to the Donnan effect the inorganic salt added to the system does not distribute evenly to reduce the difference between the molar fractions x_{surf} and x_{poly}. Consequently, as observed in the experiments (Figure 41), the amount of polyelectrolyte needed to induce the phase separation/ordering is lower compared to that of undoped system. Similarly, in the ionic surfactant/nonionic polymer system, the ions of the salt added are repelled by the counterions present in the surfactant-rich phase. As a result, the salt distributes unevenly and concentrates mainly in the PEG-rich phase. The presence of the salt in the polymer-rich phase counterbalances the initial excess of the ions in the surfactant-rich phase. Thus, for a given mass fraction of the polymer and the surfactant, the salt can equilibrate the chemical potentials in both the phases and induce the ordering in the system, as observed in the experiments (Figure 42).

3.1.7 Conclusions

In this Section I reported the results of studies devoted to the phase separation in four types of surfactant/polymer systems: (i) anionic surfactants and anionic polyelectrolytes, (ii) cationic surfactants and cationic polyelectrolytes, (iii) cationic surfactants and nonionic polymers either undoped or doped with different inorganic salts, and (iv) anionic surfactants and nonionic polymers. As a solvent, I have used either pure water or mixtures of water and polar solvents.

I have demonstrated experimentally that in the systems studied the phase separation can be induced in two ways:

(1) by addition of ionic polyelectrolyte having the charge of the same sign as that of surfactant,
(2) by addition of nonionic water-soluble polymer alone or along with inorganic salt.

In each case the system separates into polyelectrolyte-rich and surfactant-rich phase with hexagonal ordering. The first method can be applied for both cationic and anionic surfactants. The second method works well only for cationic surfactants. To demonstrate the robustness of my method I studied a variety of ionic surfactants and polymers.

I have found that the effect of nonionic polymers on the phase separation is significantly smaller than the effect of ionic polymers, as they can induce the phase separation only in solutions of cationic surfactants, for high mass fraction of the polymer. For anionic surfactants the addition of nonionic polymers does not result in the phase separation. I have found that the addition of inorganic salt to the mixture of cationic surfactant and nonionic polymer can induce the phase separation even for a small mass fraction of surfactant. Inorganic salt has however significantly weaker effect on the phase separation for solutions of anionic surfactants and nonionic polymers.

The method of the induction of the phase separation I developed is versatile and facilitates formation of surfactant-rich ordered phases in a broad range of surfactant mass fractions. Remarkably, the addition of ionic polyelectrolyte can trigger the phase separation even for very small surfactant mass fraction – only one order of magnitude larger than the critical micelle concentration. This makes the presented method potentially useful in industry, especially in water purification processes to remove surfactant contamination. It can be also applied in material engineering to produce hexagonal matrices that can be further processed and employed as templates to fabricate structural functional materials[159,214,215].

3.2 Nanoparticles in condensed surfactant systems

3.2.1 Introduction

In the previous Section (3.1), I discussed the polymer-induced phase separation in the systems that contain ionic surfactants. I showed that this method enables formation of condensed surfactant phases of a desired ordering. The type of ordering of surfactant phase is determined by the amount of polymer that is added to induce phase separation proces. In this Section I discuss the use of polymer-induced phase separation as a method allowing fabrication of soft and solid nanocomposites. These nanocomposites (referred to as nanostructured materials) consist of NPs embedded in ordered LLC template.

Nanostructured materials have potential applications[223,224] in a range of fields, including electronics, optics, magnetism, medical science, electrochemistry, energy storage, and material science. Among the diverse techniques[225,226] of fabrication of nanostructured materials that have been developed over the past decades, the so-called template method[227–229] has attracted special interest. The advantage of the template-based synthesis is that it offers a versatile way to transform the template into the desired nanomaterial. The templates are usually composed of soft matter, such as polymer gels, block polymers, biomolecules, fibers, emulsions, and lyotropic liquid crystals (LLC). As it was discussed in Section 1.2.3, the LLC templates[226] provide a variety of ordered phases, including lamellar, hexagonal, and cubic phases, with lattice sizes ranging from a few to tens of nanometers. These ordered phases of lyotropic liquid crystals have recently been used to fabricate nanocomposites containing metal,[52,53,152–154] semiconductor,[52,54] and magnetic[155,156] NPs (NPs) or nanorods[55,56]. In the existing techniques, the nanoobjects have been either grown in the LLC template[52–56] or are mixed with surfactant[152–156]. In the later case, the desired ordered phase is obtained by the evaporation of solvent or by a change in temperature.

As it was raised in Section 1.2.7, surfactants forming the LLC phases are known to act as structure-directing agents in the formation of silica-based mesophases that are an intermediate step in forming mesoporous materials with a well-defined pore structure. Such mesophases, doped with noble metal NPs, are very promising nanocatalysts[87,165,230]. The silica-based mesophase is obtained by introducing a silica precursor into the surfactant template. The silica precursors undergo hydrolysis and then condense to form walls with a well-defined structure.

Depending on the type of silica precursor, surfactant, and pH conditions, different types of the silica-based mesophase can be obtained[161].

It has recently been shown[146,147,191] that the surfactant LLC template can be obtained by inducing phase separation by adding polymer to an aqueous solution of surfactant. Upon the addition of polymer, the system separates into polymer-rich and surfactant-rich phases. Depending on the amount of polymer, the surfactant-rich phase can exhibit different types of ordering. This method works for nonionic surfactants and polymers[146,147] as well as ionic surfactants and polyelectrolytes[191], as it was discussed in details in Section 3.1.

In aqueous micellar surfactant solutions, phase separation is driven by the dehydration of the surfactant hydrophilic heads. At a fixed temperature, this process can be controlled by the concentration of the surfactant molecules in the system. The dehydration enhances the van der Waals attractive interactions between the micelles.

In aqueous solutions of nonionic surfactant and polymer, the phase separation is driven by different mechanism. In this case, the attractive interactions between micelles is induced by the presence of polymer molecules. These attractive forces are referred to as the depletion forces and are due to the conformational entropy of the polymer chains[149,150,202,203]. As it was discussed in Section 3.1.1, if the distance between micelles in the solution is small enough, the polymer coils cannot enter between them. This causes, that the space between micelles is depleted with respect to the polymer concentration. The polymer molecules outside the depletion zone induce an osmotic pressure that pushes the micelles together and leads to the phase separation into the surfactant-rich phase and the polymer-rich phase[151].

In the case of an ionic surfactant, the repulsive electrostatic interactions stabilize the micellar solution, and the entropic forces caused by the nonionic polymer are usually too weak to induce the phase separation. However, as I discussed in previous Section (3.1), the phase separation can be induced by adding polyelectrolyte having the same sign of the charge as that of the surfactant. In this case, the electrostatic interactions between the charged micelles and the polyelectrolyte molecules enhance the depletion forces and lead to the phase separation and further ordering of ionic surfactants.

The phenomenon of polymer-induced phase separation (PIPS) has already been used[231] to obtain dispersions of uncharged carbon nanotubes in the LLC templates formed by nonionic surfactant. Here, I deal with ionic systems and propose a method of incorporating charged

NPs into LLC templates. In terms of the interactions, method of treatment, and solubility, ionic and nonionic solutions are completely different. Dispersions of charged particles are stabilized by electrostatic repelling interactions. For this reason, it is very difficult to overcome the electrostatic energy barrier and bring the system into an ordered phase. For example, the addition of salt reduces the repulsive forces but usually results in the formation of amorphous aggregates.

In this Section of the dissertation, I make use of the PIPS phenomenon to develop a method providing a convenient way to transform the dispersion into an ordered, thermodynamically stable phase. I demonstrate that my method enables the incorporation of charged NPs into the LLC matrices composed of both ionic and nonionic surfactants.

3.2.2 Polymer-induced phase separation (PIPS) method

In this part of the dissertation, I make use of the phenomenon of polymer-induced phase separation to introduce charged NPs into the LLC surfactant templates. The idea of the PIPS method is explained in Figure 43.

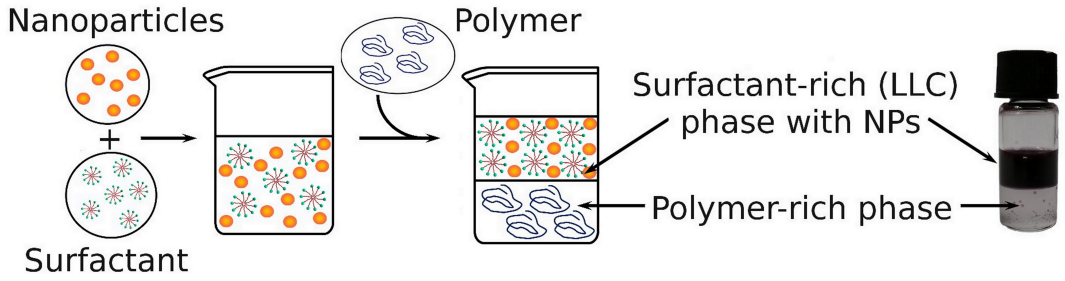

Figure 43: Schematic representation of the PIPS method. At the beginning, surfactant is dissolved in an aqueous solution of NPs, and homogeneous solution is formed. Then, polymer is added and dissolved. Finally, the sample is allowed to relax to complete the phase transition.

To obtain the LLC matrix doped with NPs, I applied the following two-step procedure. First, surfactant is dissolved in an aqueous solution of NPs and well mixed at 30 °C. Such a mixture can be easily processed to obtain the desired properties of the NPs. In particular, other nano-objects and chemicals can be added. In the second step, polymer is added to this solution and thoroughly stirred at about 30 °C. Then, the sample is allowed to relax for about an hour at the same temperature to complete the phase transition. In the process, the system separates into two phases: the ordered surfactant-rich (upper) phase that is also rich in NPs and the polymer-

rich (bottom) phase. The ordering of the resulting LLC phase is controlled by the proportion between surfactant and added polymer.

I applied the PIPS method to introduce NPs of either charge into the nonionic LLC phase as well as into ionic (both cationic and anionic) LLC phases. The mixtures used in my experiments were characterized by the initial content of polymer, surfactant, and NPs in the homogeneous phase, before the phase separation. The proportion between surfactant and polymer was represented by their mass fractions (as for surfactant/polymer/water systems, cf. Section 3.1.2). The number of NPs was characterized by molar concentration. The time lapse of the phase separation process occurring in the system $C_{12}E_6$/PEG/Au(-) is shown in Figure 44.

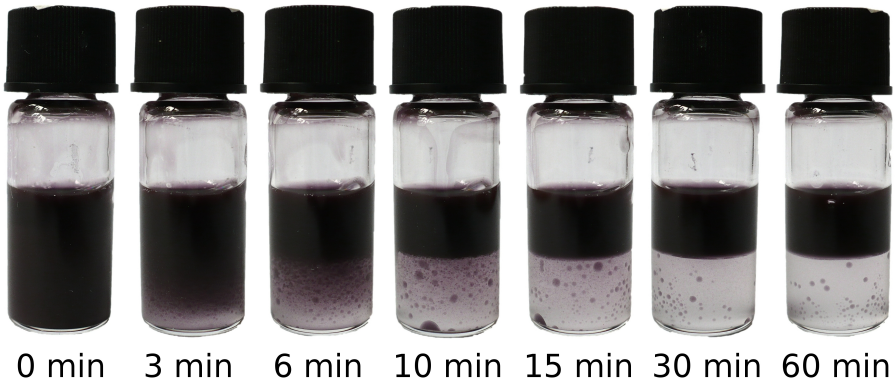

Figure 44: The time lapse of the process of the phase separation occurring in the aqueous solution of $C_{12}E_6$, PEG, and Au(-) (b). The initial composition of the sample was 20% $C_{12}E_6$/10% PEG w/w; the initial concentration of the NPs in the solution was 1.9 10^{-7} M. The upper (dark) phase is the surfactant-rich LLC phase, the bottom phase is the polymer-rich phase. During the phase separation process all NPs moved into the upper surfactant-rich phase.

3.2.3 UV-vis absorbance measurements

To determine the concentration of metal NPs in the system both before and after phase separation, I applied the UV-vis absorbance technique. As I found, for the concentrations of NPs used, the absorbance of the NP/polymer/water system was a linear function of the concentration of the NPs. An example of the calibration plot for Ag(+) is shown in Figure 45.

Because the surfactant-rich phase is very cloudy (cf. Figure 44), it was impossible to determine the concentrations of the NPs in the LLC matrix on the basis of direct UV-vis absorbance measurements. To circumvent this problem and find the concentration of metal NPs transferred into the LLC phase, I investigated the NPs that were left in the transparent polymer-rich phase.

I did it in the following way: denoted the initial (i.e., before phase separation) volume of NP solution and the initial concentration of NPs as V^0 and $C^0_{\rm NP}$, respectively, and then calculated the number of NPs transferred into the LLC phase, $N^{\rm LLC}_{\rm NP}$, from the relation

$$N^{\rm LLC}_{\rm NP} = V^0 C^0_{\rm NP} - V^{\rm pol} C^{\rm pol}_{\rm NP}, \tag{45}$$

where $V^{\rm pol}$ and $C^{\rm pol}_{\rm NP}$ are the volume of the polymer-rich phase and the concentration of the NPs remaining in this phase after the phase separation, respectively. The volume $V^{\rm pol}$ was measured directly using a syringe.

To find the ratios of the absolute values of the net charges on the surfaces of NPs, we performed titration studies based on the UV-vis absorbance. The number of negatively and positively charged NPs was characterized by the molar fraction, χ, defined as

$$\chi = \frac{N_-}{N_- + N_+}, \tag{46}$$

where N_- and N_+ denote the number of moles of the negatively and positively charged NPs in the system, respectively. The titration point, χ^*, corresponds to the electroneutrality of the system. This condition is fulfilled when

$$N_- Q_- = N_+ Q_+, \tag{47}$$

where Q_- and Q_+ denote the total net charge over the negatively and positively charged NPs, respectively.

From Equations (46) and (47), the charge ratio is calculated as

$$\frac{Q_-}{Q_+} = \frac{(1-\chi^*)}{\chi^*}. \tag{48}$$

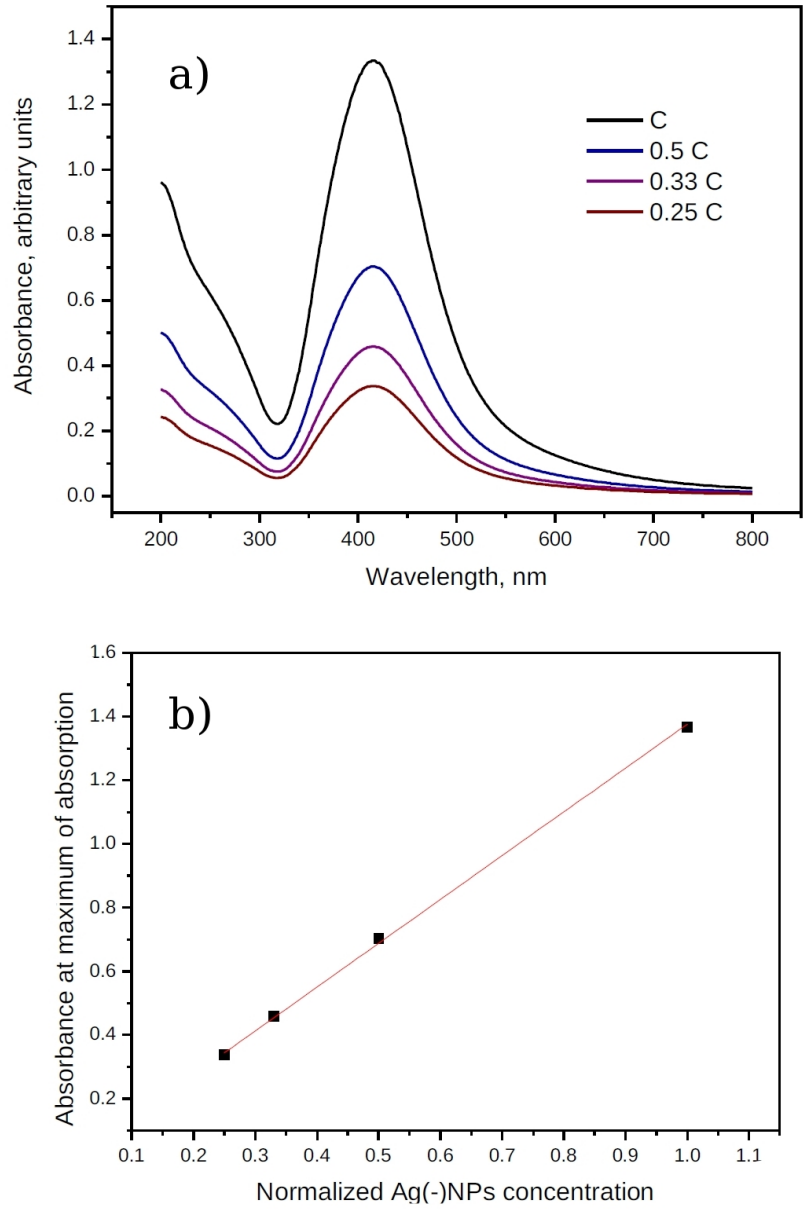

Figure 45: Absorbance-concentration calibration for the Ag(+)/polymer/water mixture. (a) Changes of the absorbance spectrum for different concentrations of NPs (for fixed polymer content). (b) Absorbance at the maximum of absorption vs. normalized concentration of NPs solution. The value of the normalized concentration is equal to unity for the NPs concentration $c = 2.68 \times 10^{-7}$ M. The plot shows that absorbance changes linearly with the NPs concentration. Based on this calibration plot I calculated NPs concentrations.

NPs of opposite charge are known[67,232] to form clusters, especially near the electroneutrality point. The presence of the metal-metal clusters strongly affects the UV-vis absorption spectrum. For this reason, it is impossible to determine the concentration of NPs in mixtures of metal NPs. To quantify the PIPS method, I employed mixtures of QD(-) and Ag(+). Using

mixtures of QDs and metal NPs instead of mixtures of metal NPs offered two important advantages. First, as I verified, the metal-semiconductor clusters formed in the QD(-)/Ag(+) system do not affect the UV-vis spectrum, and the calculation of the NP concentration based on the UV-vis data was possible. Second, the absorbance of QD(-) is very low compared to that of the metal NPs (Figure 46).

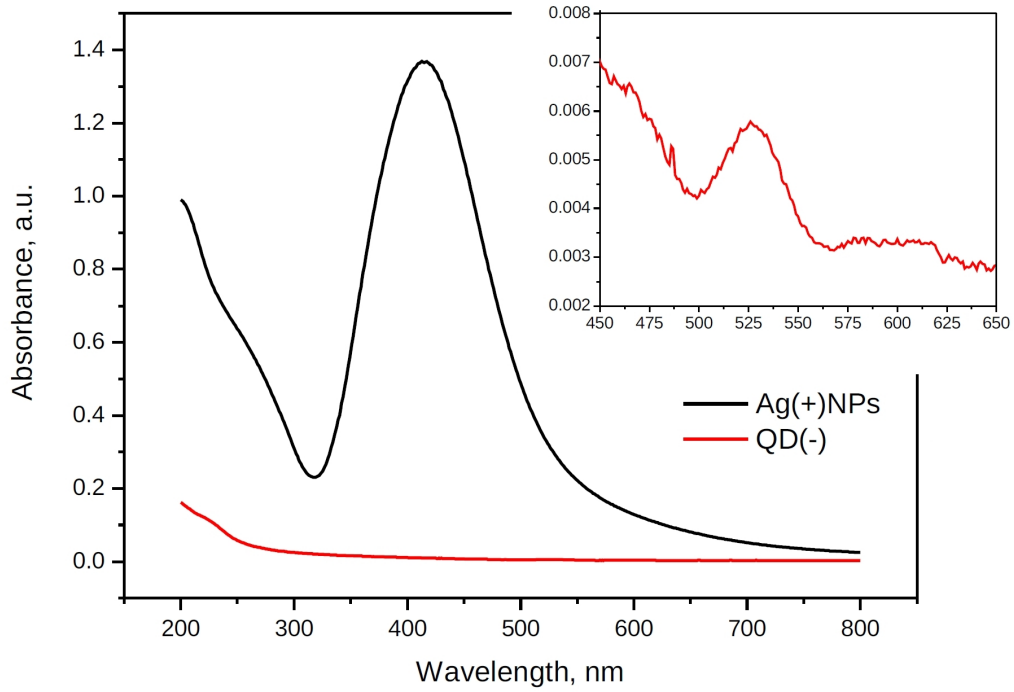

Figure 46: Comparison of the absorption spectra of positively charged silver NPs, Ag(+), and negatively charged semiconductor QD(-), used in the experiments with mixed NPs solution. The absorbance of the OD(-) is negligible compared with that of Ag(+) NPs. Inset: magnification of the QD(-) absorption spectrum.

For this reason, the absorbance spectrum of the metal NPs was not altered by the presence of the QDs. Results of the titration of Ag(+) with QD(-) are presented in Figure 47. I found that for χ below the threshold value, $\chi^* = 0.67 \pm 0.01$, the solution is stable and no aggregates are present. The threshold value χ^* corresponds to the electroneutrality of the system. At this point, precipitation of the clusters composed of Ag(+) and QD(-) occurs and an abrupt decrease in absorbance is observed.

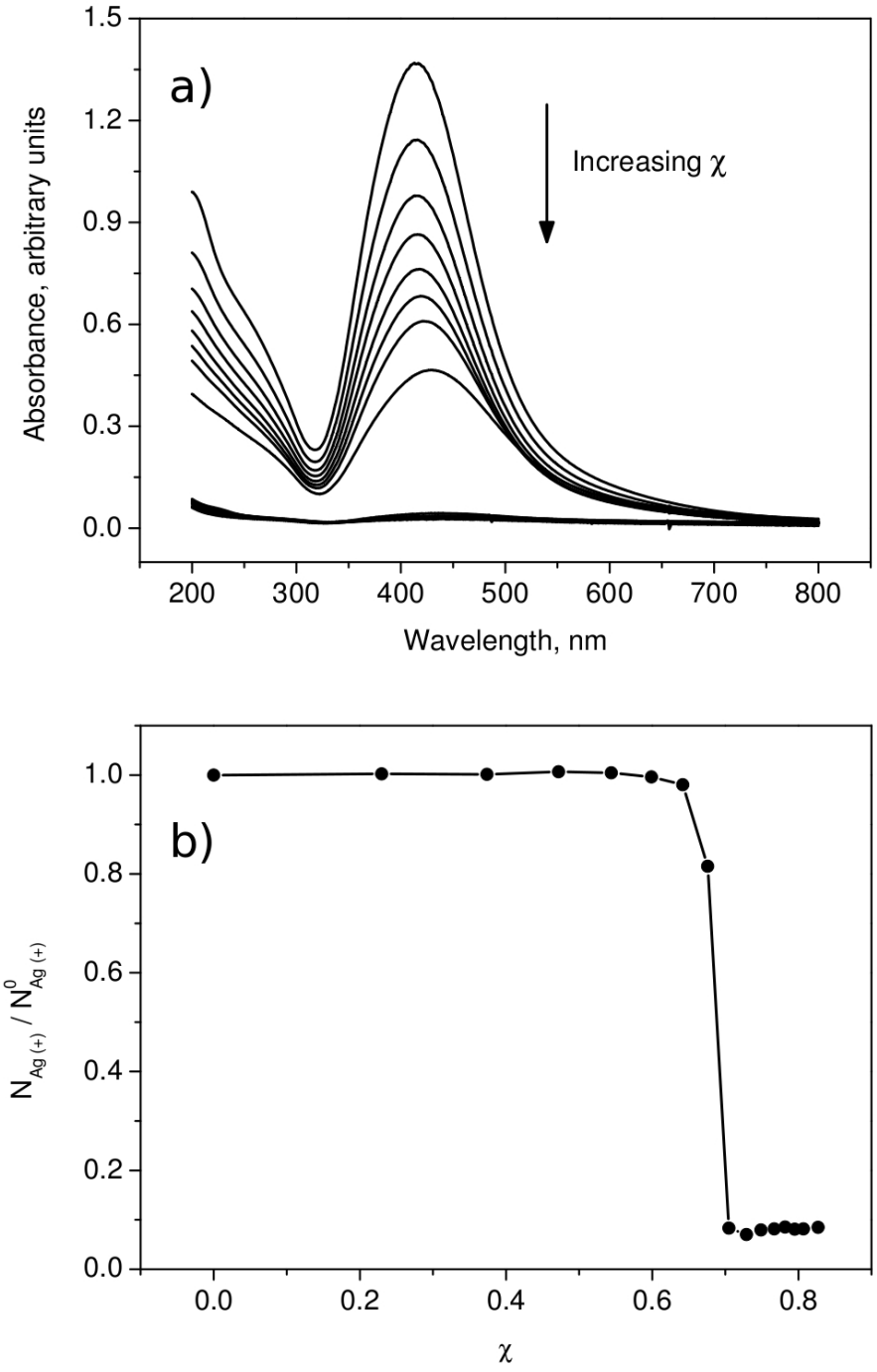

Figure 47: Titration of Ag(+) with QD(-). (a) Changes of the absorbance due to Ag(+) observed during the titration process. (b) Amount of moles of Ag(+) present in the solution – measured relative to the initial number of moles $N^0_{\mathrm{Ag}(+)}$ in the system – plotted as a function of the molar fraction, χ, of QD(-) added.

3.2.4 PIPS in Nonionic Systems

I employed the PIPS method to introduce NPs into LLC phases of a nonionic surfactant ($C_{12}E_6$) induced by a nonionic polymer (PEG). To demonstrate the versatility of the method, I also applied PIPS to two ionic systems: (i) a cationic surfactant (CTAB) and cationic polyelectrolyte (PDDAC) and (ii) an anionic surfactant (SDS) and anionic polyelectrolyte (PSS).

I. Ordering of the LLC Matrix

In the case of nonionic $C_{12}E_6$/PEG/water systems, the PIPS method enabled the introduction of charged NPs into the hexagonal and lamellar LLC phases. In Figure 48, the SAXS patterns of the LLC (a) hexagonal and (b) lamellar phases doped with Au(-) are shown. The hexagonal and lamellar phases were obtained, respectively, for $C_{12}E_6$/PEG weight fractions of 20%/10% and 10%/36%. In each case, the concentration of Au(-) was 1.91 10^{-7} M. For comparison, in Figure 48, the patterns of the corresponding pure LLC phases (without NPs), are also shown. The positions of SAXS reflections as well as resulting characteristic parameters of pure and doped hexagonal and lamellar phases are collected in Table 5. All the characteristic parameters were determined on the basis of Equations (7) and (11) described in Section 2.1.2.

type of LLC	doping		(010)	(110)	(020)	LLC characteristic parameter
hexagonal	pure	2θ, °	1.60	2.77	3.20	a = 6.37
		d, nm	5.52	3.19	2.76	
	Au(-)	2θ,°	1.58	2.73	3.16	a = 6.47
		d, nm	5.58	3.23	2.79	
lamellar	pure	2θ, °	1.91	-	3.82	d = 4.62
		d, nm	4.62	-	2.31	
	Au(-)	2θ, °	1.90	-	3.80	d = 4.65
		d, nm	4.65	-	2.32	

Table 5: The positions of SAXS reflections as well as resulting characteristic parameters of pure and Au doped hexagonal and lamellar phases. The errors of positions of SAXS reflections as well as of resulting characteristic parameters do not exceed 1%.

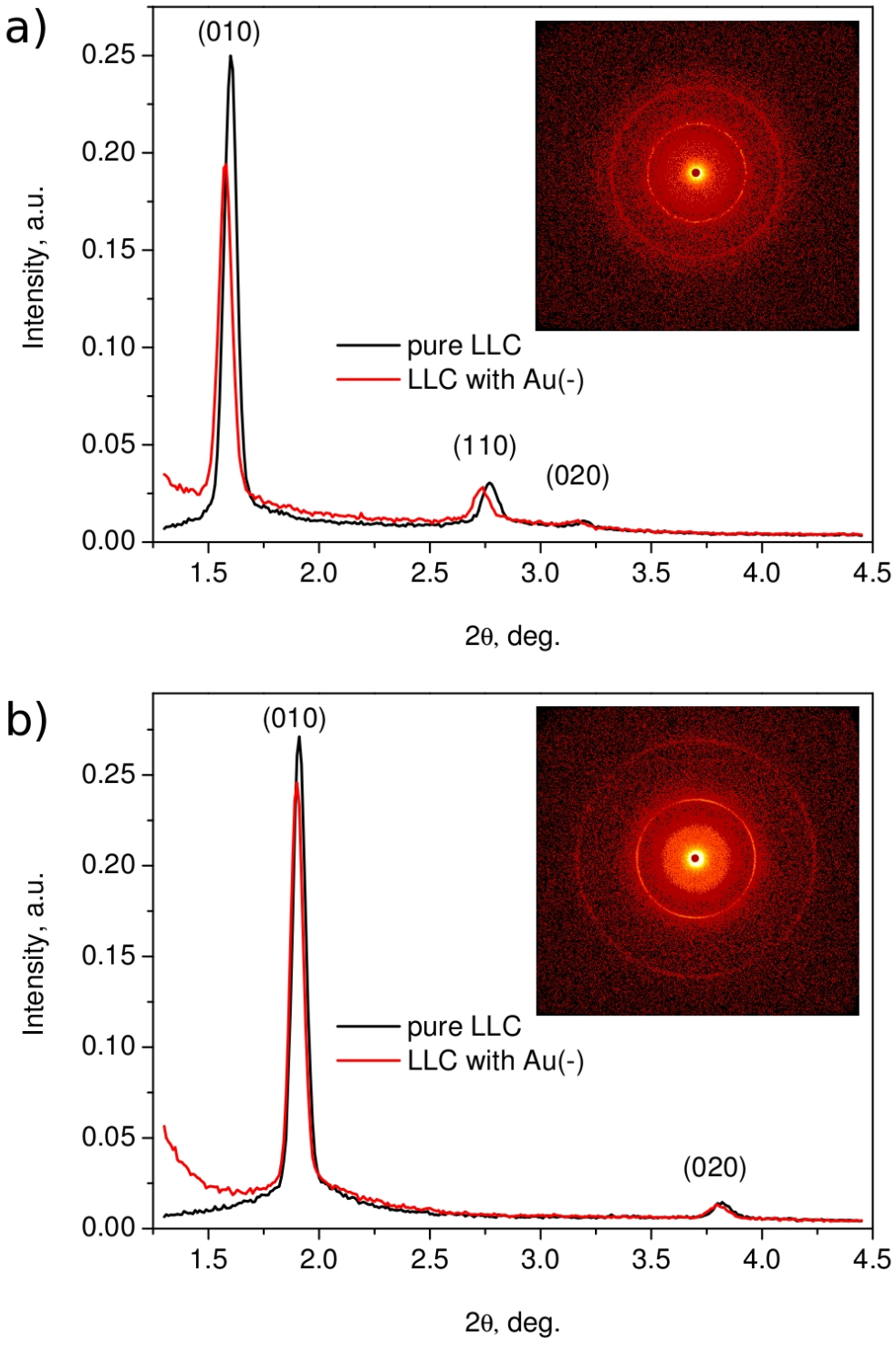

Figure 48: SAXS patterns of the hexagonal (a) and the lamellar (b) LLC phase formed in the $C_{12}E_6$/PEG/water system. The red and black lines correspond, respectively, to the LLC phase containing Au(-), and the same phase without Au(-). The presence of the NPs causes the increase of the lattice constant of the hexagonal phase and the layer thickness of the lamellar phase.

On the basis of the SAXS data, the lattice constant, a, of the doped and pure hexagonal phase was 6.47 and 6.37 nm, respectively. The layer thickness, d, of the doped and pure lamellar phase was 4.65 and 4.62 nm, respectively. It follows that the presence of the NPs results in "swelling" of the LLC matrix for each type of the ordering. This fact indicates that most of the NPs are dispersed homogeneously in the LLC phase. That is because the increase in the average values of d and a can be observed only if the NPs, having a diameter of 7.3 nm that is larger than both d and a, are uniformly distributed between the columns or the lamellas. The spatial arrangement of the NPs dispersed in the two LLC phases is shown in Figure 49. It should be also noted that the SAXS measurements revealed that the swelling of the LLC matrix is more pronounced in the case of the hexagonal phase. This difference can be attributed to the fact that the hexagonal columnar structure is much stiffer than the lamellar one.

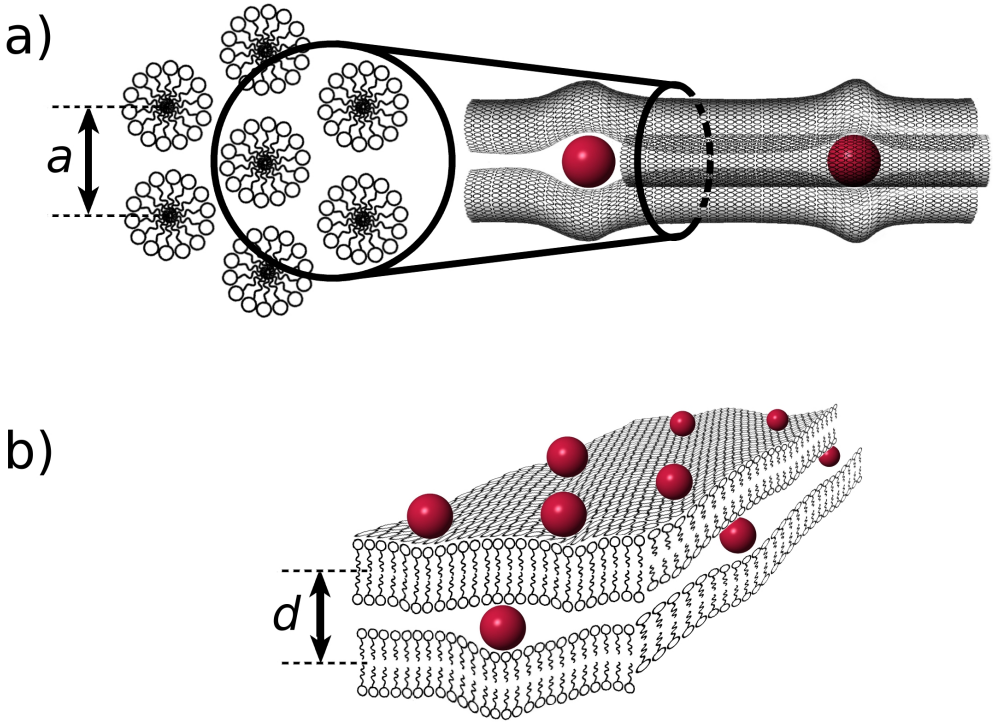

Figure 49: Spatial arrangement of the NPs in the hexagonal (a) and lamellar (b) LLC phase. In both cases, NPs are located in aqueous regions of the LLC phase, that is between columns in the case of hexagonal phase, and in water layers in the case of lamellar phase. The presence of NPs results in "swelling" of the LLC matrix for each type of the ordering.

Importantly, it was noted that the doped LLC phases obtained using the PIPS method are very stable against the aggregation of NPs. For example, I checked that the hexagonal phase containing Au(-) preserved its ordering and did not exhibit any measurable change in the lattice constant for 11 months. The SAXS patterns of the freshly prepared sample and the same sample after 11 months are shown in Figure 50. As can be seen, the positions of peaks (010), (110), and (020) remain unchanged which confirms the stability of the ordering of LLC matrix.

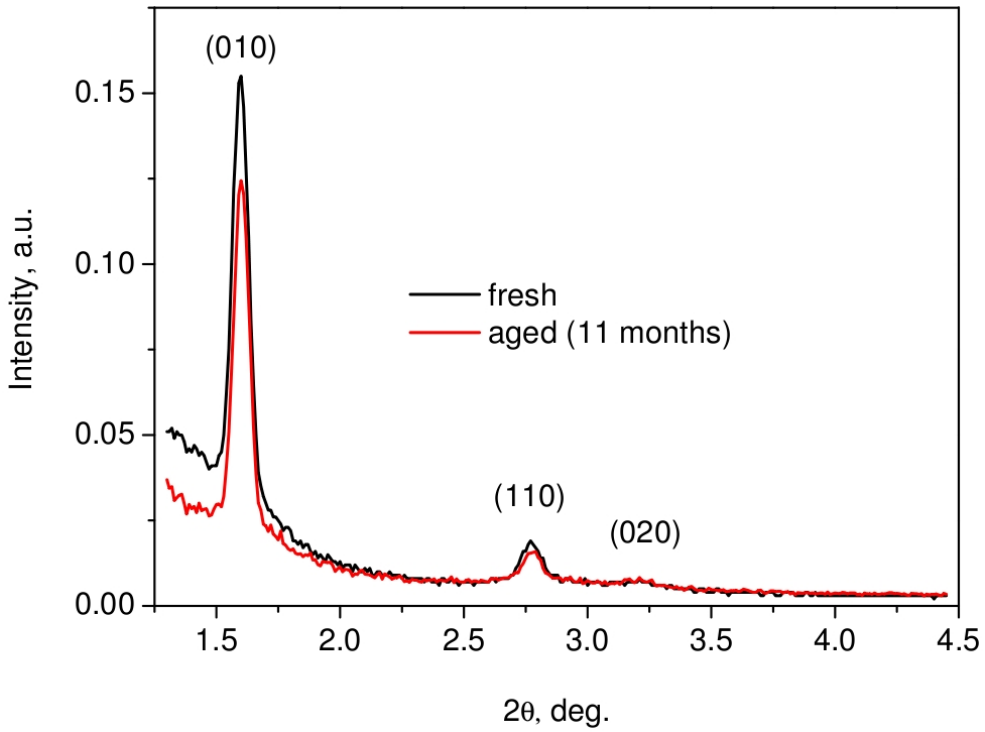

Figure 50: SAXS patterns of the LLC phases doped with Au(-) (obtained from the aqueous solution of 20% $C_{12}E_6$/10% PEG/Au(-)). The black curve corresponds to the freshly prepared sample, and the red curve corresponds to the same sample aged for 11 months. The positions of the Bragg peaks did not change over this time.

Besides the SAXS measurements, to determine the ordering, I analyzed textures of the LLC phases using polarized optical microscopy. For each type of ordering, the texture of the doped phase was very similar to that of the pure surfactant, as shown in Figure 51.

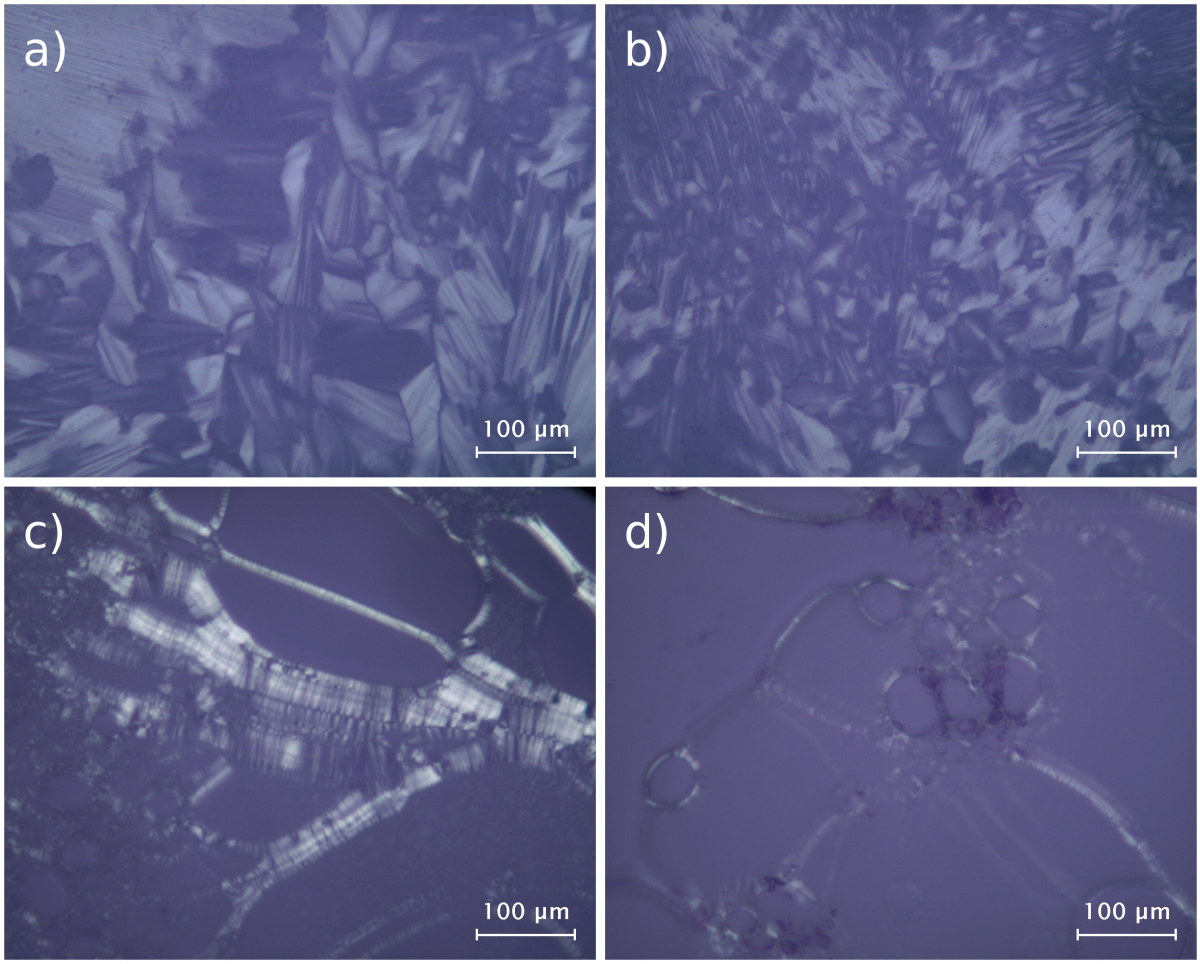

Figure 51: Polarized microscopy textures for representative samples. The hexagonal columnar phase obtained from 20% $C_{12}E_6$/10% PEG and water (a) or Au(-) (b). The lamellar phase obtained from 10% $C_{12}E_6$/36% PEG and water (c) or Au(-) (d).

II. Effect of Nanoparticle Charge.

To study the effect of the sign of the charge of the NPs on the efficiency of their transfer into the LLC phase, I compared the initial number of NPs in the solution and the number of NPs present in the surfactant-rich phase after phase separation. The UV-vis absorbance spectroscopy studies revealed that after the phase separation the negatively charged metal NPs (Au(-) and Ag(-)) were not present in the polymer-rich phase. That is, in each experiment, they were all transferred from the solution into the LLC phase. In the case of QD(-), I observed the sample in UV light. (The absorbance of the semiconductor NPs is to low to be used to determine the presence of QD(-) in the polymer-rich phase based on the UV-vis measurements.) I found that for each initial concentrations, after the phase separation, all QD(-) were transferred into the LLC phase. The results of PIPS for Au(-) and QD(-) are shown in Figure 52a.

I found, however, that PIPS is not symmetric with respect to the sign of the charge of the NPs. Namely, I observed that, in contrast to the negatively charged NPs, some fraction of the positively charged NPs (Au(+) and Ag(+)) always stayed in the polymer-rich phase for any surfactant/polymer proportion used. For example, for the system consisting of 20% $C_{12}E_6$ and 10% PEG, all Ag(+) is in the polymer phase, as shown in Figure 52b.

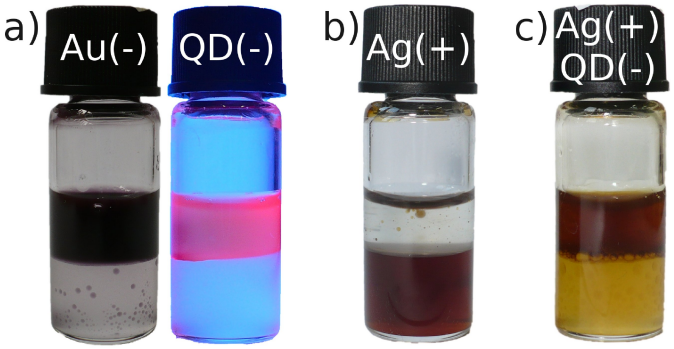

Figure 52: Results of PIPS for the $C_{12}E_6$/PEG/water mixture doped with negatively (a), positively (b), and a mixture positively and negatively (c) charged NPs. Photograph of the second sample was taken in the UV light. The $C_{12}E_6$/PEG proportion was identical for all samples. In each case the upper phase is the LLC matrix.

Interestingly, I found that the fraction of positively charged NPs transferred into the LLC phase increases when negatively charged NPs are present in the solution before the phase separation. This cooperative effect can be clearly seen in Figure 52c. The admixture of QD(-) made the majority of Au(+) move into the LLC phase, and only a small fraction of Au(+) was present in the polymer-rich phase. I also observed that the number of positively charged NPs incorporated into the LLC phase increases with the amount of PEG added. For example, for the system consisting of 20% $C_{12}E_6$ and Au(+) the fraction of incorporated NPs increases significantly when the polymer content increases from 10% to 20%, as shown in Figure 53b. The cooperative behavior is discussed in more detail in the next Section.

From Equation (48), the ratio of the absolute values of the charges on QD(-) and Ag(+) is

$$Q_{\mathrm{QD}(-)}/Q_{\mathrm{Ag}(+)} = 0.49 \pm 0.05.$$

It follows that the ratio of the charge densities on QD(-) and Ag(+) is

$$r^2_{\mathrm{Ag}(+)}Q_{\mathrm{QD}(-)}/r^2_{\mathrm{QD}(-)}Q_{\mathrm{Ag}(+)} = 0.53.$$

Here, $r_{\mathrm{Ag}(+)} = 5.25$ and $r_{\mathrm{QD}(-)} = 5.05$ nm are the radii of Ag(+) and QD(-), respectively. To determine whether the observed asymmetry in the transfer of NPs into the LLC phase is caused

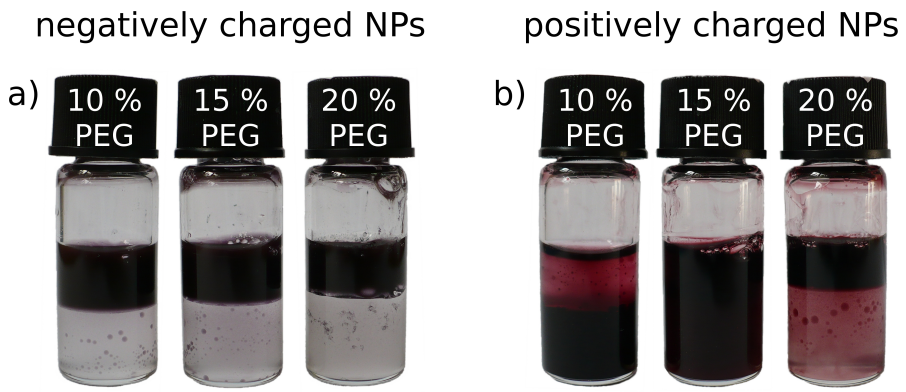

Figure 53: The influence of polymer content on the incorporation of (a) negatively or (b) positively charged Au NPs in 20% $C_{12}E_6$/PEG/water mixtures doped with Au NPs.

by the difference in the charge density on the NPs surface, I also investigated other systems. Using UV-vis spectroscopy, I studied PIPS for Au(-), Ag(-), and Au(+) and found that Au(-) and Ag(-) were completely transferred into the LLC phase independently of the polymer and surfactant content used whereas the majority of Au(+) stayed in the polymer-rich phase. From the titration studies, I obtained the following charge ratios:

$$Q_{\mathrm{Au}(-)}/Q_{\mathrm{Au}(+)} = 0.43 \pm 0.03$$

and

$$Q_{\mathrm{Ag}(-)}/Q_{\mathrm{Au}(+)} = 1.86 \pm 0.14.$$

The ratios of the charge densities are estimated to be 0.50 and 1.15 for the Au(-)/Au(+) and Ag(-)/Au(+) pairs, respectively. (The radii of Au(+), Au(-), and Ag(-) are 3.92, 3.65, and 4.98 nm, respectively.) The asymmetry in the transfer is observed between NPs with the charge density varying from 0.50 to 1.15. This fact indicates that the asymmetry is actually due to the difference in the sign of the charge on NPs.

III. Effect of NPs(-) and Polymer Content on the Incorporation of NPs(+) into the LLC Phase.

To investigate the effect of negatively charged NPs and the concentration of the polymer on the transfer of positively charged NPs into the LLC phase, I studied the $C_{12}E_6$/PEG/water system doped with Ag(+) and QD(-). I quantified the amounts of NPs in the initial and resulting solutions using the molar fraction, χ, defined in Equation (46). For each system studied, all QD(-) were transferred into the LLC phase. (Confirmed by the observation of the sample in the UV light.) The use of QD(-) facilitated the determination of the concentration of Ag(+) based on the UV-vis measurements (as it is shown in Figure 45).

I carried out a series of experiments for the $C_{12}E_6$/PEG/water system by changing either the content of PEG (10, 11, 15, and 20%) or the initial proportion of Ag(+) to QD(-) (χ = 0.0, 0.1, 0.2, 0.3, 0.4, and 0.5). The dependence of the concentration of Ag(+) remaining in the polymer-rich phase is plotted as a function of the PEG concentration in Figure 54a for six different values of χ. The cooperative effect of the presence of the oppositely charged NPs on the transfer of Ag(+) into the LLC phase is clearly seen. Even a small admixture of QD(-) increases the amount Ag(+) moved into the LLC phase to a great extent. I also found that for a fixed polymer content the concentration of Ag(+) in the polymer-rich phase decreases approximately linearly with χ, as it is shown in Figure 55. This proves that the presence of negatively charged NPs helps to incorporate positively charged ones. In Figure 54b, values of χ observed in the LLC template after the phase transition are plotted as a function of the initial values of χ. To calculate the amount of Ag(+) transferred into the LLC phase, Equation (45) was used. As seen, when the concentration of PEG is smaller than $\sim$15 wt%, the ratio of QD(-) to Ag(+) in the LLC phase differs from the initial one. In this regime, the NP composition in the LLC template can be controlled by the amount of polymer added. The effect of NPs(-) and polymer content on the transfer of NPs(+) into the LLC phase is shown schematically in Figure 56.

The LLC phases doped with mixtures of positively and negatively charged NPs exhibited SAXS patterns similar to that of an LLC phase doped with Au(-). I did not detect any structure formed by the NPs within the lamellar or hexagonal templates. NPs with opposite charge do not form aggregates as long as the overall charge in the system is nonzero (the electroneutrality point). In my studies, the molar fractions, χ, both in the initial mixture and in the resulting LLC phase did not reach the threshold value χ^* (cf. the titration curve shown in Figure 47). This

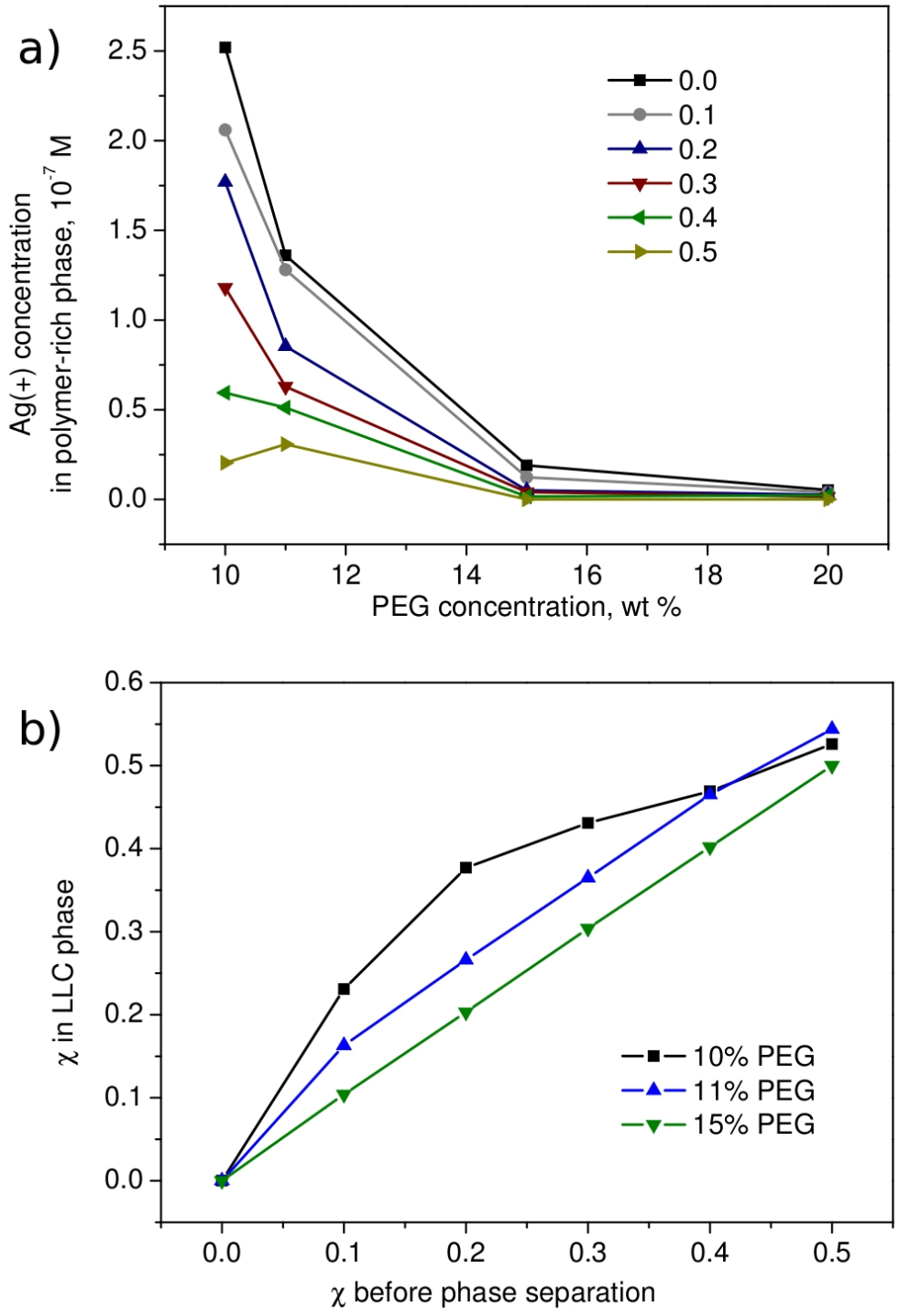

Figure 54: (a) Concentration of Ag(+) in the polymer-rich phase as a function of the PEG content for different NP compositions (six values of χ). (b) Fraction of QD(-) observed in the LLC phase vs. the initial fraction of QD(-).

suggests that Ag(+) and QD(-) do not form aggregates in the LLC phase.

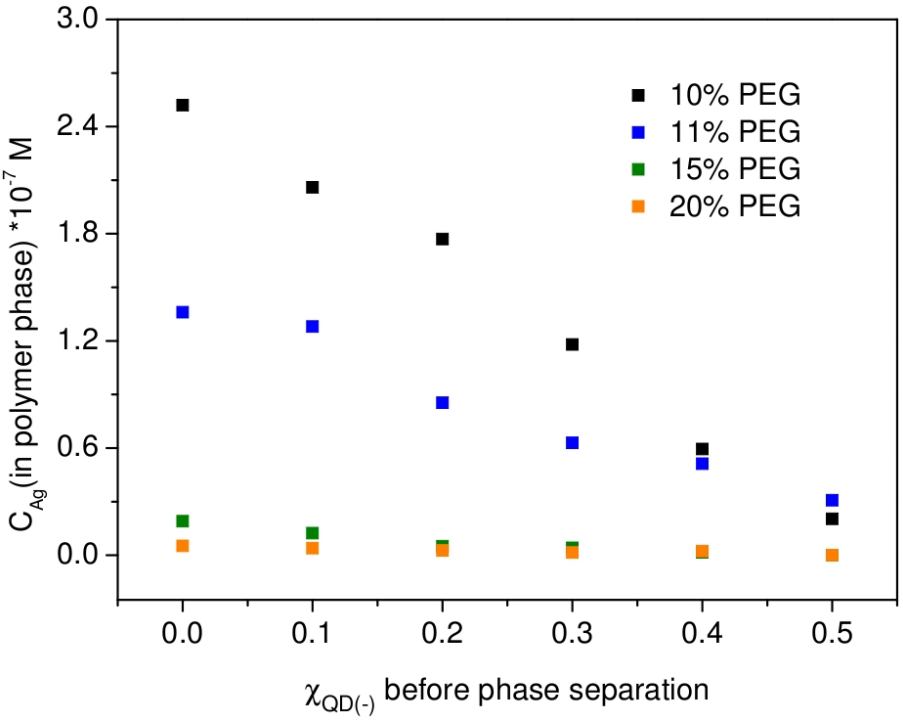

Figure 55: Concentration, C_{Ag}, of Ag(+) in the polymer-rich phase as a function of the initial fraction χ (i.e., before the phase separation) of QD(-). As seen, for a fixed polymer (PEG) content, the amount of Ag(+) left in the polymer-rich phase decreases, with a good approximation, linearly with increasing fraction of QD(-) in the initial mixture. This means that the negatively charged NPs help to transfer the positively charged ones into the LLC matrix.

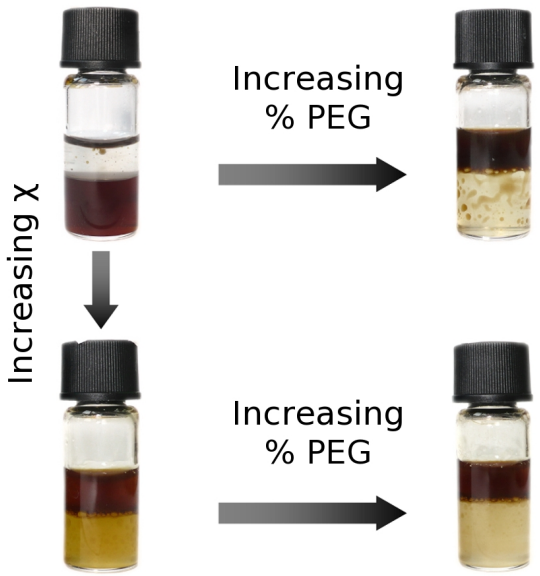

Figure 56: Schematic representation of the effect of NPs(-) as well as polymer content on the incorporation of NPs(+) into the LLC phase.

3.2.5 PIPS in Ionic Systems.

PIPS can be employed to incorporate charged hydrophilic NPs into ionic LLC templates. To obtain such templates, I applied the method described in Section 3.1 of this dissertation and induced the phase separation by adding to the solution of ionic surfactant polyelectrolyte of the same charge.

I investigated qualitatively PIPS in two ionic systems:

- anionic template – SDS/PSS/water
- cationic template – CTAB/PDDAC/water

In both systems I employed Au(+) and Au(-) NPs. Surprisingly, I found that the PIPS method enables incorporation into the ionic LLC matrix NPs of either charge. That is, I managed to dope both the anionic and cationic LLC phases with charged NPs of either sign. The experiments revealed that for the two ionic systems considered, the number of NPs transferred into the LLC phase depended, irrespective of the charge of the NPs, on the surfactant/polyelectrolyte proportion. The results are summarized in Table 6. I also checked using the SAXS technique that for both the anionic and cationic systems hexagonal ordering was induced.

Surfactant	Polyelectrolyte	Nanoparticles	Result
10% SDS	20% PSS	Au(-)	P
20% SDS	15% PSS	Au(-)	C
10% SDS	20% PSS	Au(+)	C
10% CTAB	15% PDDAC	Au(-)	C
12% CTAB	10% PDDAC	Au(-)	C
15% CTAB	12% PDDAC	Au(-)	C
12% CTAB	10% PDDAC	Au(+)	P

Table 6: Results of the experiments with the ionic LLC matrices (both anionic and cationic): C – NPs are completely incorporated to the upper, surfactant-rich phase, P – NPs are partly incorporated to the upper phase, some fraction of them is left in the bottom, polymer-rich phase.

3.2.6 Silica-Based Mesophase Doped with Nanoparticles.

The silica-based mesophases were fabricated according to the procedure described in Section 2.2.3. Its structure was investigated using the WAXS technique. The WAXS pattern shown in Figure 57 indicates that during the formation of the silica network the initial hexagonal structure of the LLC template changes to the lamellar one. The first three peaks located at 2θ = 3.4°, 6.8°, and 10.2° correspond to the reflections from the (010), (020), and (030) planes of the lamellar phase, respectively, with a layer spacing of $d = 2.59$ nm. From the comparison of the layer spacing, d, with the length of the CTAB molecule (2.173 nm), it follows that within the bilayers the hydrocarbon chains overlap. The spatial arrangement of the surfactant molecules within the layers is reflected in the central region of the diffraction pattern for angles ranging from 15 to about 30°[160,233]. The presence of the peaks located at 16.36°, 18.46°, and 21.5° indicate[234] that the molecules form the triclinic lattice characterized by three distances: 0.541, 0.480, and 0.413 nm (Figure 57). The presence of the gold NPs dispersed within the silica-based mesophase is confirmed in the WAXS pattern by the small peak at 2θ = 35.63°. This peak is assigned to the reflection from the (111) plane of the face-centered-cubic Au. Note that the relatively low intensity of the Au(111) peak and the lack of reflections from other planes are characteristic of small gold NPs having a diameter of a few nanometers. Because of the finite-size effect[235], the full X-ray diffraction pattern is displayed only by sufficiently large NPs. As it is shown in Figure 58, the Au (111) peak is better visible after the calcination of the sample for 24 h at 500 °C. The calcinated sample does not contain the surfactant template and the diffraction peaks corresponding to the lamellar structure and the peaks resulting from the ordering of the surfactant chains are not present.

The fact that the NPs remain dispersed in the sample after the solidification is confirmed by other observations. First, the silica-based mesophase has a light violet color (see Figure 59), that is characteristic for the nano-sized gold crystals. Second, the intensity of the color does not change even after boiling the sample in water for a couple of hours, what indicates that the NPs are permanently embedded in the silica-based framework.

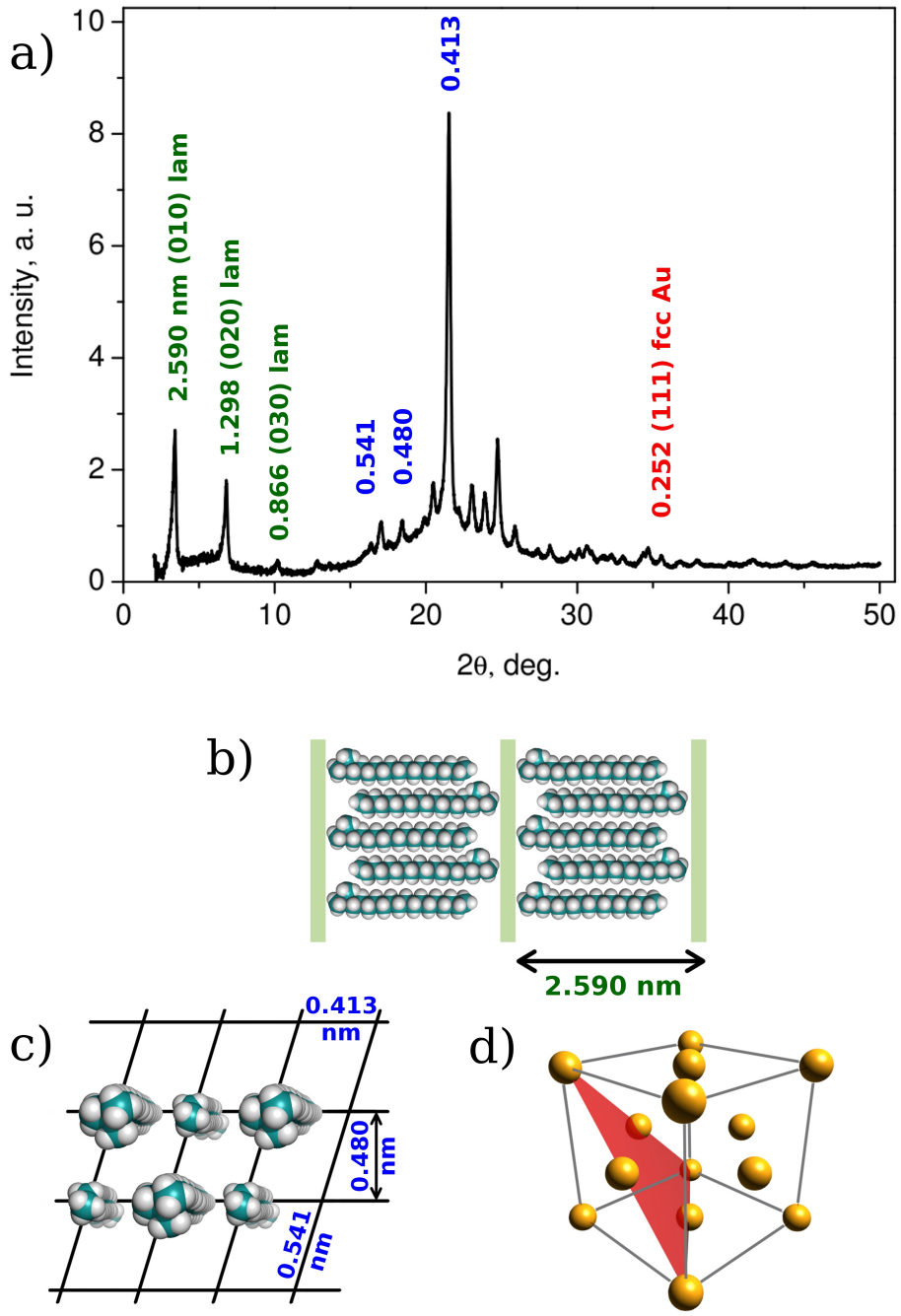

Figure 57: WAXS pattern of the silica-based mesophase obtained from hexagonal template with NPs (15% CTAB, 10% PDDAC and Au(-)) (a). The diffraction peaks located at 2θ = 3.4°, 6.8°, and 10.2° correspond, respectively, to reflections from the (010), (020), and (030) planes of the lamellar phase with the layer spacing $d = 2.59$ nm (b). The peaks at 16.36°, 18.46°, and 21.5° reflect the arrangement of CTAB molecules forming the triclinic lattice in the plane of bilayer (c). The small peak at 2θ = 35.63° is assigned to the reflection from the (111) plane of the face-centered-cubic Au (d).

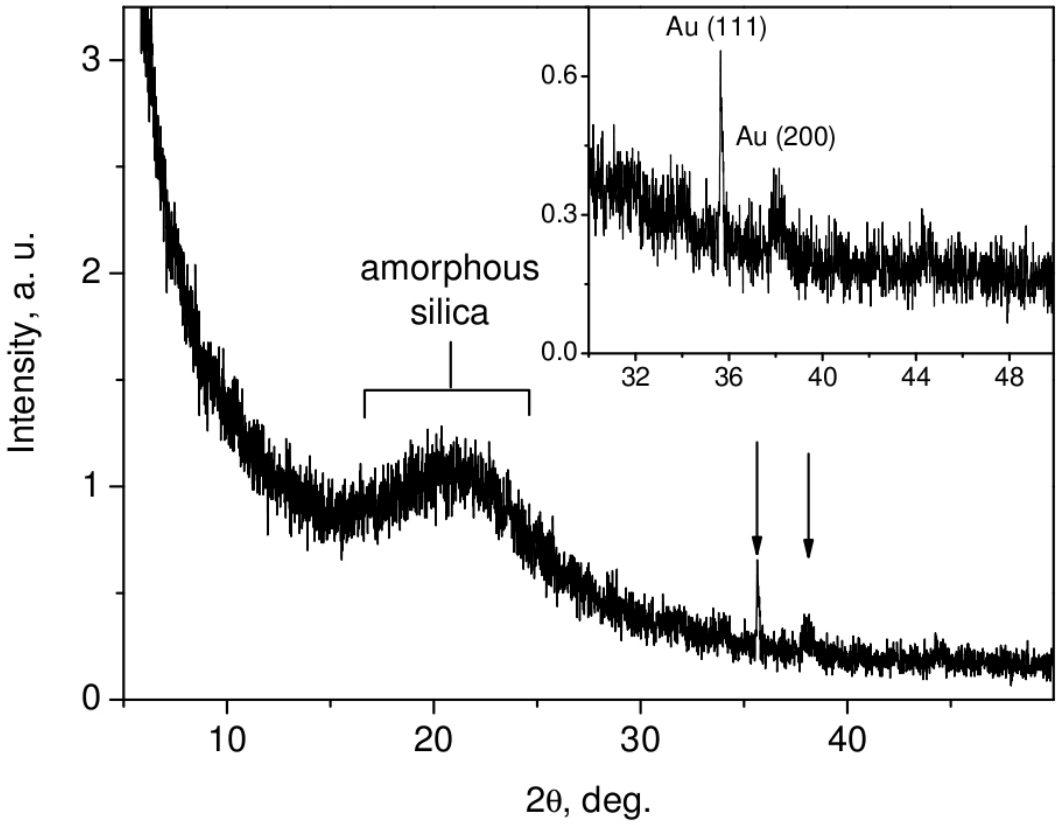

Figure 58: WAXS pattern of the calcinated sample (24 h at 500 °C) containing gold NPs. The broad peak at $2\theta \sim 23°$ corresponds to the amorphous silica. The sharp peak at $2\theta \sim 35.63°$ comes from the presence of Au NPs and is assigned to the reflection from the (111) plane of face-centered-cubic Au.

Figure 59: The picture of as prepared solid silica mesophase doped with Au NPs. Slightly violet color of obtained material, results from the presence of gold NPs.

3.2.7 Conclusions

I presented a facile new technique for incorporating hydrophilic charged NPs into the LLC template. In this technique, called the PIPS (polymer-induced phase separation) method, phase separation is induced upon adding polymer to an aqueous solution of NPs and surfactant. As a result, the system separates into polymer-rich and ordered surfactant-rich (LLC) phases. The type of ordering (hexagonal or lamellar) of the LLC phase can be easily controlled by the amount of polymer added. In the process of phase separation, the NPs are transferred into the surfactant-rich phase and form a uniform dispersion in the LLC matrix. The resulting LLC template containing NPs is very stable against NPs aggregation. As I demonstrated, the PIPS method enables the incorporation of NPs into the LLC templates composed of both nonionic and ionic (anionic and cationic) surfactants.

I found that the PIPS method enables incorporation into the ionic LLC matrix NPs of either charge. In particular, I found that, unexpectedly, my method enables the incorporation of charged NPs into the liquid-crystal matrix composed of ionic surfactant with the same sign of the charge as that of the NPs. That is, I could incorporate negatively charged particles into anionic templates and positively charged NPs into cationic ones. Using the PIPS method, we obtained both cationic and anionic LLC templates doped with positively and negatively charged NPs. The number of NPs transferred into the template was controlled by the surfactant/polyelectrolyte proportion.

I also found that in the nonionic systems the PIPS method is not symmetric with respect to the charge of the NPs. That is, negatively charged NPs are transferred into the LLC template much more easily than positive ones. Moreover, I discovered that the presence of negatively charged NPs has a cooperative effect on the transfer of the positively charged NPs into the LLC matrix. This feature opens up a way to fabricate templates containing different types of NPs in prescribed proportions. Namely, the composition of the template can be controlled by the initial proportion between NPs carrying a positive net charge and NPs carrying a negative net charge.

The PIPS method offers potential industrial applications. It can be used as a simple way to separate NPs from different water solutions. Also, as I demonstrated, the PIPS method can be successfully employed to fabricate solid silica-based mesophases containing different well-dispersed types of NPs in prescribed proportions.

3.3 Nanoparticles in diluted surfactant solutions

3.3.1 Introduction

Mixing of surfactants with NPs may give unexpected results. One of them is fluorescence quenching of semiconductor QDs[236,237] – the phenomenon that is sometimes used to sense the presence of surfactants in solution[238,239]. Fluorescence quenching of QDs, that is described in literature, is the strongest in the case of negatively charged QDs and cationic surfactants[236]. It is however observed for other types of surfactants[236,237].

The exact mechanism of this phenomenon is still the matter of debate. In the case of negatively charged QDs and cationic surfactant the fluorescence quenching is ascribed to the aggregation mediated by the electrostatic interaction[236,240]. For negatively charged QDs and nonionic surfactant, mechanism of quenching is not fully understood, however it seems that the adsorption of surfactant molecules to the particles surface may be crucial in this process[236].

The adsorption of surfactants to nano-sized particles was recently intensively studied. One of the most extensively studied system is the mixture of nonionic (polyoxyethylene-based) surfactants and negatively charged silica particles[241–244]. It is believed that the nonionic PEO-based surfactants bind to negatively charged silica surface through hydrogen bonds between oxygen atoms of ethoxyethylene groups and hydrogen of the silanol group[245]. Below critical micelle concentration (CMC) the adsorbed surfactant molecules form a monolayer at the surface of the particle. It was recently shown[246] that the adsorbed hydrophilic groups lie flat on the silica surface while the hydrophobic chain extends towards a solution. Such modified silica surface becomes more hydrophobic which may result in the flocculation of particles from the solution. With increasing concentrations (near the CMC), additional surfactant molecules are bound to the first monolayer forming bilayer. The binding of these molecules is based on hydrophobic interactions between hydrophobic parts (alkyl chains) of surfactant molecules. Such quazi-micellar aggregates composed of particle with adsorbed surfactant bilayer are typically referred to as hemimicelles[247].

In the previous Section of this dissertation I showed that the sign of charge on the NPs may play a key role in the spontaneous incorporation of NPs into ordered matrices formed by nonionic surfactants via polymer-induced phase separation method[146,191]. In particular, I showed that the process is not symmetric with respect to the sign of NP charge, that is: negatively

charged NPs are incorporated much easier than positive ones. I suppose that the easiness of incorporation of negative NPs result from the adsorption of surfactant molecules at the surface of NPs. In this Section I combined the experimental results from different techniques (DLS measurement of hydrodynamic radii, ζ-potential measurements and spectroscopic real time studies of fluorescence quenching) to gain a new insight into the mechanism of fluorescence quenching of negatively charged QDs in the presence of nonionic surfactants.

3.3.2 Characterisation of quantum dots

Commercially available semiconductor NPs of a core/shell (CdSe/ ZnS) type were used in the experiments. These NPs, called also quantum dots, were coated with two stabilizing organic layers. The first one was octadecylamine and the second – amphiphilic polymer having carboxylic acid functional groups. The presence of the latter provided a water solubility as well as the negative charge at the surface of these NPs. Schematic representation of the structure of the QDs used in experiments is shown in Figure 60.

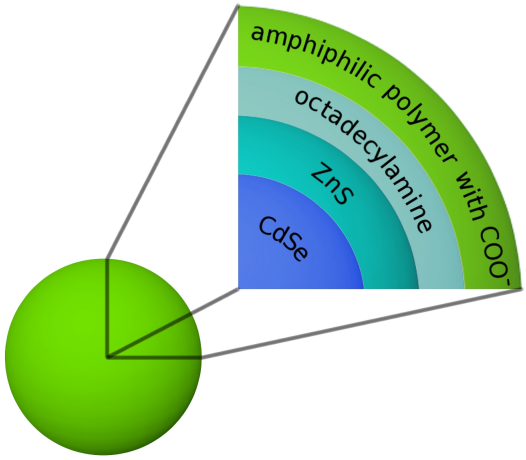

Figure 60: Schematic structure of QDs used. Each particle consisted of CdSe core surrounded by a ZnS shell. The particles were stabilized by octadecylamine layer and the layer of amphiphilic polymer with carboxylic acid groups.

QDs were characterized by performing: (i) measurement of the hydrodynamic radius of QDs, $R_{\mathrm{h,QD}}$ (using DLS), (ii) measurement of the ζ-potential of particles and (iii) absorption and fluorescence spectra in the UV-vis spectral range. The stability of the particles against aggregation was also determined.

I.The size of the quantum dots

To determine the size of QDs I performed the measurement of hydrodynamic radius using DLS technique. The resulting data are plotted in Figure 61. The experimental data were easily fitted with double-exponential fitting curve. This indicate the presence of two types of objects in the sample, moving with different diffusion coefficient and as a result - having different hydrodynamic radius. The values of diffusion coefficient and corresponding hydrodynamic radii obtained for QDs are collected in Table 7.

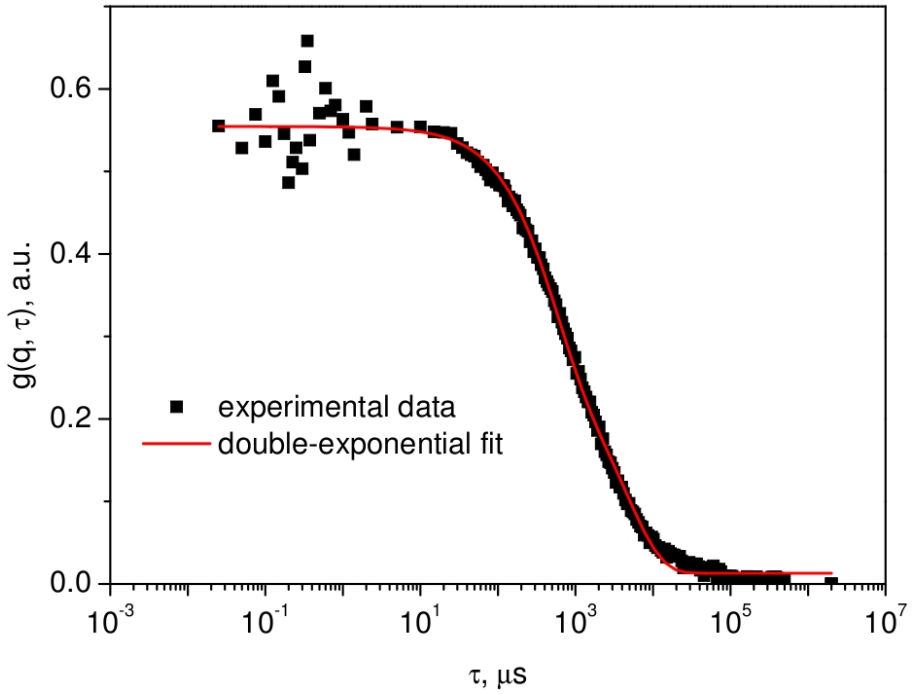

Figure 61: The DLS data obtained for QDs dissolved in water together with double-expomential fitting curve. The data was collected at 45°.

D (10^{-12} m^2/s)	R_h (nm)	I (a. u.)	interpretation
28.5 ± 2.5	8.6 ± 0.8	0.24	single QD
2.9 ± 0.3	83.8 ± 8.6	0.50	aggregates of QDs

Table 7: The values of diffusion coefficients, D, and corresponding hydrodynamic radii, R_h, and relative intensity of the DLS signal components obtained for QDs dispersed in water.

As it was indicated in Table 7, the smaller hydrodynamic radius (8.6 nm) was ascribed to single QDs, whereas the bigger ones (83.8 nm) corresponded to the aggregates of QDs. To estimate the relative number of aggregates I took the advantage of the fact that the intensity of

the DLS signal scales with the sixth power of the particle size[172]:

$$\frac{I_{\mathrm{b}}}{I_{\mathrm{s}}} \approx \frac{N_{\mathrm{b}}}{N_{\mathrm{s}}} \frac{R_{\mathrm{h,b}}^6}{R_{\mathrm{h,s}}^6} \Longrightarrow \frac{N_{\mathrm{b}}}{N_{\mathrm{s}}} \approx \frac{I_{\mathrm{b}}}{I_{\mathrm{s}}} \left(\frac{R_{\mathrm{h,s}}}{R_{\mathrm{h,b}}} \right)^6 . \tag{49}$$

In Equation (49), I_{b} and I_{s} is the intensity of DLS signal comming from big and small particles, N_{b} and N_{s} is the number density of big and small particles, $R_{\mathrm{h,b}}$ and $R_{\mathrm{h,s}}$ is the hydrodynamic radius of big and small particles respectively. In the case of QDs, the intensity of signal coming from aggregates (I_{b}) was approximately two times bigger than intensity of signal corresponding to isolated quantum dots (I_{s}) (see Table 7). By applying this value as well as the values of the hydrodynamic radii of QDs and aggregates from Table 7 to Equation (49) I got:

$$\frac{N_{\mathrm{b}}}{N_{\mathrm{s}}} \approx 2.3 \times 10^{-6} \tag{50}$$

which indicates that the number of aggregates was about two million times smaller than the number of non-aggregated QDs.

II. The ζ-potential of quantum dots

The outer stabilizing layer of QDs has carboxylic acid functional groups. This means, that in proper condition QD should exhibit negative ζ-potential. To verify this, I performed the measurement of ζ-potental of QD solution in deionized water in pH = 7.20. The resulting averaged ζ-potential of QDs was negative and equal to (-41.2 $\pm$ 3.9) mV.

III. Absorption and fluorescence spectra of quantum dots in the UV-vis spectral range

The normalized absorption and emission spectra of QD solution is plotted in Figure 62. As it is show in this figure, QDs exhibit strong absorption in UV and visible spectral range, with relatively small maximum at 523 nm. In the emission spectra of QDs there is a single band, whose maximum falls at 540 nm, and its full width at half maximum is 30 nm.

In studies, I collected fluorescence spectra of a series of samples containing QDs. In order to minimize the differences in experimental conditions (such as the laser power), and ensure the comparability of the results, the results were referred to the results obtained for the reference sample. Namely, the fluorescence spectrum of rhodamine B solution (0.0001 M in water) was collected before every measurement. The intensity of fluorescence of rhodamine B solution at

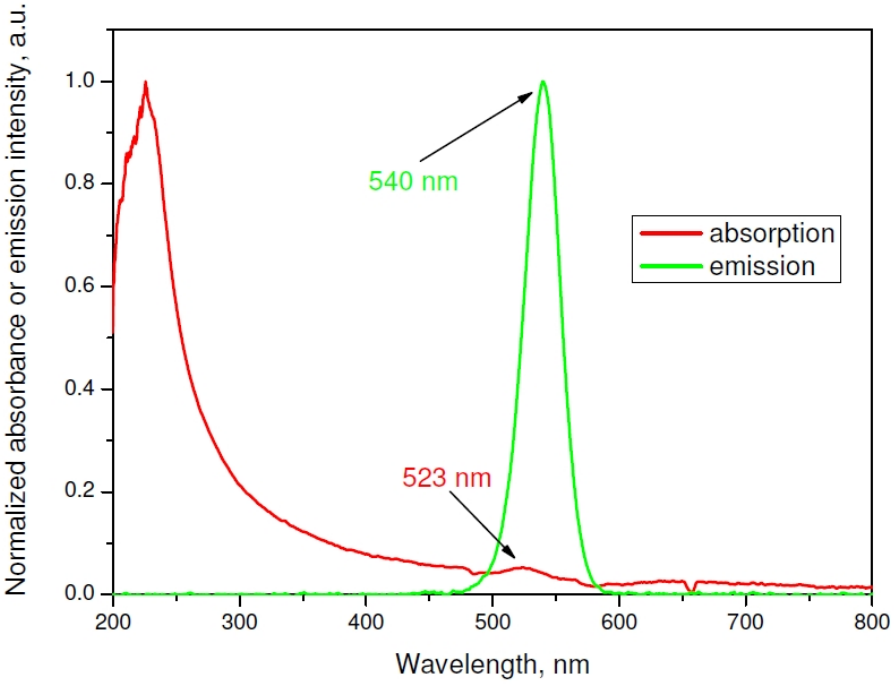

Figure 62: Normalized absorption and emission spectra of QDs used in the experiments.

λ_{max} = 594.8 nm was used as reference value.

IV. Stability of quantum dots

The QDs used in the experiments were very stable in water. Their fluorescence intensity was high and does not change much in time. The total quenching of QDs fluorescence in water was not observed even after very long storage of the sample (few months) or long (16 h) constant illumination. QDs used in experiments exhibited stability against aggregation in wide range of pH values. As it was noted, the aggregation of QDs in water solution was observed only if the pH of the solution was lower than 3. Importantly, the aggregation was not accompanied by any fluorescence quenching (aggregates of QDs exhibit very strong emission). The fluorescence of QD acidified to pH = 1 (measured in the center of the cuvette) decreased in time nearly to zero reflecting the precipitation process (see Figure 63). Importantly, the pH-induced aggregation of QDs did not cause any change in the position of emission maximum what indicates that the process did not cause any change of QD composition. Furthermore, the increase of the pH of the aggregated sample resulted in re-dispersing of QDs without any significant change in their emission intensity.

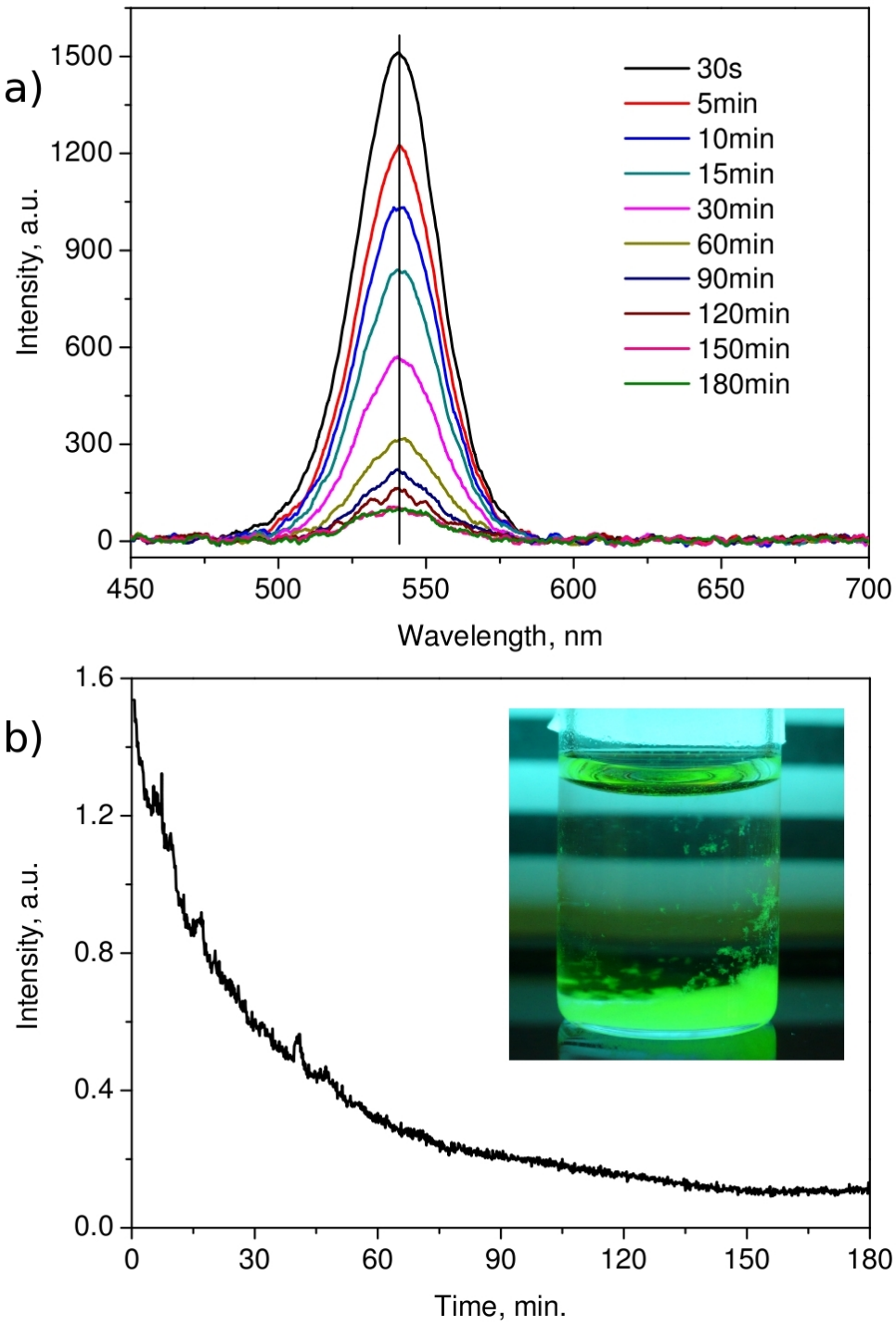

Figure 63: a) Changes of the emission spectra of QDs in water acidified to pH = 1. The curves plotted in different colors correspond to the absorption spectra measured at different times (indicated in legend) from the change in pH. b) Changes of the emission intensity of QDs in water acidified to pH = 1 at the emission maximum (540 nm). The intensity of fluorescence was normalized with respect to the fluorescence intensity of 0.0001 M rhodamine B in water. In the insert – the picture of aggregated QD solution taken in the UV light.

3.3.3 Characterization of $C_{12}E_n$ micellar system

To characterize the nonionic surfactant media I performed:

- detailed DLS measurements of hydrodynamic radii of micelles, $R_{\mathrm{h,mic}}$
- the measurements of pH of surfactants' solutions

The hydrodynamic radii of $C_{12}E_n$ micelles (n = 5 - 10, 23), were determined for five selected surfactant molar concentration, c_{surf}: 0.001 M, 0.01 M, 0.05 M, 0.1 M and 0.2 M. The changes of $R_{\mathrm{h,mic}}$ as a function of surfactant concentration are plotted in Figure 64.

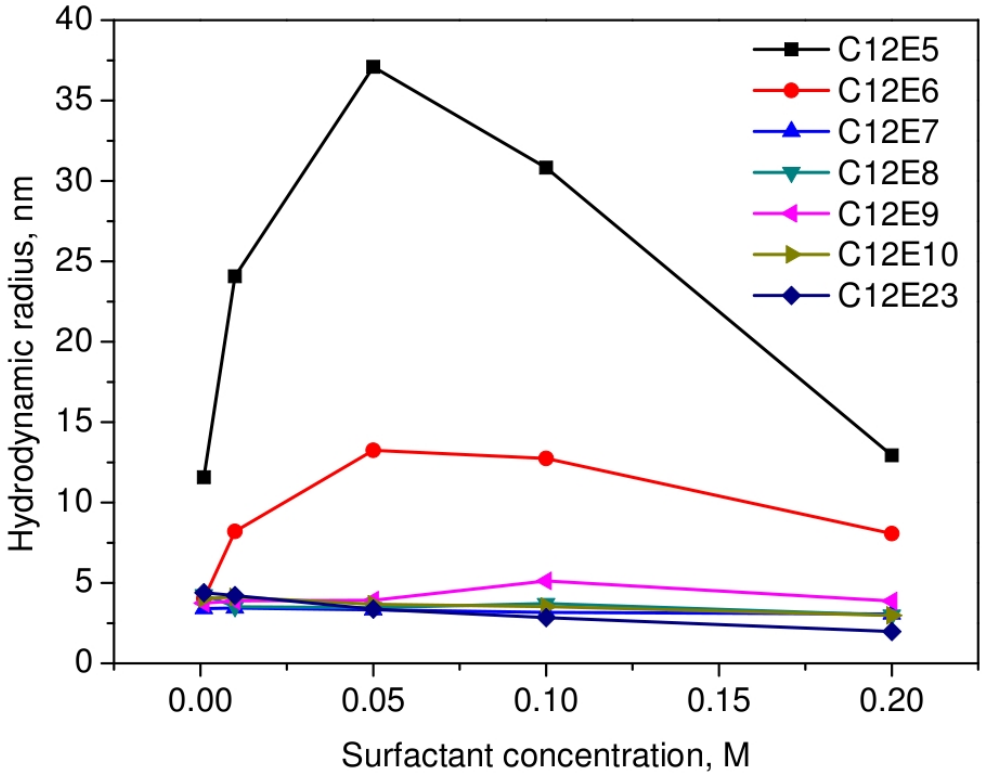

Figure 64: Comparison of $C_{12}E_n$ surfactant micelle hydrodynamic radii.

For most of the $C_{12}E_n$ surfactants (n = 7 - 10, 23), hydrodynamic radii of micelles were very similar to each other (about 3 - 4 nm) and varied only slightly with surfactant concentration. This results are consistent with literature, as it is known that those surfactant form small spherical micelles of a roughly constant size. For the remaining two surfactants, $C_{12}E_5$ and $C_{12}E_6$, the values of $R_{\mathrm{h,mic}}$ were significantly higher (up to 37 nm) and varied strongly with c_{surf}. Based on the literature[248], this behavior can be ascribed to the growth of $C_{12}E_5$ and $C_{12}E_6$ micelles into elongated or worm-like structure.

Measurements of pH were made using a pH meter equipped with a glass electrode suitable for viscous solutions. Measurements were performed at 25 °C. The obtained pH values are collected in Table 8.

surfactant	$C_{12}E_5$	$C_{12}E_6$	$C_{12}E_7$	$C_{12}E_8$	$C_{12}E_9$	$C_{12}E_{10}$	$C_{12}E_{23}$
0.2 M	2.73	2.51	2.70	2.42	2.47	2.40	2.67
0.1 M	2.86	2.61	2.94	2.51	2.49	2.50	2.61
0.05 M	3.08	2.68	3.28	2.73	2.89	3.60	2.95
0.01 M	3.97	3.31	3.98	3.20	3.21	3.88	3.23
0.001 M		4.22	4.30	4.24	3.88	4.26	4.43

Table 8: pH values of the surfactant solution for five molar concentration.

3.3.4 Fluorescence studies of QD quenching

The term: "fluorescence quenching" refers to the loss of fluorescence intensity of the emitting species, regardless of the nature of the process that leads to it.[249] Due to the relative proportions between the number of excited molecules of the fluorophore and quencher molecules as well as due to the possibility of their contact during the lifetime of the fluorophore excited state, one can distinguish three cases of fluorescence quenching.[249]

The first case of fluorescence quenching occurs when the quencher is in large excess relative to the fluorophore and the probability of their meeting during the lifetime of the fluorophore excited state is high. This case splits into two. If the probability of contact is equal to unity, we have photoinduced photon or electron transfer. If this probability is less than unity then we observe **static quenching**. Static fluorescence quenching is associated with two possibilities. The first is the existence of the so-called sphere of effective quenching which occurs when the mutual distance between the fluorophore and quencher can not be changed (e.g., when the reaction occurs in a rigid matrix). In such a case, the quencher affects the fluorescence of the fluorophore only if it is located within a certain sphere surrounding the fluorophore molecule. The second possibility of static quenching of fluorescence is associated with formation of ground-state non-fluorescent complex. The creation of fluorophore-quencher complex, results in the lack of fluorescence of fluorophore. In some cases, the formation of ground-state non-fluorescent

complex can be confirmed by the change in absorption spectrum of the fluorophore during the complexation process.

The second case of fluorescence quenching occurs when the quencher is not present in large excess relative to the fluorophore and, in addition, these species are not able to be in close proximity during the lifetime the fluorophore excited state. In this case, the fluorescence quenching of fluorophore is observed only when the interaction between the fluorophore and quencher is significant at long (about 8 nm) distances. This case is known as long-range non-radiative energy transfer.

The third case of fluorescence quenching occurs when the quencher is not present in large excess relative to the fluorophore (as in the second case) however the species can reach each other during the lifetime the fluorophore excited state. In this case, the process is diffusion-controlled and this type of quenching is referred to as **dynamic quenching**. It should be noted that for high concentrations of quencher, static quenching can occur together with the dynamic quenching.

The observed quenching of QD fluorescence in the presence of $C_{12}E_n$ nonionic surfactants was orders of magnitude slower than typically observed quenching of fluorophores (minutes/hours vs. nanoseconds). *This gave us the unique opportunity to monitor the process in real time.* I performed real-time fluorescence studies were performed to find time characteristics of the quenching process as well as its dependence on the surfactant concentration (c_{surf}). Importantly, I made sure that QD quenching is caused by the presence of surfactant itself, not by the presence of metal cation impurities. It is known that metal cations, especially Cu^{2+}, can affect the fluorescence of quantum dots[236,252–254]. On the other hand, surfactants often contain metal impurities that are remnants after the synthesis process. For most of $C_{12}E_n$ surfactants used, the total amount of metallic impurities (specified by the manufacturer) was in the order of 650 mg/kg whereby the contents of Cu^{2+} was $\leq$ 50 mg/kg. To eliminate the influence of metallic impurities, I used ethylenediaminetetraacetic acid, disodium salt (EDTA), a typical chelating ligand which complexes metal ions. The fluorescence of QDs was quenched by $C_{12}E_n$ surfactants even at large excess of EDTA, confirming that the QD quenching process is caused by the presence of surfactant.

I traced QD fluorescence changes in the aqueous solutions of nonionic surfactants, $C_{12}E_n$ for n = 5, 6, 7, 8, 9, 10 and 23. In a typical experiment, 10 μl of QDs (8 μM in water, original solution) were added to 410 μl of micellar solution of surfactant. The resulting QD concentration was 0.19 μM. The measurements were performed for five selected surfactant concentration, that is c_{surf} = 0.2 M, 0.1 M, 0.05 M, 0.01 M and 0.001 M. All the surfactants concentration used were above the value of critical micelle concentration, which for $C_{12}E_n$ surfactant series is of the order of 10^{-5} M. The exact literature values of CMCs are collected in Table 1 (Section 2.3). The molar concentrations were used to ensure the same number of surfactant molecules per one QD ($N_{\mathrm{surf/QD}}$) for all samples having same surfactant concentration. The exact numbers of surfactant molecules that accrue to one QD are collected in Table 9. The as prepared mixture of QDs and micelles was hand shaken for few seconds and then the fluorescence intensity was measured under continuous laser illumination. The first spectrum was collected 30 seconds after the addition of QDs to the surfactant solution and further spectra were recorded automatically every 10 seconds. Typical changes of the emission spectra of QDs in the solution of nonionic

c_{surf}	0.001	0.01	0.05	0.1	0.2
$N_{\mathrm{surf/QD}}$ [$\times 10^3$]	5.13	51.3	256	513	1026

Table 9: The number of surfactant molecules that accrue to one QD, $N_{\mathrm{surf/QD}}$, in the surfactant solution of a given concentration, c_{surf}.

surfactant in time is shown in Figure 65a. The corresponding time-characteristics of observed surfactant assisted QD quenching, that is, changes of fluorescence intensity at λ_{max} = 540 nm, is shown in Figure 65b. For most of surfactants and surfactant concentrations, the fluorescence of QD was fully quenched. In all cases, for c_{surf} down to 0.01 M, the fluorescence decay were fitted by the mono-exponential function,

$$I(t) = I_0 \exp\left(-\frac{t}{\tau_{\mathrm{q}}}\right), \tag{51}$$

where I is the intensity of fluorescence whereas t and τ_{q} correspond to time and time of quenching, respectively. For the lowest surfactant concentration, c_{surf} = 0.001 M the fluorescence intensity was not changed even after long time. For $C_{12}E_{23}$ only the highest concentration, 0.2 M, was examined. Even that concentration did not cause quenching of QDs fluorescence

within 24 h.

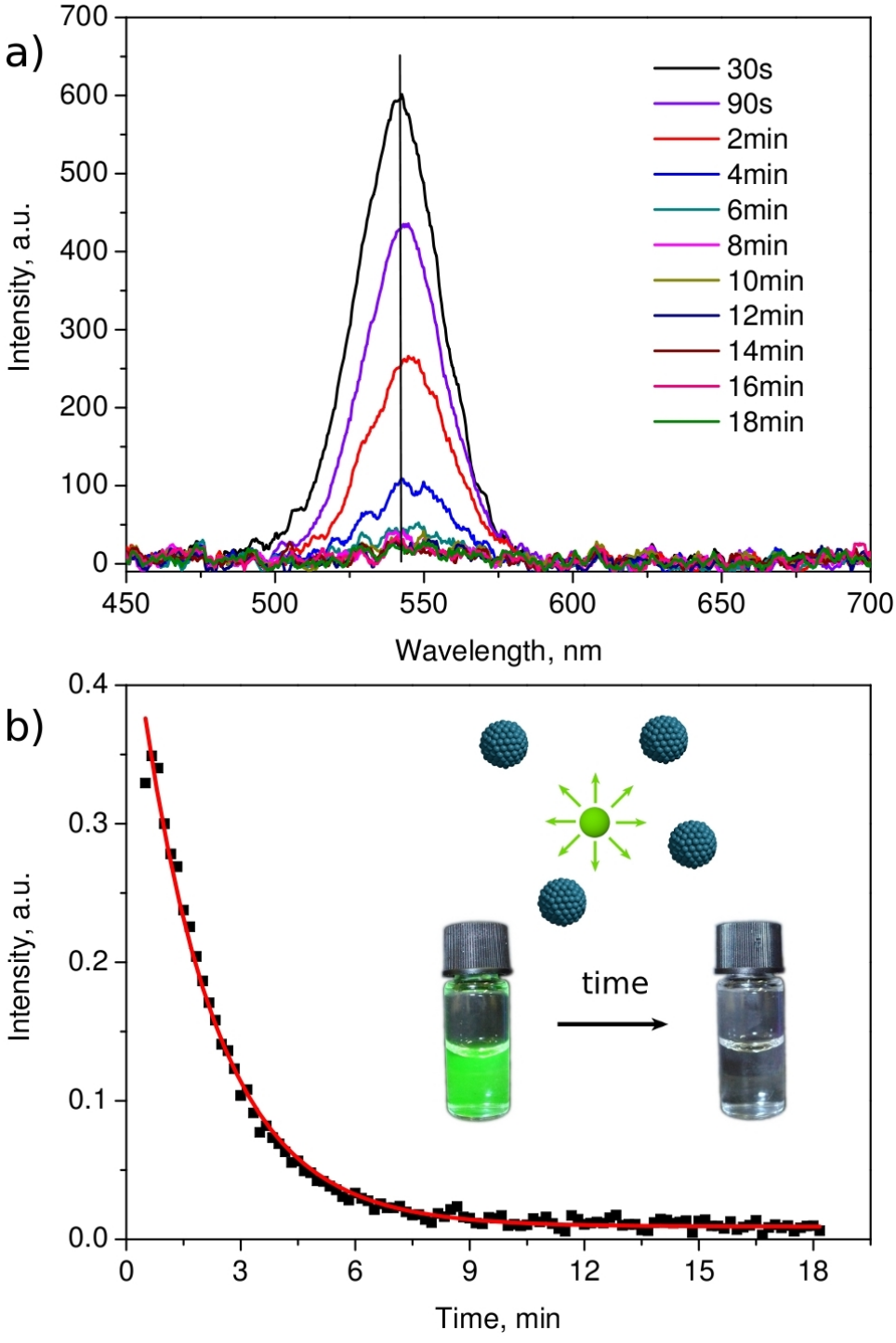

Figure 65: Representative results of QD quenching in the solution of nonionic surfactant. a) Changes of the emission spectra of QDs in 0.2 M $C_{12}E_8$ in time. b) Time characteristics of fluorescence quenching of QD in 0.2 M $C_{12}E_8$ at the wavelength of emission maximum: black points - experimental data, red curve - mono-exponential fit. Resulting quenching time is (1.99 $\pm$ 0.03) min. In the insert - photographs of a QD solution before and after quenching, taken in the UV light.

All quenching times taken from mono-exponential fitting were analyzed in terms of surfactant concentration dependence. The result for all the surfactants are plotted in Figure 66. Three basic trends were observed:

- quenching time decrease with surfactant concentration
- quenching time decrease with decreasing the number of oxyethylene groups (n) in $C_{12}E_n$ surfactant molecule.
- quenching was not observed in the case of solutions containing ethylene glycol oligo- or polymers (see also point (3) in section 3.3.8). It was verified using solutions of PEG consisting of 4, 6, 9, 13 and 464 monomers.

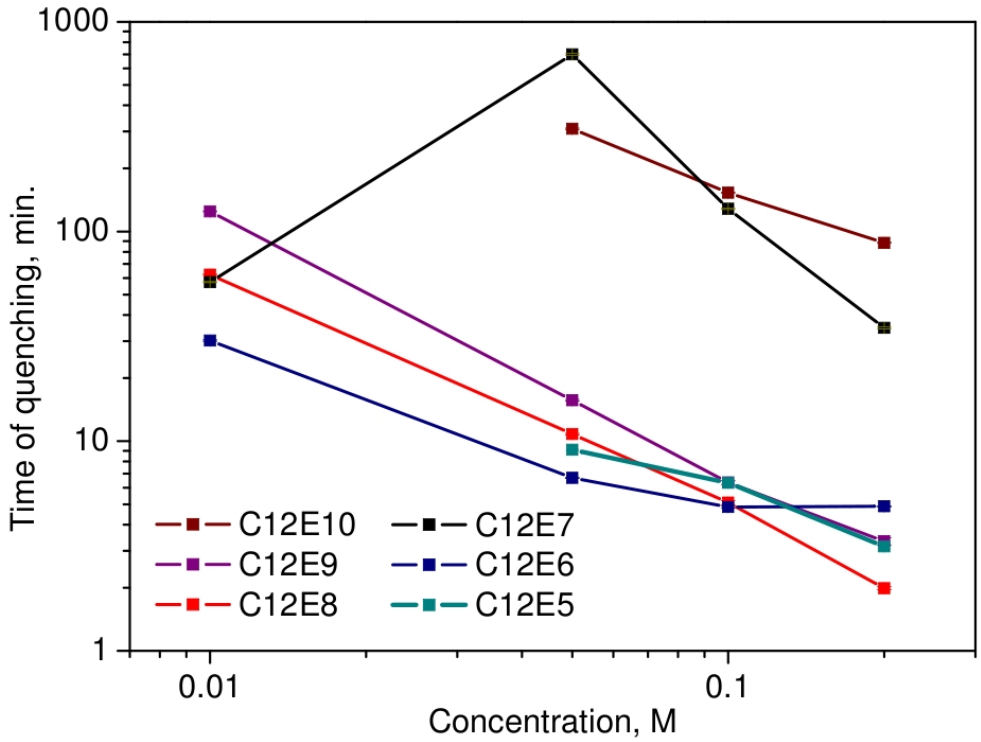

Figure 66: Quenching time of QD as a function of surfactant concentration. The lines are given as guides for the eye.

Additionally, the results plotted at the log-log plot reveal the difference between surfactants with small (n = 5 - 6) and large (n = 8 - 10) number of oxyethylene groups. In case of the latter group a linear dependence on log-log plot suggests the power law relation between quenching time, τ_q and surfactant concentration:

$$\tau_q = A \cdot (c_{surf})^B. \tag{52}$$

The values of exponent B are listed in Table 10.

surfactant	B
$C_{12}E_8$	-1.12 $\pm$ 0.03
$C_{12}E_9$	-1.28 $\pm$ 0.02
$C_{12}E_{10}$	-0.87 $\pm$ 0.08

Table 10: The values of exponent B (compare Equation (52)) for surfactants with high (n = 8 - 10) number of oxyethylene groups.

The observed difference in quenching observed for surfactants with small and large number of oxyethylene groups in hydrophilic part may be connected with size and shape of surfactant micelles. The power-low dependence is observed for $C_{12}E_8$, $C_{12}E_9$ and $C_{12}E_{10}$. These are surfactants that form small spherical micelles whose size, represented by $R_{\mathrm{h,mic}}$, does not change significantly with surfactant concentration (compare Figure 64). The second group ($C_{12}E_5$ and $C_{12}E_6$) is a group of surfactants that form elongated or worm like micelles, whose length depends strongly on surfactant concentration. From unknown reasons, QD quenching in the solutions of $C_{12}E_7$ seems to be intermediate. Namely, the power-low dependence is not observed despite the fact that $C_{12}E_7$ forms spherical micelles of a constant size.

The changes of the UV-Vis absorbance of QDs after the addition of surfactant were also investigated. As an example, the absorption spectra of QD and 0.2 M $C_{12}E_8$ in water as well as the time evolution of absorption spectra of QDs in 0.2 M $C_{12}E_8$ is shown in Figure 67. After the addition of surfactant, the absorbance of QDs decreases in time, and finally, reaches the level of the absorbance of surfactant. This means that the QDs no longer absorb the radiation – they become "invisible." This is possible only in two cases: (i) if the QDs have been destroyed by surfactant, or (ii) if the QDs have been surrounded by the surfactant in such a way that they mimic surfactant micelles. Since the first of these hypotheses seems to be impossible, I verified the second one – wrapping of the QDs by the surfactant. This issue will be discussed in subsequent Sections.

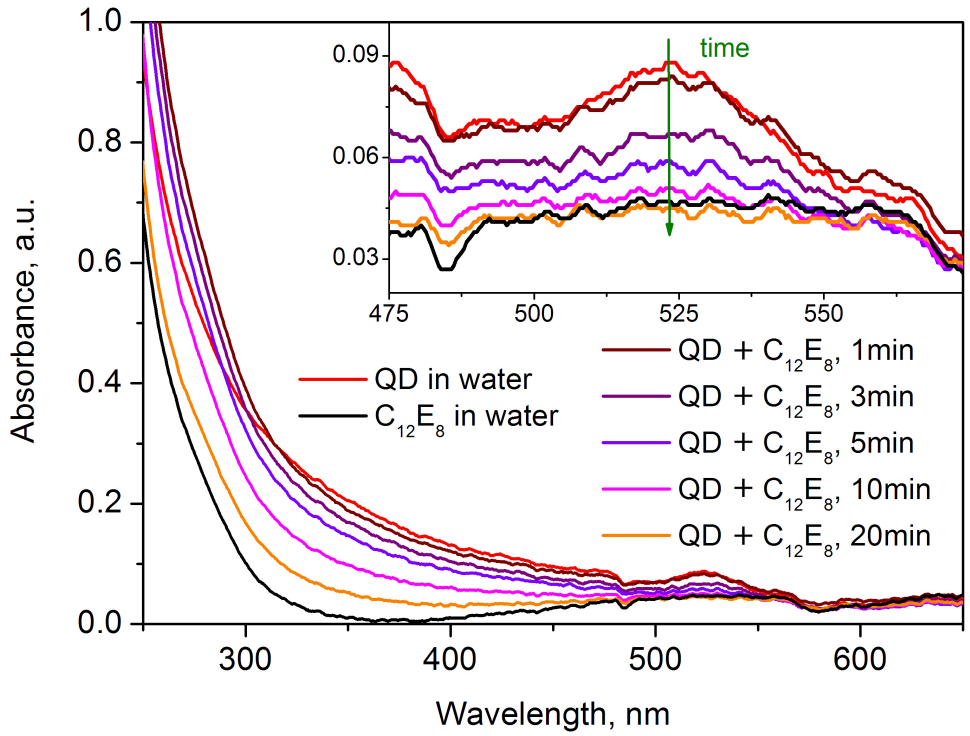

Figure 67: The absorption spectra of QD and 0.2 M $C_{12}E_8$ in water as well as the time evolution of absorption spectra of QDs after mixing with $C_{12}E_8$. As indicated in the legend, the subsequent spectra were recorded after 1, 3, 5, 10 and 20 minutes after mixing of QDs with surfactant. Insert: the enlargement of the spectra around the spectral range corresponding to the maximum of absorption of QDs in visible range.

3.3.5 DLS studies of quenched QD samples

As it was shown in previous Section, the fluorescence of QDs was quenched after mixing with surfactant solution. This process was however not accompanied by any macroscopic aggregation or precipitation, even after long time storage of the sample. Additionally, as it was discussed at the end of the previous Section, the process of quenching of QDs was associated with a decrease of their absorbance to the level of surfactant, which suggested that QDs are surrounded by surfactant. Based on these observation as well as on the literature I brought forward the hypothesis that the quenching of QDs fluorescence was a result of adsorption of surfactant micelles at the surface of QDs. It seemed that the surfactant layer adsorbed on the surface of the QD protected QD from light, which hinders the excitation of fluorescence and hence led to the quenching of fluorescence observed.

To verify this hypothesis I performed dynamic light scattering (DLS) measurements to determine the hydrodynamic radius of the quenched QD samples. I expected to see a change in

hydrodynamic radius of quenched sample with respect to both QDs and micelles. The difficulty was that the hydrodynamic radii of QDs, micelles, and sought objects (consisting of surfactant molecules adsorbed on the surface of QDs) were of the same order. Therefore, to improve the sensitivity of DLS measurements it was advisable to prepare the quenched sample containing the smallest possible amount of free surfactant micelles. Additionally, to avoid problems associated with the change of hydrodynamic radius of micelles with a change of surfactant concentration, it was desirable to use a surfactant with a relatively constant size of micelles (eg, $C_{12}E_8$). With this in mind I performed the experiment using titrated sample of QD solution with smallest amount of $C_{12}E_8$. This minimal $C_{12}E_8$ concentration was found to be 0.013 M. It meant that the proportion of QDs and micelles in the sample was about 1 : 940 (considering the fact that $C_{12}E_8$ form spherical micelles formed by about 79 molecules[251]).

DLS scattering signal from quenched sample of QD in 0.013 M $C_{12}E_8$ was fitted by the double-exponential function (as for QDs in water). The obtained values of diffusion coefficient and resulting hydrodynamic radii are collected in Table 11. The comparison of the obtained R_{h} values with the one for QD (see Table 7) and that of surfactant micelles led to two conclusions: (1) the smaller R_{h} value was intermediate between micelles and QDs, (2) the bigger R_{h} value corresponded to much larger objects compared to micelles and QDs. The bigger R_{h} value was very similar to the one of QD aggregates in water (a bit smaller) what suggested that this were the same aggregates. Additionally, the proportion between the signal intensities from big and small objects in the quenched samples was nearly the same as in the case of QD aggregates and free QD in water (the actual proportion was a little bit smaller). The observation that the aggregates were smaller in the case of quenched samples may result from surfactant molecules destroying the aggregates. The breaking of the QD aggregates was also reflected in the relative decrease in signal intensity originating from the aggregates with respect to the intensity of the signal from the smaller objects. The fact that the smaller R_{h} value was intermediate between that of QDs and micelles may be caused by two factors. Firstly, the difference in hydrodynamic radius of QD and micelles was small, only about 5 nm. For this reason, I observed one average hydrodynamic radius, that was bigger than R_{h} of micelles and smaller than that of QD. Secondly, the QD : micelles molar ratio was very small (about 1 : 940), what led to additional masking of the DLS signal coming from QDs.

surfactant	QD : micelles	D (10^{-12} m^2/s)	R_h (nm)
0.013 M $C_{12}E_8$	1 : 940	54.7 ± 0.5	4.48 ± 0.04
		4.8 ± 0.1	51 ± 1
9.25 $\times 10^{-4}$ M $C_{12}E_8$, pH $\approx$ 1	1 : 60	13.8 ± 0.5	17.7 ± 0.6
		4.5 ± 0.3	54 ± 3

Table 11: The values of diffusion coefficients, D, and corresponding hydrodynamic radii, R_h, obtained for quenched samples of QDs in $C_{12}E_8$. For each case the values of R_h were detected. The bigger one correspond to the QD aggregates.

I found that in the quenching of QD fluorescence in the presence of nonionic surfactant two parameters were crucial, that is, surfactant concentration and the appropriate pH conditions. As it was shown in Table 8, the surfactants' solutions exhibited slightly acidic pH and the majority of those solutions has pH < 4. When quantum dots were dispersed in water acidified to the same pH – it resulted in, at least partial, aggregation of QDs. On the other hand, fluorescence quenching of QDs was not observed in any of the 0.001 M surfactant solution (pH > 4). This suggested that there was a synergistic effect of pH and surfactant concentration. As a confirmation I lowered the pH (down to $\sim$ 1) in the sample consisting of QDs dispersed in 0.001 M $C_{12}E_8$ (this concentration did not normally cause QDs quenching). After lowering the pH, fluorescence quenching of ODs was observed without any detectable aggregation. With this in mind, I titrated the acidified (pH $\approx$ 1), aggregated sample of QDs with small portions of $C_{12}E_8$ to find the minimal content of surfactant needed to quench the fluorescence of QDs in low pH conditions. It was found that the addition of surfactant led to the successive breakdown of aggregates and as well as to the quenching of QDs fluorescence. The minimal $C_{12}E_8$ concentration that result in total quenching of QDs fluorescence without visible aggregation (in pH $\approx$ 1) was 9.25 $\times 10^{-4}$ M. This concentration corresponded to the proportion between QDs and $C_{12}E_8$ micelles equal to 1 : 60. The as prepared sample was further analyzed with DLS, and the result of this experiment is shown in Figure 68.

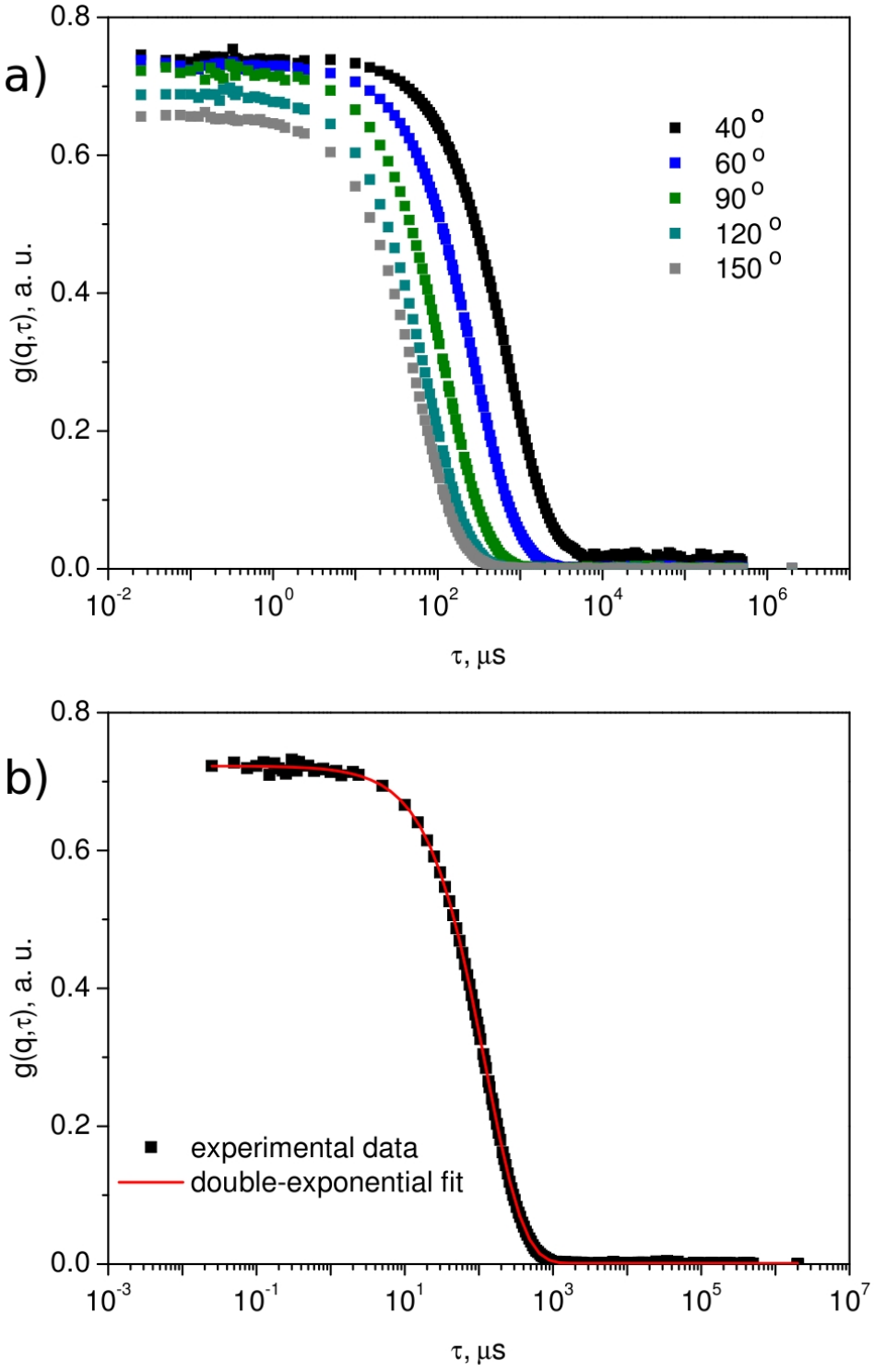

Figure 68: a) DLS experimental data collected for quenched sample of QDs and 9.25 $\times 10^{-4}$ M $C_{12}E_8$ in pH $\approx$ 1. Experimental points of different colors correspond to measurements made at different angles. b) Double-exponential fitting curve for the quenched sample of QD in pH $\approx$ 1. The data were collected at 90°.

As in previous experiments, the data from the DLS were fitted with double-exponential function (compare Figure 68b). The fitting procedure gave two distinct diffusion coefficients and as a result to two different hydrodynamic radii. The exact values of D and R_{h} are collected in Table 11. As before, the bigger R_{h} corresponded to partially broken aggregates of QDs (that were present in the pure sample of QDs in water). The difference was however observed in the case of smaller R_{h}, namely, smaller hydrodynamic radius was bigger from both QDs ($R_{\mathrm{h,QD}}$ = (8.6 $\pm$ 0.8) nm) and $C_{12}E_8$ micelles ($R_{\mathrm{h,mic}}$ = (3.7 $\pm$ 0.1) nm in pH = 1). This observation strongly supports the hypothesis of the surfactant adsorption at the surface of QDs. The obtained value R_{h} = (17.7 $\pm$ 0.6) nm agrees within experimental errors with the sum of $R_{\mathrm{h,QD}}$ and doubled $R_{\mathrm{h,mic}}$ ($R_{\mathrm{h,QD}} + 2R_{\mathrm{h,mic}}$ = (8.6 $\pm$ 0.8) nm + (7.4 $\pm$ 0.2) nm = (16 $\pm$ 3.0) nm). This fact suggests that in the quenched samples, surfactant molecules formed a bilayer at the surface of QD. The schematic representation of QD with adsorbed surfactant bilayer is shown in Figure 69.

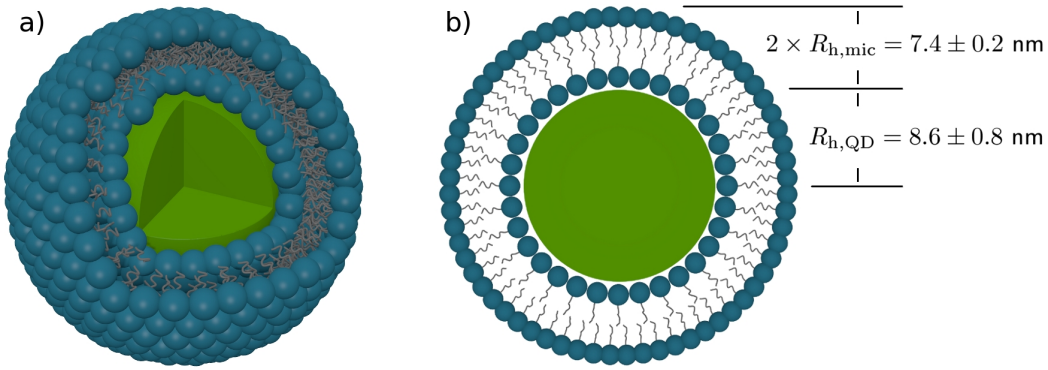

Figure 69: Three-dimensional model (a) and its cross section (b) representing QD with adsorbed surfactant bilayer. The inner green sphere represents the original quantum dot and blue shell is the surfactant bilayer.

3.3.6 ζ-potential measurements

ζ potential measurements were performed to provide additional confirmation of the adsorption of surfactants at the surface of QDs. It is known from the literature[245], that the adsorption of PEO-based surfactants to the silica particles result in masking the silica surface what cause the change of the ζ-potential of particles. Namely, ζ-potential of negatively charged particles became less negative after the adsorption of surfactant. I expected to see similar change of ζ-potential in the case of negatively charged QD in surfactant solution.

As it was mentioned in Section 3.3.2, ζ-potential of pure quantum dots in water solution (pH = 7.20) was negative and equal to (-41.2 $\pm$ 3.9) mV. Mixing of QDs with surfactant resulted in decrease of their ζ-potential. As an example, the mixing of QDs with 0.01 M $C_{12}E_8$ (pH = 3.4) resulted in decreasing the value of ζ-potential down to (-3.46 $\pm$ 6.8) mV within 10 minutes. It should be noted that within the time of the ζ-potential measurements (2 h) the fluorescence of investigated sample was almost completely quenched. The fact, that ζ-potential of QD was lowered after mixing with surfactant support the hypothesis of the adsorption of surfactant molecules to the surface of quantum dot.

3.3.7 Model of fluorescence quenching

Based on the experimental results presented in the previous sections, the exponential decay of the QD fluorescence observed in the system and the dependence of the quenching time on the surfactant concentration given by Equation (52) can be explained in terms of a simple surfactant adsorption model. This model is based on the following assumptions: First, it is assumed that the intensity, I, of the fluorescence of a selected QD decreases linearly with the amount of the surfactant molecules adsorbed on its surface. To quantify this assumption, denote by σ ($0 \leq \sigma \leq 1$) degree of saturation of the QD's surface, and by σ_0 the adsorption capacity of the QD. The quantity σ plays here a role analogous to that of the fractional coverage used in the Langmuir adsorption[250] theory. That is, when there are no surfactant molecules attached to the surface $\sigma = 0$, and when σ reaches the value of σ_0 the QD can no longer adsorb the surfactant molecules. The main difference between the fractional coverage and the degree of saturation is that the latter allows multilayer organization of the adsorbed molecules on the QD surface. Without loss the generality, we can also put $\sigma_0 = 1$. Thus, the fluorescence intensity depends

on σ according to the following formula:

$$I(\sigma) = (1-\sigma) I_{\mathrm{bare}}, \tag{53}$$

where I_{bare} is the fluorescence intensity of pristine (bare) QD. The second assumption is that the adsorption process obeys the first-order kinetics[250] with respect to surfactant concentration and σ, and that the degree of saturation changes with time according to the formula:

$$\frac{d\sigma}{dt} = \kappa_{\mathrm{a}} c_{\mathrm{surf}} (1-\sigma) - \kappa_{\mathrm{d}} \sigma, \tag{54}$$

where κ_{a} and κ_{d} are, respectively, adsorption and desorption rate constants. Both these quantities depend on the nature of the adsorption, shapes and sizes of the micelles, and on conditions such as temperature or pH. It is also assumed that the product $\kappa_{\mathrm{a}} c_{\mathrm{surf}}$ is much greater than κ_{d}, and that the concentration of surfactant does not change during the adsorption process. The first assumption is justified by the apparent irreversibility of the adsorption of surfactant observed in experiments. The latter assumption is satisfied because in the systems studied concentrations of the QDs were two or three orders of magnitude smaller than c_{surf}. By combining the solution of Equation (54) and the relation (53) we straightforwardly get the following dependence of the fluorescence intensity on time:

$$I(t) = I_{\mathrm{bare}} \exp\left(-\kappa_{\mathrm{a}} c_{\mathrm{surf}} t\right). \tag{55}$$

The above relation reproduces the exponential decay of $I(t)$ observed experimentally. In terms of the model parameters, the quenching time is given by the formula

$$\tau_{\mathrm{q}} = \frac{1}{\kappa_{\mathrm{a}} c_{\mathrm{surf}}}. \tag{56}$$

Finally, comparison of Equations (56) and (52) yields

$$B = -1. \tag{57}$$

This value of the exponent obtained agrees well with that observed experimentally, B = -1.09 $\pm$ 0.14 calculated as the average for $C_{12}E_8$, $C_{12}E_9$, and $C_{12}E_{10}$ (see Table 10).

3.3.8 Conclusions

In this Section of the dissertation I studied the fluorescence quenching of negatively charged QDs in the presence of nonionic, PEO-based, surfactants. I combined a range of experimental techniques including real-time fluorescence studies, DLS mesurements and ζ-potential measurements to elucidate the mechanism of quenching and to verify the final structure of quenched samples. My observations were as follows:

(1) QD fluorescence is quenched in $C_{12}E_n$ surfactant micellar solutions, especially for surfactants with small hydrophilic part.

(2) The process is not accompanied by any macroscopic aggregation or precipitation, even after long time storage or centrifugation of the sample.

(3) QD fluorescence is not quenched in the solutions of ethylene glycol polymers (despite the same hydrophilic units in both polymers and surfactants), what indicates that amphiphilic nature of the surfactant is crucial for the process.

(4) QD quenching is inhibited at high pH what suggests that hydrogen bonds play important role in the process.

(5) QD quenching is irreversible with respect to the pH. Changing the pH of quenched sample (both into acidic or basic) does not restore the fluorescence of QDs.

(6) Fluorescence intensity of QD in the presence of surfactants decays mono-exponentially in time and the quenching time is the power-law function of surfactant concentration. These two facts were explained using a simple model of adsorption of surfactant on the surface of QD (see Section 3.3.4).

(7) In the process of the fluorescence quenching, the absorbance of the QDs decreases to reach the level of surfactant. QD becomes "invisible". This fact may also reflect the process of adsorption of surfactant to the surface of the QD.

(8) DLS measurements of quenched samples revealed the presence of objects with a hydrodynamic radius that is larger than both the QD and the surfactant micelles. The resulting hydrodynamic radius was, in fact, comparable to the radius of QD increased by a diameter of micelle. This suggests the adsorption of surfactant bilayer on the surface of the QD.

(9) The adsorption of surfactant to the surface of the QD is also reflected in the change of ζ-potential. Namely, ζ-potential QD surrounded by surfactant is less negative than the ζ-potential of bare QD.

As it was mentioned at several points above, I found that the quenching of QD fluorescence is caused by the adsorption of surfactants at the surface of QD. This adsorption of surfactant was confirmed by both DLS and ζ-potential measurements. By the analysis of DLS experimental data I estimated that in the quenched samples, each QD is surrounded by the bilayer of surfactant. The first layer within bilayer is formed by the adsorption of the hydrophilic segments of surfactants to the surface of QD and it is stabilized by hydrogen bonds between QD surface (namely protonated carboxylic acid groups) and oxyethylene groups of the surfactant. The second layer of surfactant molecules is stabilized by hydrophobic interaction between the alkyl chains of surfactants. The fact, that the first layer is stabilized by the hydrogen bonds explains the observed comparative effect between surfactant concentration and the low-pH condition. At lower pH the fraction of protonated COOH groups increases which causes more surfactant molecules can adsorb to the QD surface. Similarly, at higher pH most of the COOH group is deprotonated, which hinders the binding of surfactant molecules to the surface of the QD and thus weakens the fluorescence quenching. The presence of the second layer of surfactant molecules at the surface of QDs explains the lack of aggregation in the quenched samples. QDs with adsorbed surfactant bilayer were found to be stable in water by the analogy to normal surfactant micelles (due to the interaction between hydrophilic segments of surfactant with water molecules). The ζ-potential measurements also supports the hypothesis of the surfactant adsorption to the surface of QDs. As it was shown, in the presence of surfactant, the ζ-potential of QD became less negative and additionally it changes in time which suggest that the surfactant molecules rearranges at the surface of QD. The adsorption of surfactant to QDs is also evidenced by the change of absorption spectra of QDs during the process. As it was noted, the absorbance of QDs in the presence of surfactant decreases in time to the level of pure surfactant. It means that QDs became "invisible". This fact indicates the role of the surfactant shell in the quenching process. It seams that it absorbs the energy of the excitation and also the energy emitted by the excited QDs.

At the beginning of Section 3.3.4, I presented three basic cases of fluorescence quenching observed for typical fluorophores. The location of observed QD quenching among these three cases is not a simple issue. I have shown that QD quenching process (its dependence on time and on surfactant concentration) can be modeled by a simple model in which the adsorption of surfactant to the QD is limited by diffusion. According to the presented classification, the

diffusion-controlled processes are observed in the case of dynamic fluorescence quenching. On the other hand, the observed changes in absorption spectrum of QD in the presence of surfactant seem to support the "formation of ground-state non-fluorescent complex" scenario, which is a variant of the static quenching. According to the literature[249], both types can coexist if the quencher concentration is high, which probably takes place in this case. In order to classify the observed fluorescence quenching properly, one needs to perform additional series of experiments, including measurements of fluorescence lifetimes and quantum yields for bare and surfactant-coated QDs.

4 Summary

As the first thesis of this dissertation, I postulated that the ordering in solutions of ionic surfactants can be achieved through a polymer-induced phase separation. To confirm this thesis I conducted experiments in four experimental systems, that is: (i) anionic surfactants and anionic polyelectrolytes, (ii) cationic surfactants and cationic polyelectrolytes, (iii) cationic surfactants and nonionic polymers either undoped or doped with different inorganic salts, and (iv) anionic surfactants and nonionic polymers. As described in details in Section 3.1, I confirmed postulated thesis. The desired ordering in solutions of ionic surfactants can be achieved by: (a) adding an appropriate amount of ionic polymer (polyelectrolyte) having the charge of the same sign as that of surfactant (b) adding a nonionic polymer (c) adding a nonionic polymer with the addition of inorganic salt. First method is appropriate for ionic surfactant of either charge whereas the second and the third works well only in solutions of cationic surfactants. Importantly, presented method enables the phase separation and ordering of the surfactant phase even in very dilute surfactant systems – for surfactant concentrations that are only one order of magnitude larger than the critical micelle concentration. Additionally, I studied in details the effect of inorganic salt on the phase separation with both ionic and nonionic polymers. I found that the presence of inorganic salt has a positive effect on the phase separation involving both ionic and nonionic polymers, that is it minimizes the amount of polymer needed to induce the phase separation.

The second thesis of this dissertation concerned the use of polymer-induced phase separation (described in Section 3.1) as a potential method to incorporate NPs into ordered phases of surfactants. To verify this thesis, I used ternary systems consisting of surfactant, polymer, and hydrophilic NPs. As presented in Section 3.2, I examined both non-ionic matrices (nonionic surfactant/nonionic polymer system) and ionic matrices (anionic surfactant/anionic polyelectrolyte and a cationic surfactant/cationic polyelectrolyte systems). I demonstrated that polymer-induced phase separation is an effective method for incorporation of hydrophilic NPs for a variety of ordered phases including hexagonal and lamellar phase. I showed that embedded NPs are uniformly distributed within the considered phase and aggregate insignificantly. The resulting soft composite is stable even after long storage of the sample (about 11 months). Moreover, the presented method allows the incorporation of NPs of any charge to the LLC ma-

trix formed by both ionic and nonionic surfactants. In case of nonionic matrices I considered the impact of NP charge on the efficiency of its incorporation to the LLC phases. Surprisingly, I found that there is a difference in the incorporation of negatively and positively charged NPs. As I demonstrated, NP having negative charge are incorporated far more easily (i.e. at lower polymer concentrations) than those with a positive charge. The number of positive NPs embedded can be increased in two ways: (i) by increasing the polymer concentration and/or (ii) by adding negatively charged NPs. This means that it is possible to obtain a composite material consisting of ordered matrix and two different types of NPs in prescribed proportions.

The third thesis of this dissertation concerned the adsorption of nonionic surfactants to the surface of negatively charged NPs, especially semiconductor QDs. As I presented in Section 3.2 and the preceding paragraph of this summary, the negatively charged NP were incorporated more easily to nonionic matrices than those with a positive sign. Additionally, I observed that the fluorescence of semiconductor quantum dots is rapidly quenched in the presence of non-ionic surfactants. I brought forward the hypothesis that these unusual behaviors arise from the adsorption of molecules at the surface of NP or QDs. As I presented in Section 3.3, in order to verify this thesis I conducted a series of experiments including real time measurements of fluorescence of QDs in the presence of surfactants, DLS measurements of hydrodynamic radius in solutions of QDs and surfactants and ζ-potential measurements. Obtained results show that: (i) non-ionic surfactants adsorb at the surface of NPs that have COOH groups at the surface, (ii) the adsorption is stabilized mainly by hydrogen bonds between protonated COOH groups and ethoxyethylene groups of surfactants (iii) the successive adsorption of surfactant molecules to the surface of QDs leads to a gradual quenching of QD fluorescence, (iv) in the quenched samples, each quantum dot is surounded by a bilayer of surfactant. Fluorescence quenching caused by adsorption of surfactant is a result of two factors. Firstly, the gradual shielding of the QDs surface by adsorbed micelles leads to a reduction of radiation that excite QD fluorescence. Secondly, the photons emitted by the QD are effectively dissipated by surfactant coating.

References

[1] Feynman, R. P. *Miniaturization*. Gilbert H. D. Ed., Reinhold Publishing Corporation, New York, (1961).

[2] Taniguchi, N. On the basic concept of nano-technology. In *Proc. ICPE*, (1974).

[3] Chemicool.com., G. C. P. T. http://www.chemicool.com/elements/gold.html.

[4] Rao, C. N. R., Thomas, P. J., and Kulkarni, G. U. *Nanocrystals: Synthesis, properties and applications*. Springer, (2007).

[5] Rao, C. N. R., Mu¨ller, A., and Cheetham, A. K., editors. *The Chemistry of Nanomaterials: Synthesis, Properties and Applications*. WILEY-VCH Verlag GmbH & Co. KGaA, (2004).

[6] Lee, H. M., Ge, M., Sahu, B. R., Tarakeshwar, P., and Kim, K. S. Geometrical and electronic structures of gold, silver, and gold-silver binary clusters: Origins of ductility of gold and gold-silver alloy formation. *J. Phys. Chem. B* **107**, 9994 (2003).

[7] Negishi, Y., Takasugi, Y., Sato, S., Yao, H., Kimura, K., and Tsukuda, T. Magic-numbered aun clusters protected by glutathione monolayers (n = 18, 21, 25, 28, 32, 39): Isolation and spectroscopic characterization. *J. Am. Chem. Soc.* **126**, 6518 (2004).

[8] Duffe, S., Irawan, T., Bieletzki, M., Richter, T., Sieben, B., Yin, C., von Issendorff, B., Moseler, M., and H¨ovel, H. Softlanding and stm imaging of ag561 clusters on a c60 monolayer. *Eur. Phys. J. D* **45**, 401 (2007).

[9] Curley, B. C. and Johnston, R. L. Combining theory and experiment to characterize the atomic structures of surface-deposited au309 clusters. *J. Phys. Chem. C* **111**, 17846 (2007).

[10] Roduner, E. *Nanoscopic materials. Size-dependent phenomena*. The RoyalSociety of Chemistry, (2006).

[11] Corma, A. and Garcia, H. Supported gold nanoparticles as catalysts for organic reactions. *Chem. Soc. Rev.* **37**, 2096 (2008).

[12] Johnson, B. F. G. Topics in catalysis. *Top. Catal.* **24**, 147 (2003).

[13] Zheng, N., Fan, J., and Stucky, G. D. One-step one-phase synthesis of monodisperse noble-metallic nanoparticles and their colloidal crystals. *J. Am. Chem. Soc.* **128**, 6550 (2006).

[14] Sharma, V., Park, K., and Srinivasarao, M. Shape separation of gold nanorods using centrifugation. *PNAS* **106**, 4981 (2009).

[15] Zhang, J., Langille, M. R., Personick, M. L., Zhang, K., Li, S., and Mirkin, C. A. Concave cubic gold nanocrystals with high-index facets. *J. Am. Chem. Soc.* **132**, 14012 (2010).

[16] Chen, J., Wiley, B. J., and Xia, Y. One-dimensional nanostructures of metals: Large-scale synthesis and some potential applications. *Langmuir* **23**, 4120 (2007).

[17] Jana, N. R., Gearheart, L., and Murphy, C. J. Wet chemical synthesis of silver nanorods and nanowires of controllable aspect ratio. *Chem. Commun.* **7**, 617 (2001).

[18] Talapin, D. V., Nelson, J. H., Shevchenko, E. V., Aloni, S., Sadtler, B., and Alivisatos, A. P. Seeded growth of highly luminescent cdse/cds nanoheterostructures with rod and tetrapod morphologies. *Nano Lett.* **7**, 2951 (2007).

[19] Shao, Y., Jin, Y., and Dong, S. Synthesis of gold nanoplates by aspartate reduction of gold chloride. *Chem. Commun.* **9**, 1104 (2004).

[20] Lin, T.-H., Linn, N. C., Tarajano, L., Jiang, B., and Jiang, P. Electrochemical sers at periodic metallic nanopyramid arrays. *J. Phys. Chem. C* **113**, 1367 (2009).

[21] Pellegrino, T., Fiore, A., Carlino, E., Giannini, C., Cozzoli, P. D., Ciccarella, G., Respaud, M., Palmirotta, L., Cingolani, R., and Manna, L. Heterodimers based on copt3-au nanocrystals with tunable domain size. *J. Am. Chem. Soc.* **128**, 6690 (2006).

[22] Huang, L., Wang, M., Zhang, Y., Guo, Z., Sun, J., and Gu, N. Synthesis of gold nanotadpoles by a temperature-reducing seed approach and the dielectrophoretic manipulation. *J. Phys. Chem. C* **111**, 16154 (2007).

[23] Schmid, G., editor. *Nanoparticles: from theory to application*. WILEY-VCH Verlag GmbH & Co. KGaA, (2004).

[24] Medintz, I. L., Uyeda, H. T., Goldman, E. R., and Mattoussi, H. Quantum dot bioconjugates for imaging, labelling and sensing. *Nat. Mater.* **4**, 435 (2005).

[25] McNaught, A. D. and Wilkinson, A., editors. *IUPAC. Compendium of Chemical Terminology*. Blackwell Scientific Publications, Oxford, 2nd ed. (the gold book) edition, (1997). XML on-line corrected version: http://goldbook.iupac.org (2006-) created by M. Nic, J. Jirat, B. Kosata; updates compiled by A. Jenkins.

[26] Morello, G., Anni, M., Cozzoli, P. D., Manna, L., Cingolani, R., and Giorgi, M. D. The role of intrinsic and surface states on the emission properties of colloidal cdse and cdse/zns quantum dots. *Nanoscale Res Lett* **2**, 512 (2007).

[27] Njoki, P. N., Lim, I.-I. S., Mott, D., Park, H.-Y., Khan, B., Mishra, S., Sujakumar, R., Luo, J., and Zhong, C.-J. Size correlation of optical and spectroscopic properties for gold nanoparticles. *J. Phys. Chem. C* **111**, 14664 (2007).

[28] Hutter, E. and Fendler, J. H. Exploitation of localized surface plasmon resonance. *Adv. Mater.* **16**, 1685 (2004).

[29] Eustis, S. and El-Sayed, M. A. Why gold nanoparticles are more precious than pretty gold: Noble metal surface plasmon resonance and its enhancement of the radiative and nonradiative properties of nanocrystals of different shapes. *Chem. Soc. Rev.* **35**, 209 (2006).

[30] Kelly, K. L., Coronado, E., Zhao, L. L., and Schatz, G. C. The optical properties of metal nanoparticles: The influence of size, shape, and dielectric environment. *J. Phys. Chem. B* **107**, 668 (2003).

[31] Sharma, V., Park, K., and Srinivasarao, M. Colloidal dispersion of gold nanorods: Historical background, optical properties, seed-mediated synthesis, shape separation and self-assembly. *Mater. Sci. Eng., R* **65**, 1 (2009).

[32] El-Sayed, M. A. Some interesting properties of metals confined in time and nanometer space of different shapes. *Acc. Chem. Res.* **34**, 257 (2001).

[33] Mie, G. Beiträge zur optik trüber medien, speziell kolloidaler metallösungen. *Ann. Phys.* **25**, 377 (1908).

[34] Crossland, B. and Rowley, D. Contributions to the optics of turbid media, particularly of colloidal metal solutions by g. mie. *Royal Aircraft Establishment, Libary translation No.* **1876**, (english translation of the work of G. Mie) (1976).

[35] Zaluska, A., Zaluski, L., and Strom-Olsen, J. O. Nanocrystalline magnesium for hydrogen storage. *J. Alloys Compd.* **288**, 217 (1999).

[36] Yu, S., Li, N., Wharton, J., and Martin, C. R. Nano wheat fields prepared by plasma-etching gold nanowire-containing membranes. *Nano Lett.* **3**, 815 (2003).

[37] Lee, H. and Jung, G.-Y. Full wafer scale near zero residual nano-imprinting lithography using uv curable monomer solution. *Microelectron. Eng.* **77**, 42 (2005).

[38] Turkevich, J., Stevenson, P. C., and Hillier, J. Nucleation and growth process in the synthesis of colloidal gold. *Discuss. Faraday Soc.* **11**, 55 (1951).

[39] Brust, M., Walker, M., Bethell, D., Schiffrin, D. J., and Whyman, R. Synthesis of thiol-derivatised gold nanoparticles in a two-phase liquid-liquid system. *J. Chem. Soc., Chem. Commun.* , 801 (1994).

[40] Jana, N. R. and Peng, X. Single-phase and gram-scale routes toward nearly monodisperse au and other noble metal nanocrystals. *J. Am. Chem. Soc.* **125**, 14280 (2003).

[41] Rowe, M. P., Plass, K. E., Kim, K., Kurdak, C., Zellers, E. T., and Matzger, A. J. Single-phase synthesis of functionalized gold nanoparticles. *Chem. Mater.* **16**, 3513 (2004).

[42] Murphy, C. J., Sau, T. K., Gole, A. M., Orendorff, C. J., Gao, J., Gou, L., Hunyadi, S. E., and Li, T. Anisotropic metal nanoparticles: synthesis, assembly and optical applications. *J. Phys. Chem. B* **109**, 13857 (2005).

[43] Park, J., Joo, J., Kwon, G., Jang, Y., and Hyeon, T. Synthesis of monodisperse spherical nanocrystals. *Angew. Chem. Int. Ed.* **46**, 4630 (2007).

[44] Wiley, B., Sun, Y., Mayers, B., and Xia, Y. Shape-controlled synthesis of metal nanostructures: The case of silver. *Chem.–Eur. J.* **11**, 454 (2005).

[45] Herricks, T., Chen, J., and Xia, Y. Polyol synthesis of platinum nanoparticles: Control of morphology with sodium nitrate. *Nano Lett.* **4**, 2367 (2004).

[46] Chen, J., Herricks, T., and Xia, Y. Polyol synthesis of platinum nanostructures: Control of morphology through the manipulation of reduction kinetics. *Angew. Chem., Int. Ed.* **44**, 2589 (2005).

[47] Petit, C., Taleb, A., and Pileni, M. P. Cobalt nanosized particles organized in a 2d superlattice: Synthesis, characterization, and magnetic properties. *J. Phys. Chem. B* **103**, 1805 (1999).

[48] Ji, X., Song, X., Li, J., Bai, Y., Yang, W., and Peng, X. Size control of gold nanocrystals in citrate reduction: The third role of citrate. *J. Am. Chem. Soc.* **129**, 13939 (2007).

[49] Jana, N. R., Gearheart, L., and Murphy, C. J. Seeding growth for size control of 5-40 nm diameter gold nanoparticles. *Langmuir* **17**, 6782 (2001).

[50] Daniel, M. C. and Astruc, D. Gold nanoparticles: Assembly, supramolecular chemistry, quantum-size-related properties, and applications toward biology, catalysis, and nanotechnology. *Chem. Rev.* **104**, 293 (2004).

[51] Wang, X., Zhuang, J., Peng, Q., and Li, Y. A general strategy for nanocrystal synthesis. *Nature* **437**, 121 (2005).

[52] Gray, D. H. and Gin, D. L. *Chem. Mater.* **10**, 1827 (1998).

[53] Lee, M. H., Oh, S. G., Suh, K. D., Kim, D. G., and Sohn, D. Preparation of silver nanoparticles in hexagonal phase formed by nonionic triton x-100 surfactant. *Colloids Surf. A* **210**, 49 (2002).

[54] Khiew, P. S., Radiman, S., Huang, N. M., and Ahamd, M. S. Synthesis and characterization of copper sulfide nanoparticles in hexagonal phase lyotropic liquid crystal. *J. Cryst. Growth* **268**, 227 (2004).

[55] Li, M., Schnablegger, H., and Mann, S. Coupled synthesis and self-assembly of nanoparticles to give structures with controlled organization. *Nature* **402**, 393 (1999).

[56] Yu, Y.-Y., Chang, S. S., Lee, C.-L., and Wang, C. R. C. Gold nanorods: Electrochemical synthesis and optical properties. *J. Phys. Chem. B* **101**, 6661 (1997).

[57] Chen, F., Xu, G.-Q., and Hor, T. S. A. Preparation and assembly of colloidal gold nanoparticles in ctab-stabilized reverse microemulsion. *Mater. Lett.* **57**, 3282 (2003).

[58] Khomutov, G. B. Two-dimensional synthesis of anisotropic nanoparticles. *Colloids Surf., A* **202**, 243 (2002).

[59] Mafune, F., Kohno, J. Y., Y. Takeda, Y., and Kondow, T. Full physical preparation of size-selected gold nanoparticles in solution: Laser ablation and laser-induced size control. *J. Phys. Chem. B* **106**, 7575 (2002).

[60] Wilcoxon, J. P. and Provencio, P. P. Heterogeneous growth of metal clusters from solutions of seed nanoparticles. *J. Am. Chem. Soc.* **126**, 6402 (2004).

[61] Brust, M., Fink, J., Bethell, D., Schiffrin, D. J., and Kiely, C. Synthesis and reactions of functionalised gold nanoparticles. *J. Chem. Soc., Chem. Commun.* , 1655 (1995).

[62] Yonezawa, T., Yasui, K., and Kimizuka, N. Controlled formation of smaller gold nanoparticles by the use of four-chained disulfide stabilizer. *Langmuir* **17**, 271 (2001).

[63] Weare, W. W., Reed, S. M., Warner, M. G., and Hutchison, J. E. Improved synthesis of small (dcore 1.5 nm) phosphine-stabilized gold nanoparticles. *J. Am. Chem. Soc.* **122**, 12890 (2000).

[64] Love, J. C., Estroff, L. A., Kriebel, J. K., Nuzzo, R. G., and Whitesides, G. M. Self-assembled monolayers of thiolates on metals as a form of nanotechnology. *Chem. Rev.* **105**, 1103 (2005).

[65] Templeton, A. C., Hostetler, M. J., Kraft, C. T., and Murray, R. W. Reactivity of monolayer-protected gold cluster molecules: Steric effects. *J. Am. Chem. Soc.* **120**, 1906 (1998).

[66] Templeton, A. C., Wuelfing, W. P., and Murray, R. W. Monolayer-protected cluster molecules. *Acc. Chem. Res.* **33**, 27 (2000).

[67] Kalsin, A. M., Fialkowski, M., Paszewski, M., Smoukov, S. K., Bishop, K. J. M., and Grzybowski, B. A. Electrostatic self-assembly of binary nanoparticle crystals with a diamond-like lattice. *Science* **312**, 420 (2006).

[68] Hostetler, M. J., Templeton, A. C., and Murray, R. W. Dynamics of place-exchange reactions on monolayer-protected gold cluster molecules. *Langmuir* **15**, 3782 (1999).

[69] Nath, S., Ghosh, S. K., Kundu, S., Praharaj, S., Panigrahi, S., and Pal, T. Is gold really softer than silver? hsab principle revisited. *J. Nanopart. Res.* **8**, 111 (2006).

[70] Eigler, D. and Schweizer, E. Positioning single atoms with a scanning tunneling microscope. *Nature* **344**, 524 (1990).

[71] Harfenist, S. A., Wang, Z. L., Alvarez, M. M., Vezmar, I., and Whetten, R. L. Highly oriented molecular ag nanocrystal arrays. *J. Phys. Chem.* **100**, 13904 (1996).

[72] Lalatonne, Y., Richardi, J., and Pileni, M. P. Van der waals versus dipolar forces controlling mesoscopic organizations of magnetic nanocrystals. *Nat. Mater.* **3**, 121 (2004).

[73] Khanal, B. P. and Zubarev, E. R. Rings of nanorods. *Angew Chem Int Ed* **46**, 2195 (2007).

[74] Whitesides, G. M. and Grzybowski, B. Self-assembly at all scales. *Science* **295**, 2418 (2002).

[75] Grzybowski, B. A., Wilmer, C. E., Kim, J., Browne, K. P., and Bishop, K. J. M. Self-assembly: from crystals to cells. *Soft Matter* **5**, 1110 (2009).

[76] Bishop, K. J. M., Wilmer, C. E., Soh, S., and Grzybowski, B. A. Nanoscale forces and their uses in self-assembly. *Small* **5**, 1600 (2009).

[77] Grzelczak, M., Vermant, J., Furst, E. M., and Liz-Marzan*, L. M. Directed self-assembly of nanoparticles. *ACS Nano* **4**, 3591 (2010).

[78] Hamley, I. W. Nanotechnology with soft materials. *Angew. Chem. Int. Ed.* **42**, 1692 (2003).

[79] Fialkowski, M., Bishop, K. J. M., Klajn, R., Smoukov, S. K., Campbell, C. J., and Grzybowski, B. A. Principles and implementations of dissipative (dynamic) self-assembly. *J. Phys. Chem. B* **110**, 2482 (2006).

[80] Haruta, M., Kobayashi, T., Sano, H., and Yamada, N. Novel gold catalysts for the oxidation of carbon monoxide at a temperature far below 0 °c. *Chem. Lett.* , 405 (1987).

[81] Maye, M. M., Lou, Y., and Zhong, C.-J. Langmuir. *Core-Shell Gold Nanoparticle Assembly as Novel Electrocatalyst of CO Oxidation* **16**, 7520 (2000).

[82] Luo, J., Maye, M. M., Lou, Y., Han, L., Hepel, M., and Zhong, C. J. Catalytic activation of core-shell assembled gold nanoparticles as catalyst for methanol electrooxidation. *Catal. Today* **77**, 127 (2002).

[83] El-Deab, M. S. and Ohsaka, T. An extraordinary electrocatalytic reduction of oxygen on gold nanoparticles-electrodeposited gold electrodes. *Electrochem. Commun.* **4**, 288 (2002).

[84] Zhang, Y., Asahina, S., Yoshihara, S., and Shirakashi, T. Oxygen reduction on au nanoparticle deposited boron-doped diamond films. *Electrochim. Acta* **48**, 741 (2003).

[85] Mohr, C., Hofmeister, H., and Claus, P. The influence of real structure of gold catalysts in the partial hydrogenation of acrolein. *J. Catal.* **213**, 86 (2002).

[86] Schubert, M. M., Hacjenberg, S., van Vee, A. C., Muhler, M., Plzak, V., and Behm, R. Co oxidation over supported gold catalysts- inert and active support materials and their role for the oxygen supply during reaction. *J. Catal.* **197**, 113 (2001).

[87] Rioux, R. M., Song, H., Hoefelmeyer, J. D., Yang, P., and Somorjai, G. A. High-surface-area catalyst design: Synthesis, characterization, and reaction studies of platinum nanoparticles in mesoporous sba-15 silica. *J. Phys. Chem. B* **109**, 2192 (2005).

[88] Okumura, M., Tsubota, S., Iwamoto, M., and Haruta, M. Chemical vapor deposition of gold nanoparticles on mcm-41 and their catalytic activities for the low-temperature oxidation of co and of h2. *Chem. Lett.* , 315 (1998).

[89] Serna, R., Missana, T., Afonso, C. N., Ballesteros, J. M., Petford-Long, A. K., and Doole, R. C. Bi nanocrystals embedded in an amorphous ge matrix grown by pulsed laser deposition. *Appl. Phys. A* **66**, 43 (1998).

[90] Prashar, A. K., Hodgkins, R. P., Chandran, J. N., Rajamohanan, P. R., and Devi, R. N. In situ encapsulation of pt nanoarchitectures of varying morphologies in mesoporous compounds. *Chem. Mater.* **22**, 1633 (2010).

[91] Rosi, N. L. and Mirkin, C. A. Nanostructures in biodiagnostics. *Chem. Rev.* **105**, 1547 (2005).

[92] De, M., Ghosh, P. S., and Rotello, V. M. Applications of nanoparticles in biology. *Adv. Mater.* **20**, 4225 (2008).

[93] Murphy, C. J., Gole, A. M., Stone, J. W., Sisco, P. N., Alkilany, A. M., Goldsmith, E. C., and Baxter, S. C. Gold nanoparticles in biology: Beyond toxicity to cellular imaging. *Acc. Chem. Res.* **41**, 1721 (2008).

[94] Sperling, R. A., Gil, P. R., Zhang, F., Zanella, M., and Parak, W. J. Biological applications of gold nanoparticles. *Chem. Soc. Rev.* **37**, 1896 (2008).

[95] Jain, P. K., Huang, X., El-Sayed, I. H., and El-Sayed, M. A. Noble metals on the nanoscale: Optical and photothermal properties and some applications in imaging, sensing, biology, and medicine. *Acc. Chem. Res.* **41**, 1578 (2008).

[96] Hong, R., Han, G., Fernandez, J. M., Kim, B.-J., Forbes, N. S., and Rotello, V. M. Glutathione-mediated delivery and release using monolayer protected nanoparticle carriers. *J. Am. Chem. Soc.* **128**, 1078 (2006).

[97] Jain, P. K., El-Sayed, I. H., and El-Sayed, M. A. Au nanoparticles target cancer. *Nanotoday* **2**, 18 (2007).

[98] Elghanian, R., Storhoff, J. J., Mucic, R. C., Letsinger, R. L., and Mirkin, C. A. Selective colorimetric detection of polynucleotides based on the distance-dependent optical properties of gold nanoparticles. *Science* **277**, 1078 (1997).

[99] Lesniewski, A., Paszewski, M., and Opallo, M. Gold-carbon thre e dimensional flm electrode prepared from oppositely charged conductive nanoparticles by layer-by-layer approach. *Electrochem. Commun.* **12**, 435 (2010).

[100] Szot, K., Watkins, J. D., Bull, S. D., Marken, F., and Opallo, M. Three dimensional film electrode prepared from oppositely charged carbon nanoparticles as efficient enzyme host. *Electrochem. Commun.* **12**, 737 (2010).

[101] Celebanska, A., Tomaszewska, D., Lesniewski, A., and Opallo, M. Film electrode prepared from oppositely charged silicate submicroparticles and carbon nanoparticles for selective dopamine sensing. *Biosens. Bioelectron.* **26**, 4417 (2011).

[102] Bruchez, M. P. and Hotz, C. Z., editors. *Quantum dots application in biology*. Humana Press Inc., (2007).

[103] Michalet, X., Pinaud, F. F., Bentolila, L. A., Tsay, J. M., Doose, S., Li, J. J., Sundaresan, G., Wu, A. M., Gambhir, S. S., and Weiss, S. Quantum dots for live cells, in vivo imaging, and diagnostics. *Science* **307**, 538 (2005).

[104] Resch-Genger, U., Grabolle, M., Cavaliere-Jaricot, S., Nitschke, R., and Nann, T. Quantum dots versus organic dyes as fluorescent labels. *Nat. Methods* **5**, 763 (2008).

[105] Xia, F., Zuo, X., Yang, R., Xiao, Y., Kang, D., Vallée-Bélisle, A., Gong, X., Yuen, J. D., Hsu, B. B. Y., Heeger, A. J., and Plaxco, K. W. Colorimetric detection of dna, small molecules, proteins, and ions using unmodified gold nanoparticles and conjugated polyelectrolytes. *PNAS* **107**, 10837 (2010).

[106] Xue, Y., Zhao, H., Wu, Z., Li, X., He, Y., and Yuan, Z. Colorimetric detection of cd2+ using gold nanoparticles cofunctionalized with 6-mercaptonicotinic acid and l-cysteine. *Analyst* **136**, 3725 (2011).

[107] Freeman, R. G., Grabar, K. C., Allison, K. J., Bright, R. M., Davis, J. A., Guthrie, A. P., Hommer, M. B., Jackson, M. A., Smith, P. C., Walter, D. G., and Natan, M. J. Self-assembled metal colloid monolayers: An approach to sers substrates. *Science* **267**, 1629 (1995).

[108] Fukumi, K., Chayahara, A., Kadono, K., Sakaguchi, T., Horino, Y., Miya, M., Fujii, K., Hayakawa, J., and Satou, M. Gold nanoparticles ion implanted in glass with enhanced nonlinear optical properties. *J. Appl. Phys.* **75**, 3075 (1994).

[109] Colvin, V. L., Schlamp, M. C., and Alivisatos, A. P. Light-emitting diodes made from cadmium selenide nanocrystals and a semiconducting polymer. *Nature* **370**, 354 (1994).

[110] Cassagneau, T., Mallouk, T. E., and Fendler, J. H. Layer-by-layer assembly of thin film zener diodes from conducting polymers and cdse nanoparticles. *J. Am. Chem. Soc.* **120**, 7848 (1998).

[111] Tessler, N., Medvedev, V., Kazes, M., Kan, S., and Banin, U. Efficient near-infrared polymer nanocrystal light-emitting diodes. *Science* **295**, 1506 (2002).

[112] Huynh, W. U., Dittmer, J. J., and Alivisatos, A. P. Hybrid nanorod-polymer solar cells. *Science* **295**, 2425 (2002).

[113] Nozik, A. J. Quantum dot solar cells. *Physica E* **14**, 115 (2002).

[114] Gratzel, M. Solar energy conversion by dye-sensitized photovoltaic cells. *Inorg. Chem.* **44**, 6841 (2005).

[115] Robel, I., Subramanian, V., Kuno, M., and Kamat, P. V. Quantum dot solar cells. harvesting light energy with cdse nanocrystals molecularly linked to mesoscopic tio2 films. *J. Am. Chem. Soc.* **128**, 2385 (2006).

[116] Kongkanand, A., Tvrdy, K., Takechi, K., Kuno, M., and Kamat, P. V. Quantum dot solar cells. tuning photoresponse through size and shape control of cdse-tio2 architecture. *J. Am. Chem. Soc.* **130**, 4007 (2008).

[117] Kazes, M., Lewis, D. Y., Ebenstein, Y., Mokari, T., and Banin, U. Lasing from semiconductor quantum rods in a cylindrical microcavity. *Adv. Mater.* **14**, 317 (2002).

[118] Ma, J., Mo, M.-S., Du, X.-S., Rosso, P., Friedrich, K., and Kuan, H.-C. Effect of inorganic nanoparticles on mechanical property, fracture toughness and toughening mechanism of two epoxy systems. *Polymer* **49**, 3510 (2008).

[119] Bae, G. Y., Min, B. G., Jeong, Y. G., Lee, S. C., Jang, J. H., and Koo, G. H. Superhydrophobicity of cotton fabrics treated with silica nanoparticles and water-repellent agent. *J. Colloid Interface Sci.* **337**, 170 (2009).

[120] Leng, B., Shao, Z., de With, G., and Ming, W. Superoleophobic cotton textiles. *Langmuir* **25**, 2456 (2009).

[121] Lee, H. Y., Park, H. K., Lee, Y. M., Kim, K., and Park, S. B. A practical procedure for producing silver nanocoated fabric and its antibacterial evaluation for biomedical applications. *Chem. Commun.* **28**, 2959 (2007).

[122] K.Holmberg, Jönsson, B., Kronberg, B., and Lindman, B. *Surfactants and polymers in aqueous solution.-2nd ed.*, chapter Introduction to surfactants, 1–37. John Wiley & Sons LTD (2003).

[123] Hibbs, J. *Chemistry and Technology of Surfactants*, chapter Anionic Surfactants, 91–132. Blackwell Publishing Ltd (2006).

[124] Gadberry, J. F. *Chemistry and Technology of Surfactants*, chapter Other Types of Surfactants, 153–235. Blackwell Publishing Ltd (2006).

[125] Nikoobakht, B. and El-Sayed, M. A. Preparation and growth mechanism of gold nanorods (nrs) using seed-mediated growth method. *Chem. Mater.* **15**, 1957 (2003).

[126] Hepworth, P. *Chemistry and Technology of Surfactants*, chapter Non-ionic Surfactants, 133–252. Blackwell Publishing Ltd (2006).

[127] K.Holmberg, Jönsson, B., Kronberg, B., and Lindman, B. *Surfactants and polymers in aqueous solution.-2nd ed.*, chapter Surfactant micellization, 39–66. John Wiley & Sons LTD (2003).

[128] Hamley, I. W. *Introduction to Soft Matter – Revised Edition: Synthetic and Biological Self-Assembling Materials*, chapter Amphiphiles, 161–220. John Wiley & Sons, Ltd. (2007).

[129] Rosen, M. J. *Surfactants and Interfacial Phenomena, Third Edition*, chapter Micelle Formation by Surfactants, 105–177. John Wiley & Sons, Inc. (2004).

[130] Adamczyk, A. *Niezwykły stan materii- Ciekłe kryształy*, chapter Stany mezomorficzne substancji, 14–118. Wiedza Powszechna, Warszawa (1979).

[131] Janik, J. and Moscicki, J. K. Miesowicz viscosities study of a two-component thermotropic mixture. *Phys. Rev. E* **58**, 1351 (1998).

[132] Sokolowska, D. and Moscicki, J. K. Phase equilibria in solutions of platelike particles: Systems with steric and dispersive interactions between the platelets. *Phys. Rev. E* **71**, 031701 (2005).

[133] K.Holmberg, Jönsson, B., Kronberg, B., and Lindman, B. *Surfactants and polymers in aqueous solution.-2nd ed.*, chapter Phase behaviour of concentrated surfactant systems, 67–96. John Wiley & Sons LTD (2003).

[134] Myers, D. *Surfactant Science and Technology, Third Edition*, chapter Higher-Level Surfactant Aggregate Structures: Liquid Crystals, Continuous Biphases, and Microemulsions, 160–190. John Wiley & Sons, Inc. (2006).

[135] Tadros, T. F. *Applied Surfactants: Principles and Applications*, chapter Phase Behavior of Surfactant Systems, 53–72. WILEY-VCH Verlag GmbH & Co. KGaA (2005).

[136] K.Holmberg, Jönsson, B., Kronberg, B., and Lindman, B. *Surfactants and polymers in aqueous solution.-2nd ed.*, chapter Physicochemical properties of surfactants and polymers containing oxyethylene groups, 97–118. John Wiley & Sons LTD (2003).

[137] Przygocki, W. and Włochowicz, A. *Fizyka polimerów*, chapter Struktura makrocząsteczek, 15–52. Wydawnictwo Naukowe PWN SA, Warszawa (2001).

[138] Galina, H. *Fizykochemia polimerów*, chapter Rozdział 1, 9–20. Oficyna Wydawnicza Politechniki Rzeszowskiej, Rzeszów (1998).

[139] K.Holmberg, Jönsson, B., Kronberg, B., and Lindman, B. *Surfactants and polymers in aqueous solution.-2nd ed.*, chapter Polymers in Solution, 193–214. John Wiley & Sons LTD (2003).

[140] Winnik, F. M. *Principles of Polymer Science and Technology in Cosmetics and Personal Care*, chapter Elements of Polymer Science. Marcel Dekker, Inc. (1999).

[141] Jones, M. N. *J. Colloid Interface Sci.* **43**, 104 (1967).

[142] Holmberg, K., Jonsson, B., Kronberg, B., and Lindman, B. *Surfactant and polymers in aqueous solution.-2nd ed.* John Wiley & Sons Ltd, (2003).

[143] Goddard, E. D., Phillips, T. S., and Hannan, R. B. *J. Soc. Cosmet. Chem.* **26**, 461 (1975).

[144] Piculell, L., Bergfeldt, K., and Gerdes, S. Segregation in aqueous mixtures of non-ionic polymers and surfactant micelles. effects of micelle size and surfactant head-group/polymer interactions. *J. Phys. Chem.* **100**, 3675 (1996).

[145] Clegg, S. M., Williams, P. A., Warren, P., and Robb, I. D. Phase behavior of polymers with concentrated dispersions of surfactants. *Langmuir* **10**, 3390 (1994).

[146] Holyst, R., Staniszewski, K., and Demyanchuk, I. Ordering in surfactant mixtures induced by polymers. *J. Phys. Chem. B* **109**, 4881 (2005).

[147] Makulska, S., Chudy, E., Wieczorek, S. A., Zywocinski, A., and Holyst, R. Influence of poly(ethylene glycol) molecular mass on separation and ordering in solutions of ciej nonionic surfactants: Depletion interactions and steric effects. *J. Phys. Chem. B* **111**, 7948 (2007).

[148] Thalberg, K. and Lindman, B. Segregation in aqueous systems of a polyelectrolyte and an ionic surfactant. *Colloids Surf. A* **76**, 283 (1993).

[149] Asakura, S. and Oosawa, J. On interaction between two bodies immersed in a solution of macromolecules. *J. Chem. Phys.* **22**, 1255 (1954).

[150] Vrij, A. Polymers at interfaces and the interactions in colloidal dispersions. *Pure Appl. Chem.* **48**, 471 (1976).

[151] Anderson, V. J. and Lekkerkerker, H. N. W. Insights into phase transition kinetics from colloid science. *Nature* **416**, 811 (2002).

[152] Eiser, E., Bouchama, F., Thathagar, M. B., and Rothenberg, G. Trapping metal nanoclusters in soap and water soft crystals. *ChemPhysChem* **4**, 526 (2003).

[153] Bouchama, F., Thathagar, M. B., Rothenberg, G., Turkenburg, D. H., and Eiser, E. Self-assembly of a hexagonal phase of wormlike micelles containing metal nanoclusters. *Langmuir* **20**, 477 (2004).

[154] Kumar, P. S., Pal, S. K., Kumar, S., and Lakshminarayanan, V. Dispersion of thiol stabilized gold nanoparticles in lyotropic liquid crystalline systems. *Langmuir* **23**, 3445 (2007).

[155] Ramos, L., Fabre, P., and Ober, R. Existence, stability and structure of a hexagonal phase doped with nanoparticles. *Eur. Phys. J. B* **1**, 319 (1998).

[156] Ramos, L., Fabre, P., and Fruchter, L. Magnetic field induced instabilities of a doped lyotropic hexagonal phase. *Eur. Phys. J. B* **8**, 67 (1999).

[157] *Pure Appl. Chem.* **396**, 152 (1998). IUPAC Manual of Symbols and Terminology, Apendix 2, Part 1, Colloid and Surface Chemistry.

[158] Beck, J. S., Vartuli, J. C., Roth, W. J., Leonowicz, M. E., Kresge, C. T., Schmitt, K. D., Chu, C. T.-W., Olson, D. H., Sheppard, E. W., McCullen, S. B., Higgins, J. B., and Schlenker, J. L. A new family of mesoporous molecular sieves prepared with liquid crystal templates. *J. Am. Chem. Soc.* **114**, 10834 (1992).

[159] Kresge, C. T., Leonowicz, M. E., Roth, W. J., Vartuli, J. C., and Beck, J. S. Ordered mesoporous moleculer-sieves synthesized by a liquid-crystal template mechanism. *Nature* **359**, 710 (1992).

[160] Huo, Q., Margolese, D., and Stucky, G. D. Surfactant control of phases in the synthesis of mesoporous silica-based materials. *Chem. Mater.* **8**, 1147 (1996).

[161] Huo, Q., Margolese, D. I., Ciesla, U., Feng, P., Gier, T. E., Sieger, P., Leon, R., Petroff, P. M., Schüth, F., and Stucky", G. D. Generalized synthesis of periodic surfactant/inorganic composite materials. *Nature* **368**, 317 (1994).

[162] Attard, G. S., Glyde, J. C., and Goltner, C. G. Liquid-crystalline phases as templates for the synthesis of mesoporous silica. *Nature* **378**, 366 (1995).

[163] Yang, P., Zhao, D., Margolese, D. I., Chmelka, B. F., and Stucky, G. D. Generalized syntheses of large-pore mesoporous metal oxides with semicrystalline frameworks. *Nature* **396**, 152 (1998).

[164] Tanev, P. T., Chibwe, M., and Pinnavaia, T. J. Titanium-containing mesoporous molecular-sieves for catalytic-oxidation of aromatic-compounds. *Nature* **368**, 321 (1994).

[165] Corma, A. From microporous to mesoporous molecular sieve materials and their use in catalysis. *Chem. Rev.* **97**, 2373 (1997).

[166] Lee, C.-H., Lin, T.-S., and Mou, C.-Y. Mesoporous materials for encapsulating enzymes. *Nano Today* **4**, 165 (2009).

[167] http://vanha.physics.utu.fi. Electronic presentation: Optical microscopy.pdf.

[168] Feigin, L. and Svergun, D. I. *Structure Analysis by Small-Angle X-Ray and Neutron Scattering*. Plenum Press, (1987).

[169] Svergun, D. I. and Koch, M. H. J. Small-angle scattering studies of biological macromolecules in solution. *Rep. Prog. Phys.* **66**, 1735 (2003).

[170] Malvern Instruments Ltd. *Dynamic Light Scattering: An Introduction in 30 Minutes*. DLS technical note MRK656-01.

[171] Pecora, R. *Dynamic Light Scattering. Applications of Photon Correlation Spectroscopy*. Springer, (1985).

[172] Barnett, C. E. Some applications of wave-length turbidimetry in the infrared. *J. Phys. Chem.* **46**, 69 (1942).

[173] Zeta-Meter Inc. *Zeta Potential: A Complete Course in 5 Minutes*.

[174] Atkins, P. and De-Paula, J. *Atkins' Physical Chemistry*. Oxford University Press, (2006).

[175] Malvern Instruments Ltd. *Zetasizer Nano User Manual, MAN0317 Issue 5.0*, , August (2009).

[176] Zhao, D., Huo, Q., Feng, J., Chmelka, B. F., and Stucky, G. D. Nonionic triblock and star diblock copolymer and oligomeric surfactant syntheses of highly ordered, hydrothermally stable, mesoporous silica structures. *J. Am. Chem. Soc.* **120**, 6024 (1998).

[177] Dominguez, A., Fernández, A., González, N., Iglesias, E., and Montenegro, L. Determination of critical micelle concentration of some surfactants by three techniques. *J. Chem. Educ.* **74**, 1227 (1997).

[178] Noordman, W. H., Wachter, J. H. J., de Boer, G. J., and Janssen, D. B. The enhancement by surfactants of hexadecane degradation by pseudomonas aeruginosa varies with substrate availability. *J. Biotechnol.* **94**, 195 (2002).

[179] Guha, S. and Jaffé, P. R. Bioavailability of hydrophobic compounds partitioned into the micellar phase of nonionic surfactants. *Environ. Sci. Technol.* **30**, 1382 (1996).

[180] Sarkar, N., Datta, A., and Das, S. Solvation dynamics of coumarin 480 in micelles. *J. Phys. Chem.* **100**, 15483 (1996).

[181] Ruiz, C. C. Thermodynamics of micellization of tetradecyltrimethylammonium bromide in ethylene glycol-water binary mixtures. *Colloid Polym. Sci* **277**, 701 (1999).

[182] Roger, G. M., Durand-Vidal, S., Bernard, O., and Turq, P. Interpretation of conductivity results from 5 to 45 degrees c on three micellar systems below and above the cmc. *J. Phys. Chem.* **112**, 16529 (2008).

[183] Jalali, F., Shamsipur, M., and Alizadeh, N. Conductance study of the thermodynamics of micellization of 1-hexadecylpyridinium bromide in (water plus cosolvent). *J. Chem. Thermodynamics* **32**, 755 (2000).

[184] Flockhart, B. D. The effect of temperature on the critical micelle concentration of some paraffin-chain salts. *J. Coll. Sci.* **16**, 484 (1961).

[185] Matsuoka, K., Moroi, Y., and Saito, M. Thermodynamics of micelle formation of 1-dodecanesulfonic acid. *J. Phys. Chem.* **97**, 13006 (1993).

[186] Mitchell, D. J., Tiddy, G. J., Waring, L., Bostock, T., and MacDonald, M. P. Phase behaviour of polyoxyethylene surfactants with water. mesophase structures and partial miscibility (cloud points). *J. Chem. Soc. Faraday Trans.* **79**, 975 (1983).

[187] Laughlin, R. G. *The Aqueous Phase Behaviour of Surfactants*. Academic Press, London, (1994).

[188] Auvray, X., Petipas, C., and Anthore, R. X-ray dlff raction study of mesophases of cetyltrimethylammonium bromide in water, formamlde, and glycerol. *J. Phys. Chem.* **93**, 7458 (1989).

[189] Somasundaran, P. *Encyclopedia of Surface and Colloid Science*. Columbia University, New York, (2006).

[190] Rubingh, D. N. and Holland, P. M. *Cationic surfactants: physical chemistry*. Marcel Dekker, Inc., (1991).

[191] Kalwarczyk, E., Golos, M., Holyst, R., and Fialkowski, M. Polymer-induced ordering and phase separation in ionic surfactants. *J. Coll. Int. Sci.* **342**, 93–102 (2010).

[192] Kalwarczyk, E., Paszewski, M., Xin, X., Gorecka, E., Pociecha, D., Holyst, R., and Fialkowski, M. New one-pot technique to introduce charged nanoparticles into a lyotropic liquid crystal matrix. *Langmuir* **27**, 3937 (2011).

[193] Tadros, T. F. *Applied Surfactants: Principles and Applications*. Wiley-VCH, Weinheim, (2005).

[194] Ober, C. K. and Wegner, G. Polyelectrolyte-surfactant complexes in the solid state: Facile building blocks for self-organizing materials. *Adv. Mat.* **9**, 17 (1997).

[195] Vorflusev, V. and Kumar, S. Phase-separated composite films for liquid crystal displays. *Science* **283**, 1903 (1999).

[196] Penterman, R., Klink, S. L., de Koning, H., Nisato, G., and Broer, D. Single-substrate liquid-crystal displays by photo-enforced stratification. *Nature* **417**, 55 (2002).

[197] Percec, V., Glodde, M., Bera, T. K., Miura, Y., Shiyanovskaya, I., Singer, K. D., Balagurusamy, V. S. K., Heiney, P. A., Schnell, I., Rapp, A., Spiess, H.-W., Hudson, S. D., and Duan, H. Self-organization of supramolecular helical dendrimers into complex electronic materials. *Nature* **419**, 384 (2002).

[198] Lee, S. W., Mao, C. B., Flynn, C. E., and Belcher, A. M. Ordering of quantum dots using genetically engineered viruses. *Science* **296**, 892 (2002).

[199] Holyst, R. Solubility and mixing in fluids. In *Encyclopedia of Applied Physics*, volume 18, 573. VCH Publishers, New York (1997).

[200] Russel, W. B., Saville, D. A., and Schowalter, W. R. *Colloidal Dispersions*. Cambridge University Press, Cambridge, (1989).

[201] Sanyal, S., Easwar, N., Ramaswamy, S., and Sood, A. K. Phase separation in binary nearly-hard-sphere colloids: Evidence for the depletion force. *Europhys. Lett.* **18**, 107 (1992).

[202] Lekkerkerker, H. N. W., Poon, W. C. K., Pusey, P. N., Stroobants, A., and Warren, P. B. Phase behaviour of colloid + polymer mixtures. *Europhysics Lett.* **20**, 559 (1992).

[203] Zackrisson, M., Andersson, R., and Bergenholtz, J. Depletion interactions in model microemulsions. *Langmuir* **20**, 3080 (2004).

[204] Walz, J. Y. and Sharma, A. Effect of long range interactions on the depletion force between colloidal particles. *J. Colloid Interface Sci.* **168**, 485 (1994).

[205] Sharma, A. and Walz, J. Y. Direct measurement of the depletion interaction in a charged colloidal dispersion. *J. Chem. Soc. Faraday Trans.* **92**, 4997 (1996).

[206] Sharma, A., Tan, S. N., and Walz, J. Y. Measurement of colloidal stability in solutions of simple, nonadsorbing polyelectrolytes. *J. Colloid Interface Sci.* **190**, 392 (1997).

[207] Jodar-Reyes, A. B., Martin-Rodriguez, A., and Ortega-Vinuesa, J. L. Effect of the ionic surfactant concentration on the stabilization/destabilization of polystyrene colloidal particles. *J. Colloid Interface Sci.* **298**, 248 (2006).

[208] Holyst, R., Staniszewski, K., Patkowski, A., and Gapinski, J. Hidden minima of the gibbs free energy revealed in a phase separation in polymer/surfactant/water mixture. *J. Phys. Chem. B* **109**, 8533 (2005).

[209] Goddard, E. D. and Ananthapadmanabhan, K. P., editors. *Interactions of surfactants with polymers and proteins*. CRC Press, Boca Raton, (1993).

[210] Kwak, J. C. T., editor. *Polymer-Surfactant Systems, Surfactant Science Series, vol. 77*. Marcel Dekker, New York, (1998).

[211] Kokufuta, E. Polyelectrolyte complexes and gels. In Physical Chemistry of Polyelectrolytes, Surfactant Science Series, vol. 99, Radeva, T., editor. Marcel Dekker, New York (2001).

[212] Taylor, D. J. F., Thomas, R. K., and Penfold, J. Polymer/surfactant interactions at the air/water interface. *Adv. Coll. Interf. Sci.* **132**, 69 (2007).

[213] Guo, W., Sun, Y. W., Luo, G., and Wang, Y. J. Interaction of peg with ionic surfactant sds to form template for mesoporous material. *Colloids Surf. A* **252**, 71 (2005).

[214] Zhu, S., Zhou, H., Hibino, M., and Honma, I. Synthesis of hexagonal mesostructured fepo4 using cationic surfactant as the template. *Chem. Lett.* **33**, 774 (2004).

[215] Wang, L., Chen, X., Zhan, J., Chai, Y., Yang, C., Xu, L., Zhuang, W., and Jing, B. Synthesis of gold nano- and microplates in hexagonal liquid crystals. *J. Phys. Chem. B* **109**, 3189 (2005).

[216] Hertel, G. and Hoffman, H. Lyotropic nematic phases of double chain surfactants. *Progr. Colloid Polym. Sci.* **76**, 123 (1988).

[217] Kabalnov, A., Olsson, U., and Wennerstr om, H. Polymer effects on the phase equilibrium of a balanced microemulsion. *Langmuir* **10**, 2159 (1994).

[218] Salamone, J. C., editor. *Polymeric Materials Encyclopedia, Vol. 8*. CRC Press, Boca Raton, FL, (2000).

[219] Koetz, J., Reichelt, S., Kosmella, S., and Tiersch, B. Recovery of nanoparticles produced in phosphatidylcholine-based template phases. *J. Coll. Int. Sci.* **284**, 190 (2005).

[220] Cabane, B. Structure of some polymer-detergent aggregates in water. *J. Phys. Chem.* **81**, 1639 (1977).

[221] Winnik, F. M. and Regismond, S. T. A. Fluorescence methods in the study of the interactions of surfactants with polymers. *Colloids Surf. A.* **118**, 1 (1996).

[222] Guggenheim, E. A. *Theromodynamics: An Advanced Treatment for Chemists and Physicists*. North Holland Physics Publishing, Amsterdam, (1967).

[223] Caruso, F., Caruso, R. A., and Mohwald, H. Nanoengineering of inorganic and hybrid hollow spheres by colloidal templating. *Science* **282**, 1111 (1998).

[224] Bruchez, M., Moronne, M., Gin, P., Weiss, S., and Alivisatos, A. P. Semiconductor nanocrystals as fluorescent biological labels. *Science* **281**, 2013 (1998).

[225] Burda, C., Chen, X., Narayanan, R., and El-Sayed, M. Chemistry and properties of nanocrystals of different shapes. *Chem. Rev.* **105**, 1025 (2005).

[226] Wang, C., Chen, D., and Jiao, X. Lyotropic liquid crystal directed synthesis of nanostructured materials. *Sci. Technol. Adv. Mater.* **10**, 023001 (2009).

[227] Martin, C. R. Nanomaterials: A membrane-based synthetic approach. *Science* **266**, 1961 (1994).

[228] Giersig, M., Ung, T., Liz-Marzan, L. M., and Mulvaney, P. Direct observation of chemical reactions in silica-coated gold and silver nanoparticles. *Adv. Mater.* **9**, 570 (1997).

[229] Bommel, K., Friggeri, A., and Shinkai, S. Organic templates for the generation of inorganic materials. *Angew. Chem. Int. Ed.* **42**, 980 (2003).

[230] Johnson, B. F. G. Nanoparticles in catalysis. *Top. Catal.* **24**, 147 (2003).

[231] Xin, X., Li, H., Wieczorek, S. A., Szymborski, T., Kalwarczyk, E., Ziebacz, N., Gorecka, E., Pociecha, D., and Holyst, R. Incorporation of carbon nanotubes into a lyotropic liquid crystal by phase separation in the presence of a hydrophilic polymer. *Langmuir* **26**, 3562 (2010).

[232] Kalsin, A. M., Pinchuk, A. O., Smoukov, S. K., Paszewski, M., Schatz, G. C., and Grzybowski, B. A. Electrostatic aggregation and formation of core-shell suprastructures in binary mixtures of charged metal nanoparticles. *Nano Lett.* **6**, 1896 (2006).

[233] Janiak, M., Small, D. M., and Shipley, G. G. Nature of the thermal pretransition of synthetic phospholipids: dimyristoyl- and dipalmitoyllecithin. *Biochemistry* **15**, 4575 (1976).

[234] Small, D. M. Lateral chain packing in lipids and membreanes. *J. Lipid Res.* **25**, 1490 (1984).

[235] Cervellino, A., Giannini, C., Guagliardi, A., and Zanchet, D. Quantitative analysis of gold nanoparticles from synchrotron data by means of least-squares techniques - least-squares analysis of gold nanoparticles. *Eur. Phys. J. B* **41**, 485 (2004).

[236] Diao, X.-L., Xia, Y.-S., Zhang, T.-L., Li, Y., and Zhu, C.-Q. Fluorescence-detecting cationic surfactants using luminescent cdte quantum dots as probes. *Anal. Bioanal. Chem.* **388**, 1191 (2007).

[237] Hamity, M., Lema, R. H., and Suchetti, C. A. Effect of detergents on the fluorescence from cds-q clusters prepared using variable excess cd2+ concentrations. *J. Photochem. Photobiol., A* **133**, 205 (2000).

[238] Galian, R. E. and la Guardia, M. D. The use of quantum dots in organic chemistry. *Trends Anal. Chem.* **28**, 279 (2009).

[239] Frasco, M. F. and Chaniotakis, N. Semiconductor quantum dots in chemical sensors and biosensors. *Sensors* **9**, 7266 (2009).

[240] Wang, Z., Li, J., Liu, B., Hu, J., Yao, X., and Li, J. Chemiluminescence of cdte nanocrystals induced by direct chemical oxidation and its size-dependent and surfactant-sensitized effect. *J. Phys. Chem. B* **109**, 23304 (2005).

[241] Cummins, P. G., Staples, E., and Penfold, J. Study of surfactant adsorption on colloidal particles. *J . Phys. Chem.* **94**, 3740 (1990).

[242] Lugo, D., Oberdisse, J., Karg, M., Schweinsc, R., and Findenegg, G. H. Surface aggregate structure of nonionic surfactants on silica nanoparticles. *Soft Matter* **5**, 2928 (2009).

[243] Lugo, D. M., Oberdisse, J., Lapp, A., and Findenegg, G. H. Effect of nanoparticle size on the morphology of adsorbed surfactant layers. *J. Phys. Chem. B* **114**, 4183 (2010).

[244] Sharma, K. P., Aswal, V. K., and Kumaraswamy, G. Adsorption of nonionic surfactant on silica nanoparticles: Structure and resultant interparticle interactions. *J. Phys. Chem. B* **114**, 10986 (2010).

[245] Misra, P. K., Mishra, B. K., and Somasundaran, P. Organization of amphiphiles part iv. characterization of the microstructure of the adsorbed layer of decylethoxylene nonyl phenol. *Colloids Surf., A* **252**, 169 (2005).

[246] Misra, P. K. and Somasundaran, P. Organization of amphiphiles vi. a comparative study of the orientation of polyoxyethylated alkyl phenols at the air–water and the silica–water interface. *J. Surfactants Deterg.* **7**, 373 (2004).

[247] Rosen, M. J. *Surfactants and Interfacial Phenomena*. John Wiley & Sons, Inc., third edition, (2004).

[248] Gapiński, J., Szymański, J., Wilk, A., Kohlbrecher, J., Patkowski, A., and Hołyst, R. Size and shape of micelles studied by means of sans, pcs, and fcs. *Langmuir* **26**, 9304 (2010).

[249] Valeur, B. *Molecular Fluorescence: Principles and Applications*, chapter Effects of intermolecular photophysical processes on fluorescence emission, 72–123. Wiley-VCH Verlag GmbH (2001).

[250] Masel, R. *Principles of Adsorption and Reaction on Solid Surfaces*. Wiley Series in Chemical Engineering. Wiley, (1996).

[251] Johansson, L., Hedberg, P., and Lofroth, J.-E. Diffusion and interaction in gels and solutions, 5. nonionic micellar systems. *J. Phys. Chem.* **97**, 741 (1993).

[252] Gattas-Asfura, K. M. and Leblanc, R. M. Peptide-coated cds quantum dots for the optical detection of copper(ii) and silver(i). *Chem. Commun.* , 2684 (2003).

[253] Chen, Y. and Rosenzweig, Z. Luminescent cds quantum dots as selective ion probes. *Anal. Chem.* **74**, 5132 (2002).

[254] Chen, J.-L. and Zhu, C.-Q. Functionalized cadmium sulfide quantum dots as fluorescence probe for silver ion determination. *Anal. Chim. Acta* **546**, 147 (2005).

[255] Xie, J., Lee, J. Y., Wang, D. I. C., and Ting, Y. P. Identification of active biomolecules in the high-yield synthesis of single-crystalline gold nanoplates in algal solutions. *Small* **3**, 672 (2007).

Sources of images contained in Figure 1:

- Elephant: http://www.naturephoto-cz.com/asian-elephant:elephas-maximus-photo-1340.html
- Buildings: http://pl.123rf.com/photo_701383_multi-color-residental-buildings-in-a-row.html
- Cornflower: http://royaleimage.wordpress.com
- Bee: http://www.lumisfera.pl/photo/80031/Pszczoła+na+plastrze.html
- SEM picture of human hair: http://www.visualphotos.com/image/1x3746019/human _hair_ scanning_electron_micrograph_sem_of
- SEM picture of Winter's bark pollen: http://www.sciencephoto.com/images/ download_lo_res. html?id=667860786
- Microchip: http://www.industryleadersmagazine.com/5-billion-intel-chip-plant-in-arizona-by-2013/
- Microfluidic device: http://www.webbofscience.com/2009/08/26/melodies-divert-droplets
- SEM picture of red blood cells: http://www.sciencephoto.com/images/download_lo_res.html? id=802420398
- SEM picture of Escherichia coli bacteria: http://www.visualphotos.com/image/2x4139158/e_ coli_bacteria_coloured_scanning_electron
- SEM picture of human sperm: http://www.sciencephoto.com/images/download _lo_res.html?id =806240121
- Polymethylmethacrylate microparticles: http://discoveryscientific-usa.com/microparticles/pmm a-particles/polymethylmethacrylate-pmma-mi croparticles-plain-200-400-um-10g
- Double helix of DNA: http://www.dnareplication.info/dnadoublehelix.php
- Tobacco mosaic virus (TMV): http://www.britannica.com/EBchecked/media/696/Schematic-structure-of-the-tobacco-mosaic-virus
- Scheme of Fullerene C60: http://pl.wikipedia.org/w/index.php?title=Plik:Fullerene-C60.png& filetimestamp=20051001220428
- Carbon nanotube: http://www.zeitnews.org/nanotechnology/penn-researchers-help-graft-olfact ory-receptors-onto-nanotubes.html
- Nanoparticles: http://www.nanocomposix.com/gold-nanoparticles/gold-nanoparticles-spherical-colloid.html
- Nanorods: http://www.nanopartz.com/ HAR_Nanorodz.htm
- Nanocubes: see Reference no. 15.
- Nanoplates: see Reference no. 255.